University of Alberta

MICROCHIP–BASED METHODS FOR PROTEIN PROFILING

by

Mark Sax

A thesis submitted to the Faculty of Graduate Studies and Research in partial fulfillment of the requirements for the degree of **Master of Science**.

Department of Electrical and Computer Engineering

Edmonton, Alberta
Fall 2007

Your file Votre référence
ISBN: 978-0-494-33342-6
Our file Notre référence
ISBN: 978-0-494-33342-6

Abstract

Proteomic analysis is traditionally performed with techniques that suffer from low–throughput, high cost, large size, and lack of automation. Although these macroscopic techniques are well–established, miniaturisation may offer improvements beyond those that are attainable with more traditional approaches. In this work, we present the development and characterisation of a microfluidic system capable of electrophoretically separating and detecting proteins. A novel application of this system to salivary protein analysis demonstrates its applicability to proteomic–type analysis on a micro–scale. Such developments aim to lower costs, increase throughput, and increase automation, all of which are necessary to conduct widespread proteomic analyses. Preliminary work is also presented on a microfluidic device capable of coupling an electrophoretic protein separation with electrospray ionisation and ion mobility spectrometry. Such a device would permit miniaturised two–dimensional separation of the sample constituents and a technique capable of advanced proteomic analysis.

Dedication

To Nicole,
I am so thankful for your love, dedication, understanding, and support.
Without you, none of this work would have been possible.

To my family,
Thank you for your love, support, and encouragement.

Acknowledgements

Thank you to my supervisor, Dr. Christopher Backhouse, for his guidance and supervision. I also wish to thank the Applied Miniaturisation Laboratory and the Alberta Cancer Diagnostic Consortium for their support. In particular I would like to thank Dammika Manage, Jana Lauzon, and Alexey Atrazhev for their laboratory protocol support. Thank you to Alex Stickel and Ben Bathgate for their assistance with the IMS system, and to Paul Dumais and the staff of the University of Alberta Nanofab for their assistance with microfabrication.

I would also like to acknowledge Alberta Ingenuity, the Natural Sciences and Engineering Research Council (NSERC) of Canada, the Informatics Circle of Research Excellence (iCORE), the Government of Alberta, and the University of Alberta for providing research funding.

Table of Contents

List of Tables

List of Figures

Chapter 1

Introduction

The research discussed in the thesis addresses protein analysis for profiling the protein content of complex biological samples. Traditionally, such research is conducted in high cost, low–throughput instrumentation. As the study of proteomics grows and the requirement for rapid and comprehensive protein analysis and data generation becomes greater, traditional analysis techniques will not be able to keep up with demand. As such, it is important to develop analytical systems capable of providing low cost, high–throughput analyses on complex samples. This is a prototype of a class of device that might permit rapid and parallel analyses of large sample sets or could be used as personalised point–of–care diagnostic tools. With the above goal in mind, the development of microfluidic tools for protein analysis was addressed.

Originally, the research targeted the creation of a microfluidic system capable of electrophoretically separating proteins and introducing them into an ion mobility spectrometer for further separation and analysis. Also included in the research plan, was the creation of a miniature ion mobility spectrometer. As a complete system, it would be capable of two–dimensional analysis of proteins in an integrated system. Although a device capable of this type of analysis was not fully realised, critical components necessary for the implementation of such a device were developed and studied. As such, four main research components advanced the knowledge required to create such a device.

The first component of the research involved the development of a microfluidic system suitable for conducting microfluidic protein analysis (see Chapter 2). This work included the development of protocols used to modify microfluidic channel surfaces to prevent loss of protein sample due to wall adsorption. In addition, polyacrylamide gels were polymerised within the microfluidic channels to provide a sieving matrix in which electrophoretic protein separations could be conducted. The channel coatings and the polyacrylamide sieving matrix developed in this thesis permitted the miniaturisation of sodium dodecyl sulfate–polyacrylamide gel electrophoresis, or SDS–PAGE, a standard analytical technique used in proteomic studies.

The second component of the research involved characterisation of the system

to assess its suitability for performing protein analysis (see Chapter 3). This work involved the separation of standard mixtures of proteins to assess the system performance, which was evaluated on several fronts. System performance was evaluated for separation quality, conformance to known separation behaviours, system sensitivity, and system repeatability.

The third component of the research required the analysis of a complex proteomic sample. Whole unstimulated saliva analysis, or sialometry, was conducted in the characterised system and the performance of the analysis was assessed for suitability to diagnostic applications (see Chapter 4). Such work found that the system may be suitable for diagnostic applications upon the acquisition of relevant clinical samples and data. In addition, the application of the system to SDS–PAGE based salivary protein analysis proved to be novel.

The final component of the research conducted for this thesis involved the creation of a microfluidic platform for coupling a microchip capillary electrophoresis (MCE) system with ion mobility spectrometry (IMS) or mass spectrometry (MS) using electrospray ionisation (ESI) (see Appendix A). This appendix describes the linkages between the development of an IMS system outside the scope of this thesis and the concepts presented in Chapters 2, 3, and 4. In addition, it introduces the concept and preliminary design of an integrated MCE–ESI microfluidic device. The creation of a microfluidic analysis platform capable of MCE–ESI–IMS (see Figure 1.1 or MCE–ESI–MS would enable advanced proteomic analysis to be conducted primarily on–chip. With the MCE system providing pre–fractionation of the desired sample and ESI bridging MCE with IMS or MS, it is expected such an application could provide advanced high–throughput analysis of proteins with performance on par with current low–throughput and higher cost techniques. Such a system would also eliminate the need for fluorescence based sample labeling, as the IMS system could detect proteins that are not fluorescently tagged. While an entire system was not completed, the design of MCE–ESI microchip has laid the foundations for future developments.

The miniaturisation of proteomic analysis is a daunting task requiring the development of complex systems capable of countless functions. The incorporation of knowledge from many diverse areas is required to fully realise a completely integrated and functional system. The work presented herein seeks to provide a basis of research on the core components required for such analysis. This includes the development of an electrophoretic system capable of separating proteins, the electrophoretic separation of a complex proteomic sample, and the design of a microfluidic chip intended to couple electrophoresis and electrospray ionisation. These developments, supported by previous work in the field, advance the progress toward a microchip–based tool that could be used in proteomic studies.

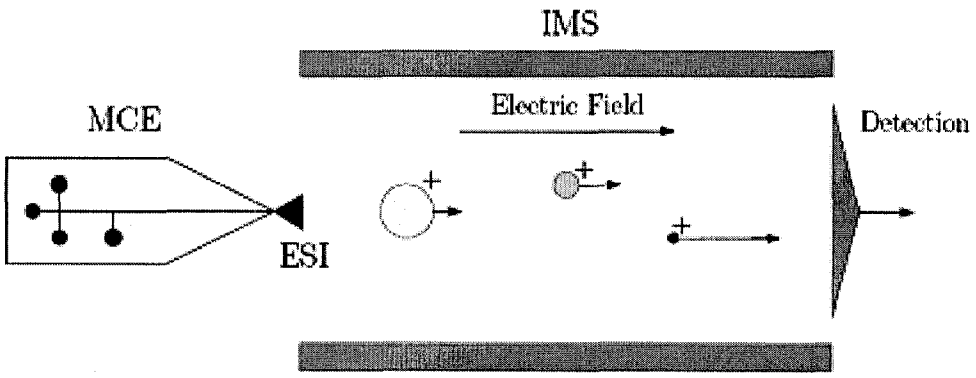

Figure 1.1: This is simplified illustration of a MCE–ESI–IMS system. The MCE and IMS portions of the instrument are coupled via ESI. The system would permit two–dimensional separation of charged analytes in a miniaturised device.

Chapter 2

Microfluidic Chip Preparation

To conduct microchip–based proteomic analyses, it is necessary to tailor the properties of microfluidic chips to fit this purpose. As noted in Chapter 1, the surface properties of the microfluidic channels were altered to suit the application and an appropriate gel matrix was also developed in which electrophoretic separations of proteins could take place. The bulk of the discussion in this chapter relates to the development of the channel surface modification techniques and gel matrix polymerisation techniques, as well as the results of these developments.

2.1 Microfluidic Channel Surface Coating

Self-assembled monolayers (SAM) and thin polymeric coatings that allow for modification of the channel surface properties are commonly recognised as key components in developing reliable electrokinetic separations of biomolecules in microfluidic devices [1, 2]. For protein–based separations, one key requirement for obtaining high quality analyses is the creation of microfluidic surface characteristics that do not allow for non–specific adsorption of proteins onto the channel wall. This is of particular concern in microfluidics, because the surface area–to–volume ratio in these devices is much larger than those of more traditional capillary electrophoresis techniques [2]. The complex structure of proteins lends itself to wide–ranging interactions with surfaces because of electrostatic or hydrophobic interactions leading to protein adsorption [3], and this larger ratio presents a more readily available substrate on which proteins can adsorb. Such adsorption could lead to modifications of the surface charge, causing inconsistent electroosmotic flow and thus separation performance, and inherently reduces the quantity of sample that is available for analysis and detection [4].

SAMs form from molecules adsorbing and assembling in a specific and ordered orientation on a substrate for which they have an affinity. They can be used as a means of protein adsorption repellence, or for anchoring thin polymer films that will provide the repellence. Polymer films or coatings can be employed in a permanent (static) or non–permanent (dynamic) fashion, and are formed by covalent

bonding or physical adsorption respectively. Typically, SAMs and polymeric films are applied to glass or one of a myriad of polymer-based substrates commonly used in microfluidic applications. Controlling microfluidic device surface characteristics via SAMs and polymeric films is critical to the success of microfluidic technology.

Microfluidic device channel coating is a field of study, especially for non–glass substrates, that is still perceived to be in its infancy [1]. Because the work described here uses glass surfaces, the techniques developed for use in traditional capillary electrophoresis are often applicable [2].

2.1.1 Permanent Surface Modification Theory

The following section is largely based on research conducted for a course (ECE 558) required for partial fulfillment of my Master of Science program. This section was derived from an extended abstract discussing the use of self–assembled monolayers for modifying the surface of microfluidic channels [5].

Preventing non-specific protein adsorption in microfluidic channels is a key aspect of providing high resolution, sensitive, reliable, and reproducible electrokinetically driven protein analyses. As such, understanding and manipulating the surface chemistry of these microchannels is paramount [4]. In many cases, permanent modification of the channel surface can be achieved by applying self-assembled monolayers (SAMs) and thin films of polymers, also known as polymer brushes [1]. In doing so, the microfluidic environment adopts a surface that prevents non-specific protein adsorption and allows for the manipulation of electroosmotic flow (EOF) [4].

Microfluidic devices feature small fluidic channels only tens of micrometers in diameter that are usually centimetres in length. As previously noted, the small channel diameter results in a very high surface area–to–volume ratio, therefore increasing the importance of surface chemistry. Microfluidic structures are typically manufactured from different types of glasses or polymeric materials such as poly(dimethyl siloxane) (PDMS). As such, the methods for modifying surfaces of different materials varies depending on the requirements of the initial surface chemistry [2]. For example, glass surfaces are hydrophilic and present silanol surface groups [2, 6], while PDMS devices are highly hydrophobic and have methyl surface groups [2]. The wide use of various polymeric materials has led to a dizzying array of surface chemistries and procedures for altering them.

Non-specific protein interactions generally occur because of electrostatic or hydrophobic interactions [3, 4]. Consequently, the need to create a surface coating that is hydrophilic and shields or eliminates surface charge is paramount [4]. While these objectives can be achieved by physical adsorption of polymeric or surface active molecules to the surface (dynamic coating), covalent modification of the surface, also known as static or permanent coating, is more stable and effective [2]. Covalent modification of surfaces was pioneered by Hjerten in the mid 1980s [7]. Today, many similar methods have been derived from this basic technique. Hjerten's

methodology modified fused silica capillaries in a two-step procedure. Initially, the surface was modified by covalently attaching bi-functional silane molecules to the surface via self–assembly. The second step involved using the head groups of the silane molecules to bind polymers to the surface [7]. While improvements to this procedure have been made in the last twenty years, the premise on which they are based is essentially the same.

As previously mentioned, the first step of Hjerten's procedure, as well as many other approaches, is to generate a SAM of silane molecules, also called silanisation. According to Kirby [8], the chemicals used to produce the SAM, and in turn functionalise the surface, primarily consist of a hydrocarbon backbone terminated by an alkoxysilyl group. Via a process of hydrolysis and condensation, these molecules covalently attach themselves to a surface that has a silanol (Si–OH) group. While native glasses typically have the silanol group, PDMS often requires an oxygen plasma, UV, or corona discharge treatment to generate the required silanol groups at its surface [6]. This covalent attachment to the ionisable silanol group helps to reduce the surface charge. Both the choice of siloxane molecule and the choice of solvent can also have an affect on the packing density of the SAM. Typically toluene or water with an acetic acid catalyst are used as solvents, with toluene being the most effective. In the case of chlorosilanes, monochlorosilanes produce the densest SAMs, while di- and trichlorosilanes produce more stable SAMs [4].

The SAMs discussed above create a covalently attached intermediate layer on which thin polymeric films can be grafted. These films, also called polymer brushes [1], can be composed of many types of polymers that are typically hydrophilic and neutral [9]. Those typically used, include polyacrylamide (PAAm), poly(vinyl alcohol) (PVA), poly(vinylpyrrolidone) (PVP), and numerous others [2]. As with silanisation, solutions are introduced directly into the microfluidic channel to react. The polymer grafting reactions generally use some means of in situ polymerisation [4]. Pallandre divides these in–situ polymerisation reactions into two distinct categories; grafting to, and grafting from [1]. In the case of grafting to, polymer chains are synthesised in the free solution within the channel and are then allowed to diffuse and covalently bond with the functional head group of the silane molecule. The grafting from methodology utilises an extra step. Before introduction of the polymer precursor solution, a polymerisation initiator is bound to the functional end of the silane molecule. When the polymer precursor solution is introduced, the polymerisation is confined to the surface [1]. Coatings that display the best performance are smooth, densely packed, and highly stable over time [4].

Characterisation of these films is often difficult given the closed nature of microfluidic structures. When conducting measurements on intact devices, quantification of the EOF via the current monitoring method [6, 10], or quantification of the surface charge using the streaming potential method [1, 6] both provide some insight into the surface charge, which in turn can help to evaluate the effectiveness of the coating. The current monitoring method is carried out by applying a potential across a microfluidic channel and monitoring the resulting current. The microfluidic

channel and the fluid reservoir at one of the electrodes are filled with an electrolyte of a given concentration and the reservoir at the other electrode is filled with the same electrolyte at a lower concentration. When a potential is applied to the system, the higher concentration electrolyte will be gradually replaced by its lower concentration counterpart, resulting in reduced channel conductivity. Stabilisation of the current indicates that the electrolyte in the channel has been completely replaced. The time elapsed can then be used to derive the EOF [6, 10]. Streaming potential measurements on the other hand, employ a pressure–induced flow to generate current in the channel. By measuring the potential generated at a given pressure, one can quantify the surface charge [1]. On open substrates numerous methods such as atomic force microscopy (smoothness), contact angle (hydrophilicity, -phobicity), and ellipsometry (thickness) can be used to characterise the thin films [1].

At present, the number and diversity of the methods seen in the literature makes it difficult to compare performance amongst various coatings [4]. Nevertheless, an understanding and use of these coatings is critical to the success of obtaining high quality protein separations in microfluidics. To date such coatings have been used extensively in microfluidic structures, but the difficulties related to surface characterisation and the variety of surface chemistries have bottlenecked the development of some microfluidic devices [1].

2.1.2 Permanent Surface Modification Protocol

For the protein separations conducted in this work (see Chapters 3 and 4), a permanent linear polyacrylamide (LPA) coating was employed. The coating protocol was primarily based on Hjerten's pioneering 1985 work that described a way of covalently bonding a hydrophilic polymer to a functionalised glass surface [7]. Han and Singh used a similar coating methodology when conducting protein separations very similar to those discussed in this thesis [11], so the LPA coating was deemed to be suitable for the desired application.

While the complete coating protocol is located in Appendix B, the following discussion will address the main points in the procedure. Beginning with a new chip, the channels were rinsed by filling the wells with water and vacuum evacuating the channels via one of the wells. Next, the wells and channels were dried using pressurised N_2. Inspection of the channels was then conducted to ensure that they were clean and dry. Channels were dried to mitigate the possible dilution and contamination caused by residual water. Use of an air purge to dry the channels between coating steps was also noted by Herr *et al.* [12]. Following this, the wells and channels were filled with a 1M NaOH (sodium hydroxide) solution and the solution was left in the chip for approximately ten minutes. Once again, the channels were vacuum evacuated, rinsed, and dried using the aforementioned method.

Before introducing the next solution, it was visually confirmed that the channels were completely dry. To functionalise the surface with silane molecules that permitted covalent attachment of LPA polymer chains, an acidic solution containing

the silane molecules was introduced into the wells and channels. The solution was an aqueous acetic acid solution with a pH of approximately 3.5, and contained 0.4% v/v 3–(Trimethoxysilyl)propyl acrylate. The wells and channels were filled with the solution via capillary forces. Once all the wells and channels were filled, the chip was covered with a glass slide to mitigate evaporation. After a one hour residence time, the solution was removed via vacuum applied to one well and the channels were rinsed and dried using the same method as was previously mentioned. Residence time refers to the quantity of time the solution was left in the channels.

The final step in the coating procedure was to apply the LPA coating. This involved introducing an aqueous solution containing 4% acrylamide monomer, 0.1% potassium persulfate, and 0.1% N,N,N′,N′-Tetramethylethylenediamine (TEMED) into the channels. The coating solution, as it will now be referred to, has a viscosity that is best described as similar to that of water. Upon proper preparation of the solution (see Appendix B), the wells and channels of the chip were filled immediately using a pipette. Any delay in filling the chip could allow premature polymerisation of the acrylamide monomer into linear polymer chains because the polymerisation process begins immediately once the TEMED and potassium persulfate are added into the solution. TEMED acts to catalyse the production of free radicals from the potassium persulfate, which in turn catalyses the polymerisation reaction [13]. Once the solution filled the wells, the chip was once again covered using a glass slide to minimise evaporation of the solution. After a thirty minute residence time in the channels, the solution was evacuated from the chip using a vacuum. At this point, the solution was more viscous due to the conversion of acrylamide monomer to linear polymer chains. This was evident, as the solution could be difficult to remove, especially from long channels or channels with small cross–sectional areas. In these cases, careful use of positive pressure applied to the channels was occasionally required to remove the polymerised solution. Since most of the work discussed in this thesis was done in chips with short channels and larger channel diameters (i.e. larger cross–sectional areas), evacuation of the polymerised solution from the channels was often easily achieved. Following inspection of the channels for debris or residual polymer, the channels and wells were refilled with water and stored submerged in water in a refrigerator. It is important to note, that the coating was not visible once it was applied to the channel.

In cases where brand new chips were not used, it was important to ensure the channel and well surfaces were very clean before proceeding with the above coating procedure. Typically, this was achieved by placing the chips in a glass annealing oven (University of Alberta, Department of Chemistry, Edmonton, AB, CAN), where any debris, coatings, or sieving matrices previously introduced in the channel could be burned out. These ovens gradually heated to a temperature of 560°C, remained at that temperature for forty–five minutes and then gradually cooled down. Two of these cycles were usually sufficient to clean chips. Because of the volume of the material removed by this process was about 1μL or less, there is little concern relating to the contamination of the ovens. Following heating in the ovens, the

channels were cleaned further with boiling sulfuric acid [14]. After all the small debris or residue had been cleaned out of the channels by the boiling sulfuric acid, the above coating procedure could be performed to coat the channel and well surfaces. A method of chip cleaning that employed H_2O_2 was also investigated (see Section 2.2.3), but it was found to be largely ineffective.

2.1.3 Permanent Surface Modification Results

Permanent surface modification of microfluidic chips with LPA permitted covalent attachment of the polyacrylamide sieving matrix (see Section 2.2.3) and the separation of proteins. While development of the permanent surface modification protocol was not without its difficulties, the results presented in Chapter 3 show that the development of the protocol was successful.

Channel Clogging

During early development of the protocol, channel clogging occurred approximately 50% of the time. Clogging can be defined as the inability to remove the liquid in the microfluidic channels after the LPA coating step. While the cause of the clogging was initially unknown, it was later determined that the clogging was due to the increase in viscosity of the LPA solution during polymerisation. When introduced into the channel, the LPA coating solution consists only of acrylamide monomer and polymerisation catalysts dissolved in water. Qualitatively, this solution has a viscosity similar to that of water. Upon polymerisation in the channels, the solution becomes more viscous because of the presence of linear polyacrylamide polymer chains. The increase in viscosity was observed qualitatively by observing the polymer solution as it was evacuated from the channels. The changes in solution viscosity during polymerisation of the LPA coating solution made it difficult to remove from the channels using the application of pressure (not recommended due to safety concerns pertaining to acrylamide monomer) or a vacuum. Channels were more likely to clog if channel coating was conducted in chips with long channels, channels with small diameters, and if the time the LPA coating solution was left in the channel was on the order of thirty minutes. It is believed that in the first two cases, clogging occurred because excessive amounts of pressure were required to flush the viscous solution from the channels. In the final case, longer polymerisation times led to more complete polymerisation of the liquid and thus, increased viscosity. Although Hjerten employed LPA polymerisation times of about thirty minutes in long capillaries without any mention of clogging [7], it is unknown what procedural differences, beyond the dimensional differences in microfluidic channels and capillaries, may have led to clogs.

Initial attempts at the coating protocol were conducted in standard Micralyne (Edmonton, AB, CAN) microfluidic chips [15]. The small channel diameter (50 μm) and longer separation channel length (80mm) likely exacerbated the clogging problems. To prevent clogging in the standard Micralyne chips, the residence

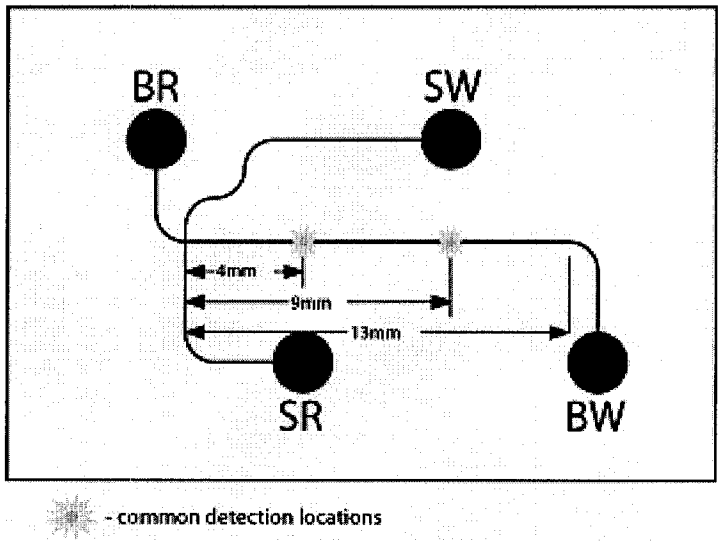

Figure 2.1: An illustration of a 4–Port Mini microfluidic chip used in protein separations. The channels used in this study were 46μm deep and 102μm wide. The chip consists of a simple design where the injection channel (between SR and SW) intersects with the separation channel (between BR and BW). The chip's wells are named as follows: SR - sample reservoir; SW - sample waste; BR - buffer reservoir; BW - buffer waste. The locations of commonly used protein detection points in the separation channel (see Chapters 3 and 4) are also indicated. Detection was also conducted at distances of 3mm and 10mm.

time of the LPA coating solution in the channels was gradually reduced from thirty minutes to six minutes. This was done to reduce the extent to which the solution had polymerised, with a lower residence time resulting in a less viscous solution. While this method did decrease the incidence of clogging in channels, the effect of reducing the coating solution residence time to six minutes was not evaluated because no successful protein separations were performed in standard Micralyne chips. Subsequent coating of 4–Port Mini chips (shorter channels with larger cross–sectional dimensions; see Figure 2.1) reverted to the thirty minute residence time described by Hjerten [7]. It was found that the polymerised LPA coating solution was much easier to evacuate out of the shorter 4–Port Mini channels due to their short length and larger diameter.

Coating Effectiveness

Experiments comparing protein separations with and without the coating were not conducted because development of the in–situ polymerisation of polyacrylamide gels (see Sections 2.2.2 and 2.2.3) dominated the majority of the experimental timetable. It is also believed that the absence of a coating may have an affect on the characteristics of cross–linked sieving media (see Section 2.2.3). Although, the successful separations of proteins discussed in Chapters 3 and 4 are a testament to the effectiveness of the permanent LPA coating, data presented in Section 3.3.3 also demonstrates that adsorption of proteins was absent or was reduced to such an extent that it did not adversely affect separation performance.

Long–term stability of the coating was also not formally evaluated. In terms of reported data on coating performance stability, little data is available. When information is available, it typically addresses stability over a short series of separations [16]. Herr *et al.* reported some degradation of separation performance over the course of approximately 500 separations in a very similar system [12], however much of this degradation was attributed to changes in the sieving matrix over time. In another example, an extensive study on the degradation of LPA coatings similar to those employed in this work showed that coating stability was present over several hundred separations. This study by Munro *et al.* also demonstrated that this stability was highly dependent on the coating procedures [17]. Procedural parameters such as surface preparation methods, silanisation solvent, degree of surface hydration before silanisation, silanising reagent, reaction temperature and time, reaction pH, and polymer reagents all affected coating performance, and in turn, separation performance. Munro *et al.* state that these factors contribute to coating homogeneity, density, and longevity. They also state that the variety of surfaces presented in the literature examining these parameters make coating optimisation difficult.

Author (Year)	Analyte Type	Separation Type	Separation Distance	Gel Preparation Method
Brahmasandra (2001) [18]	dsDNA	Electrophoretic	1.8mm	In–situ photopolymerisation
Han (2004) [11]	Proteins	SDS–PAGE and IEF*	2.0-4.0mm	In–situ photopolymerisation
Hatch (2006) [21]	Proteins	SDS–PAGE	1.0mm	In–situ photopolymerisation
Herr (2004) [12]	Proteins	SDS–PAGE	4.0mm	In–situ photopolymerisation
Herr (2005) [19]	Proteins	Native PAGE	6.0-7.0mm	In–situ photopolymerisation
Herr (2007) [20]	Proteins	Native PAGE	Unknown	In–situ photopolymerisation
Ugaz (2002) [22]	ssDNA	Electrophoretic	10-15mm	In–situ photopolymerisation

Table 2.1: Examples of published reports using cross–linked polyacrylamide gel as a sieving matrix in microfluidic separations. The electric field strengths used with these gels were 34–410V/cm for the protein separations [11, 12, 19–21], and 9–30V/cm for the DNA separations [18, 22]. **IEF=Isoelectric focusing*

2.2 Polyacrylamide Gel Sieving Matrix

Polyacrylamide gels are commonly used in macro–based applications where protein or DNA electrophoretic separations need to be performed. These cross–linked polymers can be implemented in a variety of concentrations to achieve the desired separation properties. Contrary to many applications of electrophoresis in microfluidics where a removable liquid gel is used as the sieving matrix, cross–linked polyacrylamide gels are solid and non–removable.

To date, only a handful of publications have cited the use of cross–linked polyacrylamide sieving matrices in microfluidic–based electrophoretic separations [11, 12, 18–22]. It is also important to note that these publications originate from essentially two research groups. Table 2.1 contains a brief summary of the different applications for which the polyacrylamide gels were employed. As the table demonstrates, cross–linked polyacrylamide gels have been used to separate both DNA and proteins in microfluidic channels. Amongst these published reports, numerous commonalities exist.

First, all the gels were prepared using photoactivated in–situ polymerisation, which is also the approach used in this work. Additionally, many of the applications used photopatterning to define specific areas of the microchips' channels in which the gel was polymerised [11, 18–22]. Photoactivated polymerisation permits such use of these gels because polymerisation can be locationally controlled. This was used extensively in two of these applications [20, 21], where different concen-

trations of polyacrylamide gels were polymerised to define functional regions of the chip. In each case, localised photopolymerisation permitted the creation of a high density membrane used for protein pre–concentration and a more porous gel used for electrophoretic separation of the proteins. Another feature of these microfluidic separations is the short separation distances required to resolve sample components, with most exhibiting resolution and detection of multiple analytes in less than 5.0mm. As a consequence, analysis times are commonly about thirty seconds. Other stated advantages of these gels include reusability, higher sieving power than liquid gels, and resistance to mixing and diffusion [11]. The latter is deemed to be important as microfluidic devices become more complex, and as a result, require demarcation of functional regions and higher levels of integration.

The work discussed in the following sections is strongly based on the work performed by Han and Singh [11], and Herr and Singh [12]. Such an approach was taken for several reasons. First, the aforementioned benefits including reusability, short separation distances, and rapid analysis times were all appealing. Secondly, the use of polyacrylamide gels in traditional applications such as slab gel electrophoresis and capillary electrophoresis permitted the use of some of the knowledge developed from these common techniques. Lastly, because these gels were noted to resist migration and mixing within the channels, the use of such gels could have important implications when coupling microchip electrophoresis to electrospray ionisation. As Appendix A will discuss further, these devices contain channels that open directly to the external environment (without a fluid well as an intermediary) and require the use of solvents that are incompatible with electrophoresis. So–called 'porous polymer monoliths', which are effectively porous solid gels, have been demonstrated to effectively couple microfluidic channels with electrospray ionisation [23, 24]. As such, the use of cross–linked polyacrylamide gels was pursued.

2.2.1 Polyacrylamide Gel Theory

Polyacrylamide gels consist of linear chains of acrylamide molecules that are attached to one another, or cross–linked, by a cross–linker. In many cases, this cross–linker is N,N′–methylenebis–acrylamide, also commonly known as bis–acrylamide [13]. The result is a solid and porous gel. These gels have recently been employed in microfluidics as sieving matrices in electrophoretic separations [11, 12, 18, 21, 22], but have been used in more traditional macro applications since 1959 [25].

The gels are formed when polymerisation of acrylamide monomer is initiated by catalysts such as TEMED and potassium or ammonium persulfate (see Section 2.1.2). However, unlike the polymerisation of LPA, cross–linked acrylamide differs in that the linear polymer chains are linked by a cross–linker such as bis–acrylamide. The resulting matrix forms the solid gel known as polyacrylamide gel which has a chemical structure like that seen in Figure 2.2. Varying the concentration of the acrylamide monomer and the cross–linking agent in the precursor

solution allows one to control the characteristics of the gel such as pore size. The concentration (weight per volume) of acrylamide monomer is commonly termed $\%T$, while the concentration of the cross–linking agent as a fraction of $\%T$ is commonly called $\%C$ [13]. Higher concentrations ($\%T$) of acrylamide monomer result in denser gels with smaller pores. Generally, monomer concentration in gels used for protein separations ranges from 5% to 20% but gels can form at concentration extremes of 2% and 30%. Cross–linker concentration also plays a significant role in the control of gel pore size. In general, as the $\%C$ increases, pore size decreases, up to a maximum $\%C$ of approximately 5%. After this point, gel pore size once again increases due to extensive cross–linking and the inability of the polymer chains to be packed closely [13]. A further discussion of gel characteristics in relation to protein separations will be given in Chapter 3.

Although the combination of TEMED and potassium persulfate is predominantly used to catalyse the polymerisation reaction of polyacrylamide gels, other catalysts can also be employed. For example, riboflavin is a commonly utilised photoactivated catalyst [26]. When exposed to light it decomposes and produces the free radicals necessary for polymerisation. The polymerisation catalyst referenced in the published works [11, 12] and used to develop our procedures, was an azo–initiator known as 2,2′–Azobis[2–methyl–N–(2–hydroxyethyl)propionamide] (Wako Chemical USA Inc., Richmond, VA, USA). When using this catalyst, the polymerisation reaction is initiated by exposure to ultraviolet (UV) light. Upon irradiation of the precursor monomer solution with UV light, complete polymerisation of the gel can occur in less than ten minutes [11, 12, 21]. As previously noted, this method of in–situ polymerisation is particularly useful when dealing with microfluidics because it is rapid compared to traditional polymerisation techniques and because it is photolithographically controllable.

2.2.2 In–Situ Polyacrylamide Gel Polymerisation Protocol

As previously mentioned, the work in this thesis is largely based on publications by Han [11] and Herr [12]. The following discussion will give a brief overview of the in–situ polyacrylamide polymerisation protocol. A complete version of the protocol can be found in Appendix C.

It is important to note that a wide range of polyacrylamide gel concentrations can be polymerised using this protocol. Appendix C discusses gel concentrations of $\%T = 4\%, 5\%, 6\%, 8\%, 10\%, 12\%$, and 15%, but the solution recipe can be altered to achieve any desired concentration. First, a solution containing the required concentration of acrylamide/bis–acrylamide solution was mixed. All gels used in this protocol incorporated acrylamide to bis–acrylamide ratios of 37.5:1. The solution was mixed in running buffer (the buffer present in the channels during electrophoresis) to ensure the gel was suitable for the electrophoretic separations. In addition, the solution also contained 0.5% Azo-Initiator. Upon completion of mixing the solution, which from now on will be known as the precursor solution,

Acrylamide Monomer

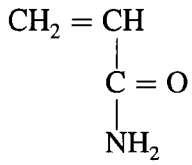

N,N′-methylene bis–acrylamide

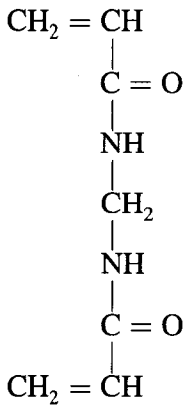

Cross–linked Polyacrylamide Gel

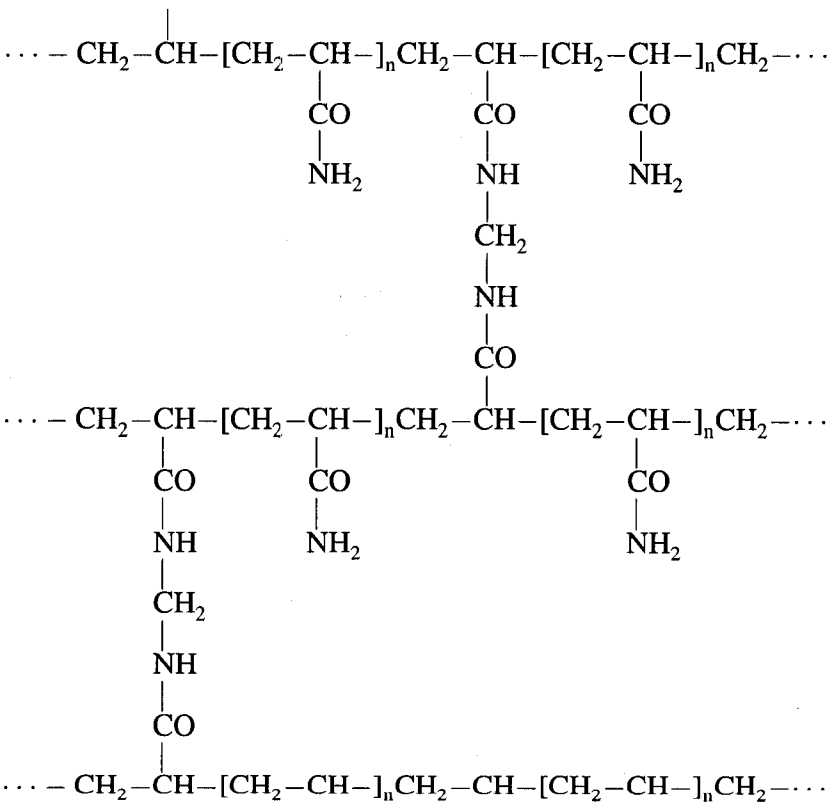

Figure 2.2: The chemical structure of acrylamide monomer, N,N′-methylene bis–acrylamide, and cross–linked polyacrylamide gel [13].

the solution's container was covered with a layer of aluminum foil to minimise the amount of light the solution was exposed to. While the UV intensity necessary to initiate polymerisation was not likely provided by ambient light, minimising exposure of the solution to light before polymerisation was done to mitigate sources of variability.

An important aspect of ensuring repeatable gel characteristics requires degassing of the precursor solution [19]. Precursor solution degassing helps to minimise the amount of dissolved oxygen in the solution. Dissolved oxygen inhibits polymerisation and may also lead to the formation of bubbles in the gel during polymerisation [13]. Due to limitations of the Applied Miniaturisation Laboratory's (AML) equipment and the use of small volumes (approximately 1mL), degassing was achieved only by sonication [27, 28]. Equipment in the AML made it difficult to conduct vacuum degassing concurrently with the ultrasonic technique. Some suggest that the simultaneous application of vacuum and sonication to the solution should be practiced [19]. On the other hand, other publications specifically note that gels were successfully polymerised with absolutely no degassing of solutions before polymerisation [18]. Because of these conflicting reports, sonication of the precursor solution for thirty minutes before being introduced into the microfluidic channels was deemed to be suitable. During solution degassing, the UV lamp was turned on and allowed to warm up for at least thirty minutes.

Approximately ten minutes before the completion of degassing, the LPA–coated chips in which new gels would be polymerised were removed from the storage water. The channels were dried thoroughly to ensure that the concentration of the cross–linked polyacrylamide gel would not be affected by residual water in the channels. Upon completion of degassing, the precursor solution was pipetted into each chip and was allowed to fill the channels completely. Because the solution was not yet polymerised, it had a viscosity similar to that of water, and filled the channels quite easily. Once the channels were filled, all the wells were topped up with precursor solution and the channels were inspected to confirm they were completely filled and free of bubbles. If bubbles were present, the solution was vacuumed from the channels followed by reintroduction of the solution into the channels. Excessive use of positive pressure to remove solutions that contained acrylamide or bis–acrylamide from the channels was avoided. Both are potent neurotoxins, and the use of positive pressure has the potential to create harmful spray or aerosols. Once the channels and wells were properly filled, the chip was placed on a microscope slide (for ease of removal from the AML UV box), and the first UV exposure was started. Exposures were conducted in the AML using a box equipped with a mercury UV lamp (Part No. 88–9213–02, BHK Inc., Claremont, CA, USA). Intensity measurements at three different wavelengths (thirty minute lamp warm–up time), 254nm, 365nm, and 400nm, yielded values of 1.64mW/cm^2, 15.7mW/cm^2, and 4.5mW/cm^2 respectively.

The stage inside the UV box was placed at its highest level for the UV exposure which located the chips approximately 3cm from the UV lamp. The duration

of the first UV exposure was eight minutes. After the chip was exposed, it was carefully removed from the UV box and inspected for defects in the gel. These defects usually consisted of bubbles that were formed in the channels during the polymerisation reaction. In this case, subsequent exposures were unnecessary and the chip was set aside for cleaning. Bubbles in the gel rendered the chip useless for electrophoretic separations. However, if the gel was free of bubbles, the wells were topped up with the precursor solution and a second UV exposure interval of eight minutes was administered. Upon completion of the exposure, the channels were inspected once again. If bubbles were present the chip was set aside for cleaning, and if not, a third exposure was conducted after the wells were topped–up with precursor solution. Following the final exposure and observation of a gel free of defects, the chip was stored in refrigerated (4°C) buffer. The storage buffer was of the same type and concentration to be used in future protein separations. Storage of the chip in water would result in buffer ions diffusing out of the channels, thus making the chip useless in electrophoretic separations.

In this procedure, the use of multiple UV exposures serves two main purposes. First, the use of multiple exposures allows the progression of the polymerisation reaction to be qualitatively monitored. This includes observing the extent of polymerisation by assessing the degree of gelation in the wells and inspecting gels for the presence of bubbles. For instance, if the gel has not polymerised after the first exposure, it may be an indication of non–ideal polymerisation conditions. The second reason for conducting multiple exposures is to ensure complete polymerisation. Although polymerisation occurs after the first UV exposure period of eight minutes, additional exposures are used to ensure complete and uniform polymerisation of the gel [12].

Once polymerised, the gel in the channel will not change in appearance. The gel cannot be flushed out with the application of pressure and liquids cannot be pumped through the gel matrix. Before conducting the first separations in the chip, the gel must be scraped out of the wells with a pipette tip to allow for filling of the wells with the appropriate buffer or sample. Freshly polymerised gels were typically stored in running buffer at 4°C for a day before use, but this was never tested to see if it was absolutely necessary.

Unlike the aforementioned papers [11, 18, 20–22], photopatterning of the gel in the channels was not employed. Although it was explored, accurate mask placement proved to be difficult and removal of the unpolymerised solution was tedious and increased the risk of exposure to acrylamide monomer. See Section 2.2.3 for a discussion of photopatterning results.

2.2.3 In–Situ Polyacrylamide Gel Polymerisation Results

In–situ polymerisation of polyacrylamide gels in microfluidic channels proved to be a challenging and particularly arduous expedition, even when photopatterning was not employed. While gels of the required quality were generated and the results of

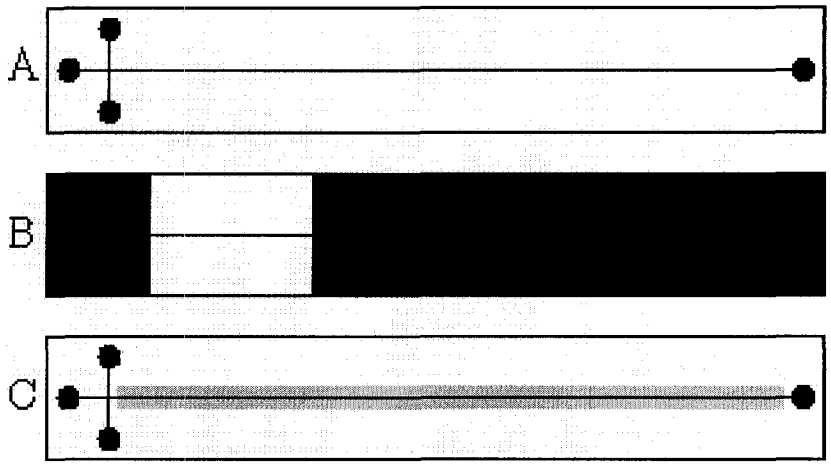

Figure 2.3: A) An unmasked 4–port standard Micralyne chip with, B) an exposure mask made from electrical tape (black indicates masked areas) designed to expose a 2cm portion of the separation channel, and C) the region (indicated in gray) from which liquid and polymer could not be removed following photopatterned polymerisation of the gel using the mask in B. Early attempts at photopatterning gels used this type of masking.

the separations permitted by these gels were positive (see Chapters 3 and 4), production of the gels was riddled with sources of variability. The following section seeks to discuss many of the obstacles that were encountered throughout the development of the in–situ polyacrylamide gel polymerisation protocol. In addition, many of the measures taken to assess variability, and mitigate it, are also addressed.

Photolithographic Gel Patterning

Initial attempts at in–situ polymerisation attempted to duplicate results published by Han [11] and Herr [12]. In the work published by Han, photolithographic patterning of the gel was employed so that only portions of the channels would contain a cross–linked polyacrylamide gel matrix.

The first microfluidic chips in which gels were polymerised were standard 4–port chips supplied by Micralyne (Edmonton, AB, CAN). These chips had channels with approximately semicircular cross–sectional dimensions of 50μm wide and 20μm deep [15]. Early misdirected attempts at patterning gels inside the channels sought to polymerise a small portion of the separation channel (see Figure 2.3). Black electrical tape was placed over areas of the chip in which gel was not desired and UV exposure was conducted using the mask aligners in the University of Alberta NanoFab. The UV light intensity at 365nm was approximately 16mW/cm^2 and 49mW/cm^2 at a wavelength of 400nm. The exposure duration was 120s.

From these initial experiments, a few key observations were made. First, the masking of the channels did not seem to provide particularly good patterning resolution. When compared to the observed resolution of 200μm for the patterning

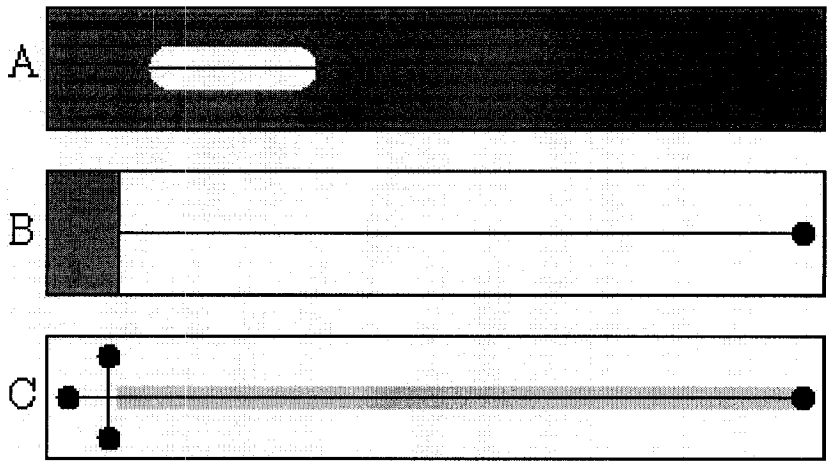

Figure 2.4: A) The first version of a PVC mask that only exposed a portion of the separation channel, B) a PVC mask used to expose and polymerise the entire separation channel, and C) the region (indicated in gray) in which polyacrylamide gel was polymerised.

of rigid polymer monoliths in microfluidic channels conducted by Throckmorton *et al.* [29], our apparent resolution of several millimeters seemed unusual. For instance, if a mask with a 2cm long exposed region was placed with an exposed region beginning 5mm from the intersection, the solution in the channels could not be removed from the majority of the separation channel (see Figure 2.3) by vacuum or pressure driven liquids or air. The other notable observation was that there is no method of visually differentiating polymerised gel from the unpolymerised precursor. Thus, it was virtually impossible to locate areas in which the gel was present and consequently, assess patterning resolution or even which general areas had been polymerised.

Initial theories behind the supposed polymerisation in unexposed regions centered on possible causes for unintended polymerisation such as light scattering or waveguiding and heat–induced polymerisation. Numerous alterations to the polymerisation method were made to induce changes that may have helped to identify the cause of the apparent problem. UV exposure times, exposure intensity, and Azo–Initiator concentrations were reduced independently to lessen the degree of polymerisation with hopes that unexposed regions would not be polymerised by suspected means such heat or scattered light. UV exposures were also performed in exposure intervals to allow the chip to remain cooler and prevent possible heat–induced polymerisation. Polyvinyl chloride (PVC) masks were also fabricated to increase mask placement repeatability (see Figure 2.4). In each of these cases, no improvement was observed in the ability to remove solution from unexposed regions of the chip. As a result, polymerisation resolution was still believed to be quite poor.

After gaining more experience with gel polymerisation, it was discovered that

these problems occurred mainly because of a lack of understanding of the properties of the gel being polymerised. In fact, the 'gel' in unexposed regions was actually just unpolymerised precursor solution that could not be flushed through polymerised regions of the gel. Initially it was assumed that because of the porous nature of the gel, liquids or gases could be pressure flushed through the gel. Experience with the gels and confirmation from Amy Herr (personal communication, e-mail, October 10, 2006) that fluids could not be pressure flushed through the gel led to a change in UV exposure methods. If only a portion of the separation channel was exposed, only that portion (with some allowance for exposure resolution and light scattering and diffraction, i.e., the aforementioned findings of Throckmorton [29]) would be polymerised into a cross–linked gel. Although the unexposed regions did not contain cross–linked gel (see Figure 2.3), the polymer's precursor solution could not be removed from certain unexposed regions in the separation channel because liquids and gases could not travel through the polymer. The inability to introduce a pressure–induced flow in a channel with polymerised gel meant that once a portion of a channel had gelled, the unpolymerised solution in the other portions of a channel could not be removed via applied pressure. So, in fact, this was not an issue of poor polymerisation resolution, but one of procedural constraints. As a result, it was more practical to avoid this issue and polymerise the entire separation channel. A closer review of Han and Herr's work [11, 12] with photopatterned gels indicated that they also polymerised the whole separation channel to avoid this issue.

Subsequent attempts at in–situ polymerisation with photopatterning were performed by exposing the entire separation channel beyond the intersection with the injection channel (see Figure 2.4). Unpolymerised solution was drawn out of the channels using the application of vacuum at each of the three head wells (three leftmost wells in Figure 2.4). This resulted in a distinct and visible interface between air and the polymerised gel (see Figure 2.5). Unfortunately, this created another problem. The space between the intersection and the gel interface could not be filled with the buffer needed for electrophoresis (see Figure 2.6). Once again, this was due to the inability of liquid or gas to be pressure or vacuum driven through the gel.

Although unpolymerised solution could be evacuated with the application of a vacuum, this was deemed to be unsuitable because it resulted in trapped volumes of air when buffer was reintroduced into the channels (see Figure 2.6). When conducting further experiments with photopatterning, flushing the unpolymerised solution was achieved using cautious application of gentle positive pressure at an unpolymerised well. Other wells were covered with the lid of a petri dish to eliminate spraying. While the channels were still filled with unpolymerised precursor solution, pressure was applied to running buffer solution in a 1mL syringe at one of the head wells. The general idea was to replace the unpolymerised precursor solution with the desired running buffer without creating any bubbles. This crude technique permitted rudimentary attempts at separating proteins.

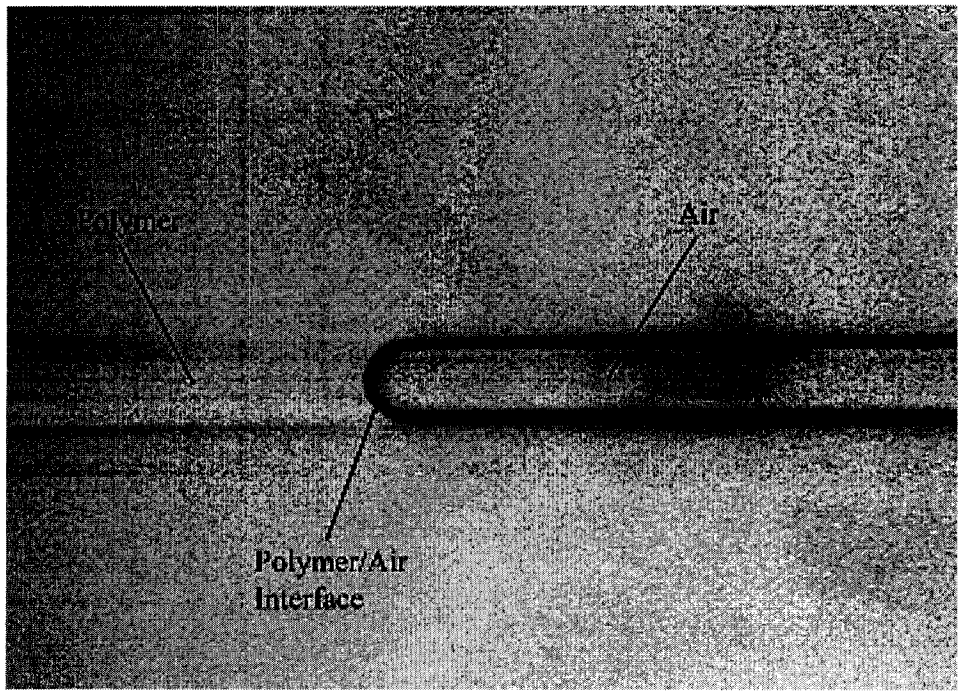

Figure 2.5: An image of the polymer/air interface. The exact shape (flat or curved) of the interface is unclear, as the curved shape could be due to residual liquid near the gel after evacuation of the unpolymerised precursor solution. Because liquids and air could not be pressure flushed through the gel, it was difficult to remove all the liquid from what was essentially a dead–ended channel.

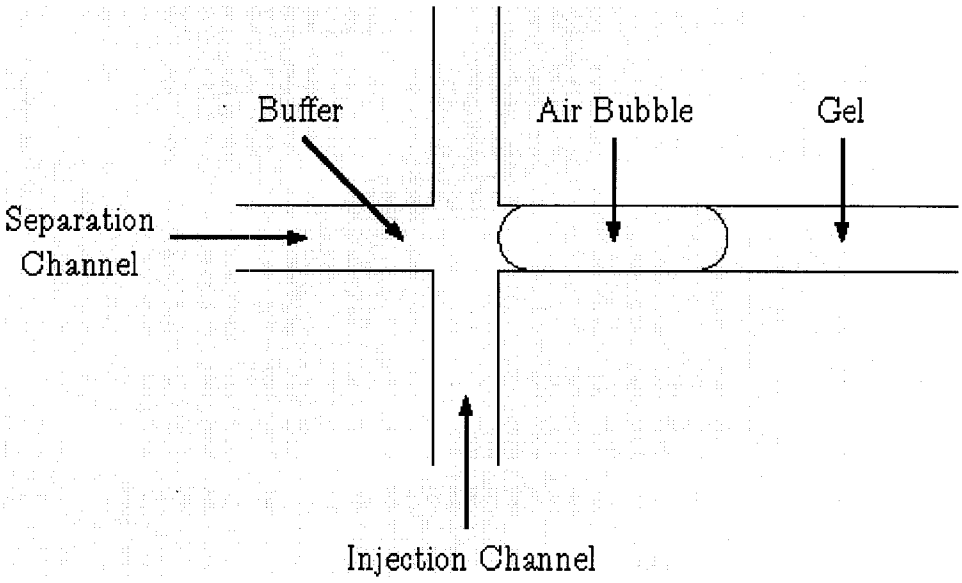

Figure 2.6: An illustration of an air bubble trapped between the polymerised gel in the separation channel and running buffer in the injection channel.

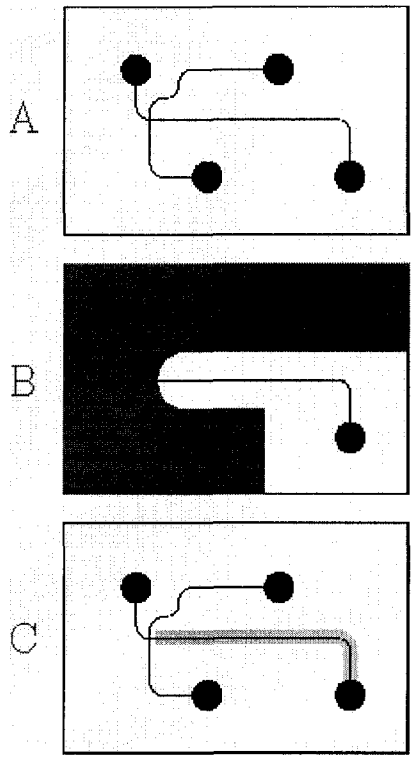

Figure 2.7: A) A 4–Port Mini chip, B) with a PVC mask for polymerising a gel in the separation channel, and C) the regions of the channels that were filled with gel (indicated in light gray) and free running buffer (not shaded).

Although extensive discussions on successful separations of proteins in 4–Port Mini chips and the standard operating procedures for those separations are available in Chapters 3 and 4, the following points are briefly noted to aid in the description of the in–situ polyacrylamide gel polymerisation protocol. When separations of proteins were attempted, performance was quite poor. It was discovered that the free running buffer present in the injection channel and the upper portion of the separation channel (portion not filled with polyacrylamide gel, see Figure 2.7) permitted pressure–induced flows of the sample and buffer in these regions. The flow of sample and buffer in the injection channel and upper portion of the separation channel disrupted proper sample plug formation at the channel intersection. Because pressure–induced flows were found to be detrimental to separation performance, all subsequent gel polymerisation was conducted with no masking to ensure polymerisation in all the channels. The presence of cross–linked polyacrylamide in the injection channel served to suppress completely any pressure–induced flows and allow proper formation of a sample plug. Consequently, photopatterning was abandoned.

Although separations using photopatterned gels were unsuccessful, separations of the BFPS ladder in these gels did reveal the location of the interface between the

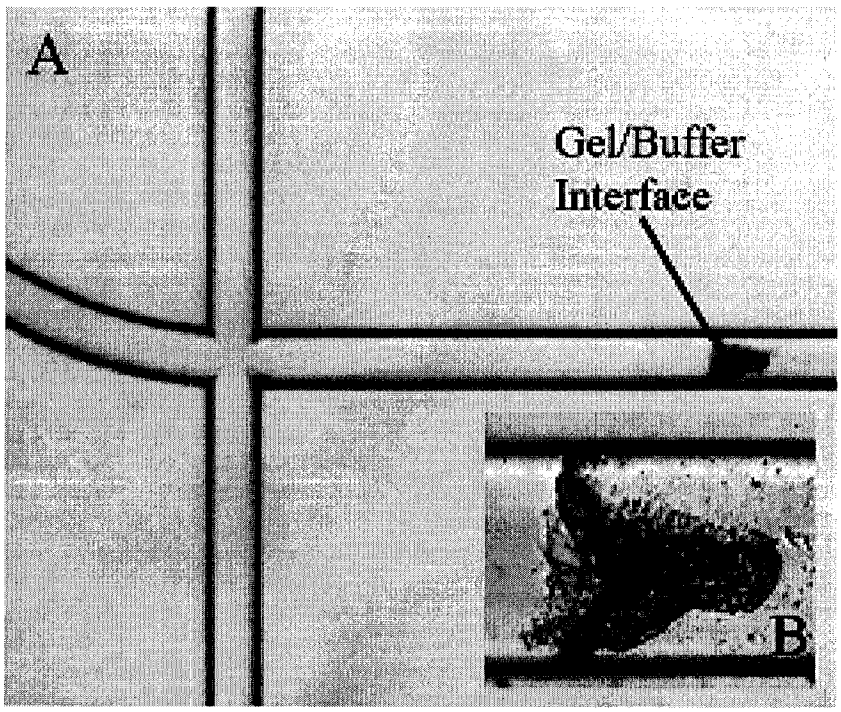

Figure 2.8: An image of the damaged gel/buffer interface. This damage resulted from a series of sixty electrophoretic separations (each approximately 120 seconds long at 230V/cm). Before conducting the separations, the gel interface was not visible. A) The interface is approximately 350μm from the intersection, and B) damage appears to be most severe in the middle of the channel.

gel and the running buffer. Figure 2.8 shows an image of the gel/buffer interface after sixty separations had been attempted. After the gel was initially polymerised, this interface was invisible. These results validate that photopatterning did in fact work. It appears that after a series of separations were performed, the gel at the interface was altered or damaged. The nature of these alterations was not explored due to the abandonment of photopatterning.

Upon reflecting on the photopatterning technique and increased experience with the gels, it was determined a diffusion or dilution based method of replacing the precursor solution with running buffer may have been more appropriate. In this case, storing photopatterned chips in running buffer solution may have allowed the unpolymerised precursor solution to diffuse out of the channels and be replaced by running buffer over time, or may have permitted dilution of the precursor solution to such a point that pressure flushing may have been safe. It is believed that this means of ridding the channels of the unpolymerised precursor solution may have been effective because a similar diffusion or dilution of buffer ions was observed when gels were accidentally stored in water instead of buffer. In this case, after being removed from the water an electric field was applied to the chip and no current flowed. This indicated an absence or drastically reduced concentration of buffer

ions in the channels likely due to diffusion or dilution mechanisms.

While the pressure–induced flushing method and the diffusion/dilution method are both potential means of removing unpolymerised solution, the former is much faster, albeit also more likely to introduce air or contaminants (i.e. debris) and pose a safety risk (acrylamide monomer is a neurotoxin) due to the potential for spraying of the precursor solution. Although not proven to be effective, the latter method is much slower but may also be much safer. The latter method was not investigated because it was devised at a point when non–photopatterned gels were generating acceptable results (see Chapters 3 and 4) and photopatterning was deemed to be unnecessary.

Although photopatterning was not used in this work, future development may make it useful, thus making these observations highly valuable. Because the publications upon which this work was largely based do not discuss many important procedural details, these observations were crucial. While photopatterning of gels is considerably more labour intensive and time consuming (preparation of a chip that contains two different gel concentrations could take about two days) than the non–photopatterning methods that were finally adopted, it does permit tailoring of gel characteristics within a single chip. This has been exploited for use in protein pre–concentration [20, 21], and to permit the simultaneous use of low and high concentration gels to ease sample injection (low concentration gels) while still attaining good sample resolution (high concentration gels) [20].

Void Formation and Polymerisation Yield

The formation of voids or bubbles, as they will subsequently be referred to, during polymerisation proved to be a major source of gel polymerisation variability. The voids formed during UV exposure of the gels and were generally the only visual indication that polymerisation had in fact taken place. Figure 2.9 shows an image of the voids that often formed during gel polymerisation. Observed traits of the bubbles in gels often included periodicity, mobility in the gel, and gradual expansion after subsequent UV exposure. While no cause for the formation of these voids was definitively determined, numerous potential causes have been explored. These include the presence of dissolved oxygen in the polymer precursor solution [13], heat–induced effects, and channel surface anomalies and hydrophilicity [30]. It is believed that some combination of these effects leads to the formation of voids and the subsequent discussion attempts to address these issues.

Initial theories regarding the formation of voids centered on the presence of dissolved oxygen in the polymer precursor solution. Degassing of the polymer precursor solution is necessary to remove dissolved oxygen. Oxygen dissolved in the precursor solution will inhibit polymerisation and may lead to the formation of bubbles during polymerisation [13]. Oxygen also inhibits polymerisation because it acts as a trap for the free radicals that are required for polymerisation to take place [26]. As a result, degassing of the precursor solution before to polymerisa-

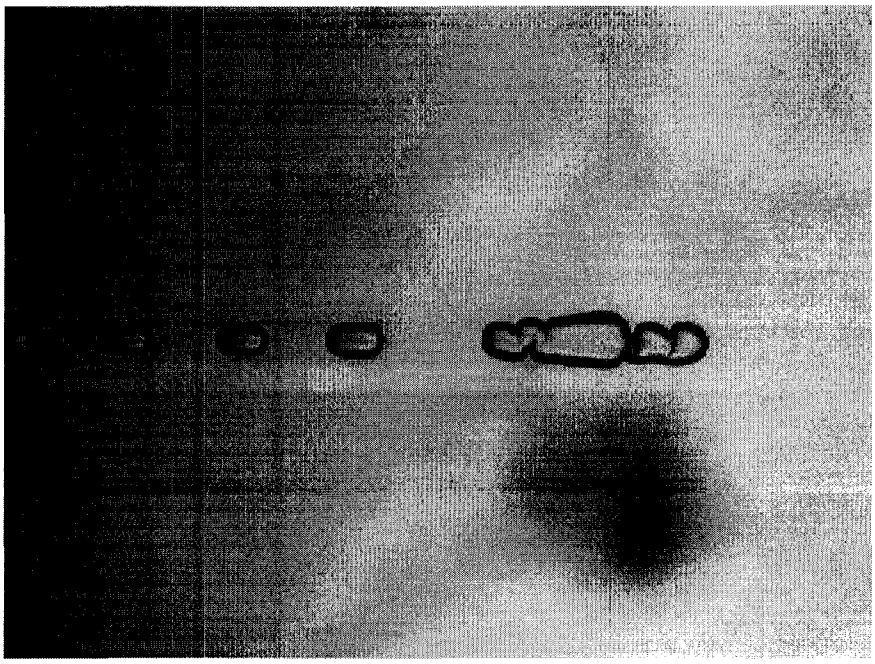

Figure 2.9: A representative image of voids that often formed during polymerisation of the polyacrylamide gel.

tion is imperative when repeatable gel characteristics are desired [19]. Sonication in conjunction with the application of a vacuum was employed by Herr *et al.* for polymerisation of polyacrylamide gels in microfluidic channels [12]. Although this is a widely accepted method of degassing solutions, previously noted equipment deficiencies (see Section 2.2.2) in the AML did not allow for both to be easily performed at the same time. Consequently, the simultaneous application of a vacuum and sonication were tested separately to see if there was a difference in degassing effectiveness. Because no difference was observed in the likelihood of bubbles to form during polymerisation using either degassing method, sonication was adopted into the protocol as it is known to be effective on its own [27, 28].

After determining different methods of degassing did not have an apparent effect on the formation of voids during polymerisation, heat–induced causes were investigated. Heat–induced effects could have been initiated by the exothermic polymerisation reaction [26] or by heat radiating from the UV lamp. Heat from the UV lamp was believed to be a larger contributor to the problem because of the much larger thermal mass of the chip and air surrounding the chip compared to the volume of solution in the channels. In addition, because the large surface area–to–volume ratio of microfluidic channels is favourable for efficient heat transfer away from the liquid in the channels, exothermic solution heating was largely ruled out. The primary method of investigating heat initiated bubble formation involved polymerising gels in different chips using a series of UV exposures with different lengths. For example, one chip received a single exposure of 12 minutes, a second

Azo–Initiator Concentration (% w/v)	Void Formation
0.10	No
0.15	No
0.20	No
0.30	No
0.40	Yes
0.50	No
0.70	Yes
1.00	No

Table 2.2: This table demonstrates that there was no clear relationship between Azo–initiator concentration and void formation. Each concentration was attempted in a different chip. While only a single trial was attempted and no conclusive results can be drawn from this data, published reports of other potential causes of void formation eliminated the need for further trials.

chip received twelve 1 minute exposures, and a third chip underwent twenty–four 30 second exposures. When multiple exposures were used, the chips were removed after each exposure to allow inspection of the gel. The time used for inspection also permitted some cooling of the chip. After observing all three exposure scenarios, no decrease in bubble formation was observed for chips that were allowed to cool between short exposure intervals. The proximity between the chip and the UV lamp was also tested to see if a greater distance between the two reduced heat transfer and thus bubble formation. An increase in distance between the two did not result in a reduction in the formation of bubbles. This seemed to rule out UV lamp generated heat as a possible cause for the formation of voids during polymerisation.

To ensure heat generated by the reaction was not the cause for void formation, a second avenue was pursued. A variety of Azo–initiator catalyst concentrations were employed to see if a change in the reaction rate would change the likelihood of bubble formation. As is shown in Table 2.2, no clear relationship between catalyst concentration and void formation was established. Only one trial was conducted, so no conclusive results emerged from this experiment. However, subsequent discussion shows that other published causes of voids have been noted. As such, experimentation on heat–induced causes for void formation was abandoned in favour of further development of the technique. Because the main goal of the research was to develop the applications discussed in Chapters 3 and 4, further experiments were considered unnecessary.

The unsuccessful attempts at eradicating the bubbles led to a more exhaustive search of literature available on the topic. During the development of cross–linked polyacrylamide gel capillaries in the 1990's, numerous papers and pa-tents described the formation of bubbles in capillaries during non–photoactivated polymerisation [30–36]. From these discussions, three methods emerged as means of mitigating bubble formation during polymerisation. Baba *et al.* vacuum–filled cap-

illaries with the polymer precursor solution in order to mitigate bubble formation, but no concrete explanation as to the underlying mechanisms of bubble formation was given [31, 32]. Dolnik *et al.* [34], Huang *et al.* [35], and Baba *et al.* [32] described the use of various techniques to initiate gradual polymerisation. While Baba *et al.* simply reduced the concentration of catalysts from typical values, Dolnik *et al.* introduced catalysts via electromigration. Huang controlled polymerisation by locally governing the temperature of the capillary. Only Huang *et al.* provided a theory as to why such a method was successful. Their explanation focused on the use of low temperatures to inhibit the polymerisation reaction. Because only small portions of their capillary were allowed to approach room temperature, and thus polymerise, any gel shrinkage (i.e. void formation) occurring during polymerisation could be mitigated by the inflow of low viscosity precursor solution that was held at temperatures between 0°C and 4°C. The low temperature solution was prevented from polymerising and consequently acted as a mobile filler for solution that was held at a higher temperature and allowed to polymerise. Therefore, any voids that formed could be refilled.

Upon reflecting on early attempts of photopatterning gels in which only a 2cm (see Figure 2.3) portion of the separation channel was polymerised, it was discovered that no voids were observed in these gels. The avoidance of void formation may have been aided by the localisation of the polymerisation to a small portion of separation channel. Due to the mechanisms described by Huang *et al.*, unpolymerised precursor solution in unexposed regions of the separation channel may have compensated for gel shrinkage and subsequent void formation by acting as a mobile filler. While this was not confirmed through further experimentation, such knowledge may be useful in future work. When gels were polymerised in all channels and wells, no unpolymerised precursor was available for use as a mobile filler. Although void formation was not always observed in these gels, the lack of a mobile filler may have contributed to the formation of voids in some cases. Further experimentation would be needed to confirm this.

Taking a different approach, Rose, Yin, and Schomburg emphasised the importance of hydrophilic surface modification of the capillary and covalent attachment of the gel to the capillary surface [30, 33, 36]. Of particular interest are the patents filed by Rose [30] and Schomburg [36]. Specifically, Rose describes the gel shrinkage that was briefly noted by Huang *et al.* [35]. Rose states that gel shrinkage occurs because the density of the polymerised gel is greater than that of the precursor solution. According to Rose, the application of a hydrophilic polymeric coating helps to create binding sites at the capillary surface for polymer molecules as well as aiding in ensuring reaction rate uniformity across the cross–section of the capillary. It is believed the hydrophilic polymer coating has the same polymerisation reactivity as other monomer molecules in the free solution, and as such, helps to ensure the reaction rate at the surface is equal to that of the reaction rate at the capillary's center. When the hydrophilic polymer is not present, the presence of an acrylic functional group at the capillary surface (e.g. 3–(Trimethoxysilyl)propyl acrylate) effectively

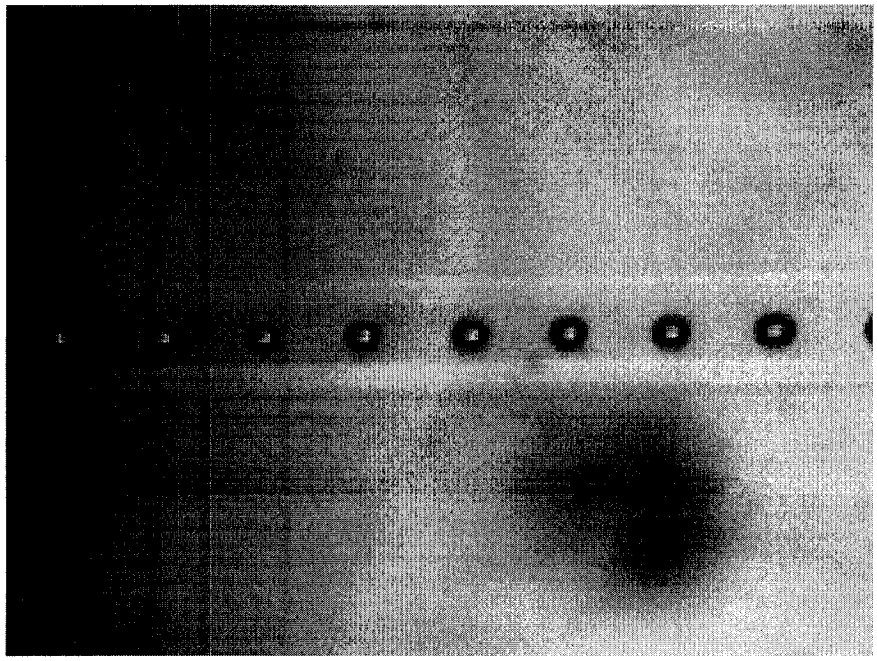

Figure 2.10: A representative image of equidistant bubbles that often formed during polyacrylamide gel polymerisation.

increases the reaction rate near the surface. This leads to a polymer concentration inhomogeneity along the cross–section of the capillary and the formation of voids or bubbles where the concentration is sufficiently low [30]. Schomburg goes on to note the formation of equidistant bubbles during polymerisation due to similar shrinkage mechanisms [36]. Equidistant bubbles were also observed during in–situ polymerisation of polyacrylamide in microfluidic channels (see Figure 2.10). As a consequence, it is believed the quality and homogeneity of the channel coating played a role in the tendency for bubbles to form during polymerisation.

Another interesting observation involved stock solution age for acrylamide and acrylamide/bis–acrylamide solutions. While the effects of solution age were not specifically quantified, it was found that polymer precursor solutions utilising stock solutions ranging from three to six months old exhibited a greater tendency to form bubbles. Typically, ordering new reagents produced a noticeable increase in the yield of bubble–free gels (i.e. increased yield from <20% to >50%). Although not confirmed, it is believed this is due to decreased reactivity of acrylamide monomer or the solvation of additional oxygen into the stock solutions. Decreased monomer reactivity might lead to less effective channel coating. As previously mentioned, dissolved oxygen in polymer precursors also has the potential to lead to the formation of bubbles during polymerisation. It should also be noted that stock solution of acrylamide and acrylamide/bis–acrylamide were always stored according to the manufacturer's recommendations.

Upon stabilisation of the polymerisation protocol, successful polymerisation

yield, defined as polymerisation in the absence of void formation, was approximately 52%. Of the successfully polymerised gels, only half performed well when separating protein ladders. Further discussion on poor separation performance in successfully polymerised gels can be found in Section 3.3.

Gel Stability and Durability

Gel stability and durability were assessed primarily by observing protein separations conducted in the gels. As a result, a complete discussion of the short– and long–term stability of gels is provided in Section 3.3.

Channel Cleaning

The cleaning of channels containing cross–linked polyacrylamide gels was time consuming and required the use of several techniques. Because the cross–linked matrix could not be flushed out via pressure or vacuum applied to the channels, an alternative means of removing the gel was required. Methods described by Ma *et al.* were inadequate for removing the gel because boiling H_2SO_4 could not penetrate into the inner portions of the gel [14]. As previously mentioned, the cleaning protocol eventually involved heating the chip to a high temperature followed by cleaning similar to that used by Ma. This brute force method proved to be effective.

Heating the chip to temperatures typically used in glass annealing (560°C) essentially burned the gel out of the channels. Figures 2.11 and 2.12 show gels in the channels of a chips that have been heated in a glass annealing oven but not completely cleaned. These results were typical for standard Micralyne chips [15]. It is believed that the debris was in fact composed of charred remnants of the polyacrylamide gel. Gel charring was also observed when polyacrylamide gel in chip wells was heated on a hot plate. In general, two or three heating cycles, as described in the cleaning protocol, were needed clean out Micralyne chips to the point where liquid could freely fill the channels. On the other hand, 4–Port Mini chips were less likely to have extensive debris present in their channels after being heated once. Debris in standard Micralyne chips was most often present in areas that were the farthest from wells, indicating that channel length likely played a role in making 4–Port Mini chips easier to clean. Chips were only subjected to the coating and gel polymerisation protocols when no debris (see Figures 2.11 and 2.11) or discolouration (see Figure 2.13) was present in the channels.

In addition to cleaning gel out of the channels, burning of the gel also contributed to the understanding and troubleshooting of the first problems seen with photopatterned gels. After one cycle of heating in the ovens, clear differences were present between debris in various regions of the channels. Regions exposed to UV light, and presumably those with polymerised gel, had dense brown debris that could not be flushed out of the channels. In contrast, unexposed areas (i.e. those containing only the unpolymerised precursor solution) had little to no debris and

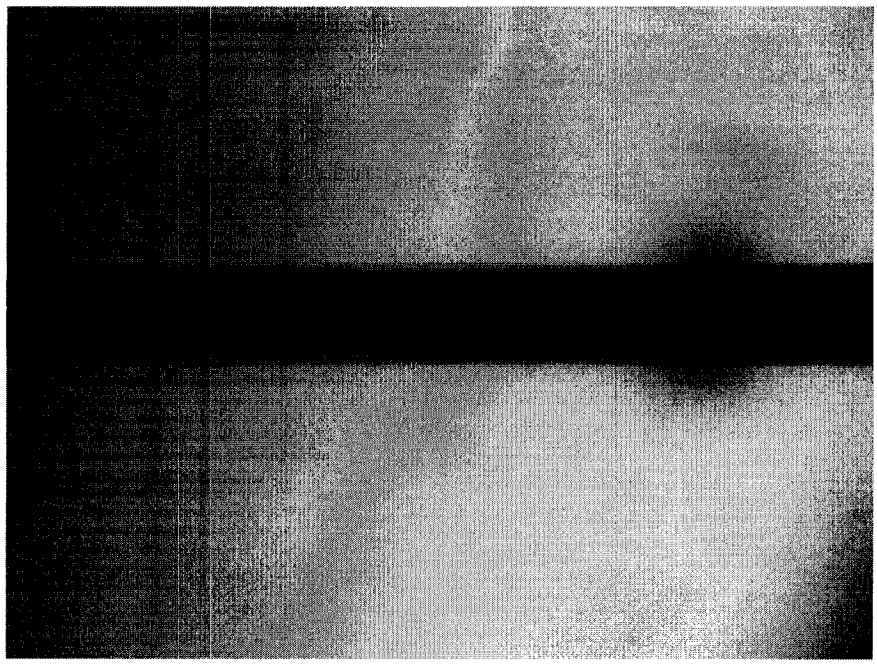

Figure 2.11: Debris that was typically found in microfluidic channels after one cycle of heating the chip in an oven (45 minutes at 560°C). This debris was moderately opaque, dark brown, and appeared to have a very dense structure. This is visible in the above photograph. A normally transparent channel when clean, is instead virtually opaque in the presence of charred gel remains. After two or three heating cycles in the oven, these charred gel remains were reduced to the string–like debris shown in Figure 2.12.

only exhibited a slight brownish tint (see Figure 2.13). The brownish tint in unexposed regions was difficult they were free of gel. Distinct changes or 'interfaces' between different debris types also coincided with the photopatterned interfaces between exposed and unexposed areas of the channel. The location of these 'interfaces' were used as one method of determining which areas of the gel had been polymerised, and which areas had not. As previously mentioned, multiple heating cycles in glass annealing ovens allowed complete removal (based on a visual assessment) of the discolouration in unexposed areas and the debris in exposed areas.

Unfortunately, repeated chip heating did have some detrimental effects. Over a series of multiple cleaning and chip preparation (coating and gel polymerisation) cycles, the glass chips showed several signs of aging that were qualitatively assessed. This included debris that was difficult or impossible to remove, discoloration of the bulk glass material, and increased brittleness of the glass. Chips also became more difficult to clean as they aged. Whereas chips that had only been cleaned two or three times were typically completely free of any visible debris after the cleaning procedure, older chips sometimes contained traces of irremovable debris. These minuscule (less than 5μm in diameter) bits of debris eventually rendered

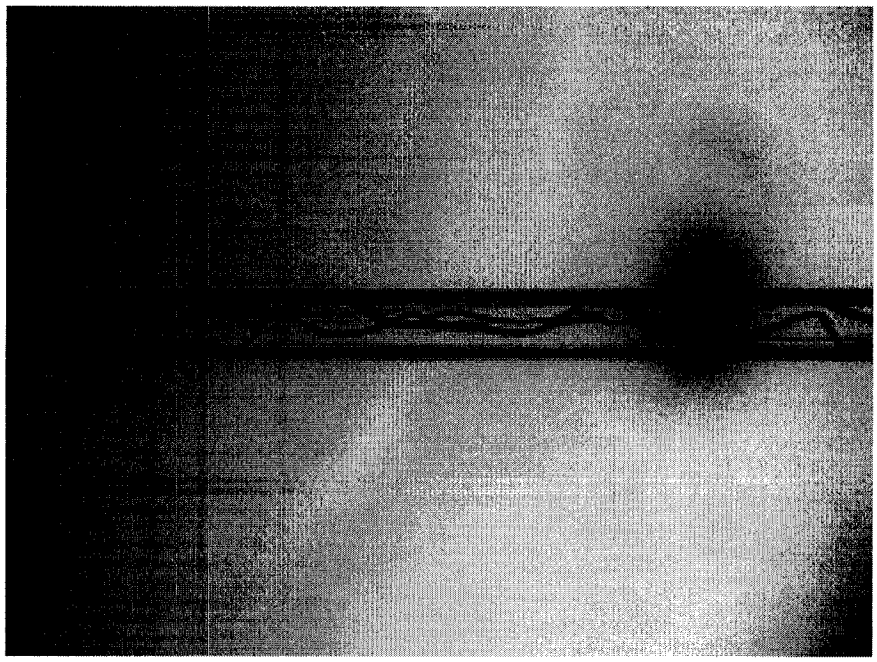

Figure 2.12: String–like debris that was typically found in the channels after heating the chip in an oven for a second or third time. The charred remains in Figure 2.11 were typically reduced to string–like debris after a second or third cycle in the annealing oven.

the chip useless as they often seemed to act as nucleation sites for the formation of bubbles during gel polymerisation. Several chips displayed the repeated formation of bubbles in specific areas where this type irremovable debris was present. Chips exhibiting repeated void formation in specific areas were deemed unsuitable for gel polymerisation and were discarded. Glass discoloration included a yellowing of the bulk material as well as browning of channel (primarily close to the wells) and well surfaces. In general, once browning of the surfaces occurred it was difficult to restore the original appearance of the material via rinsing the channels, boiling sulfuric acid in the channels, or heating the chips to glass annealing temperatures. Chips also gradually became more brittle and small fragments of glass were more likely to break away from chip edges. Because new chips were readily available, old chips were often 'retired' in favour of attempting to rejuvenate the material, and the changes to the bulk material and channel surfaces were never quantitatively measured. It is estimated that chips could withstand approximately five cleaning/chip preparation cycles before aging effects were observed to have a negative impact on chip preparation (i.e. formation of voids during polymerisation).

A published report by Ma *et al.* has suggested that glass chips can be 'rejuvenated' indefinitely via glass–annealing with no lasting effects on chip performance [14]. The main difference between that study and the work presented here involves the state of the chip when it was annealed. When annealing the glass, Ma

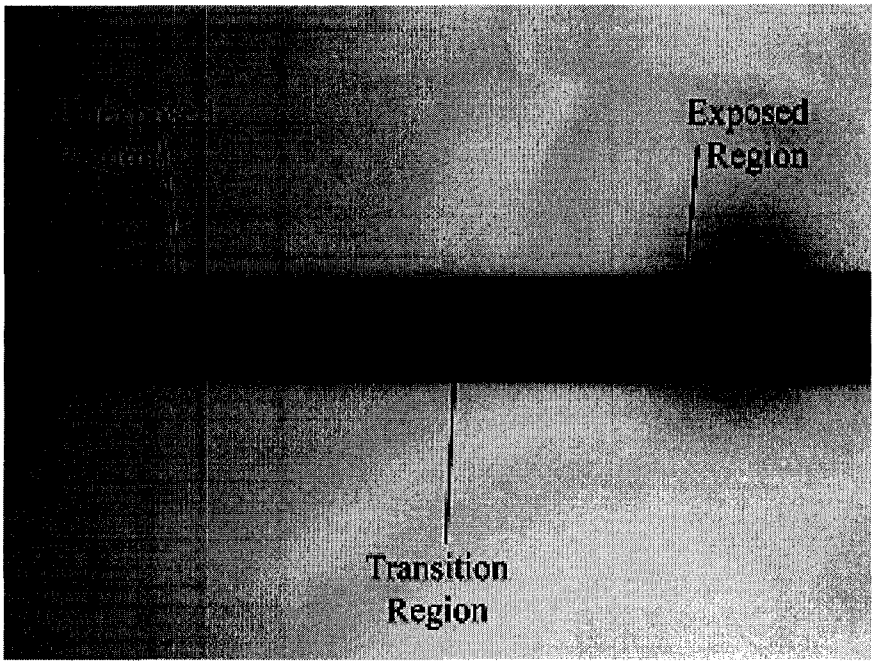

Figure 2.13: There was a noticeable difference in the debris found in exposed regions versus that found unexposed regions. The debris in exposed regions seemed to be more dense. Also noticeable is the sharp transition between debris types in an area where the channel transitioned from being exposed to unexposed during gel polymerisation. This observation helped determine that photopatterning of the gel was in fact taking place because the debris in the exposed area had a distinctly different structure from the debris in the unexposed regions. It is believed that channel contents in unexposed (unpolymerised solution) regions merely boiled off leaving only a light–brown film. In contrast, channel contents in exposed regions (polymerised gel) had to be burned out, leaving behind charred remains.

et al. ensured the channels of the chip were free of debris and void of any visible contamination. In contrast, this work presents annealing glass in the presence of channel coatings, gels, buffers, and sample contaminants. Therefore, it is not unreasonable to believe that these contaminants had effects on the channel surface materials that could not have been noted by Ma *et al.*.

Aging effects also seemed to play a role in the success of in–situ gel polymerisation. Over time, chip age seemed to contribute to the formation of bubbles during polymerisation. On several occasions this was confirmed by conducting identical iterations of the in–situ gel polymerisation protocol on old and new chips on consecutive days. In one of these occurrences, gel yield was 0% (0 out of 5) for old chips and 100% (5 out of 5) for new chips. In total, when gels were polymerised in new chips the successful polymerisation yield was 92% (11 out of 12) compared to 45% (32 out of 71) for gel polymerisations conducted in reused chips. If other protocol variations are treated as random and these results are treated as binomial

distributions, the statistical significance of the reduced formation of voids in new chips is 98.5%. Thus, it is expected that changes in surface characteristics over time contributed to decreased gel yield.

One other method for removing gels from the channels was investigated, but it was found to be more time consuming than heating. Dissolving the gel by soaking the chips in 30% hydrogen peroxide (H_2O_2) heated to 70°C proved largely ineffective. Although this procedure can be used to dissolve gels excised from traditional slab gels [13, 37], it was found that only the portions of the gel nearest to the wells dissolved in microfluidic channels. It is believed that this is primarily due to the inability of fresh H_2O_2 to diffuse to the gel at the inner portions of the channel. Even when soaked in H_2O_2 solution for two to three days, with daily solution replacement, chips were not cleaned completely. This cleaning methodology was only investigated for standard Micralyne chips. As a result, shorter channels, such as those present in 4-Port Minis, may be more effectively cleaned using this method. The advantage of this method is the lack of a need to repeatedly heat the chip to high temperatures. It is unknown if aging effects similar to those discussed above would be present if the chips were cleaned using H_2O_2.

In writing up this work, some suggestion was found that chromic acid or a phenol/chloroform/isoamyl alcohol mixture might also serve to remove the polyacrylamide gel. However, no literature report was found to support either approach and there was no opportunity to test such methods experimentally. Future work may wish to explore these methods.

2.3 Conclusions

The above discussion demonstrates the extensive protocol development required to adequately prepare microfluidic chips for protein separations. Key elements include the successful modification of a glass microfluidic channel surface with a permanent linear polyacrylamide coating, and the successful in–situ polymerisation of polyacrylamide gels. Without these developments, the research presented in subsequent chapters would not have been possible. In addition, the characterisation of protocol variability, such as the identification of the possible causes of void formation, will permit future development and refinement of these techniques. The formation of voids and bubbles during polymerisation is rarely discussed in other published works. As a consequence, knowledge pertaining to these phenomena will prove to be invaluable in the future.

Bibliography

[1] A. Pallandre, B. de Lambert, R. Attia, A. M. Jonas, and J. L. Viovy. Surface treatment and characterization: Perspectives to electrophoresis and lab-on-chips. *Electrophoresis*, 27(3):584–610, 2006.

[2] D. Belder and M. Ludwig. Surface modification in microchip electrophoresis. *Electrophoresis*, 24(21):3595–3606, 2003.

[3] J. K. Liu and M. L. Lee. Permanent surface modification of polymeric capillary electrophoresis microchips for protein and peptide analysis. *Electrophoresis*, 27(18):3533–3546, 2006.

[4] E. A. S. Doherty, R. J. Meagher, M. N. Albarghouthi, and A. E. Barron. Microchannel wall coatings for protein separations by capillary and chip electrophoresis. *Electrophoresis*, 24(1-2):34–54, 2003.

[5] M. J. Sax. Report for ECE 558: Self–assembled monolayers and thin film coatings that prevent protein adsorption in microfluidic structures (see supplementary material on DVD, "ECE558TermPaper SAMs.doc"), 2006.

[6] V. Dolnik. Wall coating for capillary electrophoresis on microchips. *Electrophoresis*, 25(21-22):3589–3601, 2004.

[7] S. Hjerten. High-performance electrophoresis - elimination of electroendosmosis and solute adsorption. *Journal of Chromatography*, 347(2):191–198, 1985.

[8] B. J. Kirby, A. R. Wheeler, R. N. Zare, J. A. Fruetel, and T. J. Shepodd. Programmable modification of cell adhesion and zeta potential in silica microchips. *Lab on a Chip*, 3(1):5–10, 2003.

[9] V. Dolnik. Capillary electrophoresis of proteins 2003-2005. *Electrophoresis*, 27(1):126–141, 2006.

[10] J. Gaudioso and H. G. Craighead. Characterizing electroosmotic flow in microfluidic devices. *Journal of Chromatography A*, 971(1-2):249–253, 2002.

[11] J. Han and A. K. Singh. Rapid protein separations in ultra-short microchannels: microchip sodium dodecyl sulfate-polyacrylamide gel electrophoresis and isoelectric focusing. *Journal of Chromatography A*, 1049(1-2):205–209, 2004.

[12] A. E. Herr and A. K. Singh. Photopolymerized cross-linked polyacrylamide gels for on-chip protein sizing. *Analytical Chemistry*, 76(16):4727–4733, 2004.

[13] B. D. Hames. An introduction to polyacrylamide gel electrophoresis. In B. D. Hames and D. Rickwood, editors, *Gel Electrophoresis of Proteins: A Practical Approach*, page 290. IRL Press Limited, Oxford, 1st edition, 1981.

[14] R. B. Ma, H. J. Crabtree, and C. J. Backhouse. A rejuvenation method for poly(n,n-dimethylacrylamide)-coated glass microfluidic chips. *Electrophoresis*, 26(14):2692–2700, 2005.

[15] Micralyne. Standard Microfluidic Chips Product Datasheet, Micralyne, Edmonton, Alberta. Website, 2007. http://www.micralyne.com/capabilities/products/standardchips.htm.

[16] M. Graf and H. Watzig. Capillary isoelectric focusing - reproducibility and protein adsorption. *Electrophoresis*, 25(17):2959–2964, 2004.

[17] N. J. Munro, A. F. R. Huhmer, and J. P. Landers. Robust polymeric microchannel coatings for microchip-based analysis of neat PCR products. *Analytical Chemistry*, 73(8):1784–1794, 2001.

[18] S. N. Brahmasandra, V. M. Ugaz, D. T. Burke, C. H. Mastrangelo, and M. A. Burns. Electrophoresis in microfabricated devices using photopolymerized polyacrylamide gels and electrode-defined sample injection. *Electrophoresis*, 22(2):300–311, 2001.

[19] A. E. Herr, D. J. Throckmorton, A. A. Davenport, and A. K. Singh. On-chip native gel electrophoresis-based immunoassays for tetanus antibody and toxin. *Analytical Chemistry*, 77(2):585–590, 2005.

[20] A. E. Herr, A. V. Hatch, D. J. Throckmorton, H. M. Tran, J. S. Brennan, W. V. Giannobile, and A. K. Singh. Microfluidic immunoassays as rapid saliva-based clinical diagnostics. *Proceedings of the National Academy of Sciences of the United States of America*, 104(13):5268–5273, 2007.

[21] A. V. Hatch, A. E. Herr, D. J. Throckmorton, J. S. Brennan, and A. K. Singh. Integrated preconcentration SDS-PAGE of proteins in microchips using photopatterned cross-linked polyacrylamide gels. *Anal. Chem.*, 78(14):4976–4984, 2006.

[22] V. M. Ugaz, S. N. Brahmasandra, D. T. Burke, and M. A. Burns. Cross-linked polyacrylamide gel electrophoresis of single-stranded DNA for microfabricated genomic analysis systems. *Electrophoresis*, 23(10):1450–1459, 2002.

[23] M. F. Bedair and R. D. Oleschuk. Fabrication of porous polymer monoliths in polymeric microfluidic chips as an electrospray emitter for direct coupling to mass spectrometry. *Analytical Chemistry*, 78(4):1130–1138, 2006.

[24] T. Koerner and R. D. Oleschuk. Porous polymer monolith assisted electrospray from a glass microdevice. *Rapid Communications in Mass Spectrometry*, 19(22):3279–3286, 2005.

[25] S. Raymond and L. Weintraub. Acrylamide gel as a supporting medium for zone electrophoresis. *Science*, 130(3377):711–711, 1959.

[26] P. Menter. Acrylamide polymerization - A practical approach, Bulletin 1156 - Revision E, Bio–Rad Laboratories Ltd., Mississauga, Ontario. Website, 2007. http://www.bio-rad.com/LifeScience/pdf/Bulletin_1156.pdf.

[27] F. P. Capote and M. D. L. de Castro. Ultrasound in analytical chemistry. *Analytical and Bioanalytical Chemistry*, 387(1):249–257, 2007.

[28] Z. Yang, S. Matsumoto, and R. Maeda. A prototype of ultrasonic microdegassing device for portable dialysis system. *Sensors and Actuators a-Physical*, 95(2-3):274–280, 2002.

[29] D. J. Throckmorton, T. J. Shepodd, and A. K. Singh. Electrochromatography in microchips: Reversed-phase separation of peptides and amino acids using photopatterned rigid polymer monoliths. *Analytical Chemistry*, 74(4):784–789, 2002.

[30] D. J. Rose Jr. Capillary gel electrophoresis columns and method of preparing the same, U.S. patent 5,282,941. Website, 1994. `http://patft.uspto.gov/netacgi/nph-Parser?u=\%2Fnetahtml\%2Fsrchnum.htm\&Sect1=PTO1\&Sect2=HITOFF\&p=1\&r=1\&l=50\&f=G\&d=PALL\&s1=5282941.PN.\&OS=PN/5282941\&RS=PN/5282941.`

[31] Y. Baba, T. Matsuura, K. Wakamoto, Y. Morita, Y. Nishitsu, and M. Tsuhako. Preparation of polyacrylamide-gel filled capillaries for ultrahigh resolution of polynucleotides by capillary gel-electrophoresis. *Analytical Chemistry*, 64(11):1221–1225, 1992.

[32] Y. Baba, T. Matsuura, K. Wakamoto, and M. Tsuhako. A simple method for the preparation of polyacrylamide-gel filled capillaries for high-performance separation of polynucleotides by using capillary gel-electrophoresis. *Chemistry Letters*, (3):371–374, 1991.

[33] H.-F. Yin, J. A. Lux, and G. Schomburg. Production of polyacrylamide-gel filled capillaries for capillary gel-electrophoresis (cge) - influence of capillary surface pretreatment on performance and stability. *Hrc-Journal of High Resolution Chromatography*, 13(9):624–627, 1990.

[34] V. Dolnik, K. A. Cobb, and M. Novotny. Preparation of polyacrylamide gel-filled capillaries for capillary electrophoresis. *Journal of Microcolumn Separations*, 3(2):155–159, 1991.

[35] A. J. Huang, Y. Chen, T. Zhu, X. H. Fang, and Y. L. Sun. Simple method for preparing cross-linked polyacrylamide gel-filled capillaries. *Journal of Chromatography A*, 755(1):138–141, 1996.

[36] G. Schomburg, J. A. Lux, and H. Yin. Production of polyacryamide gel filled capillaries for capillary gel electrophoresis, U.S. patent 5,141,612. Website, 1992. `http://patft.uspto.gov/netacgi/nph-Parser?Sect1=PTO2\&Sect2=HITOFF\&p=1\&u=\%2Fnetahtml\%2FPTO\%2Fsearch-bool.html\&r=5\&f=G\&l=50\&co1=AND\&d=PTXT\&s1=5141612\&OS=5141612\&RS=5141612.`

[37] S. B. Zhou, M. J. Bailey, M. J. Dunn, V. R. Preedy, and P. W. Emery. A systematic investigation into the recovery of radioactively labeled proteins from sodium dodecyl sulfate-polyacrylamide gels. *Electrophoresis*, 25(1):1–7, 2004.

Chapter 3

Protein Electrophoresis

The development of protein electrophoresis is a critical step in producing a microchip–based system capable of proteomic type analysis. As mentioned in Chapter 1, pre–fractionation of proteins via electrophoresis prior to analysis by ion mobility spectrometry constitutes a two–dimensional separation. The ability to separate proteins in two–dimensions in an integrated system holds great promise for the field of proteomics. As a result, the development of the protein electrophoresis component discussed in this chapter is critical in the creation of a complete proteomic analysis system.

Upon completion of the development of the procedures necessary to prepare microfluidic chips for electrophoretic protein separations (see Chapter 2), characterisation of the electrophoretic system was needed. Consequently, the majority of this chapter focuses on characterising the electrophoretic system, developing procedures for protein separations, generating a method of on–chip fluorescent protein labeling, and comparing the performance of the system with existing published data.

3.1 Microchip Electrophoresis

The following section is largely based on research conducted for a course (ECE 750) required for partial fulfillment of my Master of Science program. This section was derived from a literature review exploring the analytical techniques used in metabolomic–type analyses [1].

Electrophoresis is a commonly used technique for analyzing biomolecules. Andrews [2] offers the following definition of electrophoresis as:

> "...the migration of a charged particle under the influence of an electric field."

In initiating this migration, one is able to separate molecules based on their electrophoretic mobility [2]. As a technique, electrophoresis has seen a progression from traditional slab gels, to capillary based separations, and most recently, to chip

based separations [3]. Microchip electrophoresis (MCE) uses many of the same concepts developed for slab gel and capillary based separations and incorporates them into small chips with microfluidic channels. One of the advantages of miniaturisation is the allowance for separations to incorporate more expensive reagents because of reduced reagent consumption. In addition, incorporation of these analyses onto a chip allows multiple analytical steps such as sample preparation, sample purification, fluid pumping, and analyte detection to be combined into a single device [4]. Also not to be underestimated, is the benefit afforded by automatic digitisation of the data obtained from MCE where detection is intrinsically incorporated into the analysis [5]. Liu and Guttman also state that higher throughput, efficiency, separation speed, portability, and disposability are other advantages of MCE [6].

Current applications of electrophoresis cover a wide array of biomolecule analysis, and new applications are continually being ported to chip–based devices. At present, the applications of MCE include the analysis of amino acids [7, 8], peptides or proteins [7, 9–15], nucleic acids [7, 16–20], heavy metals [21], and other biomolecules [7, 22, 23]. Analyses of this nature can detect DNA mutations, perform DNA sequencing, profile protein expression [4], or simply detect water contamination [21].

As stated by Andrews, electrophoresis relies on charged particle migration when the particle is subjected to an electric field [2]. As a result, a positively charged particle will migrate to the electrophoretic system's cathode, while a negatively charged particle will migrate to the anode. Numerous factors determine the separation characteristics for a given analyte in an electrophoresis system. Some of these factors include electrophoretic mobility, sieving matrices, separation buffer composition, and electrophoretic analysis type.

3.1.1 Electrophoretic Mobility and Separation

The rate at which a particle migrates is determined by its electrophoretic mobility (μ), which is defined in Equations 3.1 and 3.2:

$$\mu = \frac{d}{tE} \tag{3.1}$$

$$\mu = \frac{v}{E} \tag{3.2}$$

where d is the distance traveled, t is the time traveled, E is the electric field strength, and v is the steady state electrophoretic velocity [2]. An approximation of the force ($F = qE$) causing the particle to migrate is the result of multiplying its charge (q) and the electric field strength [24]. This holds true when the migrating particle is at a very low concentration in a non–conducting solvent [2]. Opposing this force is friction within the separation medium. When not using a sieving matrix (see Section 3.1.2), this frictional force (f) is given by Equation 3.3:

$$f = 6\pi r\eta v \tag{3.3}$$

where r is the ionic radius of the migrating particle, and η is the viscosity of the separation medium, and v is the electrophoretic velocity [24]. However when a sieving matrix is used, as is often the case with electrophoresis, this relation no longer holds true. Instead the friction opposing electrophoretic movement is dependent on matrix pore size and migrating particle size [2]. In either case, different electrophoretic mobilities between two analyte particles will result in a separation. For example, a smaller particle will have a higher mobility than a larger particle with equal charge, and as a result will move faster along the separation channel. Two particles equal in size, but differing in charge will also be separable by electrophoresis.

3.1.2 Sieving Matrices

Sieving matrices are used to alter the mobility of charged particles in an electrophoretic system. In the case of DNA, if left to migrate in a simple buffer solution, no separation would occur. The addition of a sieving matrix will produce a separation where mobility is partially determined by size [3]. The size of pores in the sieving matrix, often called a gel, partially determine the rate at which analyte particles will migrate. Manipulating the pore size (based on gel type or composition) will permit different separation characteristics [2].

Sieving matrices often consist of water–soluble entangled polymers [3, 25], or cross-linked polymers [3, 9, 26]. Khandurina offers a fairly extensive list of entangled polymers that are used in DNA analysis. These include several derivatives of linear polyacrylamide (LPA), and other polysaccharide variants. Also cited are various types of "thermoresponsive polymers" whose viscosity, and thus matrix properties, are temperature controllable [25]. For protein analysis, sieving matrices are often composed of a polymer such as LPA or poly(dimethyl acrylamide) [4]. That being said, cross–linked acrylamide polymers have been implemented in microchannels, and have resulted in protein and DNA separations that are highly resolved over a distance of millimeters [9, 19].

3.1.3 Channel Surface Characteristics

Microfluidic channels present a few unique challenges regarding electrophoretic separation. In traditional slab gel electrophoresis, the surface area–to–volume ratio of the separation system is much smaller than in capillary or chip–based electrophoretic techniques. As a result, influences such as electroosmotic flow (EOF) and solute adsorption to the microchannel walls can have a significant effect on separation quality [27].

EOF, also known as electroendosmosis [28], results from channel walls adopting a surface charge when in contact with an electrolyte. In turn, the charged surface groups attract a cloud of mobile electrolyte ions of the opposite polarity which create a thin layer known as the Debye layer. This Debye layer, or electric double layer (EDL) as it is also known, consists of two distinct regions. The Stern layer

consists of a thin immobilised layer of counterions (ions of opposite charge to the surface charge) immediately adjacent to the surface. A second layer, known as a Gouy or diffuse layer, consists of mobile counterions and its thickness is known as the Debye length (on the order of nanometers) [29, 30] When an electric field is applied to the channel, the charged fluid in the Debye layer is attracted to an electrode of opposite polarity and develops momentum that is then transferred to the adjacent fluid in the channel via viscous mechanisms [31]. The resulting EOF can contribute to the migration of neutral particles at the EOF velocity (v_{EOF}) described in Equation 3.4:

$$v_{EOF} = \frac{E\epsilon\zeta}{\eta} \tag{3.4}$$

where E is the electric field strength, η is the separation solvent viscosity, ϵ is the permittivity (dielectric constant) of the separation solvent, and ζ is the zeta–potential of the inner channel surface. Zeta–potential is the charge present on the channel wall [32], and is generally a result of either protonation, deprotonation, or adsorption at the channel surface in the presence of an electrolyte [29]. When EOF is present, separation resolution can be reduced, especially when separating complex analytes such as proteins or DNA [27]. Controlling EOF is also important to ensure proper sample injection, prevent hydraulic pumping, and create a flat flow profile that minimises band broadening [33].

Analyte adsorption to the channel walls is also highly dependent on channel wall characteristics. For instance, the adsorption of proteins to a channel wall occurs in a time–dependent fashion and will affect the channel walls inhomogeneously. This creates surface abnormalities that can lead to band broadening, asymmetrical detection peaks, inadequate separation quality, and reduced peak concentration [31]. Surface–analyte interactions are particularly present when analyzing complex molecules such as proteins or DNA [27].

Controlling surface characteristics thus becomes of great concern to practitioners of MCE. Numerous reviews exist on manipulating surface characteristics of microfluidic channels to optimise performance [27, 31, 33]. An example of polymer based channel coating for protein separation can be found in a paper published by Han and Singh. In this paper, a polyacrylamide based coating, based on techniques pioneered by Hjerten [28], is used to coat the microchannels of a glass chip. Along with a polyacrylamide sieving matrix, this permanent coating produced channels that allowed for highly efficient separations [9]. Another paper by Ullsten *et al.* actually uses channel coating to induce electroosmotic flow in a fused–silica capillary. Doing so enabled Ullsten to use electrospray ionisation (ESI) (see Section A.1.1 on page 127) compatible buffers for coupling protein electrophoresis to mass spectrometry (MS) [34]. Additional discussion of channel coatings, their implementation, and their effects can be found in Chapter 2.

3.1.4 Separation Efficiency

Electrophoretic separations often refer to the theoretical number of plates or plate height as an indicator of performance. Each band of analyte in an electrophoretic separation consists of a concentration distribution. Often approximated as an ideal (Gaussian) distribution, each band has a variance (σ^2). Plates are essentially a theoretical construct designed to divide the separation capillary into a number of bands or plates that help to quantify the effects of band (peak) broadening by measuring σ^2 [32]. In capillary electrophoresis, the primary causes of band broadening are molecular diffusion, inhomogeneous temperature within the capillary, and adsorption of the analyte to the channel surface [31]. Using band variance, the concept of plate height (H) emerges in Equation 3.5 as an indication of the variance per unit of column length,

$$H = \frac{\sigma^2}{L} \tag{3.5}$$

where L is the length of the separation column, or in the case of this work, the distance at which detection of the analytes was performed. Plate height is typically expressed in micrometres (μm). A smaller plate height indicates less band variance, and consequently a more efficient separation [32]. The total number of theoretical plates, N, in a capillary is therefore given by Equation 3.6,

$$N = \frac{L}{H} \tag{3.6}$$

A higher number of theoretical plates indicate better separation efficiency (i.e. less band variance). The number of theoretical plates can also be described by Equation 3.7,

$$N = 5.54 \left(\frac{t}{\Delta t_{1/2}} \right)^2 \tag{3.7}$$

where t is the migration time of the detected peak, and $\Delta t_{1/2}$ is the full–width half maximum of the detected peak [26]. Equation 3.7 is essentially derived by combining Equations 3.5 and 3.6. Migration time (t) is substituted for migration length (L) and the full–width half maximum ($\Delta t_{1/2}$) of the band is substituted for variance [32]. The value of $\Delta t_{1/2}$ is considered to be 2.35σ [26].

Another method of determining separation performance is by determining the separation resolution (R_s). R_s can be defined by Equation 3.8,

$$R_s = \frac{t_2 - t_1}{\frac{1}{2}(W_1 + W_2)} \tag{3.8}$$

where t_1 and t_2 are the migration times of two peaks, and W_1 and W_2 are the bandwidths of the peak bases. Higher values of R_s indicate better resolution [35]. Baseline resolution of two peaks is achieved when R_s is greater than 1.25 [36]. Although both N and R_s were developed for chromatographic separations, they are also used in describing electrophoretic separations. Examples of plate number are

far more prominent in the literature because comparing R_s values between different papers becomes very difficult because of the variety of techniques, channel lengths, and samples used.

Of particular interest in microchip electrophoresis is the theoretical number of plates per meter, N/m. Because the aim of microfluidics is to miniaturise and accelerate separations, theoretical plates per meter emerges as a very relevant performance metric. The number of theoretical plates per meter is obtained by calculating the number of theoretical plates (see Equation 3.7) and dividing by the detection distance [26].

3.1.5 Signal–to–Noise and Limits of Detection

The signal–to–noise and limits of detection for a system are important operating characteristics that aid in establishing detectable levels of analytes. The signal–to–noise ratio (SNR) is typically calculated by dividing the background corrected fluorescence signal by the standard deviation of the noise signal taken over a given period of time [37]. This is expressed by Equation 3.9,

$$SNR = \frac{S - \overline{N}}{\sigma_N} \tag{3.9}$$

where S is the peak amplitude of the signal, $\overline{N}$ is the average of the baseline noise observed at a time prior to the signal occurring, and σ_N is the standard deviation of the baseline noise observed during the same time period as $\overline{n}$. The limit of detection of a system, is established by measuring the concentration of analyte that produces a signal with a SNR value of 3 [37].

3.1.6 Types of Electrophoresis

Since electrophoresis is a well–established technique, numerous variants of electrophoretic techniques exist. Techniques such as isoelectric focusing (IEF) have been performed with success in microchips in recent years [9, 12]. This technique uses a pH gradient to separate proteins based on their isoelectric point (pI) [12]. Proteins adopt a charge based on the pH of their environment. At pHs above their isoelectric point, proteins will adopt a negative charge and at pHs below their isoelectric point, proteins adopt a positive charge. However, at their isoelectric point proteins are neutral. If a potential is applied to a system with a pH gradient, the proteins will migrate until they reach their isoelectric point and become neutral. Consequently, the proteins are separated based on their isoelectric point [38]. Other techniques such as sodium dodecyl sulfate–polyacrylamide gel electrophoresis (SDS–PAGE) have also been implemented on a microfluidic chip [9]. SDS–PAGE allows proteins to be separated on the basis of molecular weight (MW) [2]. A review by Dolnik and Liu also mentions other variants of conventional electrophoresis such as zone electrophoresis, multi–dimensional electrophoresis, and affinity electrophoresis, all of which have been implemented in microfluidics [4].

3.2 SDS–PAGE

As previously mentioned, sodium dodecyl sulfate polyacrylamide gel electrophoresis (SDS–PAGE) permits the separation of proteins on the basis of their MW [2]. Traditionally performed in large slab gels [2, 39], recent papers have discussed the use of this technique in microfluidic structures [9, 26].

3.2.1 SDS–PAGE Theory

SDS–PAGE involves the electrophoretic separation of denatured proteins. Proteins are denatured by a process that involves heating in the presence of SDS and 2–mercaptoethanol or dithiothreitol (DTT). 2–mercaptoethanol and DTT are thiol reagents that serve to cleave the proteins' disulphide bonds, and thus allow complete denaturation and saturation of the protein with SDS. This results in proteins with SDS bound in a constant weight ratio, such that the negatively charged SDS molecules create proteins with virtually uniform charge densities regardless of protein size. When migrating in the presence of an electric field, the migration behaviour of a series of proteins is such that a linear curve can be plotted using the logarithm of protein MW in relation to the proteins' relative mobilities. Such curves are useful in determining the size of unknown proteins [39]. As a result, SDS–PAGE is a highly useful technique capable of providing information on protein content in a sample along with the MW of those proteins.

Proteins and Protein Denaturing

Although a large portion of this thesis discusses proteins, little has been said as to their nature. Proteins are essentially polymers of amino acids. Every protein is constructed from a set or subset of the twenty standard amino acids. Each amino acid consists of an amino and carboxyl group bonded to the same carbon atom. The unique properties of each amino acid are determined by their side chains, also known as R-groups. R-groups influence amino acid structure, charge, size, and water solubility. Amino acids are zwitterionic when dissolved in water. Essentially this means that amino acids can act as either a proton donor (acid) or proton acceptor (base) when in solution. Based on the pH of the solution in which they are dissolved, amino acids will assume a positive or negative net electric charge. When the amino has no net electric charge, it is said to be at its isoelectric point, pI, which occurs at a given pH. If the solution pH is below the pI of the amino acid, the amino acid will present a net positive charge. In contrast, when in a solution with a pH above its pI, the amino acid will assume a net negative charge [38].

As previously mentioned, proteins are chains of amino acids that are joined by covalent bonds known has peptide bonds. Typically, proteins contain hundreds to thousands of amino acids, and form long chains. As such, unique sequences of amino acids generate unique proteins with unique properties. In terms of structure, proteins are characterised by four levels of protein structure. Primary structure is

described by observing the sequence of amino acid residues (the term applied to amino acids in a polypeptide) linked together by covalent bonds. These covalent bonds include previously discussed peptide bonds, as well as disulfide bonds which are formed by thiol groups of cysteine amino acid residues. Secondary structure refers to stable amino acid arrangements that result in the formation of repetitive structural patterns. The third level of structure, tertiary, describes how the protein folds in three–dimensional space, while quaternary structure, refers to the arrangement of multiple polypeptide subunits that may make up a protein. Protein structure determines its functionality and is also known as protein conformation [38].

While information on protein structure is valuable when determining a protein's function, SDS–PAGE is primarily concerned with the size of the protein of interest. As such, disturbing the secondary, tertiary, and quaternary structure of the protein is essential to separate proteins purely based on size. This process is known as denaturing the protein, and is a necessary sample pre–treatment step when utilizing SDS–PAGE.

The native protein state or conformation can be defined as the structure a protein assumes in its natural environment, i.e. a living organism. On the other hand, a denatured protein refers to a protein that has undergone a significant structural alteration without disturbing the primary structure. Consequently, denaturation involves disturbing the secondary, tertiary, and quaternary structure of a given protein. In general, denaturation can be reversible or irreversible and can be achieved using various methods [40].

When using SDS–PAGE, three distinct components of denaturation are essential to ensure repeatable results. These are the presence of SDS and a thiol reagent, and the addition of heat. An excess of sodium dodecyl sulfate (SDS) as well as thiol reducing reagent, such as dithiothreitol (DTT) or 2–mercaptoethanol, must be present. When heat is applied in the presence of the additives, protein secondary, tertiary, and quaternary structure will be disturbed. The thiol reagent acts as a means of cleaving disulfide bonds [39]. SDS, an anionic detergent, serves to denature the protein into a random coil configuration as well as place a large negative charge on the protein [2]. Because SDS binds to proteins in a constant weight ratio when disulfide bonds are reduced, 1.4g SDS per 1g protein, the charge assumed by the protein–SDS complex is proportional to the mass of the protein and greatly overwhelms the charge resulting from the proteins' zwitterionic amino acids. In order to ensure complete denaturation and reliable migration of the sample during electrophoresis, boiling of the sample is required prior to analysis [39].

Sieving Matrices

As is evidenced from its name, sodium dodecyl sulfate–polyacrylamide gel electrophoresis utilises polyacrylamide gel as a sieving matrix. Polyacrylamide gels used for SDS–PAGE are cross–linked and are formed by the polymerisation of acrylamide monomer into long chains that are cross–linked by bifunctional cross–

Polyacrylamide Gel Concentration ($\%T$)	Separable Protein MWs (Da)
5%	60,000–200,000
10%	16,000–70,000
15%	12,000–45,000

Table 3.1: Theoretical polyacrylamide gel concentrations and separable molecular weight ranges in slab gel electrophoresis [39].

linking reagents, typically N,N′–methylene bisacrylamide (more commonly known as bisacrylamide). See Figure 2.2 for a chemical representation of the final gel structure. The result is a porous gel in which the pore size is determined by the total monomer concentration (acrylamide monomer and cross–linker monomer), $\%T$, and cross–linker concentration, $\%C$. When the proportion of monomer to cross–linker is kept constant, the pore size of the gel decreases as the $\%T$ increases. The proportion of $\%C$ to $\%T$ has additional effects on the porosity, stiffness, brittleness, light scattering, and swelling properties of the gel. Typically, pore sizes are at a minimum when $\%C$ is approximately 5% of the total monomer concentration, $\%T$. Typical values for $\%T$ in SDS–PAGE are 5% to 15%, while the ratio of $\%T$ to $\%C$ is typically 37.5:1. Gels using a concentration gradient are also used. Gradient gels offer the advantage of being able to separate a wider MW range of protein in a single gel [39].

Choosing the appropriate gel concentration for separating the proteins in the sample of interest is critical to ensure adequate separation of the constituent proteins. Improper gel concentration choice may lead to complete exclusion of the proteins from entering the gel or the inability to separate protein species. Table 3.1 contains general guidelines for traditional SDS–PAGE applications in terms of gel concentration and separable protein size range [39]. These should be considered as general guidelines as experience with use of the gels may result in different observed separable MW ranges. Refer to section 3.2.1 for further discussion on determining the appropriate gel concentration for a set of proteins and determining the porosity of polyacrylamide gels. For additional discussion on the polymerisation and characteristics of polyacrylamide gels, see Section 2.2.

Molecular Weight Estimation

Because SDS–PAGE separates proteins on the basis of the MW, one of the primary uses of the technique is to generate information on the MW of proteins within a given sample. As with other separation techniques, the ability to adequately separate and detect proteins within a sample is also of great importance. Consequently, metrics and methods have been developed for analysing data generated by SDS–PAGE. These include molecular weight curves (MWC), Ferguson plot analysis, resolution and plate number, and signal to noise and limit of detection. Each of these concepts are presented in the subsequent discussion.

Molecular weight curves offer a convenient means of calculating the MW of unknown proteins. These curves are generated by the separation of a series of standard (known molecular weight) proteins. By normalising the standard proteins' mobility to that of the buffer front and plotting that against the logarithm of the known MW of the standard proteins, a linear curve is generated [39]. This curve can then be used to evaluate the MW of unknown sample proteins [41]. There are two main assumptions associated with this method. First, one assumes the protein molecules being separated have a uniform charge density. As previously mentioned, this is typically achieved by binding large amounts of SDS to the protein as well as reducing disulfide bonds using reagents such as 2–mercaptoethanol or DTT. Even in the presence of SDS and a thiol reducing agent, some proteins have been known to behave anomalously. Second, one assumes that the relationship between mobility and MW is linear throughout a given range [2].

At this point it would be appropriate to introduce the concept of Ferguson plot analysis and its impact on the use of molecular weight curves. The foundations of Ferguson plot analysis are rooted in the knowledge that the electrophoretic migration of a molecule is influenced by both the gel concentration, $\%T$, and the degree of gel cross–linking, $\%C$. As long as the degree of cross–linking ($\%C$) remains constant over a range of gels concentrations ($\%T$), so as to maintain a consistent relationship between gel concentration and gel porosity, Equations 3.10 and 3.11 apply to observed mobilities of molecules in a gel [2],

$$\log_{10}\mu = \log_{10}\mu_0 - (K_R \times \%T) \tag{3.10}$$

$$\log_{10} R_f = \log_{10} Y_0 - (K_R \times \%T) \tag{3.11}$$

where μ is the mobility of the molecule, R_f is the normalised mobility of the molecule (normalised to the dye front that moves ahead of proteins in a slab gel), K_R is the retardation coefficient of the molecule, and μ_0 and Y_0 are the free mobility and relative free mobility respectively. Free mobility is the mobility of the molecule in a $\%T = 0\%$ gel [2].

Figure 3.1 contains an example of a Ferguson plot using artificially constructed data. The base ten logarithm of R_f is plotted against gel concentration ($\%T$). Although R_f is used in this plot, it can be used interchangeably with μ. In Ferguson plots, each linear curve (described by either Equation 3.10 or 3.11) links the measured mobilities of a single protein in several different gel concentrations ($\%T$). From this, one can gather that Ferguson plot analysis was performed on seven proteins (i.e. seven curves) in Figure 3.1. Each linear curve, and in turn each protein, has a unique slope known as K_R. When Ferguson plots display data gathered from proteins of known molecular weights, the data can then be used to plot K_R versus the MW of the proteins. This will produce another linear curve. Based on this, the MW of an unknown protein can be established by measuring its K_R value and fitting it to the linear plot of K_R versus MW that was generated by proteins with known molecular weights [2]. The retardation coefficient is characteristic of protein size and the sieving capabilities of the gel matrix [26].

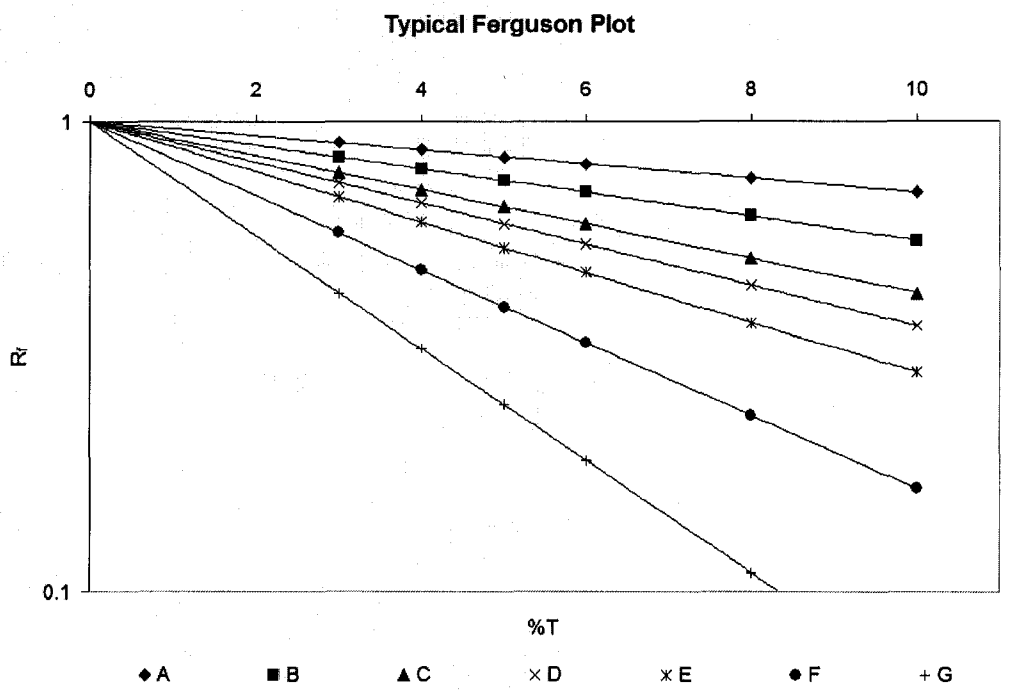

Figure 3.1: This example of a Ferguson plot depicts a separation of seven proteins in gels of six different concentrations ($\%T = 3\%, 4\%, 5\%, 6\%, 8\%, 10\%$) using artificial data constructed for the purpose of demonstration. The x–axis represents the gel concentration ($\%T$) and the y–axis represents the proteins' normalised mobilities (R_f). Values for R_f are generated by normalising protein mobilities to the mobility of the buffer front. In the case of slab gel electrophoresis, the buffer front is indicated by a dye front that moves faster than the proteins during electrophoresis. The proteins in this plot exhibit identical free solution (i.e. $\%T = 0\%$) mobilities indicating that they have uniform charge densities. This free solution mobility is described by μ_0 or Y_0 (y–intercept) in Equation 3.10 or Equation 3.11 respectively. The retardation coefficient, K_R, for each protein is quantified by measuring the slope of each line. Proteins having unique molecular weights will have unique K_R values. There is a linear relationship between K_R and MW [39]. The separation of proteins using SDS–PAGE would produce a Ferguson plot of this type because ideally SDS–denatured proteins will exhibit identical charge densities (i.e. $Y_0 = 1$) [39]. It is also important that no data point was given for protein G at $\%T = 10\%$ because it was size–excluded (too large to enter the gel pores) from the gel. As a result, it never migrated to the detector and could not be detected.

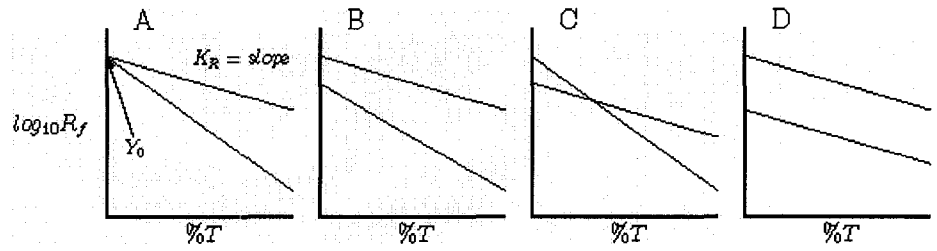

Figure 3.2: Examples of different behaviours in protein separations as described by Ferguson plot analysis. Artificial data adapted from another source is used to demonstrate these concepts [39]. A) Proteins have identical charge densities, and thus, identical mobilities in free solution ($Y_0 = 1$). Proteins are separated strictly on the basis of size [42]. As previously noted, SDS–PAGE separations produce Ferguson plots of this nature (see Figure 3.1). B) The protein with the greater mobility in free solution is also the smaller protein. Separation is based on both size and charge. C) The protein with the greater mobility in free solution is actually the larger protein because it has a higher charge density than the smaller protein. Separation is based on both size and charge. Such circumstances are common in non–denaturing protein separations because native proteins can adopt a wide range of charges. D) Two proteins have the same size (same K_R values) but different free mobilities (different Y_0 values) caused by differences in charge [39].

Ferguson plot analysis is particularly useful when examining the anomalous mobility behaviour of proteins in SDS–PAGE separations. Because it can differentiate between protein mobility governed strictly by size (i.e. SDS–PAGE) and protein mobility governed by size and charge, it is useful in cases where SDS–denaturing is ineffective at generating the uniform charge density required for SDS–PAGE. In these cases, a smaller protein may actually migrate more slowly than a larger protein because it has less SDS per unit mass, and therefore a lesser charge density than a larger protein that is completely saturated with SDS [39]. Figure 3.2 identifies different scenarios where both the size and charge density of two proteins affect their mobility relative to one another.

Relative mobility, R_f, is also a good indicator of the validity of protein MW measurements. Values of R_f between 0.25 and 0.85 are considered to be valid measurements of the relative mobility of proteins due to the linearity of the relationship between R_f and MW in this range [41]. Such information is useful, in that it also permits optimisation of the gel concentration ($\%T$) by allowing one to ensure that the values of R_f for the proteins of interest remain within this range. The application of Ferguson plot analysis to the data gathered in this work will be discussed in Section 3.3.2.

Given this knowledge of Ferguson plot analysis, it is clear that with proper techniques most proteins can be sized using molecular weight curves established from separating standard proteins. However, it is also important to note that when anomalies are observed, Ferguson plot analysis will aid in determining the cause of

the anomalies (i.e. non–uniform charge density in SDS–denatured proteins) and the true MW of the protein under scrutiny.

In addition to Ferguson plots, molecular weight curves are another good source of experimental information. MWCs are constructed using the least squares regression method. The common form of the equation for these curves is found in Equation 3.12. Essentially the curves are in the form of a straight line,

$$\log MW = SR_F + \log MW_{Ex} \tag{3.12}$$

where MW is the molecular weight of the protein, S is the sieving capability of the gel, R_f is the mobility of the protein normalised to the mobility of the buffer front, and MW_{Ex} is the size exclusion limit of the gel. The size exclusion limit refers to the size of proteins that will be completely excluded from the gel, while the sieving capability is an indicator of how effectively the proteins are being separated [26]. Size exclusion limit can be used to ensure that proteins of interest are able to effectively enter the gel to be separated, but can also be used as a measure of assessing the consistency of gel polymerisation procedures. Uniform size exclusion limits among different gels of the same concentration and degree of cross–linking indicate stable polymerisation procedures [43]. This is particularly useful during protocol development. The sieving capability, or slope of the molecular weight curve, is equally important. A near vertical slope, indicates ineffective separation capability of the gel relating to proteins of interest, while a flatter slope indicates more effective sieving of the proteins [26]. Figure 3.3 illustrates this point.

3.2.2 SDS–PAGE Protocols

Separations employing SDS–PAGE in microfluidics are not well–established in the literature and only a handful of published works are available on the subject [9, 14, 26, 44–47]. In conjunction with the work discussed in Chapter 2, procedures for conducting SDS–PAGE separations were derived from information in these sources. Additionally, techniques for labeling denatured protein in microchip wells (developed within the scope of this work) were derived from capillary based SDS–protein separations of single cell lysates [48, 49]. Because many information gaps were present in these publications, standard SDS–PAGE procedures were also adapted for use in microfluidics from more traditional sources [2, 39] and product datasheets. These protocols serve to outline sample injection and separation parameters, sample handling, on–chip protein labeling methods, and general procedures related to conducting such separations.

The following discussion will give a brief overview of the various procedures used to separate protein ladders via SDS–PAGE. Complete versions of these protocols, including solution recipes, can be found in Appendix D. These separations were also used to refine the protocols discussed in Chapter 2, provide data on separation performance, and supply data needed for experiments conducted in Chapter 4. All separations in this thesis were performed using μFluidic–Toolkits

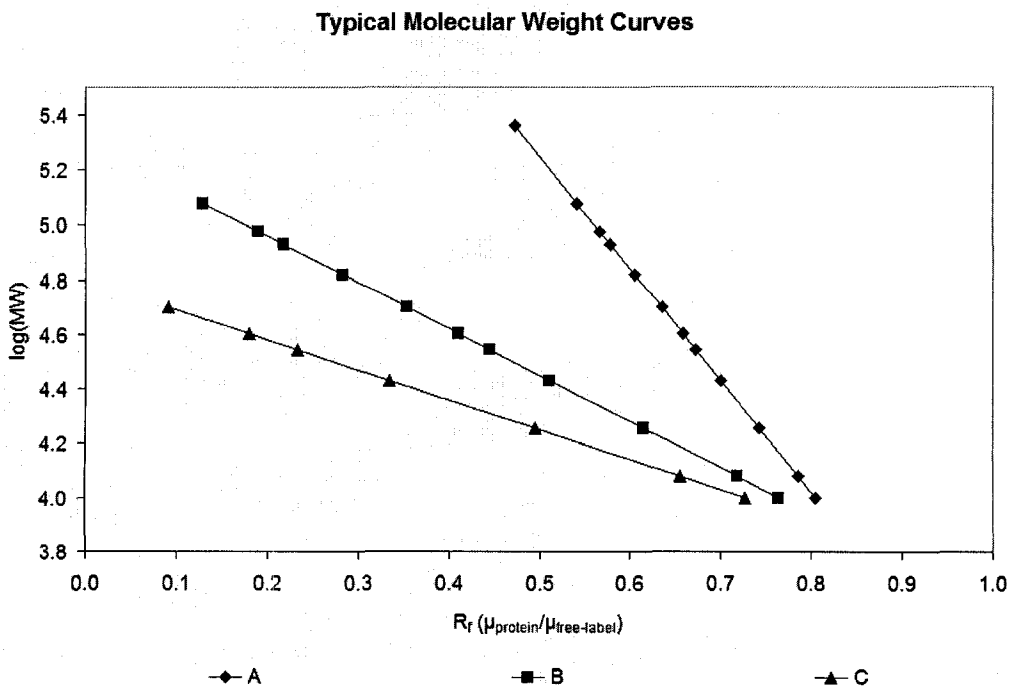

Figure 3.3: A theoretical example of the separation of twelve proteins using SDS–PAGE. These plots are derived from artificial data designed to demonstrate these concepts. These molecular weight curves illustrate the results from the separation of these proteins in three different gel concentrations. Curve A resulted from a separation conducted in the gel having the lowest concentration, while Curve C was generated by a separation in the gel with the highest concentration. Proteins (data points) are best separated when the horizontal distance between two proteins on the same curve is large. Curve A shows that although all of the proteins were detected, the mobilities of each protein were very close, so each protein peak was probably not well–resolved. Curve C shows proteins that have very different mobilities, indicating a well–resolved separation, but only seven proteins were detected. This occurred because five of the proteins were beyond gel C's size exclusion limit. The size exclusion limit of a gel can be approximated by the y–intercept of the curve. In general, a greater curve slope means the separable size range of proteins is greater, but also means that the separation capability is lower.

(μTk) supplied by Micralyne (Edmonton, Alberta, Canada). The μTk's utilised laser–induced fluorescence (LIF) based detection with an excitation wavelength of 532nm and optimal emission detection between 563.2 and 573.2nm [50].

Microfluidic Chips

All SDS–PAGE separations were conducted in 4–Port Mini microfluidic chips (see Figure 2.1). The channels in these chips had an approximately semicircular cross–sections with a depth of approximately 46μm and a maximum width of approximately 102μm. The chips were fabricated from borosilicate glass substrates using traditional glass fabrication methods at the University of Alberta NanoFab facility. Prior to conducting separations in these chips, the channels were coated using the protocol discussed in Section 2.1.2 and polyacrylamide gels were polymerised in the channels using protocols described in Section 2.2.2.

Pre–Labeled Protein Ladder Separations

Pre–labeled protein ladder separations were conducted using the BenchMark™ Fluorescent Protein Standard (BFPS) supplied by Invitrogen (Carlsbad, CA, USA). This protein ladder consists of seven standard proteins with MWs of 11, 21, 32, 40, 60, 98 and 155kDa. Proteins in this ladder are SDS denatured and conjugated to a fluorescent dye, Alexa Fluor 488. The ideal excitation wavelength of the Alexa Fluor 488 fluorophore is 494nm and maximal emission occurs at 519nm (see Figure 3.4). No modifications were made to this ladder and as a sample it was analysed in its as–shipped state. It should be noted that all parameters discussed below are typical values and do not necessarily reflect the operating parameters used in all experiments.

The microfluidic chips used for the separations were removed from the storage buffer and the outer surfaces of the chip were dried using absorbent clean wipes. If a new gel was being used (i.e. first separation after gel polymerisation), polymerised polyacrylamide gel was scraped from the chip wells using a 10μL pipette tip. If the chip had been previously used, storage buffer was removed from the wells using a pipette. It is important to note that the chip wells were never left dry for a time greater than two minutes. When this occurred, the gel inside the channel began to dry out. This drying had the potential to make the chip unusable. Dried out gel contains air bubbles that disrupt or prevent current and sample flow during injection and separation.

Prior to performing sample separations, the channels were inspected and electrokinetically flushed. This was done to introduce fresh buffer into the system, test gel integrity, and minimise cross–contamination from previous samples when the gel was being reused [26]. In instances where a new gel was being used for the first time, fluorescence was measured during the initial electrokinetic flushing step. Since no fluorescent proteins had been introduced into the gel, the exact cause of the fluorescence was unknown. For this reason, electrokinetic flushing was always

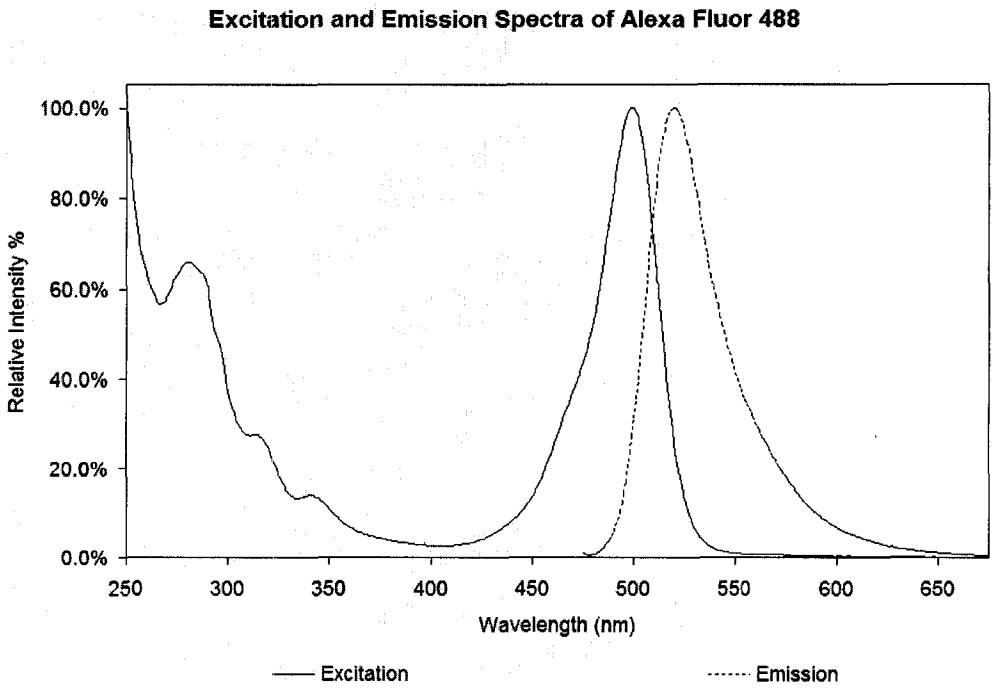

Figure 3.4: A plot of the Alexa Fluor 488 fluorophore's emission and excitation spectra obtained from Invitrogen (Carlsbad, CA, USA) [51].

conducted on new chips, as well as those that were being reused. This type of flushing prior to use has also been noted in other published reports of capillary gel electrophoresis [52, 53].

Electrokinetic flushing was achieved by placing 3μL of 1X NEXT GEL Running Buffer (1XNGB) in each of the chip's four wells. The channels were then inspected under a microscope to ensure no bubbles were present in the gel. If bubbles were present, the chip was deemed to be unusable and was set aside for cleaning. If no bubbles were found, the chip was then loaded into the μTk and the laser was focused at the channel intersection. The fluorescence signal was monitored at the intersection to ensure any sample remaining the chip was flushed out. A potential of 300V was first applied across the injection channel (approximately 160V/cm, SR = GND, SW = 300V) for ten minutes followed by the application of a 300V across the separation channel (approximately 140V/cm, BR = GND, BW = 300V) for an equal duration. When residual sample from previous experiments was still in the chip, this procedure was repeated until the baseline sample fluorescence generated a photomultiplier tube (PMT) voltage of less than 0.5V (PMT gain = 0.8) during the injection phase of the electrokinetic flushing. Flushing the gel and lowering the baseline fluorescence meant that a reasonably low concentration of the previous sample was present in the injection channel. The PMT voltage level of 0.5V was chosen because at this low level of injection channel fluorescence, old sample did

not interfere with detection of the new sample. It also ensured analysis of the new sample was less likely to be affected by old running or sample buffers because new running buffer had been introduced into the gel. Once this was complete, the chip was prepared for separation of the BFPS ladder.

First, 1XNGB was removed from each of the wells using a pipette. The SW, BR, and BW wells were filled with 3μL of 1XNGB each. After vortexing the sample tube to ensure a homogeneous sample concentration within the vial, 0.5μL of BFPS sample solution was pipetted into the SR well. 2.5μL of sample buffer was then pipetted into the SR well and it was mixed with the BFPS sample solution using the pipette. The sample buffer consisted of 2.4mM sodium borate buffer (pH = 8.5) with 2.0% SDS. Because the BFPS sample contained SDS–denatured proteins, there was no need apply heat to denature the proteins. Once the solution contained in the SR well was thoroughly mixed, the chip was placed in the μTk for the injection and separation of the sample proteins.

When the chip, gel concentration, sample content, or the protocol were unfamiliar, it proved useful to initially detect fluorescence at the intersection to determine an appropriate injection time for the first injection of the sample. Typically the initial injection duration was approximately 90 to 120 seconds at an injection voltage of 400V (approximately 215V/cm, SR = GND, SW = 400V) in gels with $\%T$ from 6% to 10%. Because sieving of proteins occurred in the injection channel, subsequent injections were sometimes needed to ensure all of the sample constituents reached the channel intersection. Separations were conducted with voltages of 500V to 1000V (approximately 230V/cm to 460V/cm, BR = GND, BW = 500–1000V) and detection was usually performed at 3mm or 10mm. These detection points were chosen because they were easy to approximate using the wells as landmarks (see Figure 2.1). Subsequent injections of sample used the same injection electric field strength and were 10 to 20 seconds in duration.

Following completion of the experiments, the channels were electrokinetically flushed using the aforementioned procedure. Throughout the entire process, special care was taken to ensure the chip's wells did not dry out. Such occurrences typically rendered the chip unusable for reasons previously noted.

Unlabeled Protein Ladder Separations

Unlabeled protein ladder separations were conducted using the BenchMark™ Protein Ladder (BPL) supplied by Invitrogen (Carlsbad, CA, USA). This protein ladder consists of 15 standard proteins with MWs of 10, 15, 20, 25, 30, 40, 50, 60, 70, 80, 90, 100, 120, 160 and 220kDa. The proteins are SDS–denatured and each is present at a concentration of approximately 0.1μg/μL. The 20 and 50kDa proteins are designed to be highlights in the ladder, and as such, may have an actual concentration higher than 0.1μg/μL. This protocol contains a simple method of conjugating the proteins to a fluorescent dye while the sample is in the SR well. The fluorescent label used was 3–(2–furoyl)quinoline–2–carboxaldehyde (ATTO–TAG FQ), which

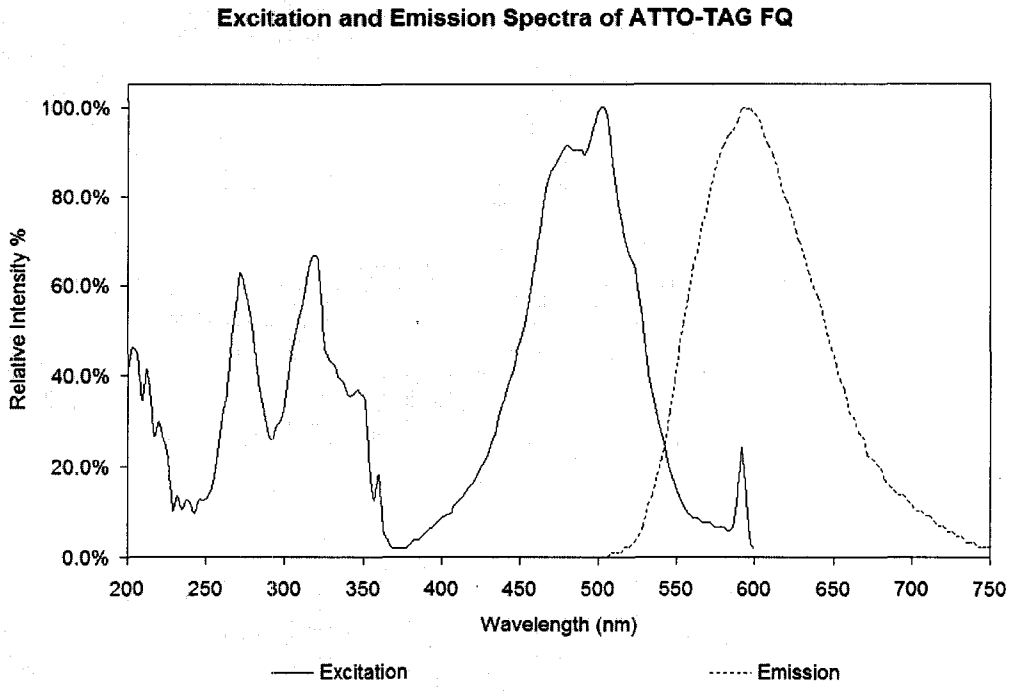

Figure 3.5: A plot of the ATTO–TAG FQ fluorophore's emission and excitation spectra obtained from Invitrogen (Carlsbad, CA, USA) (personal communication, e-mail, September 1, 2006)

was also supplied by Invitrogen. The ideal excitation wavelength of the ATTO–TAG FQ fluorophore is 489nm and maximal emission occurs at 591nm (see Figure 3.5).

ATTO–TAG FQ was chosen because of its reasonable excitation/emission efficiency (approximately 3% see Section 3.3.4), use in published works for labeling proteins in single–cell lysates [48, 49], and its relatively simple conjugation procedures. ATTO–TAG FQ covalently labels primary amines and is not fluorescent until it reacts with an amine in the presence of a cyanide anion [48]. Consequently, fluorophores not conjugated to sample proteins do not generate detrimental background noise. Unfortunately, the fluorescence enhancement of bound versus unbound ATTO–TAG FQ was not quantified in published works discussing development of the fluorophore [54].

Because ATTO–TAG FQ covalently labels primary amines, it is incompatible with sample buffers containing Tris. Tris is a primary amine, and its presence during the labeling reaction may result in higher levels of background noise due to labeled buffer components, or reduced labeling efficiency of proteins. Although data on the composition of 1XNGB is largely proprietary, the suppliers did reveal that it contained Tris. As a result, a dilution of 1XNGB could not be employed as a sample buffer and a sodium borate based buffer was used instead.

With the exception of the in–well protein labeling procedure, the protocol for

separating the BPL was essentially the same as the protocol for separating the BFPS ladder. Electrokinetic flushing with 1XNGB was followed by chip well loading, sample injection and separation, and finally, electrokinetic flushing.

In–well protein labeling was achieved by mixing the required reagents in the sample well prior to conducting the initial injection of the sample. Reagent quantities were determined based on data provided in Invitrogen datasheets for both the BPL and ATTO-TAG FQ. Using 0.5μL of BPL sample solution diluted in a total of volume 3μL of liquid in the SR well, it was determined that the approximate total concentration of proteins in the SR well was 7μM. According to Invitrogen's recommendations, a six–fold molar excess of ATTO-TAG FQ and five–fold molar excess of potassium cyanide (KCN) compared to sample proteins at a concentration of 10^{-4} to 10^{-6}M is required to properly label the sample in a time period of one hour. Given these parameters, an eighteen–fold molar excess of both reagents was used to accelerate the reaction. This was achieved by adding 0.2μL of 2mM aqueous KCN was added to the 0.5μL of BPL solution, followed by 0.2μL of 2mM ATTO-TAG FQ (dissolved in methanol). Because these labeling reagent solutions were stored at -20°C, it was imperative that aliquots of these solutions were completely thawed and mixed prior to use. Once aliquots were thawed, they were stored in the refrigerator at 4°C for approximately one week before being disposed of. Following the addition of the labeling reagents, 2.1μL of 2.8mM sodium borate buffer (pH = 8.5) with 2% v/v SDS was added to the SR well. The contents of the SR well were subsequently mixed with the pipette and allowed to react for a duration of 10 minutes. The chip sat in the stage of the μTk to allow the reaction to proceed in the dark. During this reaction and subsequent separation of the proteins, 3μL of 1XNGB was present in the SW, BR, and BW wells.

After the ten minute labeling reaction was complete, the injection and separation of the proteins was carried out as described in Section 3.2.2 with gel concentrations of $\%T = 6\%$ or $\%T = 8\%$. Detection was typically carried out at 10mm because it was difficult to adequately resolve the proteins in the ladder at a separation distance of 3mm. In comparison to separations of the BFPS, the BPL ladder was a much more complex mixture with closer MW spacing of proteins. Consequently, resolving a complex mixture over a distance of 3mm would have resulted in poorly resolved proteins. See Section 3.3.3 for a further discussion of this topic.

3.3 SDS–PAGE Results

The following discussion is intended to provide an extensive characterisation of the microchip–based SDS–PAGE separation technique and draw comparisons with existing examples of SDS–PAGE in microchips. This characterisation sets the stage for future real–world use of the technique and attempts to establish it capabilities and limitations.

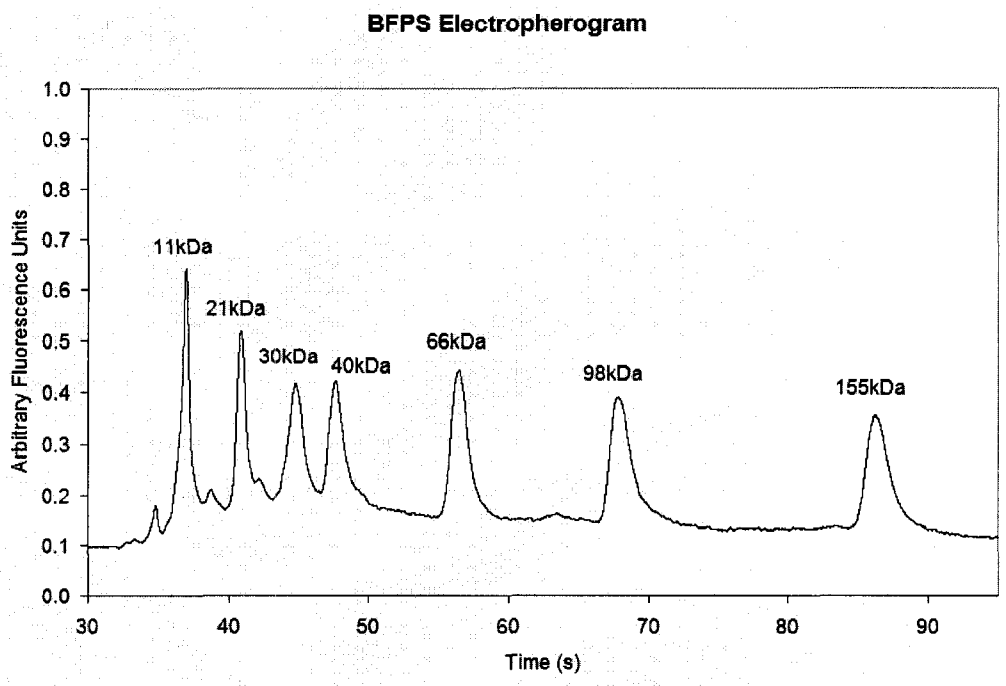

Figure 3.6: This is an example of a successful separation of the BFPS protein ladder. It was conducted in a $\%T = 6\%$ polyacrylamide gel in a 4–Port Mini chip with 46μm deep channels. The separation field strength was 230V/cm. All seven proteins in the ladder were detected at a distance of 10mm.

3.3.1 Electropherograms

Electropherograms resulting from the separation of the BFPS and BPL protein ladders can be found in Figures 3.6 and 3.8 respectively. While variations did exist between separations, the general peak profiles shown in these electropherograms were typical. In total, 54 successful separations of the BFPS ladder and 136 successful separations of the BPL protein ladder were conducted. The term 'successful separation' refers to separations which met all of the following qualitative criteria. First, protein peaks had to be of sufficient amplitude to be visually identifiable in electropherogram plots generated by the AML's μTk data analysis program (AnDna). This was a largely qualitative evaluation, and was merely used as pre–screening measure for determining which electropherograms were subjected to further analysis. Second, protein peaks had to be resolved to the point where they could be easily identified as unique peaks. Finally, the peak identities had to be intuitive. The applicability of the final criterion was facilitated by the emergence of typical electropherogram profiles (see Figures 3.6 and 3.8) in which the peak identity and the relative spacing between peaks were familiar. Upon satisfaction of these three criteria, 'successful separations' were then subjected to further analysis.

In many ways, the BFPS ladder was easier to separate than the BPL ladder. For

one, the ladder was shipped pre–labeled with Alexa Fluor 488. This meant that any unconjugated, or free–label was removed from the ladder before it was supplied to consumers. As a consequence, unconjugated fluorescent label is barely detectable (small bump in electropherogram at approximately 32.5s of Figure 3.6). Secondly, all of the proteins are present in equal concentrations. As a result, no single peak has the ability to overwhelm other peaks. Lastly, the number of proteins is lower, and the differences in MW between those proteins is much greater. The BFPS ladder has only six proteins with a MW of less than 100kDa, while the BPL ladder has twelve.

Separations of the BFPS often resulted in very 'clean' electropherograms, like the one seen in Figure 3.6. However, on numerous occasions additional peaks were detected. Figure 3.7 shows a few examples of unexpected peaks that were often present in BFPS electropherograms. Although the exact origin of these peaks is largely unknown, they were easily identifiable. The appearance of these peaks was not related to sample buffer composition nor were they dependent on gel concentration or the electric field strength. One theory as to the origin of these peaks relates to age–induced sample degradation. Early separations of the ladder (see Figure 3.6) exhibited smaller versions of these peaks, while later separations (see Figure 3.7) yielded unexpected peaks that were much larger in amplitude. These later separations were conducted on sample that had exceeded its six month recommended shelf life. While age–induced sample degradation was not confirmed by separating freshly ordered sample, such action was not deemed necessary as the appearance of the extra peaks was not adversely affecting the work being conducted.

Typical electropherograms produced by separating the BPL ladder, like the one found in Figure 3.8, consisted of the easily recognisable pattern of peaks. The first peak in the electropherogram was generated by free–label that was not conjugated to a protein. As mentioned in Section 3.2.2, unconjugated or free ATTO–TAG FQ does not exhibit fluorescence. This seems to contradict the free–label peak concept, but control runs confirmed the presence of a singular peak in separations conducted without a protein sample. From the observations made during this work, it is believed that some unbound ATTO–TAG FQ and KCN anions in the sample may actually react with the primary amines contained in the Tris component of the NEXT GEL Running Buffer upon entering the gel. As expected, this peak arrived before the protein peaks because its mobility would be on the order of that of the buffer ions. Consequently, the mobility of the free–label peak should agree with values obtained for free–solution mobility (μ_0). Similar peaks were observed before the arrival of protein peaks in works published by Hu *et al.* in which ATTO–TAG FQ was used in conjunction with a Tris–based separation buffer [55, 56].

The values obtained for the free–label peak mobility in BPL separations ranged from $1.84 \times 10^{-4}\text{cm}^2/\text{V}\cdot\text{s}$ to $2.14 \times 10^{-4}\text{cm}^2/\text{V}\cdot\text{s}$ (95% confidence interval). These values agree with the approximate values provided by Gerstner *et al.* ($\mu_0 \approx 2.2 \times 10^{-4}\text{cm}^2/\text{V}\cdot\text{s}$) [57], and are slightly less than those observed by Herr *et al.* ($2.8 \times 10^{-4}\text{cm}^2/\text{V}\cdot\text{s} \leq \mu_0 \leq 3.6 \times 10^{-4}\text{cm}^2/\text{V}\cdot\text{s}$) [26]. The lack of protein sep-

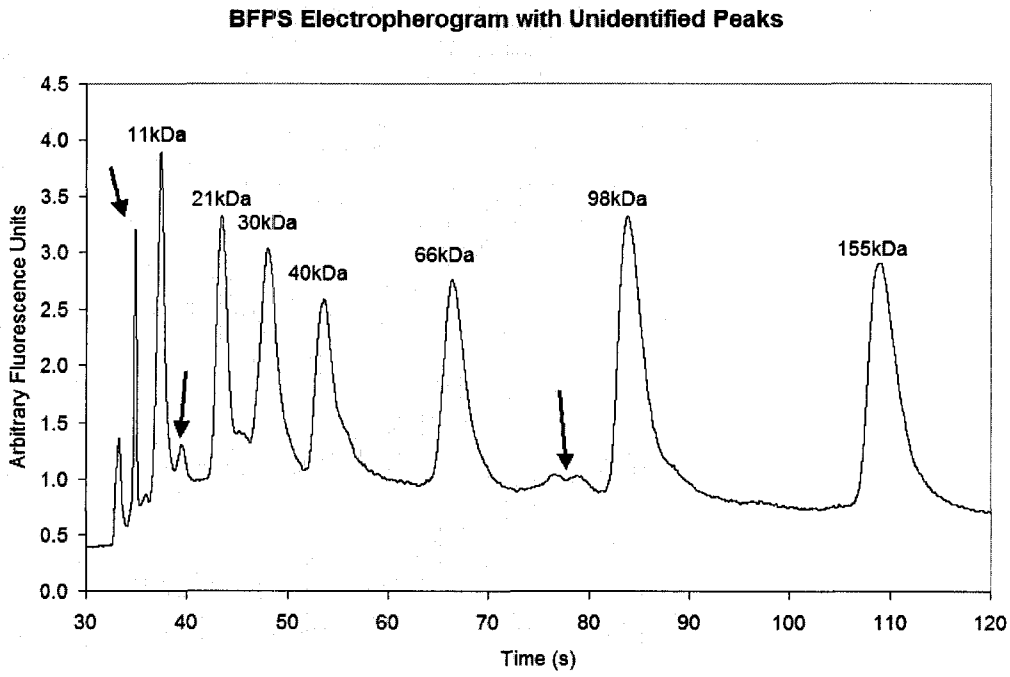

Figure 3.7: This is an example of a successful separation of the BFPS protein ladder. It was conducted in a $\%T = 8\%$ polyacrylamide gel in a 4–Port Mini chip with 46μm deep channels. Detection was conducted at 10mm. The separation field strength was 230V/cm. Unexpected peaks (those that do not result from the main protein constituents) denoted in the electropherogram were easily identifiable by their peak shape.

aration data from multiple gel concentrations and the irregular behaviour of some proteins did not allow Ferguson plot analysis to be applied to the determination of the free–solution mobility (see Section 3.3.2). No attempt was made to eradicate this peak because it was useful as a reference in determining the normalised protein mobilities used in the molecular weight curves.

SDS–PAGE separation of the BPL protein ladder was significantly more difficult than separation of the BFPS ladder for the aforementioned reasons. As a result, some key features of the electropherograms made protein peaks initially harder to identify and interpret. Unlike the BFPS ladder, peak amplitudes varied widely amongst proteins. As one can see in Figure 3.8, the peak amplitude of the 50kDa protein (seventh protein peak) was significantly greater than that of its counterparts. This likely resulted from its greater concentration, as it is designed to be a ladder 'highlight'. In addition, it is unlikely that its greater amplitude is due to some type of injection effect because relative to the amplitude of other peaks, it did not change much over multiple injections (see further discussion in Section 3.3.4. As a result of the 50kDa protein's greater concentration, the peak of the 40kDa protein (sixth protein peak) was nearly overwhelmed. The 20kDa (third protein peak) protein was also designed to be a ladder highlight, but its peak amplitude was not much larger than adjacent peaks. Peak amplitudes of higher MW proteins sized 120kDa to 220kDa (peaks thirteen through fifteen) were likely smaller due to sieving experienced during injection. Molecular weight, however, does not explain the lower signal amplitudes of proteins sized 40, 70, and 100kDa (sixth, ninth, and twelfth protein peaks respectively). In each of these cases, adjacent peaks have significantly greater amplitudes. The combination of the large number of proteins and the in–well pre–column labeling resulted in a very challenging separation. It should be noted that of the papers published on SDS–PAGE performed in microfluidic chips, the greatest number of off–chip labeled proteins separated was thirteen [58], and the greatest number of on–chip labeled proteins was eight [44].

Some qualitative assessment of the separations of both protein ladders can be found in Tables 3.2 and 3.3. From this brief analysis, a few key trends emerge. In the case of both ladders, a large portion of the peaks were detected greater than 95% of the time indicating sufficient resolution and detection limits. In general, it is also evident that larger proteins were detected less frequently than their smaller counterparts. This can be attributed to a one key attribute of the electrophoretic system. As mentioned in Chapter 2, the sieving gel was present in all of the channels of the chip. As such, migration rates of the larger proteins toward the channel intersection were significantly retarded when compared with the migration rate of smaller proteins. This often resulted in the detection of only smaller proteins during the first few separations after the initial injection of the sample. Figure 3.9 shows electropherograms obtained from a series of separations of the BPL performed on a chip. The first separation resulted in the detection of eleven proteins with a cumulative injection time of 50s. By the time the last separation was performed, the cumulative injection time was 100s and all fifteen proteins were detected. A gradual increase

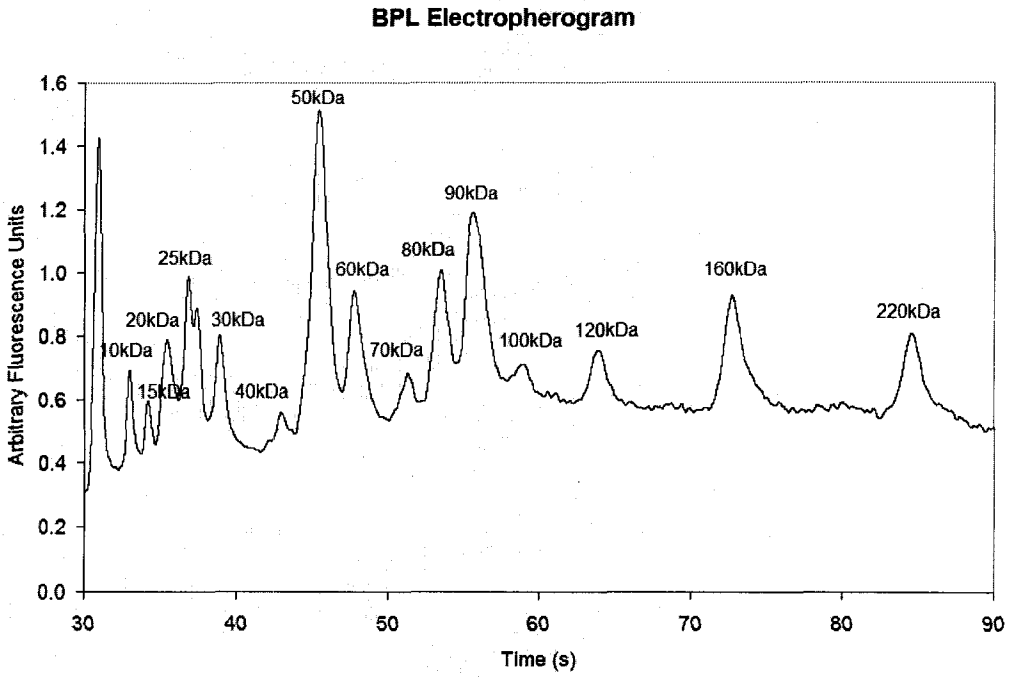

Figure 3.8: This is an example of a successful separation of the BPL protein ladder. It was conducted in a $\%T = 6\%$ polyacrylamide gel in a 4–Port Mini chip with 46μm deep channels. The separation field strength was 230V/cm and detection was performed at 10mm. Fluorescent labeling of the proteins with ATTO–TAG FQ was conducted in the chip's sample well. All fifteen proteins were detected. The first peak in the electropherogram represents free–label present at the buffer front.

Protein Ladder	BFPS	BPL
Number of Successful Separations	54	136
Mean # of Proteins Detected/Successful Separation	6.43	13.76
% of Separations Where All Proteins Were Detected (%)	57	49

Table 3.2: General performance of separations of the BFPS and BPL protein ladders. The influence of injection time was the main reason some proteins were not detected 100% of the time. In most cases where large proteins were not detected, the separation was conducted when the total injection time was insufficient to permit larger proteins to reach the intersection. As a result, the largest proteins were not detected at the start of a series of separations. As the series of separations continued, the cumulative injection time increased, thus permitting the larger proteins to reach the intersection and be included in the sample plug. This is further illustrated in Table 3.3.

BFPS Separations		BPL Separations	
Protein Size (kDa)	Successful Detection (%)	Protein Size (kDa)	Successful Detection (%)
11	100	10	100
21	100	15	98
30	100	20	100
40	100	25	99
63	98	30	100
98	86	40	100
155	57	50	100
-	-	60	99
-	-	70	95
-	-	80	97
-	-	90	96
-	-	100	85
-	-	120	84
-	-	160	72
-	-	220	52

Table 3.3: Statistics stating the percentage of separations in which proteins in each ladder were detected. The majority of the time, larger proteins were not detected due to injection effects (had not yet reached intersection at time of separation) or size exclusion effects of the gel.

in the amplitude of the peaks and the baseline fluorescence level were also evident as more sample reached the channel intersection. The observed increase in baseline fluorescence will be discussed in Section 3.3.3.

There was also some drift (approximately 15% in the 50kDa peak) in the absolute mobilities of the proteins in Figure 3.9. In the case of this series of separations, the drift seemed to be particularly pronounced. In contrast, the data shown in Table 3.4 indicates much lower levels of variability. The separations shown in Figure 3.9 seemed to be particularly prone to mobility variations, but the values in Table 3.4 are more indicative of the typical performance of the system. Quantification of the mobility drift and discussion of the potential causes are discussed in Section 3.3.2.

3.3.2 Molecular Weight Curves and Ferguson Plot Analysis

The molecular weight curves generated by protein ladder separations (BFPS and BPL) demonstrate the validity of the separation method and permitted evaluation of the separations. MWCs were generated using least squares regression analysis to fit a line to the data points generated by protein ladder separations. Figures 3.10 and 3.11 exhibit typical molecular weight curves for the BFPS and BPL protein ladders respectively. These MWCs were generated from multiple separations of

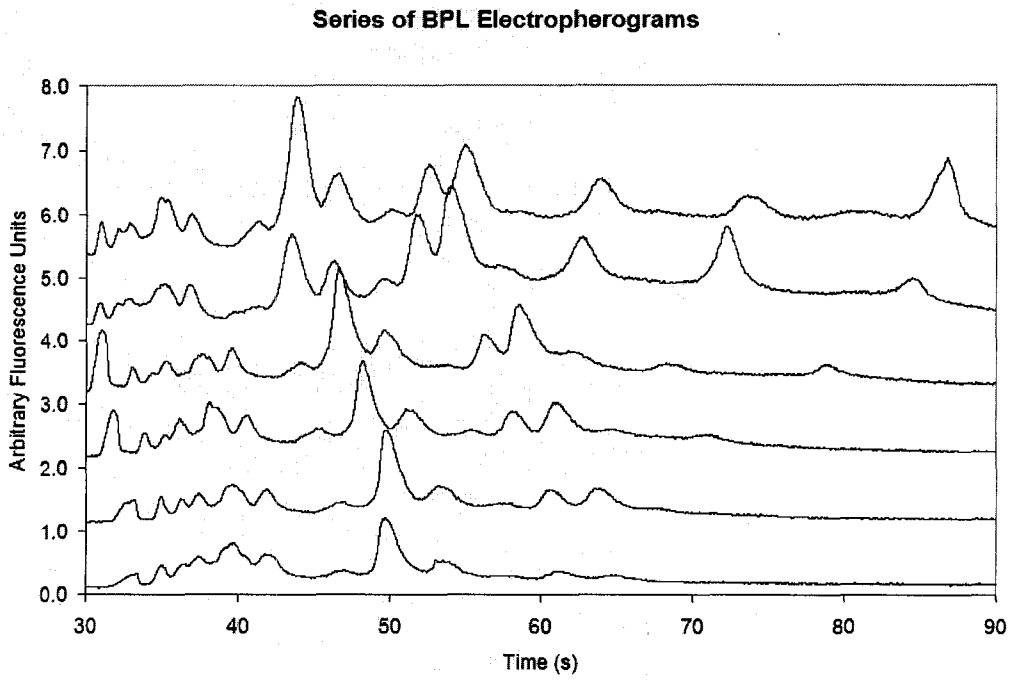

Figure 3.9: These electropherograms depict a series of separations in which the increase in the cumulative injection time increases the number of proteins that are detected. The electric field strength used in the separation was 230V/cm and detection was conducted at 10mm. The electropherogram on the bottom represents the first separation, while the top electropherogram resulted from the last separations. Increased baseline fluorescence levels are likely due to a higher than required sample concentration. Some drift (see Section 3.3.2) in the absolute mobilities of the proteins was also observed. The drift in the absolute mobilities had little effect on the normalised mobilities. The cumulative injection time was 50s for the first separation. Each subsequent injection was 10s in duration, leading to a cumulative injection time of 100s at the last separation.

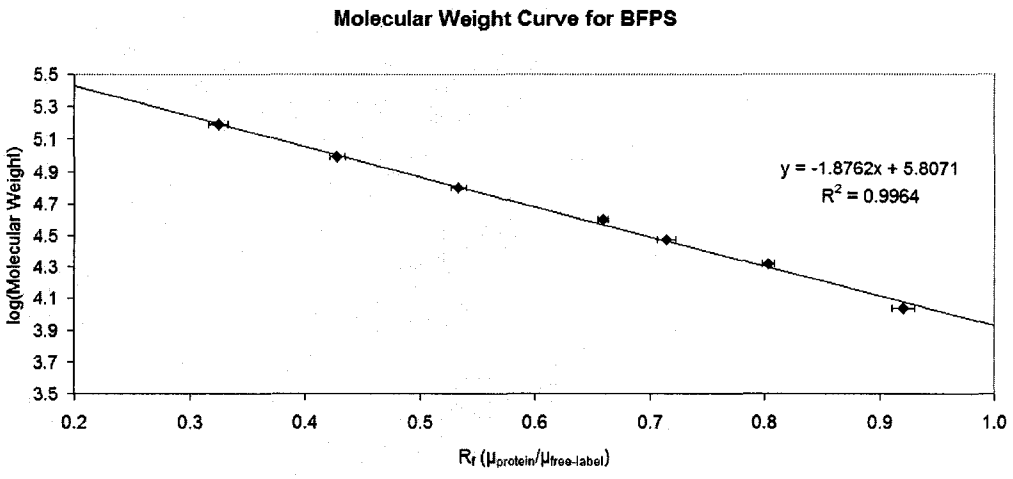

Figure 3.10: The linear molecular weight curve generated by the BFPS separation electropherogram in Figure 3.6. The BFPS ladder was separated in a $\%T = 6\%$ gel with a size exclusion limit of 640kDa. Based on several ($n = 4$) separations of the same protein ladder conducted in the same gel, the relative standard deviation of the normalised mobility of the various peaks ranged from 0.72% to 2.72% as indicated by the error bars. Curves similar to these were used to calibrate gels and permit sizing of the detected salivary proteins in Chapter 4. Gel calibration refers to the generation of characteristic MWC plot using standard proteins. Using normalised mobilities, this MWC plot could then be used to size unknown proteins that were separated in subsequent analyses.

each protein ladder. From these plots, the linear relationship between the logarithm of protein MW and normalised mobility is clear. On average, the 54 successful separations of the BFPS ladder yielded relationships with $R^2 = 0.998$, while separations of the BPL protein ladder resulted in average values of $R^2 = 0.995$. This is comparable to other SDS–PAGE microfluidic separations where R^2 values between 0.984 and 0.999 were observed [26].

Because all efforts at sizing proteins rely on consistent protein mobility, it is critical to assess the variability in mobility amongst separations. Both absolute mobility, a reflection of repeatable gel characteristics, and normalised mobility, a reflection of repeatable gel characteristics and separation mechanisms, are critical. As a result, the repeatability of separations conducted in the same gel, as well as separations conducted in different gels was assessed. In terms of repeatability within the same gel, Table 3.4 shows values (mean $\pm$ standard error) for the absolute and normalised mobility for proteins in the BPL ladder separations ($n = 31$) to be on the order of $\pm 0.69\%$ and $\pm 0.32\%$ respectively. For the purposes of comparison, this represents an average relative standard deviation (RSD) of 3.74% for absolute mobility and 1.72% for normalised mobility. By comparison, Nagata *at al.* achieved

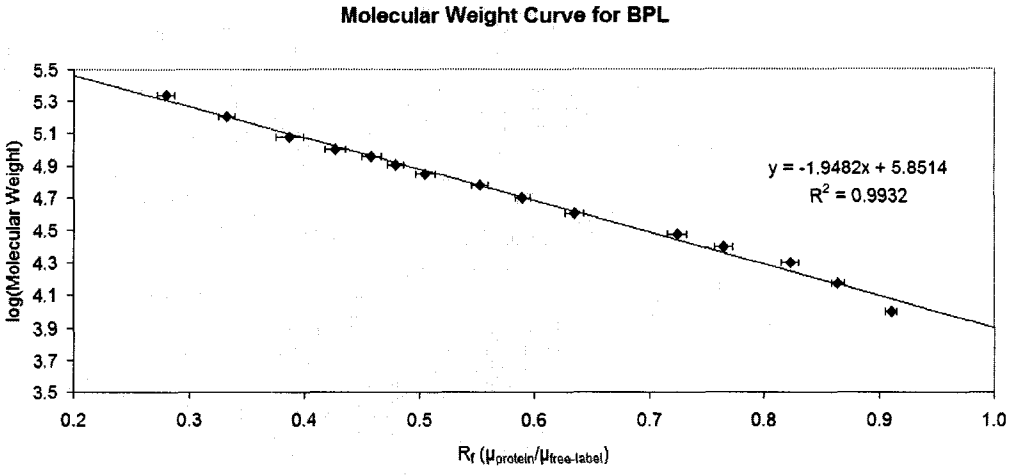

Figure 3.11: The linear molecular weight curve generated by the BPL separation electropherogram in Figure 3.8. The BPL ladder was separated in a $\%T = 6\%$ gel with a size exclusion limit of 710kDa. Based on several ($n = 23$) separations of the same protein ladder conducted in the same gel, the relative standard deviation of the normalised mobility of the various peaks ranged from 0.81% to 1.93% as indicated by the error bars.

average absolute mobility RSD equal to 5.7%, while Herr *et al.* claimed and RSD of approximately 7% from run to run. Figures 3.10 and 3.11 visually demonstrate that the variability of R_f for each protein is quite small, indicating good reproducibility for protein mobility within individual gels. When mobility was assessed across multiple gels ($n = 14$) for a large number of BPL separations ($n = 123$), the average RSD for absolute protein mobility was 10.8% and the average RSD for normalised protein mobility was 5.7%. Compared to Herr *et al's* stated values of RSD$\leq$ 13% for normalised mobility in multiple gels ($n = 2$), the repeatability of the system discussed in this work is superior.

The causes for the absolute mobility drift (as seen in Figure 3.9) and absolute or normalised mobility variability (see Table 3.4) were not studied in depth. Because the impact on normalised mobility, the critical value required for protein sizing, was so minuscule (standard error averaging 0.32%), characterisation and mitigation of the phenomenon were not vigorously pursued. That being said, future work may be directed at characterising this phenomenon, as it is likely that variations in EOF contributed to the absolute mobility variations. As seen in Figure 3.9, there were instances where such variations were large. It is well–known that variability in buffer characteristics such as pH, ionic strength, and temperature have been shown to cause changes in EOF [30]. In particular, the low solution volume in microchip wells makes microfluidic systems particularly susceptible to changes in buffer composition due to evaporation.

Protein Size (kDa)	Mean Absolute Protein Mobility (mm^2/Vs)	Mean Normalised Protein Mobility
10	0.1886 ± 0.0013	0.9147 ± 0.0020
15	0.1793 ± 0.0012	0.8693 ± 0.0021
20	0.1701 ± 0.0013	0.8249 ± 0.0025
25	0.1618 ± 0.0010	0.7848 ± 0.0021
30	0.1504 ± 0.0010	0.7296 ± 0.0021
40	0.1325 ± 0.0008	0.6424 ± 0.0018
50	0.1242 ± 0.0008	0.6024 ± 0.0020
60	0.1156 ± 0.0008	0.5607 ± 0.0019
70	0.1063 ± 0.0007	0.5155 ± 0.0018
80	0.1012 ± 0.0007	0.4909 ± 0.0018
90	0.0964 ± 0.0007	0.4674 ± 0.0019
100	0.0900 ± 0.0007	0.4369 ± 0.0018
120	0.0814 ± 0.0006	0.3949 ± 0.0015
160	0.0696 ± 0.0004	0.3367 ± 0.0011
220	0.0580 ± 0.0003	0.2801 ± 0.0007

Table 3.4: This table represents the variability present in protein mobility (mean $\pm$ standard error) in the BPL ladder. The data was gathered over a series of thirty-one ($n = 31$) separations performed in a single chip ($\%T = 6\%$) at the same electric field (E=230V/cm). Three separate sample loads were conducted during these thirty–one separations. Overall, the standard error for absolute mobility averaged $\pm 0.69\%$, while the standard error for normalised mobility was only $\pm 0.32\%$. Such values indicate good separation reproducibility and minimal degradation of the separation system over time. The separations shown in Figure 3.9 seemed to be especially prone to mobility variations and are not representative of the typical performance of the system.

Gel Concentration (%T)	6	8
Mean Size Exclusion Limit (kDa)	688	371
Mean Minimum Separable Size ($R_f = 0.85$) (kDa)	15.3	10.9
Mean Maximum Separable Size ($R_f = 0.25$) (kDa)	212	131
Mean Selectivity Factor	-1.91	-1.79

Table 3.5: These gel characteristics were calculated using observations garnered from separations of the BFPS and BPL protein ladders.

Separations of the ladders also permitted the gels to be characterised for features such as size exclusion limit. The data for $\%T = 6\%$ gels in Table 3.5 was generated using separations of the BPL and BFPS ladders, while $\%T = 8\%$ gels were evaluated using BFPS separations. Based on the values observed by Herr *et al.* [26] for size exclusion limit and selectivity (slope of the MWC), gels polymerised in the Applied Miniaturisation Laboratory (AML) appeared to be more porous in spite of using the same cross–linking ratio and the same polymerisation catalyst. The observed size exclusion limits are approximately three times greater than those calculated by Herr. When comparing selectivity of the gels, Herr states MWC selectivity of -1.7 and -1.1 for $\%T = 6\%$ and $\%T = 8\%$ gels respectively, while those polymerised in the AML exhibited values of -1.91 and -1.79.

The exact causes for the discrepancy between Herr's results and the results presented in this work are unknown. These differences were not characterised beyond this point because of the acceptable performance of the protein separations. In addition, because the size exclusion limit is a value extrapolated from the MWC, it is more appropriately used as a means of measuring consistency of gel porosity amongst gel batches characterised by the same means [43], as opposed to a means of direct comparison between different systems. Menter notes that the use of different protein standards to characterise the size exclusion limit can also have an effect on the extrapolated value [43]. Due the magnitude of the discrepancy it is still believed that some influence from polymerisation conditions may have led to the disparity. Factors such as UV intensity, dissolved oxygen content in the polyacrylamide precursor solution, and catalyst concentration may have all played a role. Further characterisation of the polymerisation reaction and gel characteristics may yield more conclusive answers, but such experimentation was not warranted in this work.

While conducting separations with different electric field strengths, an interesting observation was made. As the field strength increased, so too did the apparent size exclusion limit (see Table 3.6). Over a series of separations performed on a single gel, the separation field strength was increased from 230V/cm to 460V/cm over the course of five separations. Each increase in field strength was accompanied by an increase in the size exclusion limit of the gel and a decrease in selectivity (steeper slope of the MWC). Upon returning the field strength to 230V/cm, the apparent size exclusion limit returned to the values initially obtained at that field strength.

Because the values returned to normal, it is unlikely that the apparent change in gel porosity were caused by irreversible changes to the gel such as the damage seen in Figure 2.8. As a result, investigations into changes in protein mobility were conducted using the same data. Evidence of alterations in the way proteins migrated at different fields, similar to that observed by Han *et al.*, emerged from the data. The increase in size–exclusion limit was in fact an artifact of changes in the normalised mobility of proteins at different electric fields. Because the size–exclusion limit is merely an extrapolation of the MWC, any changes in the normalised protein mobilities used to construct that curve will also be reflected in the extrapolated size–exclusion limit.

Although their data was not stated in terms of size exclusion limit, Han *et al.* reported similar protein mobility changes in SDS–PAGE separations with field strengths ranging from 34V/cm to 170V/cm [9]. In this case, the normalised mobility changes were assessed by plotting the logarithm of the normalised mobility versus the proteins' MW. Figure 3.12 shows a similar plot composed by using the data that was gathered to generate the values in Table 3.6.

According to Ogston theory [59], a linear relationship should occur for such a plot since the logarithm of mobility is approximately linearly proportional to the length of a polymer molecule such as an SDS–denatured protein [9]. More specifically, Ogston theory states that mobility is a function of the probability that a spherical particle will have no contact with rigid gel fibers. This in turn results in the retardation coefficient, K_R (previously discussed in Section 3.2.1), as described by Equation 3.13,

$$K_R = pil'(r + R)^2 \tag{3.13}$$

where l' is the gel polymer length per unit volume, r is the radius of the polymer fibers, and R is the radius of the migrating particle [60]. In the case of SDS–denatured proteins, which are elongated, a spherical representation of the molecule is defined by the radius of gyration of the protein [60]. According to Han [9], when SDS–denatured proteins are treated as ideal polymers, the radius of gyration is closely approximated by protein length, and thus their MW. Therefore, K_R is linearly related to the MW of SDS–denatured proteins [61], and because Equation 3.14 (previously discussed in Section 3.2.1) also notes a linear relationship between K_R and $\log_{10} R_f$,

$$\log_{10} R_f = \log_{10} Y_0 - K_R \times \%T \tag{3.14}$$

a similar linear relationship can be drawn between MW and $\log_{10} R_f$ [9].

In the case of the separations performed on the BFPS ladder at fields between 230V/cm and 460V/cm, the linear behaviour is not observed, especially for larger fields and larger proteins. Such observations were confirmed by the findings of Han. Han attributed these mobility changes to possible conformational changes of the protein–SDS complex at high electric fields [9]. Westerhuis's in–depth assessment of the migration of SDS–protein complexes in polyacrylamide gels showed that proteins, especially those larger than 65kDa, do not conform solely to the Ogston

Separation Run Number	Electric Field Strength (V/cm)	Gel Size Exclusion Limit (kDa)	Gel Selectivity Factor (Da)
1	230	880	136
2	230	886	138
3	277	932	144
4	323	971	153
5	369	1019	168
6	415	1061	177
7	460	1214	207
8	460	1187	202
9	230	873	135

Table 3.6: Electric field strength altered the size exclusion limit and selectivity of the gels. This data was gathered by performing a series of separations at progressively higher separation field strengths. Upon returning to an electric field strength of 230V/cm after conducting separations at higher field strengths (separation run number nine), the size exclusion limit and selectivity values returned to the original values.

theory [61]. Instead, they exhibit intermediate properties to those described by Ogston and reptation theories. Reptation theory describes migrating particles as snake–like, with migration occurring through defined 'tubes' in the gel. These migrating particles are also oriented along the electric field. Reptation occurs when pores in the gel approach a size in which they no longer permit free–migration of a spherically shaped molecule. As a result, migrating particles are strung out and progress 'head–first' through the gel matrix [60].

Because Westerhuis states that neither Ogston nor reptation models completely describe the migration behaviour, the door is also opened to other models in which protein mobility is also dependent on electrokinetic forces determined by electric field strength. The door–corridor model discussed by Kozulic proposes that the gel matrix is deformable (it is considered to be rigid in the Ogston and reptation models). Regions of higher flexibility are termed as doors, while regions of lower flexibility are termed corridors. The proportion of doors that are opened compared to the proportion of corridors opened is a function of the ratio of electrokinetic force to polymer resistance. As electrokinetic force increases, so too will the number of doors opened in proportion to corridors [60]. As such, a small particle may not experience much change in normalised mobility with an increase in electric field strength because it opened a high proportion of doors even at low field strengths. However at increased fields, a larger particle may experience a greater increase in normalised mobility because of a larger change the door/corridor ratio. While interesting, characterisation of this model with SDS–proteins has been minimal.

Table 3.7 contains the values for K_R for the rudimentary Ferguson plot analysis conducted using $\%T = 6\%$ and $\%T = 8\%$ gels and the BFPS ladder. Although the smaller proteins in the BFPS protein ladder adhered to typical Ferguson

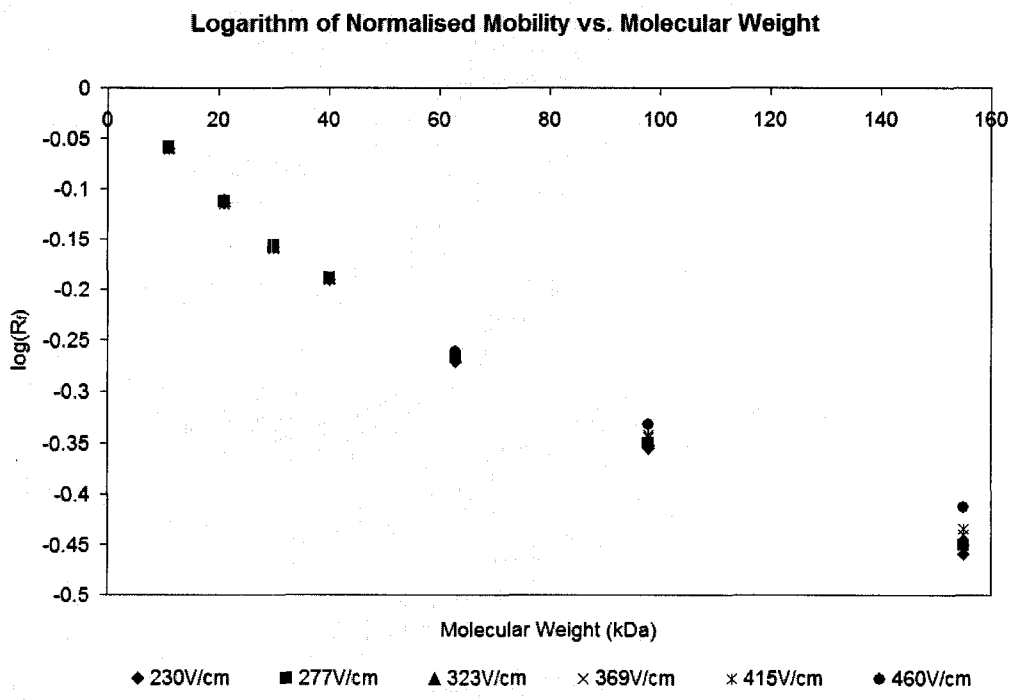

Figure 3.12: This plot illustrates the effect of the electric field on the migration behaviour of BFPS proteins in a polyacrylamide gel. BFPS proteins were separated at electric fields of 230V/cm, 277V/cm, 323V/cm, 369V/cm, 415V/cm, and 460V/cm in consecutive separations beginning with the lowest field strength. According to Ogston theory, a linear relationship should exist between MW and the logarithm of the normalised mobility (R_f) [59]. One can see that at all of the observed electric field strengths this is not the case, and as the electric field strength increases, the relationship becomes less linear. The non–linearity is especially pronounced for proteins having a greater MW. These findings indicate that a combination of Ogston and reptation mechanisms may have contributed to the migration behaviour of these proteins.

Molecular Weight (kDa)	Measured K_R	Measured Y_0
11	0.0164	0.978
21	0.0379	0.998
30	0.0460	0.980
40	0.0537	0.962
63	0.0631	0.916
98	0.0653	0.836
155	0.0581	0.699

Table 3.7: The K_R values obtained from analysing the separating the BFPS at 230V/cm. Detection for these separations was conducted at 10mm in $\%T = 6\%$ and $\%T = 8\%$ polyacrylamide gels. As expected, values increase along with MW for the smaller proteins (11, 21, 30, and 40kDa). However due to possible reptation mechanisms [9, 61, 62], values of K_R cease to increase with MW when considering the 63, 98, and 155kDa proteins. This data supports the Ferguson plot in Figure 3.13

plot findings for SDS–denature proteins, larger proteins in the ladder did not (see Figure 3.13). The curves generated by the 63, 98, and 155kDa are nearly parallel (equivalent K_R values for proteins of differing MW) to each other and their y–intercept (Y_0) does not approach 1. The research conducted into the effects of electric field on protein mobility yielded some explanation as to this irregularity. According to Westerhuis [61], the large proteins' Ferguson plot curves may actually represent reptation behaviour. Because only two different gel concentrations ($\%T$) were used in the Ferguson plot analysis, conclusions about the migration behaviour of the proteins are hard to reach. Additionally, it is not known if a concave Ferguson plot curve shape for larger proteins, as observed by Westerhuis, would actually emerge if migration in lower concentration gels was assessed. Nevertheless, the combination of the electric field dependent normalised mobility and the anomalous Ferguson plot curves indicate that the larger proteins in the ladder were not strictly adhering to the Ogston theory of migration. Because of the anomalous behaviour noted, Ferguson plot analysis could not be used for sizing the unknown proteins in Chapter 4. It should also be noted that although Herr *et al.* did observe linear Ferguson plots with $Y_0 \approx 1$ for similar separations [26], the proteins used to produce these plots were all smaller than 40kDa.

3.3.3 Separation Efficiency and Resolution

Separation efficiency and resolution are two key metrics that are necessary for evaluating any electrophoretic separation. Based on subsets of data gathered on the BFPS and BPL separations, some generic statistics have been compiled concerning the resolution and efficiency of the SDS–PAGE based separations (see Tables 3.9, 3.11, and 3.10). For the purposes of comparison, Table 3.8 has been

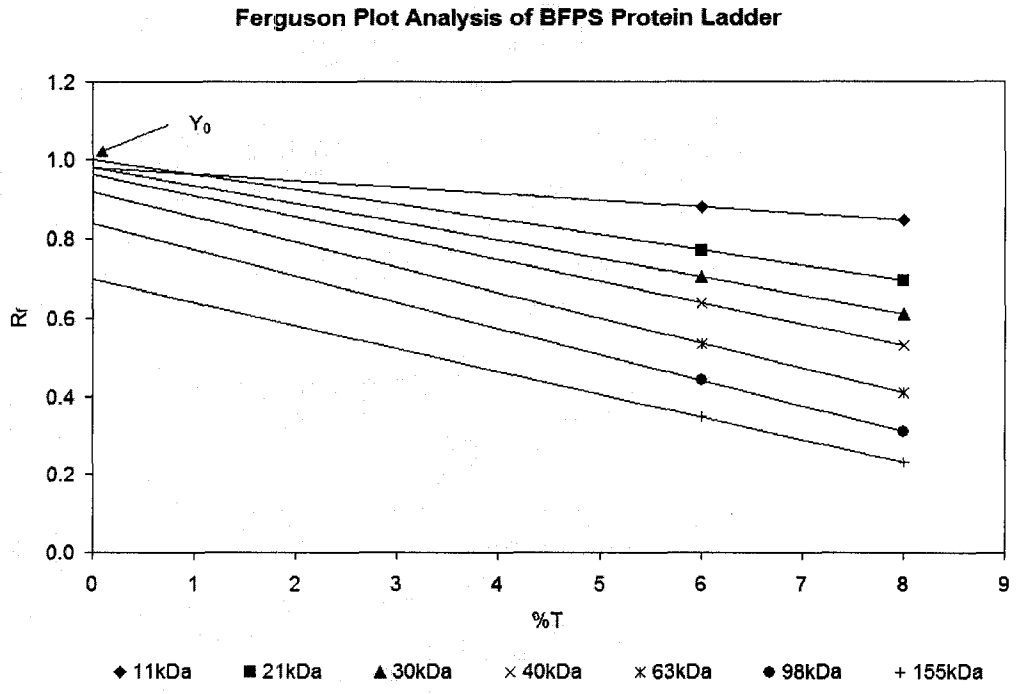

Figure 3.13: A Ferguson plot constructed from data gathered from separating the BFPS at 230V/cm. Detection for these separations was conducted at 10mm in $\%T = 6\%$ and $\%T = 8\%$ polyacrylamide gels. This plot illustrates that the larger proteins (63, 98, and 155kDa) in the BFPS were not adhering strictly to Ogston migration behaviour because their slopes (K_R values) are nearly parallel and are not proportional to MW and their Y_0 values are not equal to one [61]. The proteins that seem to be obeying Ogston migration mechanisms (11, 21, 31, and 40kDa), have K_R values that increase along with protein size and have Y_0 close to one. According to Westerhuis [61] and Guo [62], Ferguson plot curves would be parallel for SDS–denatured proteins that are reptating through a matrix. Although separations in more gel concentrations would be needed to reach conclusions about the mode of large proteins' migration behaviour at high electric field strengths, these results serve to support the data presented in Figure 3.12 and indicate that protein migration did not strictly adhere to the Ogston regime. In addition, the use of Ferguson plots for the determination of retardation coefficient values may not be a valid exercise in these gels due to the non–Ogston migration behaviours.

Author (Year)	Number of Proteins Detected	MW Range of Detected Proteins (kDa)	N/m (10^3)	Additional Notes
Bousse [44] (2001)	8	14.4 – 200	5600 – 9600	Non–covalent on–chip labeling
Hatch [45] (2006)	4	14 – 66	8.3 – 309	On–chip protein pre–concentration
Han [9] (2004)	6	20.1 – 205	150 – 400	–
Herr [26] (2004)	5	6.5 – 39	400	–
Nagata [46] (2005)	3	21.5 – 166	38 – 620	–
Nagata [14] (2005)	8	5.7 – 116	97 – 1350	–
Nagata [47] (2005)	3	21.5 – 116	90 – 2300	–

Table 3.8: Examples of published microfluidic separations of SDS–denatured proteins separated in microfluidic chips.

populated with data from other microfluidic SDS–denatured protein separations.

When looking at N/m values, separations of the BFPS ladder averaged approximately $10^6 N/m$ in both the $\%T = 6\%$ and $\%T = 8\%$ gels (see Tables 3.9), while separations of the BPL ladder averaged $3.4 \times 10^5 N/m$ in $\%T = 6\%$ gels. These values are comparable or superior to many of the values noted by the publications cited in Table 3.8. Only values reported by Bousse *et al.* are higher. In this case, Bousse *et al.* attribute the increase in resolution to the use of non–covalent labeling techniques that reduce heterogeneous labeling, and thus peak broadening [44]. Bousse *et al.* claim that variable quantities of covalently attached fluorophores (i.e. hetergeneous labeling) lead to peak broadening by creating a larger mass range for a given protein species. This technique, in which dye molecules were incorporated into the separation buffer, also requires post–column dilution of SDS to permit detection of the proteins. Background fluorescence caused by non–covalent attachment of the dye to SDS micelles resulted in significant levels of background noise in the absence of the SDS dilution step. Post–column SDS dilution was achieved by applying an electrical current to channels that intersect on either side of the separation channel. This confines the SDS to the center of the channel where it was left to diffuse within the post–column separation buffer. The diffusion takes place over several hundred milliseconds and results in dilution of the SDS. With BPL separations, such a dilution step was unnecessary because ATTO–TAG FQ only fluoresces when covalently bound to a primary amine.

In terms of resolution, it is more difficult to compare BFPS and BPL separation results with published values. Only Herr *et al.* have published values for resolution

Protein Size (kDa)	Mean N/m (10^3) ($\%T = 6\%$)	Mean N/m (10^3) ($\%T = 8\%$)
11	1484 ± 60	1008 ± 263
21	687 ± 111	1034 ± 239
30	200 ± 11	681 ± 199
40	297 ± 29	882 ± 220
63	456 ± 58	663 ± 158
98	577 ± 58	905 ± 137
155	689 ± 75	1721 ± 153

Table 3.9: Theoretical plate per meter values (mean $\pm$ standard error) calculated for two sets of separations of the BFPS ladder in different polyacrylamide gel concentrations. The separations in the $\%T = 6\%$ gel ($n = 11$) were conducted in a single chip at electric field strengths of 230V/cm to 460V/cm. The separations in the $\%T = 8\%$ gel ($n = 6$) were conducted in a single chip at electric field strengths of 230V/cm and 460V/cm.

Protein Size (kDa)	Mean N/m (10^3)
10	1135 ± 92
15	742 ± 128
20	49 ± 17
25	208 ± 19
30	297 ± 48
40	85 ± 59
50	426 ± 32
60	118 ± 28
70	61 ± 59
80	155 ± 40
90	277 ± 28
100	84 ± 81
120	215 ± 110
160	535 ± 120
220	670 ± 229

Table 3.10: Theoretical plate per meter values (mean $\pm$ standard error) calculated for separations of the BPL ladder. The separations were conducted in a $\%T = 6\%$ gel ($n = 32$) in a single chip at electric field strengths of 230V/cm.

Protein Size (kDa)	R_s for $\%T = 6\%$	R_s for $\%T = 8\%$
11	1.98 ± 0.08	2.47 ± 0.10
21	1.47 ± 0.06	1.98 ± 0.08
30	0.79 ± 0.03	1.39 ± 0.08
40	1.18 ± 0.05	1.94 ± 0.09
63	2.02 ± 0.10	2.73 ± 0.12
98	2.60 ± 0.16	2.64 ± 0.19
155	2.92 ± 0.20	2.76 ± 0.25

Table 3.11: Resolution values (mean $\pm$ standard error) for protein peaks from the same data sets assessed in Table 3.9. Resolution values were calculated by averaging the calculated resolution for each peak in relation to each of its two adjacent peaks. The peaks for the 11kDa and 155kDa proteins only have one adjacent peak, so no average value needs to be calculated. Peak bandwidth was calculated by relating the full–width half maximum ($\Delta t_{1/2}$) to the base width (BW) of a Gaussian curve. $BW = 6\sigma$, $\Delta t_{1/2} = 2.35\sigma$ [26], therefore, $BW = 2.55\Delta t_{1/2}$.

in microfluidic SDS–PAGE based separations [26]. For a separation of five proteins, ranging in size from 6.5kDa to 39kDa, resolution values averaging 4.1 were reported for detection at 4mm. While these values are greater than those shown for the BFPS separations (detection at 10mm) in Table 3.11, there are a few key reasons for this. First, Herr *et al.* treated the peak's full–width half maximum (2.35σ) as the peak bandwidth, whereas the values in Table 3.11 resulted from using a peak bandwidth of six standard deviations (6σ) of the peak. Secondly, Herr *et al.* do not calculate the resolution of adjacent protein peaks, but rather the resolution between the second (14.2kDa) and fifth (39kDa) protein peaks. In order to perform a better comparison, results from a BFPS separation (detection at 3mm) were assessed for the resolution between the 11kDa and 40kDa protein peaks. When using the same resolution formula as Herr *et al.*, the resolution between these two peaks was found to be approximately 11.8 ± 1.5 (mean $\pm$ standard error, $n = 6$) in $\%T = 8\%$ gels (no BPL separations in $\%T = 6\%$ gels were performed with detection conducted at 3mm). This represents a nearly three–fold improvement in resolution beyond Herr *et al's* results.

Given that the separation systems were very similar, it is possible that the nature of the detection instrumentation played a role in the resolution differences. A confocal system was used in this work, while a CCD was used by Herr *et al.* [26]. However, with the modest number of details available on their system, it is difficult to compare performance. Beyond differences in detection equipment, it is also possible that the more porous nature of the gels used in the AML actually played a role. Herr *et al.* note that their $\%T = 6\%$ gels performed better than their $\%T = 8\%$ gels ($R_s = 4.6$ versus $R_s = 3.6$ respectively), and attribute this to less band broadening resulting from of the lower sieving power of the $\%T = 6\%$ gels [26]. In observations made in the AML, a reduction in gel pore size typically improved res-

olution (see Table 3.11). Only the resolution of the largest protein's (155kDa) peak experienced an insignificant reduction. Another possibility includes the presence of increased Joule heating due to the higher electric fields employed by Herr *et al.*. This, however, is also unlikely because they found that they had poorer separation performance with electric field strengths comparable to those used in this work. They also used microfluidic channels with very similar dimensions, meaning that differences in heat transfer away from the channel would be relatively similar. Beyond this, it is difficult to speculate what differences may have led to this improvement in performance. The effects of differences in running buffers and other operating parameters are difficult to quantify without direct experimental results.

Although comparisons on the effects of Joule heating and electric field strength are difficult to conduct when referencing others' work, an evaluation of these operating parameters was possible with the data gathered in BFPS separations. In particular, Van Deemter plots proved to be useful tools in evaluating the detected protein peaks. Traditionally used in applications of chromatography, Van Deemter plots can also be used to describe the dependency of theoretical plate height on migration velocity in electrophoresis [63]. Plate height (H) is easily calculated by dividing the detection distance by the theoretical number of plates (see Equation 3.6). These plots also attempt to quantify the effects of different causes of peak broadening, also known as band broadening or dispersion. As previously noted in Section 3.1.4, plate height is a reflection of band dispersion, also known as variance (σ). A larger plate height indicates greater dispersion. Characteristically, there are four main contributors to band dispersion in capillary electrophoresis described the Van Deemter equation (see Equation 3.15). These are injection parameters (i.e. initial plug width) (A), longitudinal diffusion (B), analyte adsorption (C_1), and temperature (C_2) [63, 64]. When combined with the migration velocity (v) of the analyte, the Van Deemter equation [63] is:

$$H = A + \frac{B}{v} + (C_1 + C_2)v \tag{3.15}$$

The A term, is largely governed by the initial plug width, which in the case of the separations conducted in this work is defined by the approximate width of the injection channel. As one would expect, analytes migrating at a slower velocity will be more susceptible to longitudinal diffusion (B), which increases with time [64]. On the other hand, analytes migrating at higher velocities are more susceptible to band broadening due to analyte adsorption to channel surfaces. This is reflected in the C_1 term. Compared to slower moving analytes, the impact of the duration of analyte adsorption and desorption processes is proportionally larger when analytes are moving quickly [63]. Higher analyte velocity is often achieved by increasing the electric field strength, and thus, the susceptibility of the channel to Joule heating. Joule heating causes radial temperature gradients to form in the channel as cooling at the surface of the capillary counteracts the Joule heating of the material within the capillary [65]. The temperature distribution typically takes on a parabolic shape

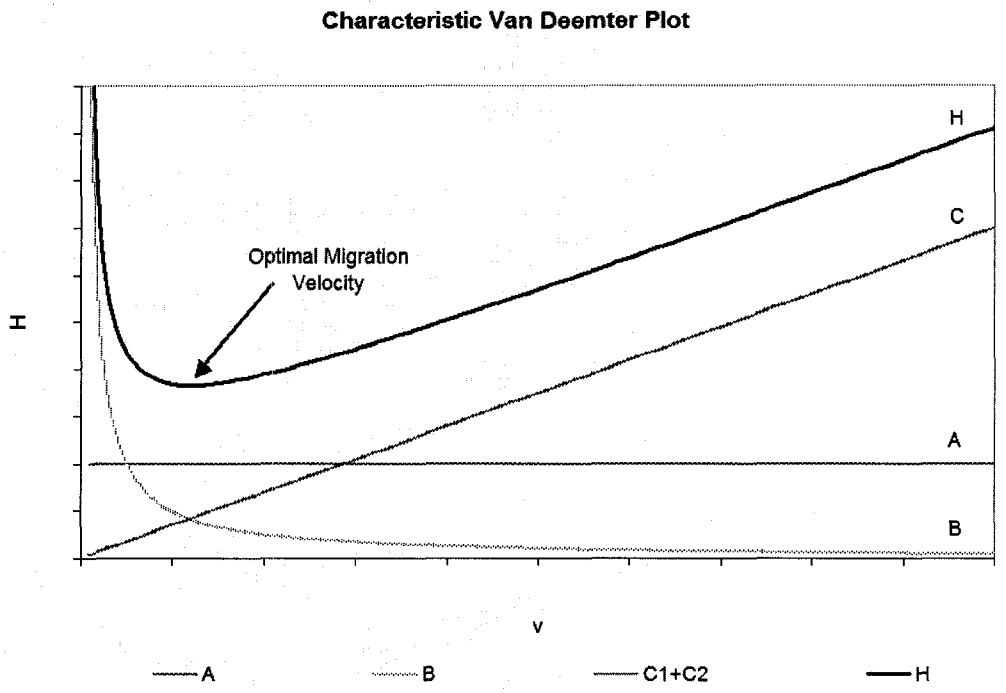

Figure 3.14: This plot is an example of a characteristic Van Deemter plot and was created using artificial data for the purpose of demonstration. Plate height, as a function of migration velocity (v), is dependent on injection parameters (A), longitudinal diffusion (B), analyte adsorption (C_1), and temperature (C_2) [63, 66]. When incorporated into the Van Deemter equation, the following curve (H) emerges.

with the coolest temperatures being along the capillary wall. Temperature influences electrophoretic mobility and results in a radial distribution of mobility along the temperature gradient [64]. This is reflected in the C_2 term. Equation 3.15 results in the characteristic curve seen in Figure 3.14. The minimum of the curve (minimum plate height) indicates the optimal migration velocity, since this point represents the best separation efficiency.

Data on the BFPS separations conducted at different electric field strengths permitted Van Deemter plot analysis of the SDS–PAGE protein separations. The Van Deemter plots for the BFPS separations in Figure 3.15 were constructed from five consecutive separations conducted at electric field strengths between 230V/cm and 415V/cm. As Figure 3.15 illustrates, the Van Deemter plots for all of the proteins are reasonably flat. This indicates that the band broadening contributions of Joule heating (C_2) and adsorption of analytes to the wall (C_1) are relatively non–existent. It is believed that Joule heating was minimised because of the efficient cooling afforded by the microfluidic channels' high surface area–to–volume ratio. Analyte wall–adsorption was reduced by the permanent LPA coating applied to the channel walls. Adsorption of analytes to capillary walls has been shown to significantly

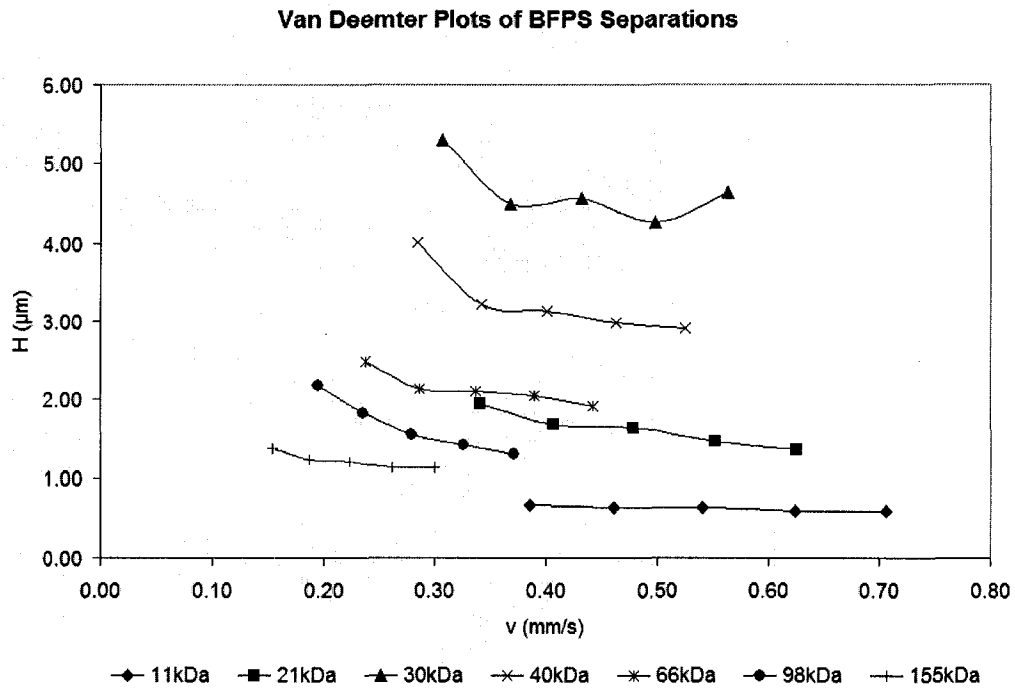

Figure 3.15: These plots demonstrate the effect of electric field strength (i.e. migration velocity (v)) on separation efficiency. The separations ($n = 5$) were conducted consecutively at electric field strengths of 230V/cm, 276V/cm, 322V/cm, 368V/cm, and 415V/cm. Detection of the proteins was carried out at a distance of 10mm. As the curves demonstrate, longitudinal diffusion is minimised (slight negative slope in curves at $v \leq 0.4$mm/s), and Joule heating and analyte wall–adsorption are kept to a minimum (flat curves at $v \geq 0.4$mm/s). It is unknown what the effects of using electric fields outside of the 230-415V/cm range would be. Further experimentation would be required to see if Joule heating would have a greater effect at higher fields and if longitudinal diffusion would be more pronounced at lower fields.

affect plate height [63], so it is expected that the analyte–wall interactions in the separations presented in this work are suppressed to a point such that they did not adversely affect separation efficiency. The relatively flat plots also indicate that longitudinal diffusion (B) had a small effect at these electric field strengths. It is only visible as a slight slope in the plots at migration velocities below 0.4mm/s. Palonen *et al.* state that if migration velocity is high enough, longitudinal diffusion becomes negligible and plate height becomes largely dependent on injection plug length [63].

Although the performance of the BFPS and BPL separations was on par with published results, an increase in the baseline fluorescence level between peaks was a problem encountered with both ladders. It had a particularly negative impact on the resolution and separation efficiency of smaller peaks and peaks located in

close proximity to more dominant peaks in the BPL separations (see Figure 3.9). The presence of an excess of labeling reagents was initially investigated as a cause, however this was largely discounted for numerous reasons. First of all, unbound (i.e. excess) ATTO–TAG fluorophores do not fluoresce. Although the fluorescence enhancement of bound versus unbound ATTO–TAG FQ has not been quantified in published works discussing development of the fluorophore [54], subsequent points show that this was not likely a factor. Secondly, separations incorporating reduced labeling reagent concentrations produced inconclusive results. Also, the presence of a free–label peak meant that the majority of fluorescent ATTO–TAG fluorophores attached to buffer amines arrived before the protein peaks. Finally, BFPS separations (labeled by the supplier using an optimised protocol) exhibited similar issues.

Because of these findings, another possibility was explored. When a series of separations was conducted, a rise in baseline fluorescence was most present in the intermediate separations during the series. This will be further addressed in Section 3.3.4, but in general, the total protein concentration present in the injection channel varied over a series of consecutive injections and separations. From this, it was determined that excess protein available for injection into the separation channel resulted in constructive interference amongst peaks which decreased the separation performance.

3.3.4 Sensitivity and Limits of Detection

Although no direct measurement of the system's sensitivity or limit of detection (LOD) were conducted, extrapolations of existing data and the availability of data from similar applications provided a reasonable estimate of the system's potential. Actual values were not pursued because the nature of the applications this work is concerned with (see Chapter 4) do not require the detection of proteins at concentrations approaching the projected detection limits of the system.

By using peak amplitude as a estimation of relative protein concentration and calculating the signal–to–noise ratio (using Equation 3.9) of peaks in electropherograms, estimates of the system's LOD could be attained. The LOD was defined by a critical signal–to–noise ratio of three [26]. Because separations of 'real–world' proteins in Chapter 4 used ATTO–TAG FQ as a fluorescent label, only LOD values for the BPL separations were estimated. Based on data gathered from a series of BPL separations, the curve in Figure 3.16 was established. Estimated concentrations for the system's LOD (mean $\pm$ standard error) range from 22 $\pm$ 3nM for the 10kDa protein to 515 $\pm$ 78pM for the 220kDa protein. Other data presented in Chapter 4 exhibits similar values.

Keeping in mind that these figures are only estimates, it is also crucial to take into account the optical inefficiencies in the excitation and detection of the ATTO–TAG FQ fluorophores with the Micralyne μTk. Based on data from the ATTO–TAG FQ excitation and emission spectra (see Figure 3.5), it is estimated that excitation efficiency was approximately 37%, while only 8.5% of emitted light was detected.

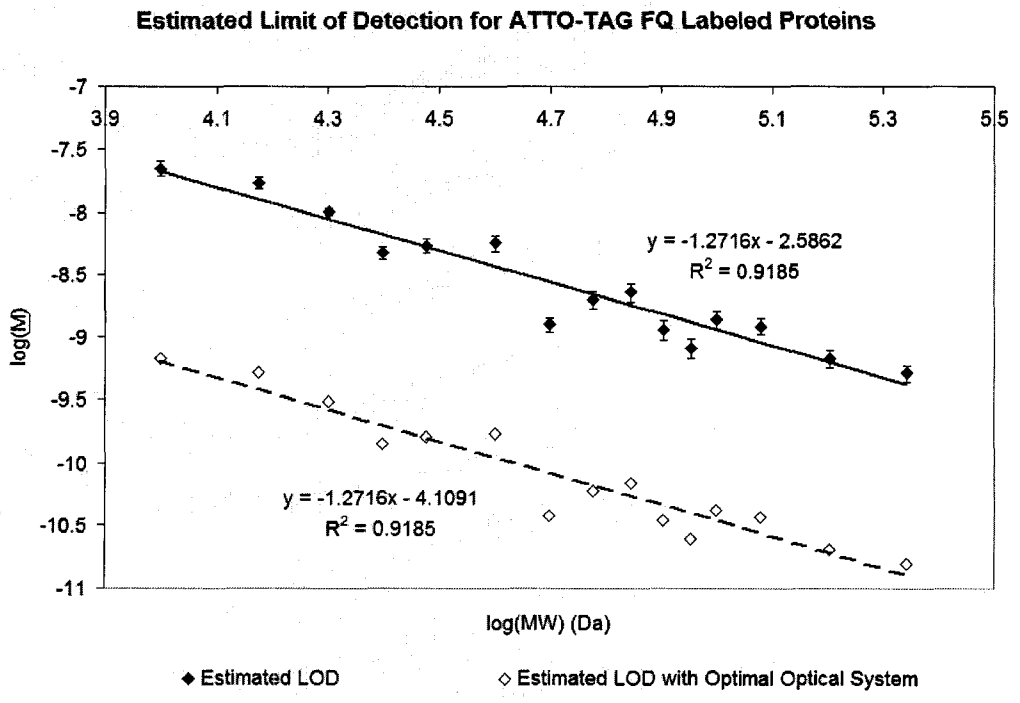

Figure 3.16: These estimates of the system's limit of detection are based on data gathered from ten consecutive ($n = 10$) separations of the on–chip ATTO–TAG FQ labeled BPL performed on a single chip. The error bars represent the standard error. Baseline noise was sampled over a ten second separation period prior to the arrival of the free–label peak. This data was used to determine the values needed for the SNR calculation. Estimates for a limit of detection with improvements made to the optical system are based on knowledge of inefficiencies in the excitation and detection of ATTO–TAG FQ fluorophores. It is estimated that the combined excitation and detection efficiency of the current Micralyne μ Tk is only 3%, due to mismatches in excitation wavelength and fluorescence emission filtering.

Excitation efficiency was calculated by comparing the relative intensity of the excitation spectrum at 532nm and 489nm. Detection efficiency was calculated by comparing the area under the emission curve for a notch filter between 563 and 573nm with the total area under the emission curve. This method of calculating optical efficiency is believed to be adequate for the purposes of this thesis, because in many cases the excitation spectrum of a fluorophore is similar to its adsorption spectrum [67]. Under these circumstances, the emission spectrum is said to be independent of the excitation wavelength [68] and the intensity of the emission spectrum is proportional to the excitation efficiency [69]. Thus, by multiplying the excitation and detection efficiencies, an approximate overall efficiency of 3% was obtained.

Optimising the excitation wavelength could result in a nearly three–fold improvement in signal levels, while better matching of the detection filters may result in a signal improvement of approximately ten–fold. Therefore, an ideal increase of approximately thirty–fold in the signal–to-noise ratio may be possible with better matching of the optical system to the ATTO–TAG FQ fluorophore. It is possible that these improvements may also lead to higher noise levels, but because unbound ATTO–TAG FQ fluorophores do not fluoresce, this increase would governed by the limited number of fluorophores bound to Tris in the separation buffer. While the LOD claims are not confirmed in this work, comparable limits of detection (70–290pM) have been achieved with SDS–denatured proteins labeled with ATTO–TAG FQ in a capillary electrophoresis separation [55].

Separations of SDS–denatured proteins in microfluidics have yielded similar estimates of detection limits, albeit with the use of extra sample processing or off–chip preparation. Bousse *et al.* attained a limit of detection of 30nM using SYPRO Orange as a fluorescent label. However, this separation required on–chip dilution of SDS to reduce the background noise caused by fluorophores bound to SDS micelles [44]. Hatch *et al.* attained an extremely low detection limit of 50fM, but this required an on–chip sample pre–concentration (10,000x) step lasting a total of thirty minutes. The simplicity of the method demonstrated in this work, coupled with the estimated limit of detection (even without optical system improvements), places it among state–of–the–art techniques (see Figure 3.17).

The main contributors to SNR variability are inherently changes that occur to the baseline noise and protein peak amplitude over time. Figures 3.18 and 3.19 show the changes in baseline noise levels and peak signal over a series consecutive separations. Noise is seen to increase over the series of separations and is most likely due to residual fluorophores labeling running buffer and contaminating the separation channel. As noted in the SDS–PAGE protocol (see Section 3.2.2), the baseline fluorescence level could be restored after a series of separations by electrophoretically flushing the channels with fresh running buffer. Peak signal, on the other hand, has a more bell–shaped curve over a series of separations. If peak signal is once again taken as a measure of protein concentration, then Figure 3.19 shows that the protein concentration at in the injection channel increases to a maximum

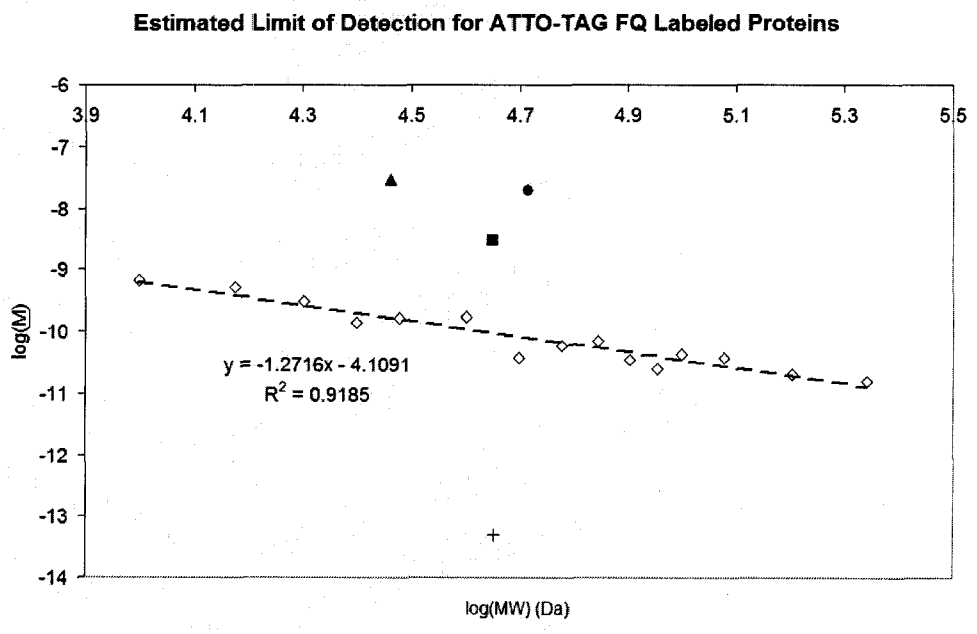

Figure 3.17: This plot provides a comparison of the limit of detection values published for microfluidic separations of SDS denatured proteins separated in microfluidic chips [14, 26, 44, 45] with the projected optimal limit of detection for the system used in this work (see Figure 3.16).

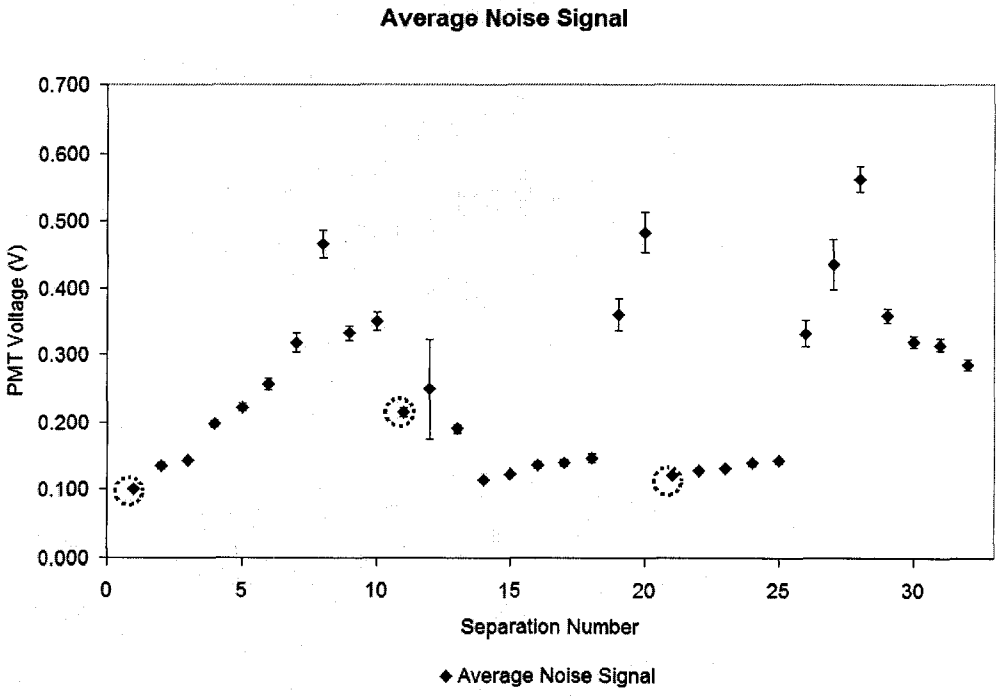

Figure 3.18: This plot illustrates the changes that occurred in the baseline fluorescence level (noise level) over a series of thirty–two separations of the BPL. The electric field strength used for these separations was 230V/cm and detection was conducted at 10mm. Three separate sample loads were conducted during these separations, and the first separation from each load is circled. As one can see, the electrophoretic flushing between loads permits extended reuse of the chip by lowering the noise level back to original values. The error bars indicate the standard deviation of the noise, which is used in the SNR calculation

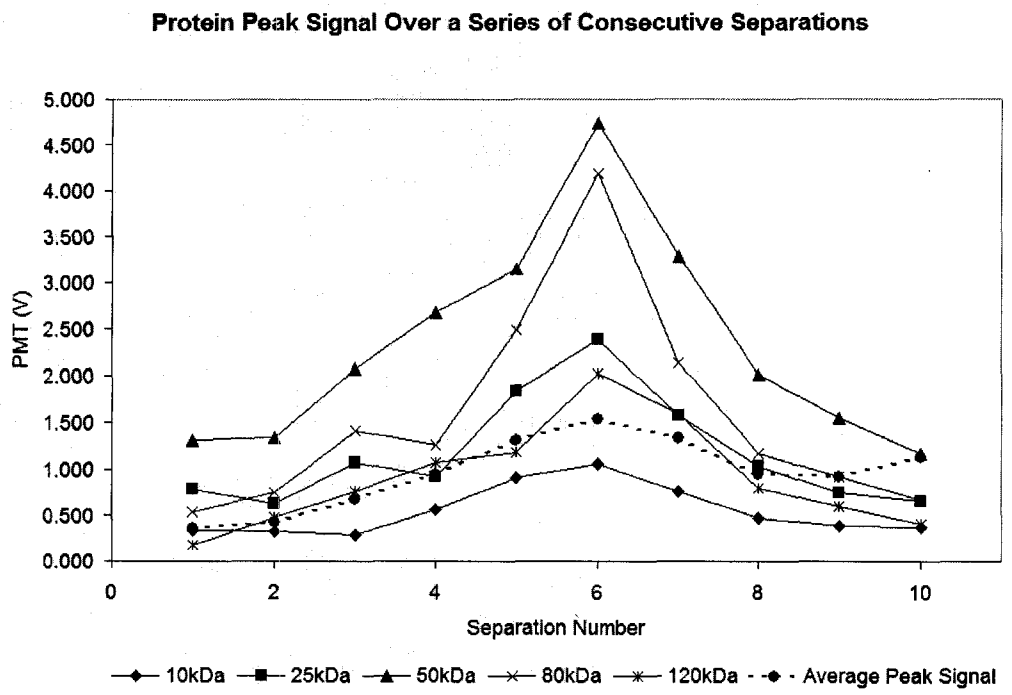

Figure 3.19: The plot illustrates the protein peak signal amplitudes of a few proteins in the BPL ladder over the course of ten consecutive separations. Injection duration for each separation was ten seconds at 215V/cm. Separations were conducted at 460V/cm, and detection was performed at 10mm. It demonstrates that the amplitudes of the peaks of each protein generally increase and decrease in a relatively proportionate fashion. This likely represents a gradual increase in protein concentration in the injection channel over time, followed by a gradual decrease. Refilling the sample well with new sample permitted signal levels to increase once again, indicating that a reduction in the amount of sample available for injection was likely the cause for the decrease. The average peak amplitude was obtained by surveying the amplitude of all the peaks in the BPL ladder over the course of the same ten separations. If peak amplitude is used as a measure of the protein concentration in the separation channel, the maximum concentration was present in the sixth separation.

Protein Size (kDa)	Mean Normalised Signal
10	0.034 ± 0.002
15	0.027 ± 0.002
20	0.043 ± 0.002
25	0.077 ± 0.003
30	0.058 ± 0.003
40	0.039 ± 0.002
50	0.192 ± 0.007
60	0.085 ± 0.003
70	0.050 ± 0.002
80	0.104 ± 0.004
90	0.134 ± 0.005
100	0.057 ± 0.002
120	0.055 ± 0.002
160	0.070 ± 0.004
220	0.058 ± 0.004

Table 3.12: If data is gathered over a series of separations, a characteristic protein peak amplitude curve is obtained for each protein. When peak signal is taken as a measure of protein concentration, it is clear that over the course of several separations the protein concentration available for separation gradually increases, reaches a peak, and subsequently decreases (see Figure 3.19). As such, if the protein peak signal is normalised to the sum of the peak signals (a rudimentary indicator of total protein concentration) in the separation in which the protein is detected, the repeatability of peak signal is fairly good. The above table gives the statistics (mean $\pm$ standard error) for a series of thirty–two ($n = 32$) separations of the BPL ladder performed in a single chip. The average RSD of all of the peak signals was 26.5%. Three separate sample loads were conducted during these thirty–two separations.

value, then subsequently decreases. Consequently, determining the repeatability of peak signal is only useful if it is normalised to the total protein concentration (approximated by the sum of the protein peak signals) available for injection into the separation channel. Table 3.12 shows that standard error values for the protein amplitudes normalised to the estimated total protein concentration are on average less than $\pm 5\%$.

3.3.5 Gel Quality and Durability

One of the key advantages of using a cross–linked polyacrylamide gel as a sieving matrix in microfluidic channels is the ability to reuse the gel multiple times. To the best of our knowledge, little data has been published on the durability and stability of such gels, with only Herr *et al.* briefly mentioning that approximately 500 separations had been performed on a single chip. While none of the gels discussed in this work were reused to that extent, many gels were 'retired' after logging hours

Gel Concentration (%)	6	8	10	Overall
% Gels that Produced Successful Separations (%)	63	50	0	52
% Gels that had Current Instability (%)	31	40	67	38
% Gels that Experienced Poor Performance* (%)	6	10	33	10

Table 3.13: This table shows the proportion of successfully polymerised gels that were used successfully and the proportion of gels that exhibited gel failure or poor gel performance. Of the chips that performed poorly, no overwhelming mode of failure or deficiency was observed. Typically these gels suffered from poor resolution and/or poor sensitivity, neither of which could be attributed to any visually apparent flaws or deficiencies in operating parameters such as injection or separation current.

of separation time even though they had not failed. In many cases, gels were retired in favour of conducting new experiments. Previous discussions have shown that repeatability in the gels over time was good and on par with other state–of–the–art applications. Because chips were regularly cleaned and new gels were polymerised in the channels, no long–term (greater than one month) studies of performance stability or maximum storage lifetime were conducted. In addition, gels were not stored for periods longer than one month to ensure that buffer freshness was preserved. The discussion presented in preceding sections generally involved data gathered on individual gels or batches of gels from experiments conducted over the course of a week to two weeks. As such, the following section discusses troubleshooting issues encountered during those time frames.

As previously discussed, the successful polymerisation yield for polyacrylamide gels was approximately 52% (see Chapter 2). Out of the gels that were successfully polymerised, approximately 52% performed well during separations, leading to an overall yield (percentage of chips used in successful separations) of approximately 27%. Table 3.13 summarises the modes of failure for gels that were successfully polymerised.

As Table 3.13 shows, the majority of gel failures occurred due to some presence of current instability. Current instability came in two forms; catastrophic failure, and gradual current degradation. The former was relatively easy to characterise, as it presented itself as an abrupt decrease in current due the formation of voids (complete mechanical failure) in the channel during the application of an electric field. The voids were similar in appearance to those discussed in Chapter 2, but were typically more elongated and were oriented along the direction of the electric field. Figure 3.20 shows an image of one of the voids formed during the application of an electric field.

While this mode of failure was present in gels that had high numbers of successful separations (hours of applied electric fields between 140V/cm and 460V/cm), some gels seemed particularly prone to this type of failure (i.e. failure within minutes of applying an electric field). It is believed that this may have been due to incomplete polymerisation (mechanical weakness) or the aging of polymerisation

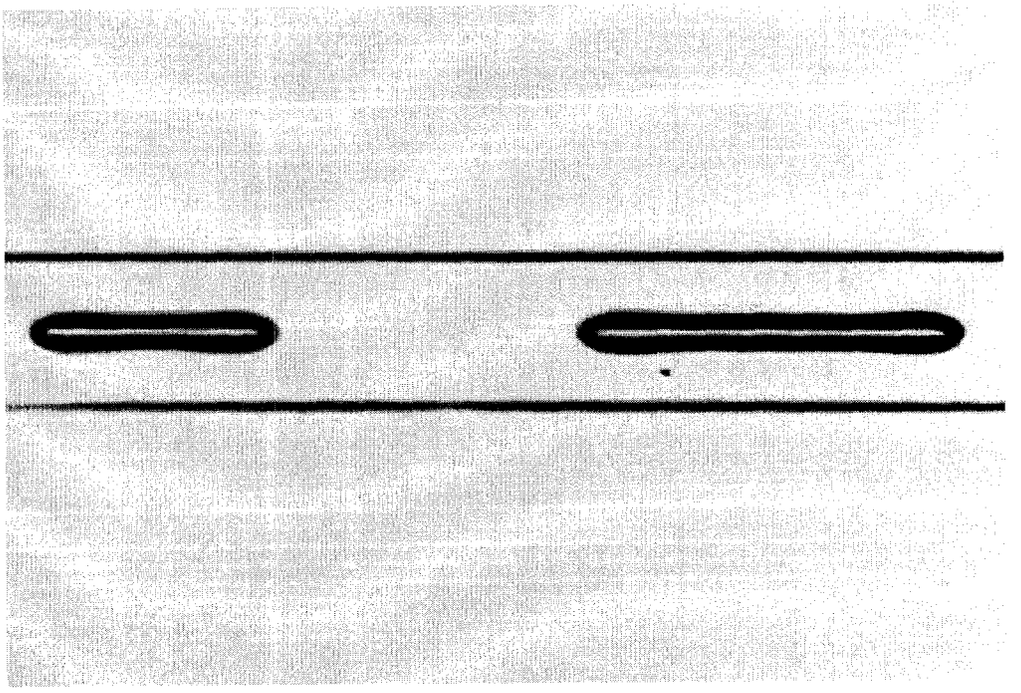

Figure 3.20: An image of a void that formed in a $\%T = 6\%$ polyacrylamide gel during the application of an $230\mathrm{V/cm}$ electric field. These voids were similar in appearance to those that formed during gel polymerisation (see Figure 2.9), but typically had a more elongated shape that was oriented along the direction of the electric field.

reagents. Reagent aging and degradation may have also contributed to the presence of the incomplete polymerisation. Herr *et al.* noted that gels that were not completely polymerised often experienced 'tearing' when they were subjected to an electric field [26]. Because characterisation of these effects was not pursued, the exact mechanisms contributing to catastrophic gel failures are unknown. Coincidentally, these gels were often prepared in the same batch as gels that were more prone to the second mode of current instability.

Gradual current degradation was also relatively easy to characterise, as it manifested itself as a reduction in injection and/or separation current over the course of one to several separations. Figure 3.21 compares current levels in 'good' gels with current levels in gels experiencing current degradation. While there was variability amongst current levels in different 'good' gels (e.g. separation currents ranged between 12μA to 20μA at 230V/cm), current stability over multiple separations was present.

The initial hypothesis for the current degradation centered on buffer age or contamination. In order to test this hypothesis, new stock solutions of buffer were obtained and tested in the gels that had exhibited current degradation. The new buffer did not improve current stability. New gels were then polymerised with the new buffer and tested for current stability. Once again, currents continued to exhibit degradation over time. After extensive troubleshooting, new gel reagents were ordered (acrylamide and bis–acrylamide) as a last resort. Gels produced using the new buffer and gel reagents demonstrated stable currents, similar to the currents of the good quality gel seen in Figure 3.21. These results revised the hypothesis, and placed the focus for the cause of current degradation on aging of the acrylamide and bis–acrylamide reagents. As mentioned in Chapter 2, old gel reagents seemed to contribute to reduced polymerisation yield, so it was not considered unreasonable to believe aging solutions could have other effects on gel characteristics and separation performance. Unfortunately, research discussing this phenomenon is relatively rare and generally limited to periods during the early development of capillary electrophoresis techniques.

Among literature found covering this phenomenon, the observed development of an ionic–depletion region at the gel–buffer interface at the end of the capillary was often cited as a primary cause for gradual current decline during electrophoresis [70–73]. The development of an ionic–depletion region is attributed to an imbalance in transference number at the gel–buffer interface [73]. Transference number is the fraction of total current carried by a type of ion in an electrolytic system [74]. An ionic depletion region forms due a discontinuity of the transference number caused by the change in the resistance to flow at the gel–buffer interface. This results in a change in the ionic concentration at the interface, and if the conditions are right, the formation of a depletion region follows [73]. The development of the depletion region, leading to an increase in the resistivity of the capillary, has been attributed to both sample–induced and sample–independent effects. Since current degradation was still present in the absence of any sample, sample–induced effects

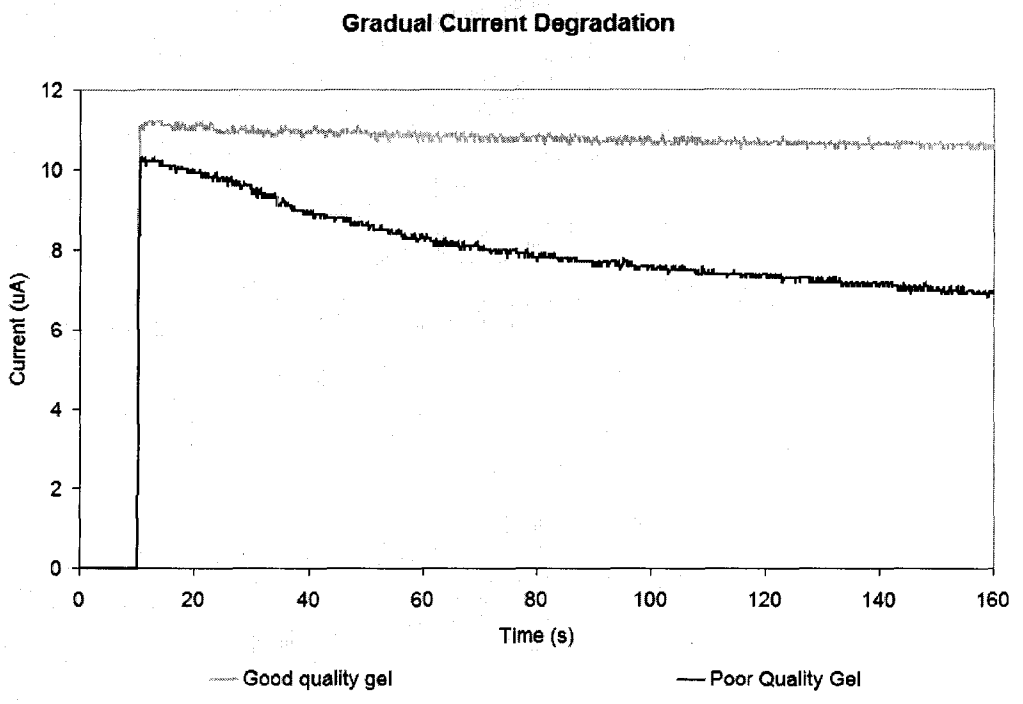

Figure 3.21: The plot shows the separation currents for two gels in 4–Port Mini chips with separation field strengths of 230V/cm. Each gel attempted a separation of the BPL in a sodium borate sample buffer with 1XNGB used as the running buffer. The good quality gel produced a stable current that decrease very little over the course of the 150s separation. On the other hand, the poor quality gel produced a current that was unstable and gradually degraded over time. This problem was not confined to the separation channel, but current degradation in the injection channel was difficult to detect over the typically short injection periods (e.g. 10-20s). If injection times were lengthened, the same degradation of current was observed in the injection channel at similar electric field strengths (215V/cm). No visible signs of gel failure, such as void formation, were present.

were ruled out. Sample–independent causes in the cited works included the formation of microscopic bubbles at the interface [70], polymer age, and buffer composition [73]. Unfortunately, Figey *et al's* study on polymer age did not address the age of polymer reagents, but rather the age of the polymer (LPA) once it had been polymerised. That being said, they did attribute differences in the formation of the depletion region to molecular degradation of the polymer itself [73]. Because these effects were not the focus of this work and were primarily viewed as a barrier to future development of the technique, the causes for the current anomalies were not explored further. While polymer reagent age did seem to play a role in the current instabilities, further characterisation of the instability and the underlying mechanisms would be required to develop links with well–established phenomena. Because of a lack of available literature, the effect of SDS on this phenomenon is not known at this time.

3.4 Conclusions

Based on the discussion in this chapter, it is clear that extensive development and characterisation of the SDS–PAGE protein separations were achieved. The performance of these separations is on par with the state–of–the–art or exceeds it in many areas. It was shown that the molecular weight curves were highly linear, the separation efficiency and resolution were representative of state–of–the–art performance, and the system's limit of detection was equally impressive. The novel and simple on–chip protein labeling procedure also expands the applicability of the techniques discussed in this chapter. Characterisation of protein migration mechanisms and polyacrylamide gel characteristics will also aid in future application of these techniques. Finally, the characterisation of protein migration behaviours and separation efficiency performance (i.e. Van Deemter analysis) provided insight to phenomena that are not often noted in published literature. Together, these developments represent a clear advance in the knowledge required to use these techniques effectively.

Bibliography

[1] M. J. Sax. Report for ECE 750: Metabolomic analysis techniques and miniaturization (see supplementary material on DVD, "ECE750TermPaper Metabolomic Analysis.pdf").

[2] A. T. Andrews. *Electrophoresis: theory, techniques, and biochemical and clinical applications.* Oxford University Press, New York, 2nd edition, 1986.

[3] C. W. Kan, C. P. Fredlake, E. A. S. Doherty, and A. E. Barron. DNA sequencing and genotyping in miniaturized electrophoresis systems. *Electrophoresis*, 25(21-22):3564–3588, 2004.

[4] V. Dolnik and S. R. Liu. Applications of capillary electrophoresis on microchip. *Journal of Separation Science*, 28(15):1994–2009, 2005.

[5] P. Hawtin, I. Hardern, R. Wittig, J. Mollenhauer, A. Poustka, R. Salowsky, T. Wulff, C. Rizzo, and B. Wilson. Utility of lab-on-a-chip technology for high-throughput nucleic acid and protein analysis. *Electrophoresis*, 26(19):3674–3681, 2005.

[6] S. R. Liu and A. Guttman. Electrophoresis microchips for DNA analysis. *Trac-Trends in Analytical Chemistry*, 23(6):422–431, 2004.

[7] E. M. Abad-Villar, P. Kuban, and P. C. Hauser. Determination of biochemical species on electrophoresis chips with an external contactless conductivity detector. *Electrophoresis*, 26(19):3609–3614, 2005.

[8] Y. Z. Deng, J. Henion, J. J. Li, P. Thibault, C. Wang, and D. J. Harrison. Chip-based capillary electrophoresis/mass spectrometry determination of carnitines in human urine. *Analytical Chemistry*, 73(3):639–646, 2001.

[9] J. Han and A. K. Singh. Rapid protein separations in ultra-short microchannels: microchip sodium dodecyl sulfate-polyacrylamide gel electrophoresis and isoelectric focusing. *Journal of Chromatography A*, 1049(1-2):205–209, 2004.

[10] W. Hellmich, C. Pelargus, K. Leffhalm, A. Ros, and D. Anselmetti. Single cell manipulation, analytics, and label-free protein detection in microfluidic devices for systems nanobiology. *Electrophoresis*, 26(19):3689–3696, 2005.

[11] H. Q. Huang, F. Xu, Z. P. Dai, and B. C. Lin. On-line isotachophoretic preconcentration and gel electrophoretic separation of sodium dodecyl sulfate-proteins on a microchip. *Electrophoresis*, 26(11):2254–2260, 2005.

[12] X. Y. Huang and J. C. Ren. On-line chemiluminescence detection for isoelectric focusing of heme proteins on microchips. *Electrophoresis*, 26(19):3595–3601, 2005.

[13] M. Kato, Y. Gyoten, K. Sakai-Kato, T. Nakajima, and T. Toyo'oka. Analysis of amino acids and proteins using a poly(methyl methacrylate) microfluidic system. *Electrophoresis*, 26(19):3682–3688, 2005.

[14] H. Nagata, M. Tabuchi, K. Hirano, and Y. Baba. Automatic protein separation by microchip electrophoresis using quartz chip. *Chromatography; Journal of Separation and Detection Sciences*, 26(1):23–28, 2005.

[15] B. Yao, G. Luo, L. D. Wang, Y. D. Gao, G. T. Lei, K. N. Ren, L. X. Chen, Y. M. Wang, Y. Hu, and Y. Qiu. A microfluidic device using a green organic light emitting diode as an integrated excitation source. *Lab on a Chip*, 5(10):1041–1047, 2005.

[16] L. M. Pilarski, J. Lauzon, E. Strachan, S. Adamia, A. Atrazhev, A. R. Belch, and C. J. Backhouse. Sensitive detection using microfluidics technology of single cell PCR products from high and low abundance IgH VDJ templates in multiple myeloma. *Journal of Immunological Methods*, 305(1):94–105, 2005.

[17] T. Ito, A. Inoue, K. Sato, K. Hosokawa, and M. Maeda. Autonomous polymer loading and sample injection for microchip electrophoresis. *Analytical Chemistry*, 77(15):4759–4764, 2005.

[18] M. Johirul, A. Shiddiky, R. E. Kim, and Y. B. Shim. Microchip capillary electrophoresis with a cellulose-DNA-modified screen-printed electrode for the analysis of neurotransmitters. *Electrophoresis*, 26(15):3043–3052, 2005.

[19] R. Pal, M. Yang, R. Lin, B. N. Johnson, N. Srivastava, S. Z. Razzacki, K. J. Chomistek, D. C. Heldsinger, R. M. Haque, V. M. Ugaz, P. K. Thwar, Z. Chen, K. Alfano, M. B. Yim, M. Krishnan, A. O. Fuller, R. G. Larson, D. T. Burke, and M. A. Burns. An integrated microfluidic device for influenza and other genetic analyses. *Lab on a Chip*, 5(10):1024–1032, 2005.

[20] P. Taylor, D. P. Manage, K. E. Helmle, Y. Zheng, D. M. Glerum, and C. J. Backhouse. Analysis of mitochondrial DNA in microfluidic systems. *Journal of Chromatography B-Analytical Technologies in the Biomedical and Life Sciences*, 822(1-2):78–84, 2005.

[21] S. H. Lee, S. I. Cho, C. S. Lee, B. G. Kim, and Y. K. Kim. Microfluidic chip for biochemical reaction and electrophoretic separation by quantitative volume control. *Sensors and Actuators B-Chemical*, 110(1):164–173, 2005.

[22] Y. Sun, X. F. Yin, Y. Y. Ling, and Z. L. Fang. Determination of reactive oxygen species in single human erythrocytes using microfluidic chip electrophoresis. *Analytical and Bioanalytical Chemistry*, 382(7):1472–1476, 2005.

[23] M. J. Schoning, M. Jacobs, A. Muck, D. T. Knobbe, J. Wang, M. Chatrathi, and S. Spillmann. Amperometric PDMS/glass capillary electrophoresis-based biosensor microchip for catechol and dopamine detection. *Sensors and Actuators B-Chemical*, 108(1-2):688–694, 2005.

[24] M. Klein. Analysis of molecules in clinical medicine. In J. G. Webster, editor, *Bioinstrumentation*. John Wiley & Sons, Inc., Hoboken, 1st edition, 2004.

[25] J. Khandurina and A. Guttman. Bioanalysis in microfluidic devices. *Journal of Chromatography A*, 943(2):159–183, 2002.

[26] A. E. Herr and A. K. Singh. Photopolymerized cross-linked polyacrylamide gels for on-chip protein sizing. *Analytical Chemistry*, 76(16):4727–4733, 2004.

[27] V. Dolnik. Wall coating for capillary electrophoresis on microchips. *Electrophoresis*, 25(21-22):3589–3601, 2004.

[28] S. Hjerten. High-performance electrophoresis - elimination of electroendosmosis and solute adsorption. *Journal of Chromatography*, 347(2):191–198, 1985.

[29] B. J. Kirby and E. F. Hasselbrink. Zeta potential of microfluidic substrates: 1. theory, experimental techniques, and effects on separations. *Electrophoresis*, 25(2):187–202, 2004.

[30] A. Pallandre, B. de Lambert, R. Attia, A. M. Jonas, and J. L. Viovy. Surface treatment and characterization: Perspectives to electrophoresis and lab-on-chips. *Electrophoresis*, 27(3):584–610, 2006.

[31] S. Ghosal. Fluid mechanics of electroosmotic flow and its effect on band broadening in capillary electrophoresis. *Electrophoresis*, 25(2):214–228, 2004.

[32] P. Kuban and P. K. Dasgupta. Capillary separations. In *Kirk–Othmer Encyclopedia of Chemical Technology*, volume 4, pages 602–647. John Wiley & Sons, Inc., Hoboken, 5th edition, 2002.

[33] D. Belder and M. Ludwig. Surface modification in microchip electrophoresis. *Electrophoresis*, 24(21):3595–3606, 2003.

[34] S. Ullsten, A. Zuberovic, M. Wetterhall, E. Hardenborg, K. E. Markides, and J. Bergquist. A polyamine coating for enhanced capillary electrophoresis-electrospray ionization-mass spectrometry of proteins and peptides. *Electrophoresis*, 25(13):2090–2099, 2004.

[35] L. R. Snyder. Theory of chromatography. In E. Heftmann, editor, *Chromatography, Fundamentals and Applications of Chromatography and Related Differential Migration Methods, Part A: Fundamentals and Techniques*, pages A151–A225. Elsevier Science Publisher B.V., Amsterdam, 5th edition, 1992.

[36] L. D. Bowers, M. D. Ullman, and C. A. Burtis. Chromatography. In C. A. Burtis and E. R. Ashwood, editors, *Tietz textbook of clinical chemistry*. W. B. Saunders, Philadelphia, 2nd edition, 1994.

[37] G. F. Jiang, S. Attiya, G. Ocvirk, W. E. Lee, and D. J. Harrison. Red diode laser induced fluorescence detection with a confocal microscope on a microchip for capillary electrophoresis. *Biosensors & Bioelectronics*, 14(10-11):861–869, 2000.

[38] D. L. Nelson and M. M. Cox. *Lehninger principles of biochemistry*. Worth Publisher, New York, 3rd edition, 2000.

[39] B. D. Hames. An introduction to polyacrylamide gel electrophoresis. In B. D. Hames and D. Rickwood, editors, *Gel Electrophoresis of Proteins: A Practical Approach*, page 290. IRL Press Limited, Oxford, 1st edition, 1981.

[40] L. Savo. *Physicochemical aspects of protein denaturation.* John Wiley & Sons, New York, 1978.

[41] A. Chrambach and D. Rodbard. "Quantitative" and preparative polyacrylamide gel electrophoresis. In B. D. Hames and D. Rickwood, editors, *Gel Electrophoresis of Proteins: A Practical Approach.* IRL Press Limited, Oxford, 1st edition, 1981.

[42] S. Rudge. Electrophoresis. In *Kirk–Othmer Encyclopedia of Chemical Technology*, volume 9, pages 738–758. John Wiley & Sons, Inc., Hoboken, 5th edition, 2004.

[43] P. Menter. Acrylamide polymerization - A practical approach, Bulletin 1156 - Revision E, Bio–Rad Laboratories Ltd., Mississauga, Ontario. Website, 2007. `http://www.bio-rad.com/LifeScience/pdf/Bulletin_1156.pdf`.

[44] L. Bousse, S. Mouradian, A. Minalla, H. Yee, K. Williams, and R. Dubrow. Protein sizing on a microchip. *Analytical Chemistry*, 73(6):1207–1212, 2001.

[45] A. V. Hatch, A. E. Herr, D. J. Throckmorton, J. S. Brennan, and A. K. Singh. Integrated preconcentration SDS-PAGE of proteins in microchips using photopatterned cross-linked polyacrylamide gels. *Anal. Chem.*, 78(14):4976–4984, 2006.

[46] H. Nagata, M. Tabuchi, K. Hirano, and Y. Baba. High-speed separation of proteins by microchip electrophoresis using a polyethylene g glycol-coated plastic chip with a sodium dodecyl sulfate-linear polyacrylamide solution. *Electrophoresis*, 26(14):2687–2691, 2005.

[47] H. Nagata, M. Tabuchi, K. Hirano, and Y. Baba. Microchip electrophoretic protein separation using electroosmotic flow induced by dynamic sodium dodecyl sulfate-coating of uncoated plastic chips. *Electrophoresis*, 26(11):2247–2253, 2005.

[48] Z. R. Zhang, S. Krylov, E. A. Arriaga, R. Polakowski, and N. J. Dovichi. One-dimensional protein analysis of an ht29 human colon adenocarcinoma cell. *Analytical Chemistry*, 72(2):318–322, 2000.

[49] S. Hu, L. Zhang, R. Newitt, R. Aebersold, J. R. Kraly, M. Jones, and N. J. Dovichi. Identification of proteins in single-cell capillary electrophoresis fingerprints based on comigration with standard proteins. *Analytical Chemistry*, 75(14):3502–3505, 2003.

[50] Micralyne. Microfluidic Tool Kit Product Datasheet, Micralyne, Edmonton, Alberta. Website, 2007. http://www.micralyne.com/capabilities/products/toolkit.htm.

[51] Invitrogen Molecular Probes. Spectra – Alexa Fluor 488 goat anti–mouse IgG antibody/pH 8.0, Invitrogen, Carlsbad, California. Website, 2007. http://probes.invitrogen.com/media/spectra/data/11001ph8.txt.

[52] A. J. Huang, Y. Chen, T. Zhu, X. H. Fang, and Y. L. Sun. Simple method for preparing cross-linked polyacrylamide gel-filled capillaries. *Journal of Chromatography A*, 755(1):138–141, 1996.

[53] Y. Baba, T. Matsuura, K. Wakamoto, and M. Tsuhako. A simple method for the preparation of polyacrylamide-gel filled capillaries for high-performance separation of polynucleotides by using capillary gel-electrophoresis. *Chemistry Letters*, (3):371–374, 1991.

[54] S. C. Beale, Y. Hsieh, D. Wiesler, and M. Novotny. Application of 3–(2–furoyl)quinoline–2–carbaldehyde as a fluorogenic reagent for the analysis of primary amines by liquid chromatography with laser–induced fluorescence detection. *Journal of Chromatography*, 499:579–587, 1990.

[55] S. Hu, L. Zhang, L. M. Cook, and N. J. Dovichi. Capillary sodium dodecyl sulfate-DALT electrophoresis of proteins in a single human cancer cell. *Electrophoresis*, 22(17):3677–3682, 2001.

[56] S. Hu, J. Jiang, L. M. Cook, D. P. Richards, L. Horlick, B. Wong, and N. J. Dovichi. Capillary sodium dodecyl sulfate-DALT electrophoresis with laser-induced fluorescence detection for size-based analysis of proteins in human colon cancer cells. *Electrophoresis*, 23(18):3136–3142, 2002.

[57] A. Gerstner, Z. Csapo, M. Sasvari-Szekely, and A. Guttman. Ultrathin-layer sodium dodecyl sulfate gel electrophoresis of proteins: Effects of gel composition and temperature on the separation of sodium dodecyl sulfate-protein complexes. *Electrophoresis*, 21(5):834–840, 2000.

[58] G. Monti, L. De Napoli, P. Mainolfi, R. Barone, M. Guida, G. Marino, and A. Amoresano. Monitoring food quality by microfluidic electrophoresis, gas chromatography, and mass spectrometry techniques: Effects of aquaculture on the sea bass (dicentrarchus labrax). *Analytical Chemistry*, 77(8):2587–2594, 2005.

[59] A. G. Ogston. The spaces in a uniform random suspension of fibres. *Transactions of the Faraday Society*, 54(11):1754–1757, 1958.

[60] B. Kozulic. Models of gel-electrophoresis. *Analytical Biochemistry*, 231(1):1–12, 1995.

[61] W. H. J. Westerhuis, J. N. Sturgis, and R. A. Niederman. Reevaluation of the electrophoretic migration behavior of soluble globular proteins in the native and detergent-denatured states in polyacrylamide gels. *Analytical Biochemistry*, 284(1):143–152, 2000.

[62] X. H. Guo and S. H. Chen. The structure and thermodynamics of protein-SDS complexes in solution and the mechanism of their transports in gel-electrophoresis process. *Chemical Physics*, 149(1-2):129–139, 1990.

[63] S. Palonen, M. Jussila, S. P. Porras, T. Hyotylainen, and M. L. Riekkola. Extremely high electric field strengths in non-aqueous capillary electrophoresis. *Journal of Chromatography A*, 916(1-2):89–99, 2001.

[64] S. P. Radko, G. H. Weiss, and A. Chrambach. Protein band spreading in capillary zone electrophoresis - effects of sample zone length and presence of polymer. *Journal of Chromatography A*, 781(1-2):277–286, 1997.

[65] H. J. Crabtree, E. C. S. Cheong, D. A. Tilroe, and C. J. Backhouse. Microchip injection and separation anomalies due to pressure effects. *Analytical Chemistry*, 73(17):4079–4086, 2001.

[66] E. Grushka, R. M. McCormick, and J. J. Kirkland. Effect of temperature-gradients on the efficiency of capillary zone electrophoresis separations. *Analytical Chemistry*, 61(3):241–246, 1989.

[67] Invitrogen Molecular Probes. Introduction to fluorescence techniques (Online Handbook), Invitrogen, Carlsbad, California. Website, 2007. `http://probes.invitrogen.com/handbook/sections/0001.html`.

[68] Invitrogen Molecular Probes. Introduction to fluorescence techniques – Jablonski diagram illustrating the processes involved in the creation of an excited electronic singlet state by optical absorption and subsequent emission of fluorescence (Online Handbook), Invitrogen, Carlsbad, California. Website, 2007. `http://probes.invitrogen.com/handbook/figures/0664.html`.

[69] Invitrogen Molecular Probes. Introduction to fluorescence techniques – Excitation of a fluorophore at 3 different wavelengths (Online Handbook), Invitrogen, Carlsbad, California. Website, 2007. `http://probes.invitrogen.com/handbook/figures/0665.html`.

[70] H. Swerdlow, K. E. Dewjager, K. Brady, R. Grey, N. J. Dovichi, and R. Gesteland. Stability of capillary gels for automated sequencing of DNA. *Electrophoresis*, 13(8):475–483, 1992.

[71] R. J. N. Coope and A. Marziali. Contaminant-induced current decline in capillary array electrophoresis. *Electrophoresis*, 26(11):2128–2137, 2005.

[72] V. Khozikov, O. Kosobokova, G. Citver, G. Tyshko, D. N. Gavrilov, G. Gudkov, and V. Gorfinkel. Experimental study of the formation of high-resistivity zones at the gel/buffer interface in CE. *Electrophoresis*, 28(3):317–321, 2007.

[73] D. Figeys and N. J. Dovichi. Change in conductivity in non-cross-linked polyacrylamide capillary electrophoresis - effects of aging polyacrylamide and buffer composition. *Journal of Chromatography A*, 744(1-2):333–339, 1996.

[74] J. R. Sandifer. Electroanalytical techniques. In *Kirk–Othmer Encyclopedia of Chemical Technology*, volume 9, pages 567–590. John Wiley & Sons, Inc., Hoboken, 5th edition, 2004.

Chapter 4

Salivary Proteome Profiling on a Microfluidic Chip Using SDS–PAGE

The work in this chapter contains an adaptation of a manuscript in preparation. The discussion contained within this chapter revisits and cites some of the concepts and data discussed in Chapter 3. This is done to maintain the flow of the discussion and support any new data that is introduced.

4.1 Introduction

Developing an understanding of the protein content of any living system is paramount to understanding its function and pathology [1, 2]. The field of proteomics, defined as large–scale analysis of the protein constituents of a living system, has great promise for better understanding of genetic function and biological systems in general [3]. Applying proteomics to the determination and profiling of disease biomarkers is another promising area of research that has far reaching implications. Traditional approaches, such as 2–dimensional gel electrophoresis followed by mass spectroscopy, are typically limited in such applications due to their high cost and requirement for larger sample quantities [1, 2, 4]. However, the miniaturisation of gel electrophoresis, through the use of microfluidics, has potential to greatly improve the analysis speed of such techniques and also reduce the amount of sample necessary for meaningful analysis [5].

As a diagnostic biofluid, saliva is particularly appealing because it does not require invasive sample collection [6–8]. Saliva also has the potential to not only provide information on oral diseases such as periodontitis, but systemic disease as well [7, 9]. Systemic diseases such as Sjögren's syndrome [10, 11], rheumatoid arthritis [11], cystic fibrosis [12], and cardiovascular disease [13] are all known to have links to the salivary proteome. Of particular interest in this study are Sjögren's syndrome [14, 15] and rheumatoid arthritis [16], which are known to have effects on the concentrations of abundant salivary proteins such as lactoferrin and α–amylase. It is also believed that the analysis of whole saliva by SDS–PAGE, the focus of

this study, may provide valuable information on the salivary profiles of connective tissue disorders in general [11].

In spite of all this promise, the proteomic analysis of saliva, and other biofluids for that matter, presents many technical challenges for analytical systems. First of all, the sheer diversity and number of proteins in these fluids greatly exceeds the separation and detection capabilities of traditional analytical methods [17]. Even multidimensional analytical techniques do not have the selectivity to distinguish all of the unique species in a given sample [18]. Additionally, the wide dynamic range of the concentrations of protein species means that in many cases, only the more abundant proteins in a given sample will be detected [17, 19, 20]. When high levels of sensitivity are attainable, comprehensive proteomic analysis renders the sensitivity irrelevant due to the masking influence of more abundant analytes [18]. Consequently, quantifying the entire proteome of a system with a single sample and single analysis methodology is difficult and not feasible with microfluidic analytical techniques available at the present time [21].

Traditionally, analysis of the salivary proteome is conducted with 2–dimensional gel electrophoresis or liquid chromatography in conjunction with mass spectroscopy [17, 22–24]. Such analyses can separate and identify large numbers of unique proteins with the use of affinity depletion of abundant salivary proteins such as amylase and immunoglobins [9]. Affinity depletion of abundant proteins eases detection of less abundant species by reducing masking effects [20, 24]. Despite their ability to identify many components of the saliva proteome, traditional techniques are expensive and lack complete automation.

Proteomic analysis in microfluidics is still in its infancy. Microfluidics were pioneered by Manz *et al.* in the early 1990's [25], and have since been applied to a wide array of biological analysis applications. The separation and analysis of the proteome has seen increasing interest as the post–genomic era has evolved, and with it an increasing abundance of protein analysis performed in capillary or microfluidic–based systems. To date, protein analysis in microfluidic platforms has worked its way toward lab–on–a–chip functionality by devising on–chip methods for sample pre–concentration [26–28], high–throughput separation [5, 27, 29–32], fluorescent labeling of proteins [29, 32], and interfacing mass spectroscopy with microfluidics [33–35]. In general, these systems aim to increase analysis throughput, reduce sample and reagent quantity requirements, increase sensitivity and performance, and reduce instrument cost.

While the development of various individual microfluidic components needed for proteomic analysis is quite prevalent, analyses involving complex samples yielding proteomic profiles are rare [20]. A recent example of proteomic profiling of urine samples was published by Thongboonkerd *et al.* [36], in which attempts were made to identify profile differences between healthy individuals, patients with diabetic nephropathy, and patients with IgA nephropathy. Using a microfluidic SDS–based separation technique, the study was able to differentiate between healthy and diseased samples on the basis of the measured molecular weight of protein peaks

and peak amplitude. Although no data was given for protein identity or absolute concentration, this study demonstrated that a protein profile was useful in differentiating between diseased and healthy subjects. Another example of microfluidic proteomic profiling involved Hellmich *et al.* demonstrating single cell protein analysis with on–chip cell lysing [37]. While analysis of the electropherograms obtained from the single cell lysates was not extensive, a total of ten peaks were detected. Using techniques similar to those used in this paper, traditional capillary electrophoresis has also been shown to be effective in generating protein profiles from single human cancer cells [38–41].

To date, published work on microfluidic analyses of saliva have only involved assays that are targeted at single protein species [13, 42, 43]. Using a modified immunoassay, Christodoulides *et al.* demonstrated the detection of clinically relevant levels ($\approx$5–11,500 pg/mL) of C–reactive protein (CRP) [13]. In another application of microfluidic salivary immunoassays, Herr *et al.* detected metalloproteinase–8 (MMP–8) via an enzyme–linked immunosorbent assay (ELISA) modified for implementation on a microfluidic chip [42]. Both of the proteins targeted in these salivary protein analyses are biomarkers related to periodontal disease. While such techniques are useful in targeted diagnostics using known biomarkers, the analysis of a single biomarker lacks the throughput necessary to determine important interactions within the biological system [44]. Such techniques may require multiple tests to elucidate information on several biomarkers of interest within the biological system under examination. Developing the capability to assess multiple biomarkers simultaneously is critical because combining information from multiple biomarkers may increase the sensitivity and specificity of analytical applications such as human cancer detection [9]. Microfluidic proteomic profiling could reduce the need for multiple analyses by examining several biomarkers simultaneously, while also alleviating the throughput issues plaguing more traditional techniques. Such techniques also cannot provide pre–screening or biomarker identification functionality.

The following discussion will address preliminary work on a simple microfluidic system capable of separating and detecting proteins from unstimulated whole saliva in a matter of minutes with minimal sample preparation. To the best of our knowledge, this is the first example of the separation and detection of multiple proteins in unstimulated whole saliva via sodium dodecyl sulfate polyacrylamide gel electrophoresis (SDS–PAGE) on a microfluidic chip. While we do not claim that the performance of the system is on par with that of advanced multidimensional analytical techniques, it is a first step towards profiling the salivary proteome in microfluidics and developing clinical diagnostic techniques. The primary objective of the current and future development of the system is to establish a profile of salivary proteins that may be used in proteomic type analyses.

4.2 Experimental Section

4.2.1 Chemicals and Samples

Solutions of 40% acrylamide/N,N′–methylene–bisacrylamide (37.5:1), 92% 3–(Trimethoxysilyl) propyl acrylate, 10% sodium dodecyl sulfate (SDS) solution, glacial acetic acid, N,N,N′,N′–Tetramethylethylenediamine (TEMED), potassium persulfate, 2–mercaptoethanol, and potassium cyanide (KCN) were obtained from Sigma–Aldrich (St. Louis, MO, USA). 2,2′–azobis[2–methyl–N–(2–hydroxyethyl) propionamide] (VA–086) Azo–Initiator was purchased from Wako Chemicals (Richmond, VA, USA). Benchmark™ Fluorescent Protein Standard (BFPS) labeled with Alexa Fluor 488, Benchmark™ Protein Ladder (BPL), and ATTO–TAG FQ were obtained from Invitrogen (Carlsbad, CA, USA). NEXT GEL Running Buffer in a 20X stock solution was obtained from Cedarlane Laboratories (Burlington, ON, CAN), and sodium tetraborate decahydrate was obtained from Fisher Scientific (Waltham, MA, USA). The chemicals used to prepare chips for SDS–PAGE separations were selected based on chip preparation methods published by Han [5] and Herr [30].

4.2.2 Microchip Fabrication

Microchips were fabricated in borosilicate glass substrates at the University of Alberta NanoFab (Edmonton, AB, CAN) using well–established glass microfabrication techniques similar to those that have been previously described [45]. The microfluidic channel pattern and well layout were photolithographically defined before the substrates were wet etched to create the microfluidic channels. After etching, the channels had an approximately semi–circular cross–section and were 46μm deep and 102μm wide. A cover plate, also made of borosilicate glass, was drilled with a water–jet to create well holes. Both the device substrate and the cover plate were cleaned, bonded together, and then thermally annealed. Each substrate yielded 24 chips measuring 16mm in width, 24mm in length, and 2.2mm in thickness. Figure 2.1 contains an illustration of the microchip's channel and well layout while Figure 4.1 contains a photograph of the microchip. The total length of the separation channel is 21.7mm, but the effective separation distance (as measured from the intersection to the curve near the end of the separation channel) is 13mm. The injection channel is 16.3mm long. Wells are 2mm in diameter and capable of holding approximately 3μL of liquid.

4.2.3 Chip Preparation

New chips were rinsed extensively with Milli–Q water (Billerica, MA, USA) to flush out any remnants of the fabrication process. In order to prevent protein adsorption, the channels were permanently coated using a method similar to the one

Figure 4.1: An image of a 4–Port Mini microfluidic chip.

pioneered by Hjerten [46]. Initially, channels were filled with 1M NaOH and allowed to sit for ten minutes. Chips were then flushed extensively with Milli–Q water and were dried using successive application of a vacuum and pressurised N_2. Following this, a 5.75mM acetic acid solution (pH $\approx$3.5) containing 0.4% v/v 3–(Trimethoxysilyl)propyl acrylate was injected into the channels to functionalise the glass surface and allow for covalent attachment of in–situ polymerised linear polyacrylamide (LPA) molecules. After one–hour in the channels, the acetic acid solution was vacuumed out. The channels were subsequently rinsed with Milli–Q water and dried extensively by applying a vacuum followed by pressurised N_2. Following this, the channels were permanently coated using in–situ polymerised LPA. The mixture used for coating the channels was an aqueous solution containing 4% acrylamide monomer and 0.1% w/v potassium persulfate. This solution was sonicated for 10 minutes prior to adding TEMED to a final concentration of 0.1% v/v. After adding TEMED, the solution was pipetted into the chip wells and allowed to fill the channels via capillary forces. Thirty minutes later, the viscous LPA solution was vacuum evacuated and excess LPA still remaining in the channel was rinsed out with water. Chips were then stored submerged in Milli–Q water at approximately 4°C.

Following the above permanent surface modification, the channels were then filled with the precursor solution necessary for creating a cross–linked polyacrylamide matrix in the channels. This precursor solution consisted of $\%T = 6\%$ or $\%T = 8\%$ acrylamide/bisacrylamide solution, with a monomer to cross–linker ratio of 37.5:1 in 1X NEXT GEL Running Buffer. The UV activated polymerisation catalyst, VA–086, was added to achieve a final catalyst concentration of 0.5% w/v.

Methods similar to those used by Han and Singh [5], and Herr [30] were used to photopolymerise the gel using a mercury UV lamp (Part No. 88–9213–02, BHK Inc., Claremont, CA, USA). Intensity measurements of the lamp at three different wavelengths (thirty minute lamp warm–up time), 254nm, 365nm, and 400nm, yielded values of 1.64mW/cm^2, 15.7mW/cm^2, and 4.5mW/cm^2 respectively. The solution was sonicated for thirty minutes prior to being injected via capillary forces into the channels.

After allowing the lamp to warm–up for thirty minutes, UV exposure was conducted at a distance of approximately 3cm from the UV lamp. Measurements conducted at three different wavelengths (thirty minute lamp warm–up time), 254nm, 365nm, and 400nm, yielded intensity values of 1.64mW/cm^2, 15.7mW/cm^2, and 4.5mW/cm^2 respectively. The initial exposure lasted 8 minutes after which the chips were examined for gel defects. Polymerisation of the gel was usually complete after the first exposure, but subsequent exposures were used to ensure complete polymerisation [30]. Before further exposures, the chip's wells were topped up with gel precursor solution to ensure the wells did not dry out. Following the final UV exposure, gels were again inspected under a microscope and then stored in 1X NEXT GEL Running Buffer in the refrigerator. Unlike others who have used similar gel polymerisation techniques [5, 27, 30, 47], the gel was polymerised in all of the chip's channels and not photo–patterned to only fill a portion of the separation channel. Before the chips were used, the polyacrylamide gel in each of the wells was removed using a pipette tip. Although the preparation of chips could be time consuming, similar systems have been noted to permit reuse of the chip for several hundred separations [30]. In contrast with slab gels that need to be poured with each use, the ability to reuse these gels is particularly attractive.

When the gel needed to be removed from the channels for the purposes of cleaning, the chips were heated to 560°C. This was conducted in a glass annealing oven in which the temperature gradually increased over several hours, plateaued at the annealing temperature for 45 minutes, then decreased back to room temperature. After this process was complete, small pieces of debris remaining in the channels were cleaned out using boiling sulphuric acid. The chip's channels were filled with the concentrated sulphuric acid and placed on a hot plate at approximately 450°C for 15 minutes. After 15 minutes, all of the sulphuric acid had been boiled out of the channels. Upon removing the chip from heat, it was allowed to cool and the channels were inspected under a microscope to determine if any debris was still present. After determining that all debris had been removed, channels were rinsed. At this point the channels could once again be modified with the permanent LPA coating.

4.2.4 Sample Preparation

Two sample types were used in the SDS–PAGE separations. Standard ladders helped develop protocols and establish the mobilities for proteins of known sizes,

whereas salivary proteins were analyzed to gain qualitative information on the protein content of saliva.

The pre–labeled (Alexa Fluor 488) BFPS ladder contained seven SDS denatured proteins ranging in size from 11 to 155kDa at unknown concentrations, and the unlabeled BPL contained fifteen SDS denatured proteins ranging in size from 10 to 220kDa. Each protein in the BPL had a stock solution concentration of $0.1\mu g/\mu L$. Analysis of these ladders was achieved by placing $0.5\mu L$ of the sample into the sample reservoir (SR, Figure 2.1). In the case of the BFPS, $2.5\mu L$ of sodium borate buffer with a pH of 8.5 and 2.0% w/v SDS was added to the well to achieve a final buffer concentration of 2.0mM. For the BPL, sodium borate and SDS concentrations were identical to that used by the BFPS sample, but additional labeling reagents were also added to the well. $0.2\mu L$ of a 2mM aqueous solution of KCN, and $0.2\mu L$ of a 2mM ATTO–TAG FQ fluorescent label dissolved in methanol were added to facilitate labeling of the ladder. Hu *et al.* have used ATTO–TAG FQ in similar circumstances when analyzing single–cell protein lysates via capillary electrophoresis [39]. The labeling reagents were mixed with the buffer and sample in the well before the sample was electrokinetically injected into the microchip.

Upon receiving informed consent from the subject, unstimulated whole saliva sample collection was conducted using sialometric (whole saliva collection) methods similar to those described by Navazesh [48]. The simple procedure began with rinsing the subject's mouth with water. Over a five–minute period, saliva was allowed to gradually accumulate in the mouth, after which it was expectorated into a sterile sample tube. Immediately after sampling, $25\mu L$ of the sample was mixed with a 200mM KCN solution to achieve a KCN concentration of 2mM. This mixture was then combined 1:1 with a sample buffer consisting of 4mM sodium borate buffer, 2% w/v SDS, 5% v/v 2–mercaptoethanol, and 2mM ATTO–TAG FQ. This sample mixture was then heated to 90°C for five minutes and subsequently returned to room temperature. Heating the sample mixture facilitated proper denaturation of the proteins in the sample and also allowed adequate time for SDS and fluorescent label to bind to the proteins. $3\mu L$ of the sample mixture was then pipetted into the SR well before the electrophoretic injection and separation was performed.

4.2.5 Separation and Detection Instrumentation

Electrophoretic separation and detection of proteins on the microchip was performed using a μFluidic–Toolkit (μTk) supplied by Micralyne (Edmonton, AB, CAN). A similar instrument has been previously described in a paper by Crabtree *et al.* [49]. Separation voltages were applied to the wells via platinum electrodes. Injection of the sample typically involved applying 400V to the sample waste (SW) well and grounding the SR well (electric field strength (E) of $245\mathrm{V/cm}$). Formation of the sample plug and separation of the proteins involved applying 500V ($E = 230\mathrm{V/cm}$) or 1000V ($E = 460\mathrm{V/cm}$) to the buffer waste (BW) well and grounding the buffer reservoir (BR) well.

The μTk uses a confocal microscope apparatus for laser induced fluorescence (LIF) excitation and detection of the fluorescently labeled proteins. Unfortunately, due to the unavailability of suitable fluorescent labels and the μTk's laser excitation wavelength (532nm) and emission filtering (ideal detection wavelengths between 563nm and 573nm) [50], proteins labeled with Alexa Fluor 488 (493nm/516nm, excitation/emission) or ATTO–TAG FQ (489nm/591nm) were not optimally excited, nor was their emitted fluorescence optimally detected. Based on data gathered from the Alexa Fluor 488 and ATTO–TAG FQ excitation and emission spectra obtained from Invitrogen, overall excitation and detection efficiency could be estimated. In terms of Alexa Fluor 488, overall efficiency was estimated at around 0.25%, while the overall efficiency of the ATTO–TAG FQ fluorophore excitation was approximately 3%. Thus, the limit of detection (LOD) with Alexa Fluor 488 labeled proteins could be improved by a factor of 400 with better excitation and filter matching. Better matching would also result in a 30–fold LOD enhancement for proteins labeled with ATTO–TAG FQ. Because adequate signal was obtained for proteins labeled with both fluorophores, the performance compromise was made in the interest of both time and expense.

4.2.6 Quantifying Separation Performance

Separation performance was evaluated using several means. Separation resolution was assessed for each peak in relation to adjacent peaks using the following Equation 4.1 [51]:

$$N = 5.54\left(\frac{t}{\Delta t_{1/2}}\right)^2 \tag{4.1}$$

where N is the theoretical number of plates, t is the time between adjacent protein peaks, and $\Delta t_{1/2}$ is the peak width determined by the full–width half maximum ($\Delta t_{1/2}$). The most relevant measure of resolution that will be used in the following discussion is the number of theoretical plates per unit length, N/m, which is determined by simply dividing N by the detection distance. This metric was chosen because it facilitates comparison with other microfluidic separations conducted over different lengths, and because it has also been used to evaluate similar SDS–PAGE based protein separations [30].

Separation quality and the ability to use the system for sizing unknown proteins was also evaluated using plots of the logarithm of the proteins' molecular weight versus the proteins' mobility normalised to a single detected peak. In the case of these separations, protein mobility was normalised to the peak generated by detection of free or unbound label (i.e. the buffer front). This plot quantifies the suitability of the gel for use in sizing unknown proteins (linearity) and gives the protein molecular weight range for which the gel is most suitable for separating. In addition, by determining the y–intercept of this plot an estimation of the size–exclusion limit of the gel can be obtained [30]. This is useful in evaluating the differences between polyacrylamide gels in different chips and determining the consistency of

the gel polymerisation process [52].

4.3 Results and Discussion

4.3.1 Protein Ladder Separations

The BFPS ladder contained seven pre–labeled proteins with molecular weights of 11, 21, 30, 40, 63, 98, and 155kDa. Detection of this ladder was routinely performed at distances of 4mm and 9mm from the intersection, allowing for adequate resolution of each of the seven protein peaks. Figure 3.6 shows a typical electropherogram produced by separating the BFPS ladder.

The BPL ladder contained fifteen proteins with molecular weights of 10, 15, 20, 25, 30, 40, 50, 60, 70, 80, 90, 100, 120, 160, and 220kDa each at a stock solution concentration of $0.1\mu g/\mu L$. Closer molecular weight spacing of the proteins, the requirement for on–chip labeling, and the larger molecular weight range resulted in a separation that was far more challenging. Figure 3.8 shows a typical electropherogram for a separation of the in–well ATTO–TAG FQ labeled BPL ladder. The first peak was generated by free label that migrated along with the buffer front. While this peak was present in BFPS separations, it was far more prominent in BPL separations due to the presence of excess labeling reagents. In both cases, the free label peak was used to calculate the normalised mobilities (R_f) for protein peaks using the equation $R_f = \mu_{protein}/\mu_{free-label}$. Injection and separation field strengths for each of the ladders were identical.

Linear least–squares regression curves of the logarithm of protein molecular weight versus R_f for the above electropherograms can be found in Figures 3.10 and 3.11. As expected for SDS–PAGE separations, these molecular weight curves exhibited a highly linear relationship ($R^2 \geq 0.99$) that is comparable to values found in published data ($R^2 = 0.984$ to 0.999) [30]. The highly linear relationship of these curves also allows them to be used in protein sizing applications.

The y–intercept of these curves also indicated the approximate size exclusion limit of the gels used. $\%T = 6\%$ and $\%T = 8\%$ cross–linked polyacrylamide gels polymerised in our lab consistently exhibited size exclusion limits in the range of 600 to 750kDa and 250 to 400kDa respectively. Compared to published data for size exclusion limits of $\%T = 6\%$ gels (235kDa) and $\%T = 8\%$ gels (110kDa) [30], our gels were typically more porous. This is most likely due to differences in gel polymerisation procedures such as UV intensity and the extent to which the solution could be degassed prior to polymerisation [53].

Table 4.1 contains theoretical plate per meter values (N/m) for the separations shown in Figures 3.6 and 3.8. N/m values for the BPL separations are lower than those in the BFPS separations because of peak height variations and the close molecular weight spacing of the proteins in the ladder. Protein peaks that exhibited low amplitudes in the BPL separations had significantly lower values for theoretical plates per meter. Compared to similar separations reported by Herr *et al.* [30], we

Protein Size (kDa)	N/m (10^3)	Protein Size (kDa)	N/m (10^3)
11000	1390	10000	1870
21000	867	15000	1200
30000	274	20000	265
40000	385	25000	243
63000	557	30000	696
98000	587	40000	0.265
155000	877	50000	472
–	–	60000	406
–	–	70000	1.01
–	–	80000	60.2
–	–	90000	365
–	–	100000	2.06
–	–	120000	98.3
–	–	160000	442
–	–	220000	623

Table 4.1: Resolution values for protein peaks in Figures 3.6 and 3.8 expressed in theoretical plates per meter (N/m).

obtained higher N/m values (i.e. $\geq 5x10^5 N/m$) for many of the peaks in the BFPS ladder separations, while many N/m values in the BPL separations were comparable. Table 4.2 contains examples of protein molecular weight ranges and theoretical plate per meter values obtained from other published microfluidic SDS–based separation results. When compared with other published data, the performance of our separations is comparable in terms of theoretical plates per meter. In terms of the number of proteins separated and detected, our separation of the BPL ladder exceeds the performance of other systems reported to date [5, 27, 29, 30, 54–56].

4.3.2 Salivary Protein Separations

Using the aforementioned methods, samples of unstimulated whole saliva were collected and subsequently separated using SDS–PAGE. A collection of twelve distinct peaks formed a characteristic separation profile. The first peak in each electropherogram, which is not numbered in Figure 4.2, corresponds to fluorescence generated by free–label. To demonstrate repeatability between consecutive separations, multiple separations of the same sample were performed. Examples of these can be found in Figures 4.3 and 4.4. All separations were conducted in the same gel at a detection distance of 4mm. The separations in Figure 4.3 were conducted using $E = 230\text{V/cm}$, while those in Figure 4.4 were conducted at $E = 460\text{V/cm}$. The distinct separation profile is evident in each of these separations and the variability within the profile is relatively minimal.

In order to facilitate sizing of the detected proteins, calibration separations of the BFPS ladder were performed prior to the saliva separations. These calibrations

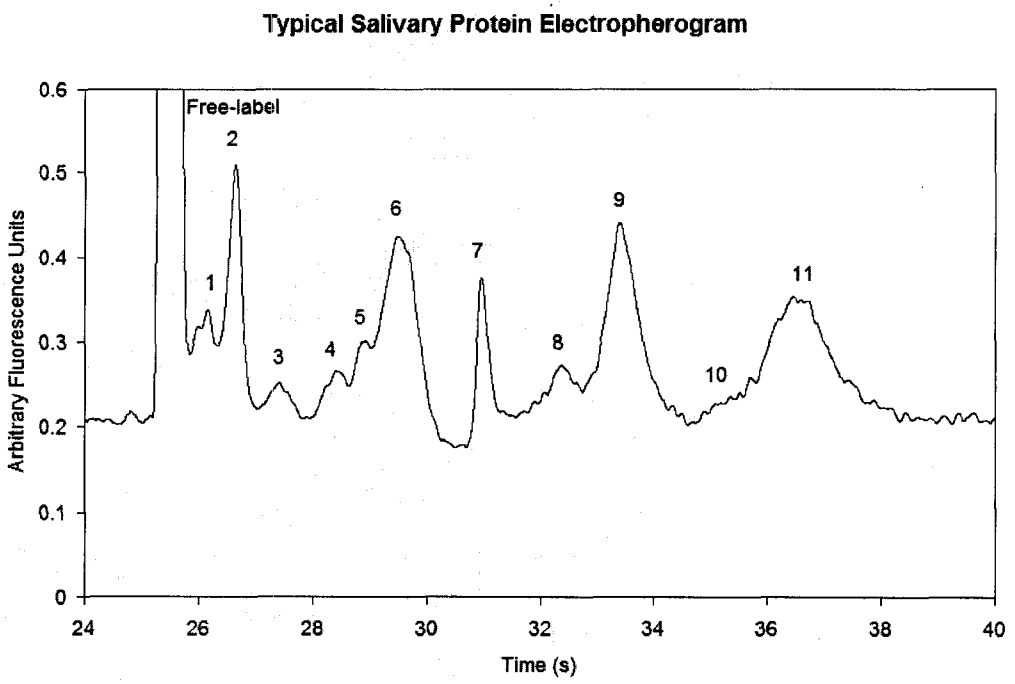

Figure 4.2: A typical electropherogram protein profile resulting from the separation of a saliva sample in an $\%T = 8\%$ polyacrylamide gel. The numbered peaks indicate the detected proteins. This separation was conducted at $460\mathrm{V/cm}$ and detection was performed at $4\mathrm{mm}$. This electropherogram is also one of the set of three presented in Figure 4.4 and is presented merely to establish peak numbers and to show what a typical protein electropherogram profile looked like.

Author (Year)	Number of Proteins Detected	Molecular Weight Range of Detected Proteins (kDa)	N/m (10^3)	Additional Notes
Bousse [29] (2001)	8	14.4 – 200	5600 – 9600	Non–covalent on–chip labeling
Hatch [27] (2006)	4	14 – 66	8.3 – 309	On–chip protein preconcentration
Han [5] (2004)	6	20.1 – 205	150 – 400	–
Herr [30] (2004)	5	6.5 – 39	400	–
Nagata [54] (2005)	3	21.5 – 166	38 – 620	–
Nagata [55] (2005)	8	5.7 – 116	97 – 1350	–
Nagata [56] (2005)	3	21.5 – 116	90 – 2300	–

Table 4.2: Examples of published microfluidic separations of SDS denatured proteins separated in microfluidic chips.

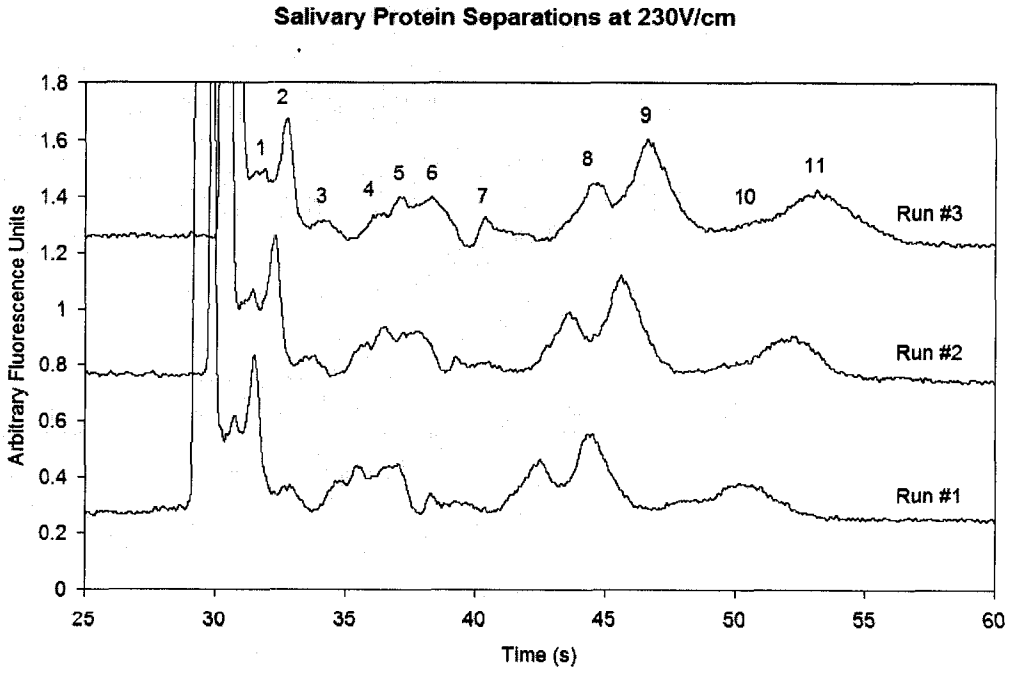

Figure 4.3: Three consecutive electrophoretic separations of the saliva sample at $E = 230\text{V/cm}$ in an $\%T = 8\%$ polyacrylamide gel. Detection conducted at 4mm.

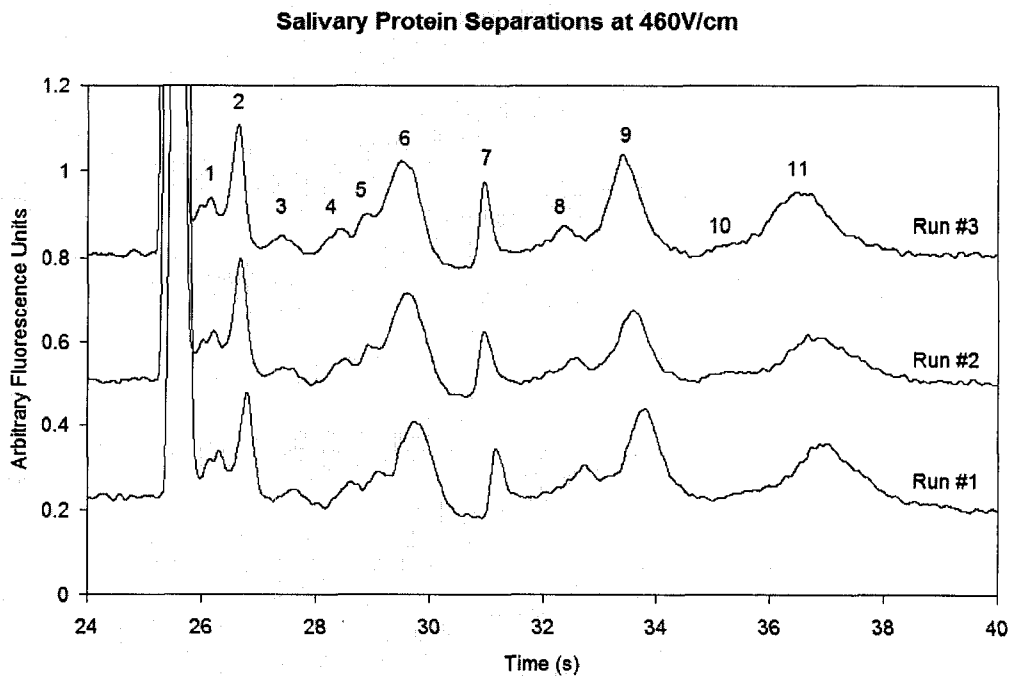

Figure 4.4: Three consecutive electrophoretic separations of the saliva sample at $E = 460\text{V/cm}$ in an $\%T = 8\%$ polyacrylamide gel. Detection conducted at 4mm.

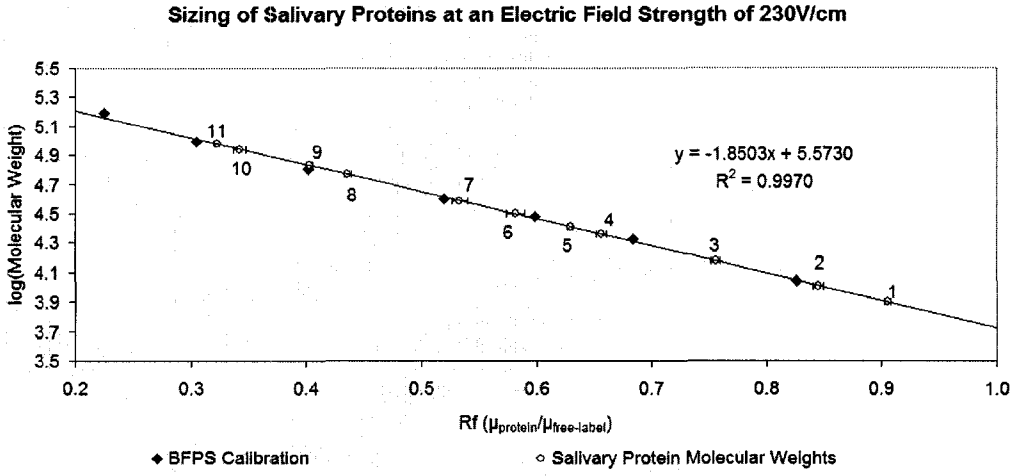

Figure 4.5: Demonstration of the use of the BFPS calibration curve for sizing proteins. The plot shows the average calculated protein molecular weights based on the electropherograms shown in Figure 4.3 ($E = 230\text{V/cm}$). When averaged from the three runs, the molecular weights of the detected proteins are 7.9, 10.2, 15.0, 22.9, 25.6, 31.4, 38.6, 58.5, 67.2, 87.0, and 94.6kDa. The inserted numbers are intended to correspond to the protein peak numbers in Figure 4.3. The RSD of R_f (used to calculate molecular weight) for the three electropherograms ranged from 0.25% to 1.62% as indicated by the error bars. The standard error of the measured R_f values for the proteins in the calibration curve is on the order of $\pm 0.3\%$. Consequently, the standard error in MW estimation is approximately $\pm 5\%$, which is similar to the values reported by Herr *et al.* [30].

were performed in the same chip as the saliva separations and also used the same detection distance and separation fields. Molecular weights of the detected proteins in the saliva sample were calculated using the molecular weight curves generated by the BFPS ladder calibrations. Similar techniques have been used to size proteins not migrating in the presence of a protein ladder [30, 36]. Based on the BFPS calibration separations, detected proteins were found to range in size from 7.7 to 98.5kDa. Figures 4.5 and 4.6 contain the calibration curves generated by the BFPS calibration separation, along with the plotted sizes of the proteins detected in the saliva sample.

Data in Table 4.3 illustrates that there is minimal variability in the calculated molecular weights for the detected proteins among separations performed at the same electric field strength. This demonstrates that run–to–run repeatability is very high. The origin of protein sizing variations amongst separations performed at different fields, particularly for peaks 5 and 7, is not yet known and requires further investigation. This will most likely involve the use of multiple gel concentrations and Ferguson plot analysis to confirm uniform protein charge densities have been

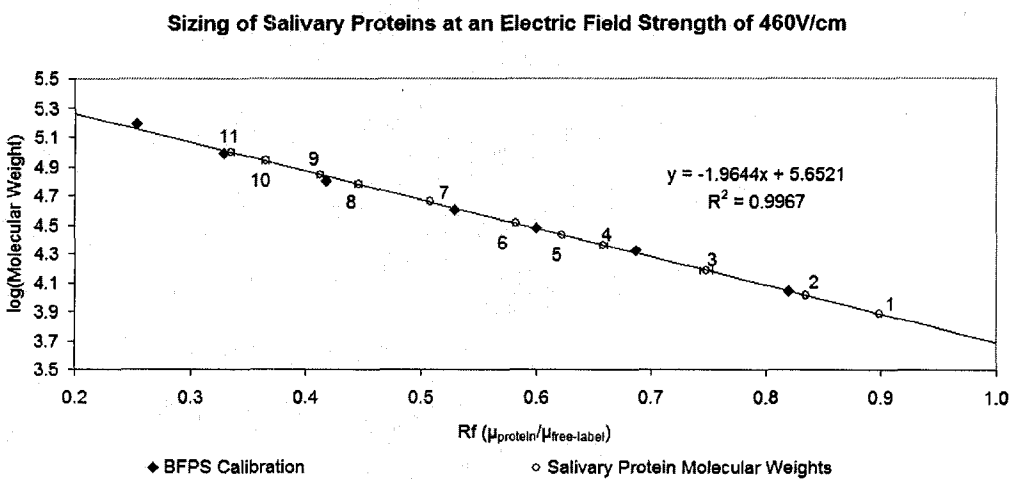

Figure 4.6: Demonstration of the use of the BFPS calibration curve for sizing proteins. The plot shows the calculated protein molecular weights based on the electropherograms shown in Figure 4.4 ($E = 460\text{V/cm}$). When averaged from the three runs, the sizes of the detected proteins are 7.7, 10.3, 15.2, 22.9, 26.8, 32.2, 45.2, 59.8, 69.6, 86.2, and 98.5kDa. The inserted numbers are intended to correspond to the protein peak numbers in Figure 4.4. The relative standard deviation, RSD, of R_f (used to calculate molecular weight) for the three electropherograms ranged from 0.24% to 1.34% as indicated by the error bars. The standard error of the measured R_f values for the proteins in the calibration curve is on the order of $\pm 0.3\%$. Consequently, the standard error in MW estimation is less than $\pm 5\%$, which is similar to the values reported by Herr *et al.* [30].

Protein Peak Number	$\overline{MW}$ (Da)		RSD (%)	
	$\overline{MW}_{230V/cm}$	$\overline{MW}_{460V/cm}$	$\overline{MW}_{230V/cm}$	$\overline{MW}_{460V/cm}$
1	7916	7695	0.97	0.92
2	10230	10291	1.78	0.55
3	14955	15244	1.77	2.32
4	22869	22863	1.89	1.40
5	25612	26800	0.83	0.71
6	31414	32229	3.45	0.95
7	38584	45158	2.72	0.42
8	58461	59755	1.35	1.37
9	67246	69550	1.02	1.20
10	87092	86165	1.87	1.44
11	94638	98532	0.66	0.97

Table 4.3: Protein molecular weight estimates and their variability determined from the electropherograms in Figures 4.3 and 4.4. Amongst separations conducted at the same field strength with the same sample, the magnitude of the RSD for the calculated protein molecular weight indicates good run–to–run repeatability.

achieved with SDS denaturing [57]. Although characterisation of such phenomena is not within the scope of this paper, the effect of electric field strength on migration behaviour, especially that of larger proteins, has been documented in similar separations [5]. In that case, the anomalies were attributed to transitions between Ogston and Reptation migration models. Such effects, however, should be mitigated in sizing salivary proteins because of the use of calibration separations conducted at identical electric field strengths as the salivary protein separations.

While the peaks that were detected in this preliminary work likely resulted from highly abundant proteins such as α–amylase, further analysis will be needed for conclusive identification. It is acknowledged that a single peak may in fact consist of multiple proteins, and that multiple peaks may actually represent a single protein species expressed in different forms [22]. Nevertheless, on the basis of molecular weight [58], its typically high abundance, and its dominance within its molecular weight range [22], it is reasonable to believe that peak 8 is composed primarily of α–amylase. The calculated molecular weight of peak 8 is close in MW to a glycosylated form of α–amylase detected by Hirtz *et al.* (59kDa) from a sample of whole saliva [58]. The MWs (at both electric field strengths) calculated for peak 8 in this sample are well within 1kDa of Hirtz's observation. Unfortunately, the concentration of α–amylase is not given in many of the salivary proteomic studies referenced by this work [16, 17, 22, 58–60], so it is difficult to specify its degree of abundance. However, for a sample of whole human saliva, Huang *et al.* noted that the intensity of α–amylase spots in 2–dimensional gels were approximately 1.5 to 10 times higher than those of other proteins that were detected [61]. In addition, 2-dimensional gels produced by Hirtz *et al.* indicate that although α–amylase was found to be present in a variety of modified and truncated forms, the majority of the

Protein Peak Number	Normalised Amplitude 230V/cm	460V/cm	RSD (%) 230V/cm	460V/cm
1	0.165	0.111	12.54	6.41
2	0.222	0.165	12.30	2.23
3	0.100	0.082	9.73	6.34
4	0.109	0.088	8.14	6.32
5	0.125	0.098	6.72	3.50
6	0.125	0.139	7.43	3.72
7	0.098	0.116	4.14	7.48
8	0.137	0.093	5.33	13.58
9	0.174	0.139	4.75	11.64
10	0.094	0.079	3.50	7.33
11	0.118	0.114	3.59	9.86

Table 4.4: Normalised saliva protein peak amplitude and variability. The free–label peak, to which the protein peak amplitudes were normalised, had an RSD of approximately 1.69% for the 230V/cm separations, and 5.27% for the 460V/cm separations. The amplitude of the free–label peak had a RSD of 23.5% for all salivary protein separations ($n = 29$) performed in this gel.

α–amylase that was detected fell within the 56 to 59kDa MW range [58]. Because many of the modified forms of α–amylase fell within this MW range and were spread out over a pI range of 5 to 8, it is possible that the elimination of the pI dimension, as seen in this work, may have resulted in a dominant α–amylase peak. It should also be noted that Hirtz *et al.* observed no other proteins having MWs between 50 and 65kDa [58], indicating that the masking of α–amylase by other proteins is unlikely. Further quantitation of the salivary proteome may be gained from a more in–depth analysis of the 2–dimensional gels presented by Hirtz.

The small run–to–run variations in the normalised amplitude of the peaks in Figures 4.3 and 4.4 also indicate that one could use the peak amplitude as an indicator of relative abundance of the protein in the saliva sample. While such data does not provide specific concentrations of the detected proteins, particularly because labeling efficiencies may differ, it does provide a consistent indication of relative peak height. Table 4.4 shows the mean and relative standard deviation for the normalised amplitude for each of the detected protein peaks at each of the separation field strengths. The peak amplitude was normalised to the amplitude of the free label peak, which had a relative standard deviation of less than 6% for the separations shown in Figures 4.3 and 4.4. When analyzing data from all of the separations conducted in the gel used for these separations, the relative standard deviation of the free–label peak ($RSD = 23\%\ for\ n = 29$) is comparable to values reported for standard protein peak heights and system spectra used in proteome profiling as demonstrated by Thongboonkerd *et al.* [36]. Further efforts will be made in future work to establish more repeatable standards that will facilitate better consistency in the normalised peak amplitude calculation, and thus in diagnostic applications.

In terms of diagnostic relevance, the concentration of α–amylase, a highly abundant salivary protein [58], has been shown to be higher in subjects with oral cancer [60]. Although this study is well cited, no quantitative data was given for the absolute concentration or the degree of change in the concentration of α–amylase. In spite of this, a simple inspection of the slab gels noted in this publication show a clear increase in the protein band intensities for diseased patients versus healthy controls. In other examples, concentrations of α–amylase have been shown to be approximately fifty percent lower in subjects with rheumatoid arthritis [16], and approximately twenty–five percent higher in patients with type 2 diabetes [59] when compared with normal controls. Given the degree of variability in our peak amplitudes (see Table 4.4), such a change would be evident. While these variations may be visible, it should also be noted that natural variations in α–amylase have been observed to be large (RSD of approximately 10%) [60]. As a result, even though the detection of a single biomarker may not be sufficient for diagnosis, our technique could be advantageous if another biomarker is known.

In another diagnostic example, two separate studies by Carpenter *et al.* [14] and Ryu *et al.* [15], have shown that the concentration of lactoferrin increases by three to ten fold (normal concentration is approximately 50nM) in the presence of Sjögren's syndrome. Although lactoferrin was not identified in this study, the concentrations discussed by Carpenter *et al.* and Ryu *et al.* are well within the detection limits of this system (see subsequent discussion), especially in the diseased state. At the expected time of lactoferrin's (80kDa) arrival in the salivary protein electropherograms, the low signal level (5-10% greater than the baseline noise level) between peaks 9 and 10 indicates that lactoferrin may not be masked by other peaks. Based on the subsequent discussion of the system's limit of detection, it is estimated that concentrations of an 80kDa protein on the order of 50nM should be detectable in the context of the salivary protein electropherograms presented in Figures 4.3 and 4.4.

As previously mentioned, proteins in salivary samples have concentrations that exist over several orders of magnitude. Consequently, a system's limit of detection can be critical if depletion techniques are used to remove the most abundant protein species. Because of the methods employed in these experiments, only more abundant protein species were detected, and values for the absolute limit of detection were not vigorously pursued.

Estimates of the system's limit of detection (LOD) were gathered by analyzing data resulting from separations of the BPL ladder. Because it was also labeled with ATTO–TAG FQ, it should provide a reasonable estimate of the limit of detection for the salivary protein samples. The electropherograms in Figure 3.8 were produced using an in–well protein concentration of approximately 16.7ng/μL for each protein, resulting in an approximate total protein concentration of 250ng/μL. Molar concentrations ranged from 1.7μM for the 10kDa protein to 77nM for the 220kDa protein. The signal–to–noise ratio (SNR) for the protein peaks ranged from 7 to 40. Based on these SNR values, estimates of the inefficiencies of the excitation wavelength and fluorescence detection, and the in–well protein concentrations, a char-

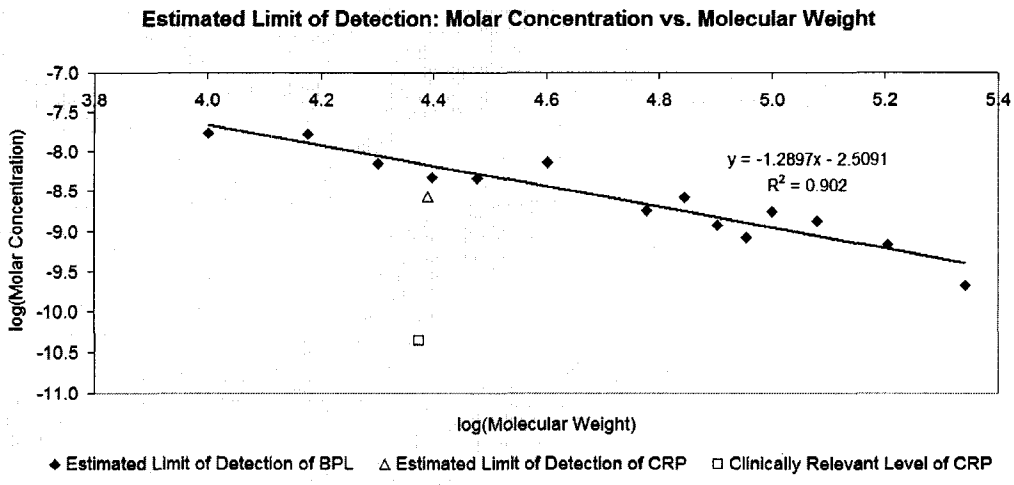

Figure 4.7: An estimate of the LOD of detection for ATTO–TAG FQ labeled proteins. The characteristic plot was produced using data from the BPL ladder electropherogram in Figure 3.8, and knowledge about fluorophore excitation and emission detection inefficiencies. In order to establish an experimentally verifiable LOD, further investigation is needed with optimised excitation wavelength and emission filtering. Data from the 50kDa protein was omitted because it existed at an unknown concentration that was greater than that of the other proteins in the BPL ladder. It is estimated that the limit of detection for this system (with optical improvements) ranges from 17nM for the 10kDa protein to 209pM for the 220kDa protein. Detection of a known concentration of C–reactive protein (CRP) in a CRP–spiked saliva sample agreed with these results. In addition, a clinically relevant level of CRP [13] is shown to be well below the LOD for this system.

acteristic plot was developed for the LOD in relation to protein molecular weight. Figure 4.7 shows that the estimated LOD ranges from 17nM for the 10kDa protein to 209pM for the 220kDa protein for in–well concentrations. Data published by Hu *et al.* on the detection limits (70 – 290pM) of standard proteins labeled with ATTO–TAG FQ indicates that even lower concentrations of proteins may be detectable [40]. Hu's detection limits permitted the detection of protein lysates from a single cell, indicating that our system may be able to detect the proteins resulting from lysing approximately 500 to 1000 cells.

To confirm that the LOD values established in Figure 4.7 corresponded well to proteins denatured and labeled in the same manner as salivary proteins, a saliva sample spiked with a known concentration of C–reactive protein (CRP) was separated in the chip. Using the same denaturing and labeling procedure that was used for saliva samples, 46ng/μL or 2μM (in–well concentration) of CRP was detected with a SNR of 63. Although the limit of detection was not firmly established (i.e. peak $SNR = 3$), the estimate of the LOD for CRP (2.68nM) fell in line with the

characteristic plot produced by the BPL ladder (see Figure 4.7). While this C–reactive protein LOD is much greater than that published by Christodoulides *et al.* (0.2fM) [13], low–abundance proteins such as CRP (clinically relevant concentrations of 3.9pM to 85pM) are not of interest because they will be overwhelmed by more abundant proteins such as α–amylase, immunoglobulin A, and cystatins [22]. Its clinically relevant concentration is plotted along with the limit of detection for this work in Figure 4.7.

4.4 Conclusions

We have demonstrated a simple and rapid method for separating and detecting multiple proteins in unstimulated whole saliva samples. The elapsed time from sample acquisition to protein separation and detection is approximately ten minutes, making this a very rapid means of gathering information on salivary protein content. While the salivary protein analysis techniques are fairly simple and the work is largely preliminary, this analysis method may be particularly powerful in that it is designed to detect multiple proteins in saliva rather than analyze single protein species. Contrary to other microfluidic salivary protein techniques where only one protein species is studied [13, 42], this technique may be useful in proteome profiling or diagnostic and pre–screening applications requiring the assessment of several salivary proteins or biomarkers. Because of the non–specific nature of this technique, the use of saliva for broad screening or proteome profiling on microfluidics may be greatly simplified, more rapid, and relevant to a wider range of applications. In addition, the non–specific nature of this technique may make it applicable for use with other biofluids. Although this analysis technique has likely detected only the most abundant proteins, potential biomarkers among abundant proteins in the salivary proteome have been identified, such as those for rheumatoid arthritis [16] and Sjögren's syndrome [14, 15]. While the investigation of the salivary proteome is still in the exploratory phases, as a diagnostic resource, it has great potential [9]. Further development of this preliminary work will likely assess further refinement of the technique, differences in proteome profiles between healthy individuals and those with oral or systemic disease, and possible identification of biomarkers of disease.

Expansion of the technique may also lead to the analysis of other biofluids and cellular samples. Numerous improvements, including further optimisation of the labeling and denaturing protocols and improvement of the laser induced fluorescence optics, may serve to further improve sensitivity, increase the number of proteins detected, and possibly enable clinical use of the technique. Other on– or off–chip enhancements such as sample pre–treatment, depletion of abundant protein species, labeling, heat denaturing [62], and protein pre–concentration will no doubt add to the functionality and degree of integration of this technique for use in profiling the salivary proteome.

Bibliography

[1] J. Hicks. Genome, proteome, and metabolome: Where are we going? *Ultrastructural Pathology*, 27(5):289–294, 2003.

[2] J. W. Cooper, Y. J. Wang, and C. S. Lee. Recent advances in capillary separations for proteomics. *Electrophoresis*, 25(23-24):3913–3926, 2004.

[3] A. Pandey and M. Mann. Proteomics to study genes and genomes. *Nature*, 405(6788):837–846, 2000.

[4] S. Hanash. Disease proteomics. *Nature*, 422(6928):226–232, 2003.

[5] J. Han and A. K. Singh. Rapid protein separations in ultra-short microchannels: microchip sodium dodecyl sulfate-polyacrylamide gel electrophoresis and isoelectric focusing. *Journal of Chromatography A*, 1049(1-2):205–209, 2004.

[6] D. Malamud. Salivary diagnostics - the future is now. *Journal of the American Dental Association*, 137(3):284–+, 2006.

[7] D. T. Wong. Salivary diagnostics powered by nanotechnologies, proteomics and genomics. *Journal of the American Dental Association*, 137(3):313–321, 2006.

[8] C. S. Miller, C. P. King, C. Langub, R. J. Kryscio, and M. V. Thomas. Salivary biomarkers of existing periodontal disease - a cross-sectional study. *Journal of the American Dental Association*, 137(3):322–329, 2006.

[9] S. Hu, J. A. Loo, and D. T. Wong. Human body fluid proteome analysis. *Proteomics*, 6(23):6326–6353, 2006.

[10] C. Baldini, L. Giusti, L. Bazzichi, F. Ciriegia, A. Tavoni, A. Lucacchini, and S. Bombardieri. Proteomic analysis of human whole saliva in Sjögren syndrome. *Annals of the Rheumatic Diseases*, 66:A58–A58, 2007.

[11] J. A. Beeley and K. S. Khoo. Salivary proteins in rheumatoid arthritis and Sjögren's syndrome: One-dimensional and two-dimensional electrophoretic studies. *Electrophoresis*, 20(7):1652–1660, 1999.

[12] D. K. Shori, T. Genter, J. Hansen, C. Koch, H. Wyatt, H. H. Kariyawasam, R. A. Knight, M. E. Hodson, A. Kalogeridis, and I. Tsanakas. Altered sialyl- and fucosyl-linkage on mucins in cystic fibrosis patients promotes formation of the sialyl-Lewis X determinant on salivary MUC-513 and MUC-7. *Pflugers Archiv-European Journal of Physiology*, 443:S55–S61, 2001.

[13] N. Christodoulides, S. Mohanty, C. S. Miller, M. C. Langub, P. N. Floriano, P. Dharshan, M. F. Ali, B. Bernard, D. Romanovicz, E. Anslyn, P. C. Fox, and J. T. McDevitt. Application of microchip assay system for the measurement of C–reactive protein in human saliva. *Lab on a Chip*, 5(3):261–269, 2005.

[14] G. H. Carpenter, G. B. Proctor, C. L. Pankhurst, J. O'Donohue, D. Scott, and M. P. Hunnable. Sialochemical markers of salivary gland involvement with Sjögren's syndrome secondary to rheumatoid arthritis and primary biliary cirrhosis. *Journal of Oral Pathology & Medicine*, 29(9):452–459, 2000.

[15] O. H. Ryu, J. C. Atkinson, G. T. Hoehn, G. G. Illei, and T. C. Hart. Identification of parotid salivary biomarkers in Sjögren's syndrome by surface-enhanced laser desorption/ionization time-of-flight mass spectrometry and two-dimensional difference gel electrophoresis. *Rheumatology*, 45(9):1077–1086, 2006.

[16] L. M. J. Helenius, J. H. Meurman, I. Helenius, K. Kar, J. Hietanen, R. Suuronen, D. Hallikainen, H. Kautiainen, M. Leirisalo-Repo, and C. Lindqvist. Oral and salivary parameters in patients with rheumatic diseases. *Acta Odontologica Scandinavica*, 63(5):284–293, 2005.

[17] T. Guo, P. A. Rudnick, W. J. Wang, C. S. Lee, D. L. Devoe, and B. M. Balgley. Characterization of the human salivary proteome by capillary isoelectric focusing/nanoreversed-phase liquid chromatography coupled with ESI-tandem MS. *Journal of Proteome Research*, 5(6):1469–1478, 2006.

[18] B. F. Liu, B. Xu, G. Zhang, W. Du, and Q. M. Luo. Micro-separation toward systems biology. *Journal of Chromatography A*, 1106(1-2):19–28, 2006.

[19] G. L. Corthals, V. C. Wasinger, D. F. Hochstrasser, and J. C. Sanchez. The dynamic range of protein expression: A challenge for proteomic research. *Electrophoresis*, 21(6):1104–1115, 2000.

[20] J. C. Smith, J. P. Lambert, F. Elisma, and D. Figeys. Proteomics in 2005/2006: Developments, applications and challenges. *Analytical Chemistry*, 79(12):4325–4343, 2007.

[21] S. L. S. Freire and A. R. Wheeler. Proteome-on-a-chip: Mirage, or on the horizon? *Lab on a Chip*, 6(11):1415–1423, 2006.

[22] B. Ghafouri, C. Tagesson, and M. Lindahl. Mapping of proteins in human saliva using two-dimensional gel electrophoresis and peptide mass fingerprinting. *Proteomics*, 3(6):1003–1015, 2003.

[23] E. Neyraud, T. Sayd, M. Morzel, and E. Dransfield. Proteomic analysis of human whole and parotid salivas following stimulation by different tastes. *Journal of Proteome Research*, 5(9):2474–2480, 2006.

[24] K. Ohshiro, D. I. Rosenthal, J. M. Koomen, C. F. Streckfus, M. Chambers, R. Kobayashi, and A. K. El-Naggar. Pre-analytic saliva processing affect proteomic results and biomarker screening of head and neck squamous carcinoma. *International Journal of Oncology*, 30(3):743–749, 2007.

[25] A. Manz, D. J. Harrison, E. M. J. Verpoorte, J. C. Fettinger, H. Ludi, and H. M. Widmer. Miniaturization of chemical-analysis systems - a look into next century technology or just a fashionable craze. *Chimia*, 45(4):103–105, 1991.

[26] Y. C. Wang, A. L. Stevens, and J. Y. Han. Million-fold preconcentration of proteins and peptides by nanofluidic filter. *Analytical Chemistry*, 77(14):4293–4299, 2005.

[27] A. V. Hatch, A. E. Herr, D. J. Throckmorton, J. S. Brennan, and A. K. Singh. Integrated preconcentration SDS-PAGE of proteins in microchips using photopatterned cross-linked polyacrylamide gels. *Anal. Chem.*, 78(14):4976–4984, 2006.

[28] S. Song, A. K. Singh, and B. J. Kirby. Electrophoretic concentration of proteins at laser-patterned nanoporous membranes in microchips. *Analytical Chemistry*, 76(15):4589–4592, 2004.

[29] L. Bousse, S. Mouradian, A. Minalla, H. Yee, K. Williams, and R. Dubrow. Protein sizing on a microchip. *Analytical Chemistry*, 73(6):1207–1212, 2001.

[30] A. E. Herr and A. K. Singh. Photopolymerized cross-linked polyacrylamide gels for on-chip protein sizing. *Analytical Chemistry*, 76(16):4727–4733, 2004.

[31] L. J. Jin, B. C. Giordano, and J. P. Landers. Dynamic labeling during capillary or microchip electrophoresis for laser-induced fluorescence detection of protein-SDS complexes without pre- or postcolumn labeling. *Analytical Chemistry*, 73(20):4994–4999, 2001.

[32] Y. J. Liu, R. S. Foote, S. C. Jacobson, R. S. Ramsey, and J. M. Ramsey. Electrophoretic separation of proteins on a microchip with noncovalent, postcolumn labeling. *Analytical Chemistry*, 72(19):4608–4613, 2000.

[33] M. H. Fortier, E. Bonneil, P. Goodley, and P. Thibault. Integrated microfluidic device for mass spectrometry-based proteomics and its application to biomarker discovery programs. *Analytical Chemistry*, 77(6):1631–1640, 2005.

[34] J. S. Kim and D. R. Knapp. Microfabrication of polydimethylsiloxane electrospray ionization emitters. *Journal of Chromatography A*, 924(1-2):137–145, 2001.

[35] S. Le Gac, S. Arscott, and C. Rolando. A planar microfabricated nanoelectrospray emitter tip based on a capillary slot. *Electrophoresis*, 24(21):3640–3647, 2003.

[36] V. Thongboonkerd, N. Songtawee, and S. Sritippayawan. Urinary proteome profiling using microfluidic technology on a chip. *Journal of Proteome Research*, 6(5):2011–2018, 2007.

[37] W. Hellmich, D. Greif, C. Pelargus, D. Anselmetti, and A. Ros. Improved native UV laser induced fluorescence detection for single cell analysis in poly(dimethylsiloxane) microfluidic devices. *Journal of Chromatography A*, 1130(2):195–200, 2006.

[38] S. Hu, J. Jiang, L. M. Cook, D. P. Richards, L. Horlick, B. Wong, and N. J. Dovichi. Capillary sodium dodecyl sulfate-DALT electrophoresis with laser-induced fluorescence detection for size-based analysis of proteins in human colon cancer cells. *Electrophoresis*, 23(18):3136–3142, 2002.

[39] S. Hu, L. Zhang, L. M. Cook, and N. J. Dovichi. Capillary sodium dodecyl sulfate-DALT electrophoresis of proteins in a single human cancer cell. *Electrophoresis*, 22(17):3677–3682, 2001.

[40] S. Hu, L. Zhang, S. Krylov, and N. J. Dovichi. Cell cycle-dependent protein fingerprint from a single cancer cell: Image cytometry coupled with single-cell capillary sieving electrophoresis. *Analytical Chemistry*, 75(14):3495–3501, 2003.

[41] S. Hu, L. Zhang, R. Newitt, R. Aebersold, J. R. Kraly, M. Jones, and N. J. Dovichi. Identification of proteins in single-cell capillary electrophoresis fingerprints based on comigration with standard proteins. *Analytical Chemistry*, 75(14):3502–3505, 2003.

[42] A. E. Herr, A. V. Hatch, D. J. Throckmorton, H. M. Tran, J. S. Brennan, W. V. Giannobile, and A. K. Singh. Microfluidic immunoassays as rapid saliva-based clinical diagnostics. *Proceedings of the National Academy of Sciences of the United States of America*, 104(13):5268–5273, 2007.

[43] R. Mukhopadhyay. Devices to drool for. *Analytical Chemistry*, 78(13):4255–4259, 2006.

[44] D. N. Breslauer, P. J. Lee, and L. P. Lee. Microfluidics-based systems biology. *Molecular Biosystems*, 2(2):97–112, 2006.

[45] H. Hartshorne, C. J. Backhouse, and W. E. Lee. Ferrofluid-based microchip pump and valve. *Sensors and Actuators B-Chemical*, 99(2-3):592–600, 2004.

[46] S. Hjerten. High-performance electrophoresis - elimination of electroendosmosis and solute adsorption. *Journal of Chromatography*, 347(2):191–198, 1985.

[47] S. N. Brahmasandra, V. M. Ugaz, D. T. Burke, C. H. Mastrangelo, and M. A. Burns. Electrophoresis in microfabricated devices using photopolymerized polyacrylamide gels and electrode-defined sample injection. *Electrophoresis*, 22(2):300–311, 2001.

[48] M. Navazesh. How can oral health care providers determine if patients have dry mouth? *Journal of the American Dental Association*, 134(5):613–+, 2003.

[49] H. J. Crabtree, E. C. S. Cheong, D. A. Tilroe, and C. J. Backhouse. Microchip injection and separation anomalies due to pressure effects. *Analytical Chemistry*, 73(17):4079–4086, 2001.

[50] Micralyne. Microfluidic Tool Kit Product Datasheet, Micralyne, Edmonton, Alberta. Website, 2007. `http://www.micralyne.com/capabilities/products/toolkit.htm`.

[51] D. J. Harrison, A. Manz, Z. H. Fan, H. Ludi, and H. M. Widmer. Capillary electrophoresis and sample injection systems integrated on a planar glass chip. *Analytical Chemistry*, 64(17):1926–1932, 1992.

[52] P. Menter. Acrylamide polymerization - A practical approach, Bulletin 1156 - Revision E, Bio–Rad Laboratories Ltd., Mississauga, Ontario. Website, 2007. `http://www.bio-rad.com/LifeScience/pdf/Bulletin_1156.pdf`.

[53] B. D. Hames. An introduction to polyacrylamide gel electrophoresis. In B. D. Hames and D. Rickwood, editors, *Gel Electrophoresis of Proteins: A Practical Approach*, page 290. IRL Press Limited, Oxford, 1st edition, 1981.

[54] H. Nagata, M. Tabuchi, K. Hirano, and Y. Baba. High-speed separation of proteins by microchip electrophoresis using a polyethylene g glycol-coated plastic chip with a sodium dodecyl sulfate-linear polyacrylamide solution. *Electrophoresis*, 26(14):2687–2691, 2005.

[55] H. Nagata, M. Tabuchi, K. Hirano, and Y. Baba. Automatic protein separation by microchip electrophoresis using quartz chip. *Chromatography; Journal of Separation and Detection Sciences*, 26(1):23–28, 2005.

[56] H. Nagata, M. Tabuchi, K. Hirano, and Y. Baba. Microchip electrophoretic protein separation using electroosmotic flow induced by dynamic sodium dodecyl sulfate-coating of uncoated plastic chips. *Electrophoresis*, 26(11):2247–2253, 2005.

[57] A. T. Andrews. *Electrophoresis: theory, techniques, and biochemical and clinical applications*. Oxford University Press, New York, 2nd edition, 1986.

[58] C. Hirtz, F. Chevalier, D. Centeno, J. C. Egea, M. Rossignol, N. Sommerer, and D. de Periere. Complexity of the human whole saliva proteome. *Journal of Physiology and Biochemistry*, 61(3):469–480, 2005.

[59] S. Aydin. A comparison of ghrelin, glucose, alpha-amylase and protein levels in saliva from diabetics. *Journal of Biochemistry and Molecular Biology*, 40(1):29–35, 2007.

[60] Y. C. Chen, T. Y. Li, and M. F. Tsai. Analysis of the saliva from patients with oral cancer by matrix-assisted laser desorption/ionization time-of-flight mass spectrometry. *Rapid Communications in Mass Spectrometry*, 16(5):364–369, 2002.

[61] C. M. Huang. Comparative proteomic analysis of human whole saliva. *Archives of Oral Biology*, 49(12):951–962, 2004.

[62] C. S. J. Hou, M. Godin, K. Payer, R. Chakrabarti, and S. R. Manalis. Integrated microelectronic device for label-free nucleic acid amplification and detection. *Lab on a Chip*, 7(3):347–354, 2007.

Chapter 5

Conclusions

In the compiling of this thesis, great care was taken to ensure that concepts and data were conveyed in an accurate, logical, and meaningful way. Upon reflecting on this work, it is clear that advances in knowledge have been attained. Chapter 2 demonstrates extensive protocol development toward permanent channel surface modification and in–situ gel polymerisation. These protocols serve to facilitate future refinements of these coating and polymerisation techniques and also act as the foundations upon which new microchip–based proteomic analytical tools will be based. The development of the SDS–PAGE and on–chip labeling techniques in Chapter 3, and the comprehensive characterisation that was associated with it, represents a progression from minimal knowledge to the state–of–the–art in a relatively short time frame. Such developments should permit the Applied Miniaturisation Laboratory to continue to make meaningful contributions to the research field in the future.

Most importantly, the application of all of these techniques to the salivary proteome profiling presented in Chapter 4 demonstrated a novel and intriguing foray into microchip–based proteomic analysis. This technique demonstrated a prototype system capable of performing diagnostic analysis in approximately ten minutes. Early testing of the system has shown that it may have the ability to screen the salivary proteome for a wide range of anomalies. Further development and integration of this technique with sample preparation procedures, and experimentation with both clinically relevant data and other biofluids, may forge a path for the realisation of point-of–care proteomic analytical tools. The potential of this system and the advances brought with it have not yet been fully realised. Further extension of this work could incorporate the concepts presented in Appendix A to achieve a two–dimensional point-of–care proteomic diagnostic tool capable of more advanced analyses. All of these advances provide a glimpse of what the future holds for microchip–based methods of protein profiling.

Appendix A

Microchip Electrophoresis–Electrospray Ionisation–Ion Mobility Spectrometry

The following appendix provides an in–depth overview of the theory, current project status, and future directions concerned with microchip electrophoresis–electrospray ionisation–ion mobility spectrometry (MCE–ESI–IMS). The combination of these analytical techniques may provide a miniaturised instrument capable of advanced proteomic analysis.

Work conducted for the purposes of creating a MCE–ESI–IMS system was centered primarily on the design and fabrication of a MCE–ESI microfluidic chip. Other work consisted of initiating the process of assembling IMS system components designed and fabricated by my predecessors. Time constraints, coupled with a change of research focus during my program, resulted in abandonment of many aspects of this project at an early stage. Nevertheless, the following discussion aims to provide a theoretical background for the MCE–ESI–IMS system as well as lay the foundations for future work in this area. Although the novel MCE–ESI chip design was not tested, it represents an extension of the work performed in Chapters 2, 3, and 4.

A.1 Instrument Theory

The following section is largely based on research conducted for two courses (ECE 559 and ECE 750) required for partial fulfillment of my Master of Science program. These works include a literature review addressing the analytical techniques used in metabolomic–type analyses [1], and another literature review discussing miniaturisation and fabrication of electrospray tips [2]. Concepts discussed in this section serve to provide a theoretical foundation for MCE–ESI–IMS and also present the

state–of–the–art in the field.

A.1.1 Microchip Electrophoresis–Electrospray Ionisation

While the theory behind MCE has been previously discussed, combining this technique with ESI requires an in-depth understanding of ESI mechanisms, as well as consideration of the implications of coupling the two technologies.

Electrospray ionisation (ESI) allows the production of gas–phase ions directly from a liquid sample. It has attractive implications in its ability to allow the analysis of macromolecules, such as biomolecules, and non–volatile analytes by methods such ion mobility spectrometry (IMS) [3] and MS [4]. In particular, ESI has proved to be very valuable in the analysis of proteins [4–7], peptides [8–19], amino acids [10, 20–23], and metabolites [24–26]. ESI's applicability to analysis of these molecules has had far reaching implications regarding the use of MS in bioanalysis.

ESI was first used by Dole and co-workers in the late 1960s when they demonstrated the transfer of macromolecules to gas phase ions for use in an ion–drift spectrometer [27]. Fenn, however, is often considered to be the pioneer of modern ESI techniques because of his application of the technology to MS [3]. Developments throughout the 1990s increased the use of ESI dramatically, especially as a means of facilitating MS detection of liquid separation methods [4]. Examples of this include the coupling of CE [25, 28–30] and HPLC [31] to MS. As previously mentioned, much of the current research on ESI is centered on the ionisation of biomolecules. Another significant portion of research effort is concentrated on the miniaturisation of the ESI source to allow integration with micro–total analysis (μ–TAS) and MCE systems, as well as to introduce sensitivity improvements [7, 8, 29].

Many of the mechanisms regarding the formation of gas–phase ions from neutrally charged analytes in the liquid phase are still not fully understood. Although the fundamentals surrounding the formation of liquid droplets at the ESI tip are well-established, the physics regarding the creation of gas–phase ions is still subject to debate [32].

Taylor Cone and Ion Formation Mechanisms

The Taylor cone is formed by the application of a large potential at an ESI tip to a solution containing ions. A large potential gradient is generated by positioning a planar counter electrode at some distance from the ESI tip (see Figure A.1). The cone itself forms when the repulsive force generated by the high potential acts on like charges and causes them to migrate to the surface of the liquid. Surface tension of the liquid opposes the repulsive force [33]. Equation A.1 describes the electric field, E_c, at a conventional capillary style ESI tip:

$$E_c = \frac{2V_c}{r_c \ln\left(\frac{4d}{r_c}\right)} \tag{A.1}$$

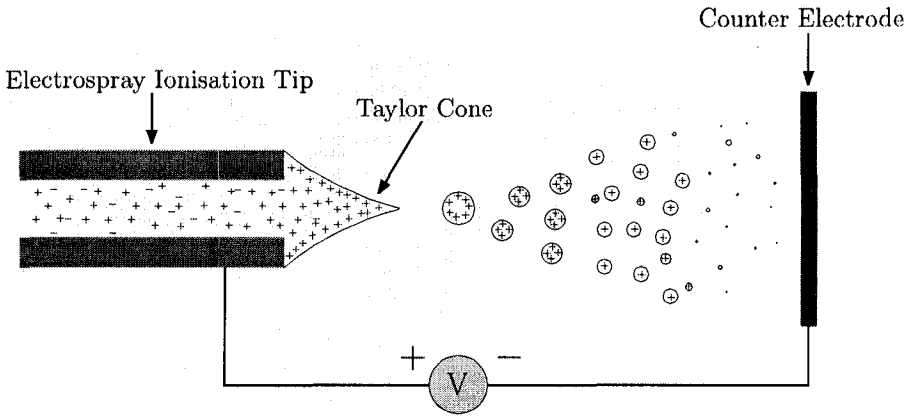

Figure A.1: Depiction of a Taylor cone and the droplet fission process that leads to gas–phase ions. This figure is adapted from another source [32].

where V_c is the electrospray potential, r_c is the outer capillary radius, and d is the distance to the counter electrode [33]. When the repulsive force experienced by the ions on the surface of the liquid exceeds the surface tension of the liquid, a Taylor cone forms. With a sufficiently high field, a stream of charged droplets is emitted from the tip of the Taylor cone [32]. These droplets move along the field gradient toward the counter electrode. During this movement, solvent evaporates, reducing the droplet radius, and causing the charge to be more condensed. As the radius (R_{Ry}) of the droplet decreases, repulsive forces (Coulombic repulsion) between charges cause the droplet to reach the Rayleigh stability limit, which is described by Equation A.2:

$$q_{Ry} = 8\pi(\epsilon_0 \gamma R_{Ry}^3)^{1/2} \tag{A.2}$$

where q_{Ry} is the droplet charge, ϵ_0 is the permittivity of a vacuum, and γ is the surface tension of the liquid. Upon exceeding this limit (through further solvent evaporation), the droplet breaks or fissures into multiple smaller droplets [32]. This process repeats as further solvent evaporation, and droplet fissions occur. Droplet fission results from a mechanism known as jet fission. In jet fission, an unstable droplet is distorted into a teardrop shape. From the teardrop tip, a stream of small droplets is released. These droplets contain approximately 2% of the initial droplet's mass, but around 15% of its charge [32]. Beyond this point, a few different theories exist on the actual mechanisms by which gas–phase ions are created.

Sample Introduction

Sample introduction consists of the flow of the sample and a solvent through a small capillary to the ESI tip. At this tip, a large positive or negative potential is applied to the liquid. Numerous factors determine the sample introduction parameters involved in ESI. These include tip configuration, capillary size and flow rate, voltage

polarity, sample content, and solvent content. When these parameters and their interdependencies are properly controlled, a Taylor cone (see Figure A.1) will form and analyte ionisation can occur.

Tip configuration refers to a sheathed or sheathless interface. A sheathed interface often consists of a larger capillary surrounding the sample capillary. This capillary supplies the solvent at the electrospray tip to ensure proper solvent composition where CE is coupled to ESI. Interfaces of this type often suffer from sample dilution because of the required solvent flow. A sheathless interface consists only of the sample capillary. In this case, solvent is introduced before entering the capillary which offers the advantage of reduced sample dilution. The obvious drawback is solvent compatibility. When ESI couples CE with another analytical instrument, the absence of an ESI compatible solvent may be detrimental to proper operation. As a result, sheathed interfaces are most commonly used as a method of providing the appropriate solvent to the ESI tip. Differences also exist in the method of applying the ESI potential to the tip. In the case of the sheathless interface, the tip receives a conductive coating treatment or is made from a conductive material. Sheathed interfaces on the other hand, often use the solvent as a method of applying the ESI potential to the sample [29].

Capillary size and solvent/sample flow rate jointly interact with many factors to play a significant role in ESI quality. These include spectrum resolution, solvent composition, fluid movement, capillary materials and construction, and ESI voltage. In both sheathless and sheathed configurations, sample is most often introduced through a capillary with inner dimensions on the order of micrometers [7]. While larger capillaries and higher flow rates were used in initial implementations of ESI, the trend has been to reduce capillary size and solvent/sample flow to reduce initial droplet size. The basic principle promoting this trend states that smaller initial droplet size formed by the capillary plays a significant role in reducing spectrum noise, and increasing sensitivity and resolution [3, 7]. This occurs because smaller initial droplets require less thermal energy to desolvate, causing the formation of more gas–phase ions at an earlier stage [15]. While large capillaries reduce the chance of clogging, they often lead to sample dilution [29] and spectrum resolution problems [7]. These capillaries also frequently rely on external pumping for sample delivery, thus providing the sample solution to the tip at a flow rate of microlitres per minute [4, 7]. The use of smaller capillaries and capillary action instead of pumping has lowered this flow to nanolitres per minute [3, 7, 8]. As a result, much of the research currently being conducted is focused on generating nanoelectrospray ionisation (nESI) using smaller capillary structures.

At the tip of the capillary, a positive (positive–mode) or negative (negative–mode) potential is applied depending on the nature of the sample under scrutiny. The high potential usually resides in the range of 2–5 kV [4], but as with flow rates, has been lowered to less than 1 kV in numerous designs [7, 8]. Cech provides a general rule for the applied voltage polarity. Positively charged ions formed from inorganic or organic molecules should be analyzed using a positive ESI potential,

whereas organic or inorganic negative ions should use a negative ESI potential [4]. Therefore, it is critical to have knowledge of the molecular properties of the targeted analyte before deciding on appropriate voltage polarity. The magnitude of the applied potential is also critical, as well as highly dependent on solvent properties and initial droplet size. Capillary construction material can also have an effect on the magnitude and placement of the applied voltage. In general, conductive capillary materials allow easier voltage application to the solution, lower voltage, and lower solvent electrolyte concentration than non-conductive capillary materials [4].

Solvent content plays a significant and very interdependent role in ESI. First and foremost, the solvent must have surface tension properties suitable for ESI. If solvent surface tension is high, stable ESI operation will require a larger potential applied to the tip. For positive–mode ionisation, solvents that contain a moderately polar organic solvent such as methanol in aqueous solution produce the most stable ESI. The organic solvent reduces the surface tension of the aqueous solution, and is usually present in concentrations of approximately 50% by volume [4]. A simple review of current literature will also show a prevalence of the use of acetic acid in positive–mode solvents [7, 20, 21, 23, 34]. The acid serves to protonate the solvent and promote analyte ionisation [4]. Negative–mode solvents differ far more in composition within the literature. For example, Chen *et al.* utilised 2–propanol, water, ammonium hydroxide in an 80:20:0.5 percentage volume ratio for a novel sheathed capillary [29], whereas Henriksen *et al.* evaluated the use of methanol or acetonitrile aqueous solutions [35]. Cech states that in order to produce stable electrospray in the negative–mode, the solvent should have the ability to produce stable anions, and to minimise the chance of electrical (also known as corona) discharge from the electrospray tip [4].

Sample content also plays an important role in electrospray performance. It determines the appropriate electrospray voltage polarity, and thus the solvent to be used as well. In addition, the method of ionisation undergone by the analyte is highly dependent on its properties. Analyte structure and the resultant properties of pH, pK_a, polarity, and charge all affect the method of ionisation [4].

Ion Formation Mechanisms

Analyte Charging Before the analytes enter the gas–phase as ions, they must undergo a process where they become charged. There are four basic mechanisms by which ions are formed. Ionisation occurs via charge separation, adduct formation, gas–phase reactions, and electrochemical oxidation or reduction. Charge separation develops from molecules that are charged in solution prior to being electrosprayed. This is the primary method of charging inorganic species, and organic and biological molecules with acidic or basic groups. Adduct formation charges molecules by the addition of a cationic (positive mode) or anionic species (negative mode) to the analyte. This process is most often present for polar analytes that do not contain acidic or basic subgroups. Charging analytes via gas–phase reactions does not refer

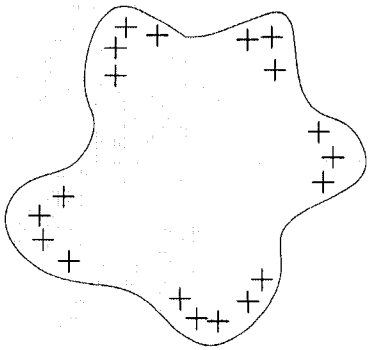

Figure A.2: Schematic depiction of inhomogeneous surface charge in an electrosprayed droplet due to highly charged analytes, such as proteins, migrating to the droplet surface. This figure has been adapted from another source [7].

to droplet fissions, but rather to interactions of molecules that have already been released from solution. In this scenario charged molecules (analyte or solvent) give up charge to molecules having a higher gas–phase proton affinity (GPPA) [4]. Cech *et al.* describe this phenomenon by stating that GPPA basically refers to the ability of a molecule to scavenge protons from another molecule. Thus, a molecule having a high GPPA will scavenge protons from a molecule having a lesser GPPA. In the case of ESI, Cech states that it is important to choose solvent with a lower GPPA than the analytes' GPPA. Failing to do this may result in the reduction of the analyte charge, and consequently, the detected analyte signal. This is not deemed to be a major issue with proteins and peptides, because they tend to possess very high GPPAs [4].

Electrochemical oxidation (positive mode) or reduction (negative mode) exists to balance the excess charge created by charge separation. This process has the ability to charge non-ionic analytes, but can be detrimental to ESI if the ions that are created compete with analyte for the extra charge [4]. According to Van Berkel, three constraints must be met for this to be an effective means of ionising neutral analyte. First, the current supplied to the ESI tip must be sufficient enough to oxidise or reduce all of the species in the solution including those that have lower redox potentials than the analyte, and the analyte itself. Second, the analyte must be present at the electrospray tip to allow for the oxidation or reduction reactions to occur. Finally, steps must be taken to ensure the first two requirements do not inhibit the formation of gas phase ions. This can be achieved by manipulating a number of parameters such as: 1) Removing or minimizing the presence of all species with lower redox potentials than the analyte, 2) increasing solution conductivity, 3) altering solution flow rate, 4) altering solvent composition, 5) altering the ESI potential, and 6) changing the capillary dimensions or geometry [36]. Most of these parameters exhibit highly complex interdependencies which will not be covered in the scope of this thesis.

Gas–Phase Ion Generation Upon ionisation of the analyte, gas–phase ions can be generated via ESI. In his 2000 paper, Kebarle revisits the two main theories explaining how gas–phase ions are produced. He addresses the charged residue model, brought forth by Dole, and the ion evaporation model, proposed by Iribarne and Thomson [32]. The charged residue model states that the cycle of solvent evaporation, and droplet fission occurs until a single analyte molecule remains in a droplet. As the last of the solvent evaporates, Dole stated that the remaining charge settles on the single analyte molecule, thus resulting in a gas–phase ion [27]. Iribarne and Thomson state that before the droplet reaches the final stage described by Dole, repulsion forces within the droplet cause the analyte molecule to break through the surface of the droplet and be released as a gas–phase ion [37, 38]. Kebarle states that it is likely that gas–phase formation results from a combination of the two mechanisms. One of the main reasons for the uncertainty of the mechanism surrounding gas–phase ion formation is the variety of results presented when using different analytes [32]. Juraschek supports Kebarle's theories during his evaluation of peptide nESI. While the main goal of his paper was to describe increased resistance of nESI to spectrum noise caused by salt contamination, he also discovered that the addition of protein to the analyte mixture altered the fission pathways experienced by the ESI droplets. Peptides have properties that allow them to carry a large majority of the excess charge in the droplet. This causes an inhomogeneous charge distribution on the droplet surface which leads to earlier droplet fission [7]. A schematic representation of this phenomenon can be seen in Figure A.2. This is further supported by Cech, who states that an analyte's tendency to migrate to the droplet surface (because of non–polar properties), promotes a higher ESI response [11]. Essentially, fission pathway, and thus ion formation are highly analyte dependent [7].

A.1.2 Miniaturisation and Integration

There are currently two main areas of interest driving current ESI research. As previously mentioned, nESI is a current area of interest because of the increased sensitivity and resolution realised by the technique. While nESI brings improved performance, integration of this type of interface with μ–TAS devices, will allow coupling of multiple analytic techniques onto affordable platforms [39].

Nanoelectrospray Ionisation

Nanoelectrospray ionisation can be defined as ESI by means of an interface capable of providing sample flow rates as low as one to tens of nanolitres per minute, with electrospray tip sizes on the order of 1μm [40]. As noted by Juraschek and El–Faramawy, flow rates of this magnitude result in smaller initial droplet sizes, and easier solvent desolvation, thus producing better sensitivity and resolution [7, 40]. Juraschek also reported better immunity to salt contamination of the sample [7]. Nanoelectrospray ionisation offers other advantages including the expansion of the

range of analyzable biomolecules, and non-covalent complexes, in addition to the use of aqueous solutions with minimal to non-existent organic additives [41]. In spite of these advantages, nESI can suffer from a lack of reproducibility. As a result, quantitative analysis is often difficult to perform [42].

Salt contamination is of particular concern when analyzing biological samples. The basic premise for increased suppression of salt contamination in nESI arises from initial droplet formation. For example, a droplet generated by conventional ESI will be larger than one resulting from nESI. Assuming these two droplets are produced from the same solution, they will have equimolar concentrations of salt when initially formed. Therefore, the amount of salt contained in the larger droplet is greater. Through the course of desolvation, the larger droplet must undergo more solvent evaporation than the smaller droplet, to produce droplet fission and the subsequent gas–phase ion. As a result, subsequent offspring droplets resulting from conventional techniques will have a higher salt concentration than nESI offspring. Because of this, analytes electrosprayed using a conventional source will exhibit less immunity to sodiation [7]. In particular, samples containing buffer salts may benefit from nESI [41].

As mentioned earlier (Section A.1.1), fission pathways in electrosprayed droplets are highly analyte dependent [7]. Creating gas–phase ions of certain types of analytes is difficult due to their physico–chemical properties. Because of this, hydrophilic or lowly charged analyte species are suppressed in analyses involving ESI [42]. For example, Karas states proteins and peptides are preferentially released as gas–phase ions in conventional ESI as compared to other types of biomolecules such as oligosaccharides, glycosides, and glycoproteins. Carbohydrate containing compounds are often lowly charged in solution, and have non–surface active properties, which prevent them from migrating to the surface of droplets to be released as gas–phase ions. Proteins and peptides on the other hand, often migrate to the droplet surface because of their charge and surface active properties, resulting in higher gas–phase ion generation [41]. In nESI, smaller droplet size increases the surface to volume ratio of the droplets, thus allowing non–surface active analyte species to get closer to the surface and be released as gas–phase ions [42]. The same holds true for inorganic analytes [41].

Although nESI does offer the aforementioned benefits, it can suffer from a lack of reproducibility. While evaluating nESI ion generation efficiency, El–Faramawy observed that a large reason for inconsistency between measurements may be due to small differences between identical nESI tips. These variations may include tip size, geometry, surface characteristics, or material impurities [40].

Electrospray Microfabrication and Micro–Total Analysis System Integration

The integration of microfabricated ESI tips with micro–total analysis systems (μ–TAS) or lab–on–a–chip (LOC) devices brings exciting possibilities, and creates interesting applications. Such integration is also necessary to create the MCE–

ESI–IMS system proposed in this thesis. Coupling glass or polymer microfluidic devices with an integrated ESI tip may allow sample preparation, and separation to be integrated with analysis by MS [39]. It should also be noted that these ESI tips usually exhibit nESI characteristics such as low flow rate and small tip dimensions [8, 14, 43–45].

Typical implementations of these devices include a glass, polymer, or silicon based substrate with a tip integrated onto one end of the device. Although the configuration of the tip can take various forms, only a few different designs will be discussed here. Historically, ESI emitters have been made from pulled fused silica or metal capillaries with dimensions on the order of around 100μm [5, 11, 22, 28]. As the availability of microelectromechanical systems (MEMS) fabrication techniques become more widespread, researchers such as Arscott and Le Gac have reduced the emitter dimensions drastically [8, 46]. The advantages of doing so are numerous. Both Arscott and Le Gac have observed the reduction of the potential required to generate electrospray from thousands of volts to less than 1000 [8], and in some cases tens of volts [47]. In addition, reducing emitter dimensions also has the potential to improve the resolution and sensitivity of analyses by reducing the solvent volumetric flow to create a nESI source [7, 40]. While the performance of nESI is typically better than conventional ESI, nESI can be subject to a lack of reproducibility. El–Faramawy cites that some of the reproducibility problems associated with nESI may be due to small variations in emitter characteristics [40]. Batch fabrication of microfabricated emitters may be able to alleviate some of the variance leading to degraded reproducibility. Given the recent advances in microfabricated LOC applications, the need for consistent and reproducible emitters, and the above motivations for miniaturisation, it is easy to see the motivation for generating microfabricated ESI emitters.

Device Geometry ESI emitter geometries can be placed into four basic categories. Planar enclosed emitters use flat or triangular shaped ESI emitters with fluidic channels that are enclosed on three or more sides and that run in parallel with the substrate surface. In contrast to planar enclosed geometries, planar open emitters employ triangular emitters with fluidic channels in which the fluid is only confined by two or fewer surfaces. In–plane conical and capillary geometries employ cylindrical or conical ESI emitters that emerge from fluidic channels that also run parallel to the substrate surface. Often, this type of geometry employs relatively crude fabrication techniques that are not suitable for mass production. The last geometry, out–of–plane, incorporates single or multiple ESI emitters fabricated onto a single substrate. Unlike the other geometries, the ESI emitters protrude perpendicularly from the substrate surface. Examples of these geometries can be found in Figure A.3.

Planar Enclosed As previously mentioned, planar enclosed emitters have been implemented with both flat ended [48, 49], and triangular ended chips [50],

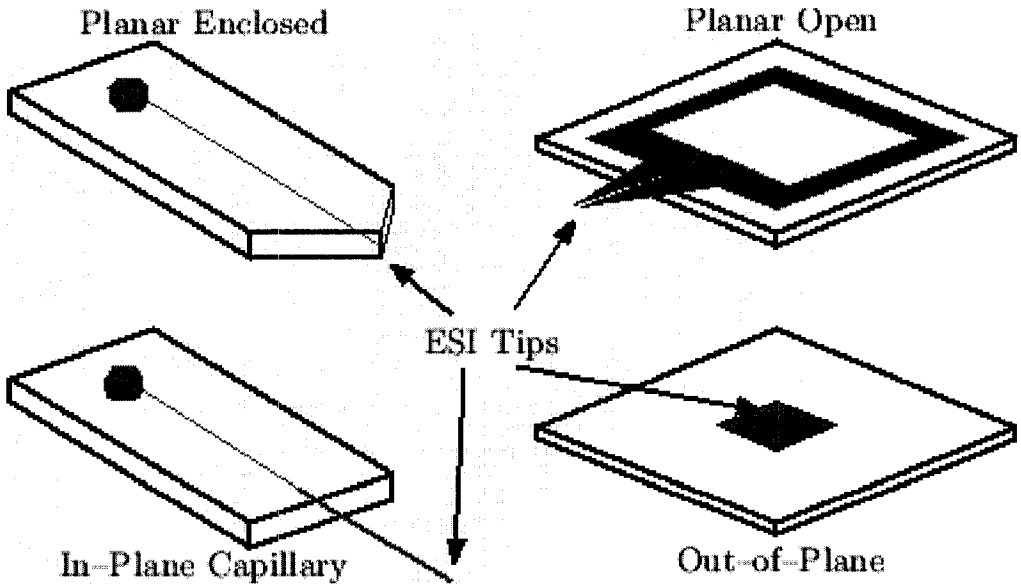

Figure A.3: This figures shows illustrations of the different geometries present in published work on micro–chip based ESI. In each case, the ESI tip (the actual fluid outlet, not the complete structure) is approximately 1μm to 100μm in diameter.

although chips with flat ends do not perform as well due to dispersed surface wetting and subsequent Taylor cone degradation [51]. These emitters are commonly fabricated in glass [48, 52], Poly(dimethylsiloxane) (PDMS) [14, 49, 50, 53–55], SU–8 [56], or other plastics [50, 56–59]. Planar enclosed emitters are likely the most widespread in the literature, but no current implementations using this type of design have been commercialised. In addition, this geometry is often a simple extension of microfluidic structures, and as such, commonly uses fabrication techniques employed by microfluidics. Many of the polymer–based devices have been fabricated using unconventional fabrication techniques such as hot embossing and replica molding.

Planar Open With only one exception [59], a single research group from France has mainly implemented this type of geometry. The majority of Arscott and Le Gac's designs have employed photolithography to pattern SU–8 and use it as a material capable of producing structures with high aspect ratios [44, 46, 60–64]. Some of Arscott's recent designs have used a more traditional MEMS material, polysilicon, as the base for the ESI emitter. The use of polysilicon required more advanced microfabrication techniques such as reactive ion etching (RIE), focused ion beam (FIB) etching, and chemical vapour deposition (CVD) [8, 47]. The unique aspect of this geometry is its method of transporting the liquid to the emitter. Contrary to planar enclosed geometries that confine the liquid from all sides, these devices only confine the liquid on the sides. Their operation has been compared to that of a fountain pen [61]. While this is mainly an operational concern, this does

bring about differing requirements for fabrication such as the lack of need for an aligned cover plate. The other type of planar open design used a triangular 5μm thick film sandwiched between two plastic plates. The tip was placed so that it protruded from the end of a microfluidic channel. Fluid exiting the channel was guided by the triangular emitter structure [59].

In–Plane Conical and Capillary In–plane conical and capillary type designs generally employ the most complex three–dimensional emitter geometries. In some cases, these geometries are achieved by mechanical machining [65, 66], insertion of a conventional capillary into the chip structure [67–71], or manual application of material to form the emitter [72]. None of these approaches really lend themselves to large–scale batch production or high levels of reproducibility. The remaining example of this type of geometry has been described papers by Fortier [58] and Yin [45]. The design used laser ablation to fabricate a conical emitter out of polyimide. Evaporation deposition was also used to form gold contact electrodes [45, 58]. Overall, the complex three–dimensional geometries demanded by such designs have probably led to their lower prevalence within the literature.

Out–of–Plane Out–of–plane devices are fairly rare within the literature, but so far the only commercial chip–based electrospray device in existence is based on an out–of–plane design [39]. Of the devices found in the literature, two designs were found. The first, implemented by Schilling *et al.*, employed the use of Computer Numerically Controlled (CNC) milling with accuracy of 0.5μm to fabricate the device [73]. The other design, discussed by Griss *et al.* [74], Schultz *et al.* [75], and Sjodahl *et al.* [76], uses deep reactive ion etching (DRIE) to pattern both silicon and silicon dioxide into ESI emitters.

MCE–ESI Integration In terms of integrating MCE and ESI specifically, several technical hurdles still exist. First, MCE buffer incompatibility with ESI must be rectified. In the past this has been achieved by using a low pH buffer [67], something that is not common in electrophoretic separations. Non–CE applications have incorporated the use of a sheathed ESI interface [16, 25, 26, 28, 29], but at present it is unknown how this could be effectively implemented on a chip. Additional challenges come in effectively coupling a microfabricated ESI tip to a microfluidic chip. Few systems have been able to accomplish this [14, 67, 72, 77], and only one of these used interfaces that were incorporated directly into the structure of the chip [14]. As a consequence, these devices required the ESI interface to be manually inserted into the chip [67], or separately fabricated after the microfluidic chip was complete [72, 77]. Combining the microfluidic channels and the ESI chip during initial fabrication stages may provide a more robust interface, and may facilitate mass production. Finally, the use of liquid polymers is not possible because they may have the tendency to migrate out of exposed microfluidic channels. Porous

polymer monoliths (i.e. solid polymers) have been shown to effectively produce nESI at the outlet of a microfluidic channel [50, 52].

A.1.3 Ion Mobility Spectrometry

As defined by Creaser *et al.*, ion mobility spectrometry (IMS) is a gas–phase electrophoretic separation technique capable of separating analytes based on mobility. Charge, mass, and collisional cross–section all play a role in determining an analyte's mobility and differences in mobility amongst various analytes allow them to be separated electrophoretically [78]. Early versions of ion mobility spectrometers, known at the time as plasma chromatographs, were introduced in the early 1970s, but the technique was virtually abandoned soon after [79]. Baumbach attributes this abandonment to a poor understanding of ion–molecule chemistry and its mechanisms [80].

IMS is perhaps most well–known for its use in airport security screening. These devices are used by security personnel to detect trace amounts of narcotics or explosives, and are in use around the world [81]. Small hand–held ion mobility systems were also used in the Gulf War for detecting chemical warfare agents [82]. Other application areas include air quality measurement [83, 84], water quality monitoring [85], food quality assessment [82], and structural determination of small molecules, biomolecules, and polymers [78]. In recent years, advances in IMS and sample introduction methods have allowed for its application to the analysis and characterisation of biomolecules [78]. Examples of biomolecules analyzed by ion mobility spectrometry include proteins [5, 12, 15, 22, 86, 87], peptides [10, 15, 17–19, 34, 88–90], amino acids [9, 20–23, 34], and various metabolites [81, 87].

Given the relative age of this technique as compared to MS it is easy to see why many analysis techniques employing IMS have not yet fully matured. Although analysis of biomolecules by IMS is still in its infancy, the potential for complimentary separations in tandem with MS, and perhaps compact equipment size explain the reason for the breadth of research being conducted in this area. One of IMS's greatest advantages lies in its simplicity. Contrary to MS, analysis by IMS is often conducted at atmospheric pressure, eliminating the need for vacuum pumps. This greatly reduces instrument cost and size, while retaining high levels of information density [80].

Theory of Operation

Separation of analytes via ion mobility spectrometry is based on a sequence of events starting with sample introduction and ion generation. There are a variety of means of introducing the sample which will be discussed below. After the sample is introduced, ions are permitted to enter a drift region, where they travel along an electric field gradient through a drift gas to a detector. The ions' mobilities determine their time of flight through the drift region, thus producing a separation based

on differing ion mobility. Upon arrival at the detector, ions produce a spectrum consisting of a number of peaks. Each peak indicates a different drift time, and consequently a different ion in the sample.

The method of introduction of sample into the drift region as ions can take many forms. Although each method has the ability to produce gas–phase ions, the nature of the sample will likely determine the mechanism used for ionisation, and the ions produced [80]. Because the main concern of this thesis is the coupling of the previously discussed ESI technique with IMS, methods such as atmospheric pressure chemical ionisation, corona discharge, matrix–assisted laser desorption/ionisation (MALDI), and photoionisation will not be addressed.

Once sample is introduced into the drift region, IMS separations are conducted based on ion mobility. Mobility results from a number of molecular characteristics and IMS operating parameters. Reduced mobility (K_0), is generally expressed using Equation A.3 and has units of $\mathrm{cm}^2/\mathrm{V}\cdot\mathrm{s}$:

$$K_0 = \left(\frac{d}{t_d E}\right)\left(\frac{273}{T}\right)\left(\frac{P}{760}\right) \tag{A.3}$$

where d is the length of the ion drift region (cm), t_d is the drift time (s), E is the electric field strength (V/cm), T is the temperature of the drift region (Kelvin), and P is the pressure in the drift region (Torr) [78]. The first part of Equation A.3 relates directly to the average ion velocity ($\bar{v}_d$), which is commonly expressed in units of cm/V-s. Equation A.4 gives the relationship which determines ion velocity:

$$\bar{v}_d = \left(\frac{d}{t_d}\right) \tag{A.4}$$

As the ion traverses the drift region, it periodically runs into neutral drift gas molecules. After the collision, the ion is accelerated by the electric field until it experiences another collision. This process continues until the ion is detected, and it results in the average velocity ($\bar{v}_d$) [21].

The following sections discuss the various molecular properties and operating characteristics that affect ion mobility [9].

Collisional Cross–Section, Mass, and Charge Collisional cross–section (Ω_m), reduced mass (μ), and charge (q) relate to ion mobility based on Equation A.5:

$$K^{-1} = \left(\frac{16N}{3}\right)\left(\frac{\mu kT}{2\pi}\right)^{1/2}\left(\frac{\Omega_m}{q}\right) \tag{A.5}$$

where K is the measured mobility, N is the number density of the drift gas, k is the Boltzmann constant, and T is the temperature [9]. In general, larger, more massive ions with a low charge will exhibit lower mobilities than smaller, less massive ions with a higher charge. An ion's mass relative to the mass of the drift gas also

plays a critical role in determining ion mobility. Reduced mass (μ) is expressed in Equation A.6:

$$\mu = \frac{mM}{(m+M)} \tag{A.6}$$

where m is the mass of the ion, and M is the mass of the drift gas. In general, ions that are small compared to the drift gas will have their mobility mainly dictated by mass, whereas ions that are comparatively large ($\mu \rightarrow 1$) will tend to have their mobility dictated more by their collisional cross–section [79, 80].

When studying the effects of drift gas composition (see Section A.1.3), Beegle noted that when modeled as a sphere, ion collisional cross–section (Ω_m) could be calculated by Equation A.7:

$$\Omega_m = \pi(r_{ion} + r_{gas})^2 \tag{A.7}$$

This means that collisional cross–section is not only a function of the ion, but also of the drift gas [9]. Creaser states that larger, more massive ions can be modeled as a solid–sphere, while smaller ions must be modeled taking into account ion–drift gas interactions (see Section A.1.3) [78]. Separations partially based on cross–sectional area gives IMS an advantage over MS. When substances have the same mass and charge, they cannot be separated by MS because their mass–to–charge ratio is identical. However, when using IMS, geometrical differences may result in a resolvable separation of the two compounds [19].

Electric Field Strength The relationship given by Equation A.5 only holds true for a limited electric field strengths. When higher field strengths are applied, ion mobility becomes field dependent [91]. In general, mobility is no longer field independent when the ratio of E/N (electric field strength to buffer gas number density) is $\leq$ 2 Td (1 Td = 10^{-17} C-cm^2) [78]. Thus, any substantial increase in field strength or decrease in drift gas pressure will make ion mobility field dependent. This simple explanation is sufficient for understanding the impact of electric field strength, but if more detail is required, a thorough paper outlining these concepts was authored by Revercomb and Mason in 1975 [92].

Drift Gas Interactions As previously stated, ion–drift gas interactions can play a large role in determining an ion's mobility. Karpas and Berant state that the drift gas polarisability as well as mass can have a significant effect on ion mobility. In general, as the mass of the drift gas molecules increases, mobility will decrease due to an increase in collisional cross–sectional area. When the drift gas polarisability is increased, the ion mobility will decrease as well [93]. Beegle attributes the decrease in mobility to increased "long–range ion–induced dipole interactions" that alter the collisional cross–section of the ion. He also introduces the relationship in Equation A.8:

$$r_{eff} = m\alpha_p + r_{act} \tag{A.8}$$

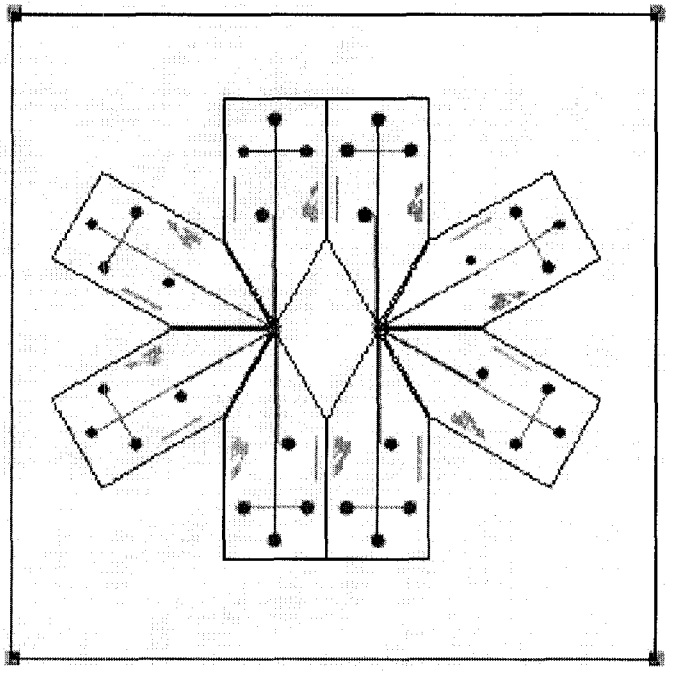

Figure A.4: An illustration of the photolithographic mask used to fabricate the MCE–ESI chips. Eight chips were fabricated on each glass wafer. The intersecting channels at the ESI tips of each chip permitted filling of the channels with wax during dicing.

where r_{eff} is the effective radius of the ion, m is an indicator of the ion's charge density, α_p is the drift gas polarisability, and r_{act} is the original radius of the ion. One can see from this relationship that as the charge density decreases (mass increases), the effect of drift gas polarisability will have a lessened impact on ion mobility. Thus, more massive ions are less affected by drift gas polarisability [9]. Drift gas composition characteristics have been exploited to separate ions that have similar mobilities [9, 87, 88].

A.2 MCE–ESI–IMS

As previously noted, much of the work with the MCE–ESI–IMS system centered on design and fabrication of the MCE–ESI microchips. Assembly of IMS components designed by Eric Cheong [5, 94], a former member of the Applied Miniaturisation Laboratory, and his successors represented a minimal proportion of the work done in this project. Aspects of the IMS system design and assembly, including portions not under my scope of work, are presented to supply continuity to the project and to discuss any issues that were encountered during device assembly.

A.2.1 MCE–ESI

As mentioned in Section A.1.1, coupling CE with ESI can be a daunting endeavour. Buffer incompatibility plays a large role in making the two techniques difficult to integrate. Nevertheless, an attempt at fabricating a MCE–ESI chip using a planar enclosed geometry with a sheath flow was made. Figure A.4 contains an image of the mask designed for these chips. The chips were constructed from borosilicate glass, according to the University of Alberta Nanofab's glass microfabrication protocols. Previous ESI devices used in the AML consisted of stainless steel hypodermic needles [5], and small capillaries manually inserted into holes drilled at the edge of a microfluidic chip. The use of a chip with a fully–integrated ESI tip has not been previously attempted in the AML.

Figure A.5 contains a detailed illustration of the chip and Figure A.6 contains a photograph of the chip that has not been diced on all sides. The channels that form a cross consist of an injection channel and a separation channel. While the design is similar to that of more conventional MCE chips used in electrophoresis (see Chapter 3), the separation channel is not terminated in a well. Instead it is designed to exit the chip at the ESI tip. A secondary channel runs parallel to the separation channel. It begins with a well and also terminates at the edge of the chip, close to the ESI tip.

The basic idea behind the chip concept is to conduct an electrophoretic separation of proteins in the separation channel while providing the necessary sheath flow solvent via the secondary channel. Originally the intention was to polymerise polyacrylamide gels in the separation channel to permit separation of proteins (or other analytes). The use of cross–linked gels was also believed to be advantageous because it may not have been subject to migrating out of the channel like liquid sieving matrices may be. As previously noted, the use of porous polymer monoliths in microfluidic ESI structures has been documented in a few publications and shown to be useful in generating stable nESI [50, 52]. It is unknown if such a porous polymer monolith would reduce the need for a sheath flow in an MCE–ESI system since both of these published examples used solvents designed for ESI. While the concept has not been tested, the electrophoretic voltage used to separate the proteins could actually be applied to the ESI solvent well (ESW). Ideally, the ESI solvent would be drawn to the ESI tip and form a liquid junction with the main channel, thus permitting electrophoretic separations. The voltage applied at the ESW would also act as the ESI tip potential required for electrospray. At the present time, the system has not been tested and numerous revisions to the chip and the concept are expected.

With the exception of chip dicing, the microfabrication protocols provided by the University of Alberta Nanofab were strictly followed. Due to the nature of the chips and the exposure of channels to diced surfaces, extra procedural steps were conducted to minimise the amount of debris that entered the exposed channels during dicing. A water soluble wax (Carbowax^{TM} 1450, Dow Chemical, Midland, MI) was melted and permitted to fill the channels of the chips before dicing. The

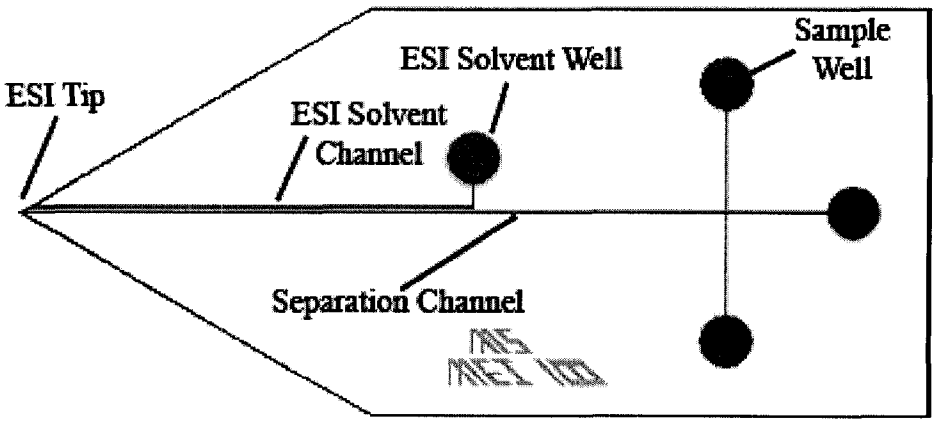

Figure A.5: A detailed illustration of the MCE–ESI chip.

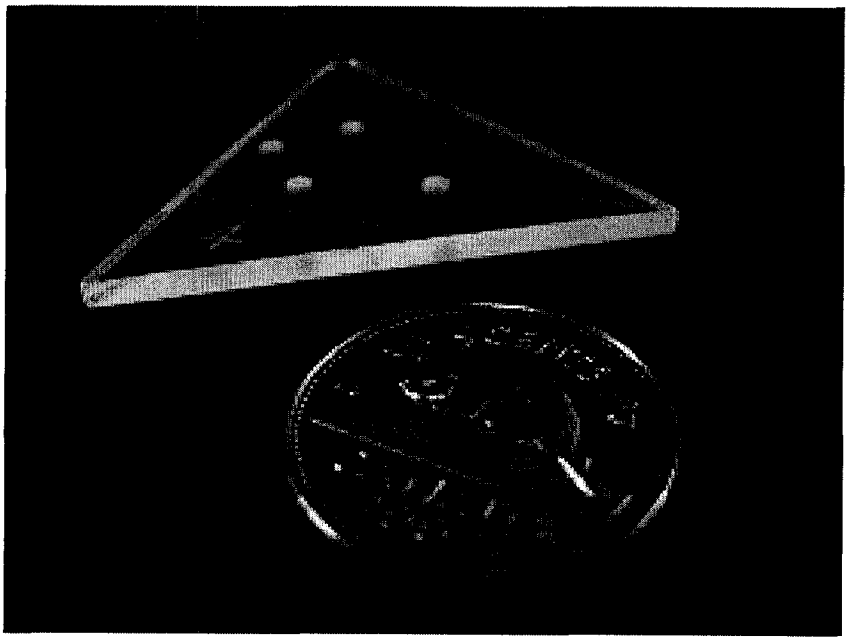

Figure A.6: An image of a partially diced MCE–ESI microfluidic chip.

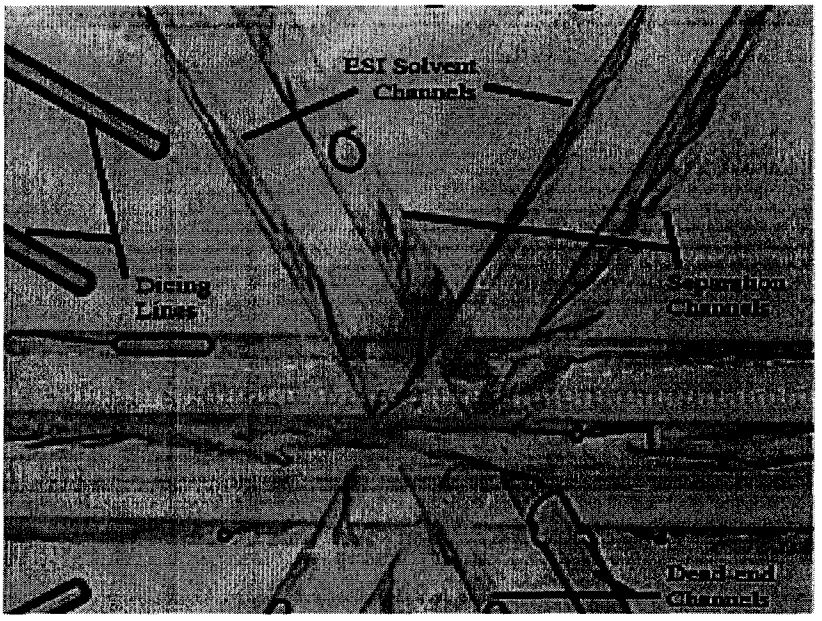

Figure A.7: An image of the tips of four MCE–ESI chips prior to dicing. Two separation and ESI solvent channels are identified in the image. The chips' channels were designed to intersect to allow filling of the channels with wax prior to dicing. The wax filling the channels in this image was intended to minimise the entry of debris into the exposed channels during dicing.

chips were placed on a hot plate and small pieces of wax were strategically placed into various wells. As the wax melted it filled the channels. The layout of the chips on the glass substrate minimised dead-end channels and promoted complete filling of the channels that would be exposed on the diced chips. See Figure A.7 for an image of the chips' ESI tips filled with wax before dicing.

After being filled with wax, the chips were diced as per normal methods. Extreme care was given to ensuring dice line accuracy. Inaccurate dicing could lead to the separation channel not exiting the chip right at the ESI tip. While the effects of this have not been tested, it is expected that such an occurrence would hamper the liquid junction and efficient ESI of the analytes.

Following dicing, the wax near the end of the exposed channels had actually been partially dissolved away (see Figure A.8). Proper alignment of the separation channel with the ESI tip was also assessed (see Figure A.9) and found to be poor in some instances. In order for ideal dicing to take place, dicing alignment and tolerances had to be on the order of half of the width of the separation channel (25μm to 50μm). Given the complex layout of chips on the substrate and the number of cuts that needed to be made, this proved to be quite difficult and led to some misalignment of the separation channel with the ESI tip. After dicing was complete, wax was easily flushed out of the channels by placing the chips on a warm hot plate. Upon being heated, the wax melted and was flushed with the application of

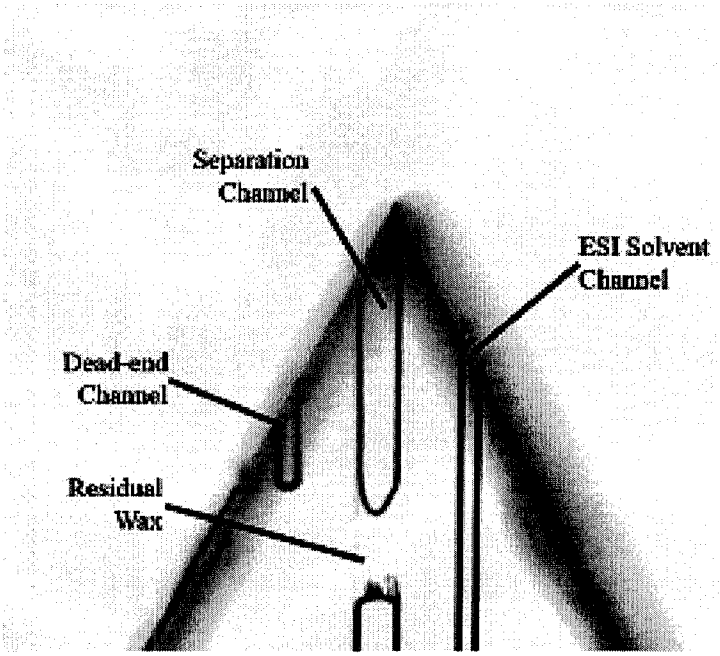

Figure A.8: An image of the tip of a MCE–ESI chip after being diced. Only some residual wax remains in the channel after dicing. The water soluble wax dissolved out of most of the channels. The alignment of the separation channel with the ESI tip is reasonably good compared to the chip shown in Figure A.9 because the separation channel emerges very close to the tip. This ESI was not damaged like the chip in Figure A.9.

pressurised water to the wells.

After conducting more work with protein separations and polyacrylamide gels, the following concerns with the MCE–ESI chip design and concept have arisen. First, polyacrylamide gel drying, similar to that experienced in the presence of dry wells, at the exposed portion of the separation channel is likely. Such drying may result in the formation of a bubble in the separation channel and the loss of the separation channel's conductive path. Without adequate testing, it is not known what amount of sheath flow will be required to prevent this drying. Secondly, the SDS–PAGE separations discussed in Chapters 3 and 4 would not be appropriate for analysis in this chip. Binding of SDS to proteins significantly alters the mass of the protein and also imparts a large negative charge on the protein. Although the SDS–PAGE separation itself could be conducted, SDS–protein complexes would not be representative of the true mass of the protein and would also be highly negative. As a result, positive mode ESI would not be feasible and drift times for SDS–protein complexes would not be representative of the original protein cross–sectional area, conformation, or native charge. It is likely that separations of native proteins or peptides would be more applicable to the MCE–ESI system. Native protein separations (native–PAGE) are attainable using similar techniques to those discussed in Chap-

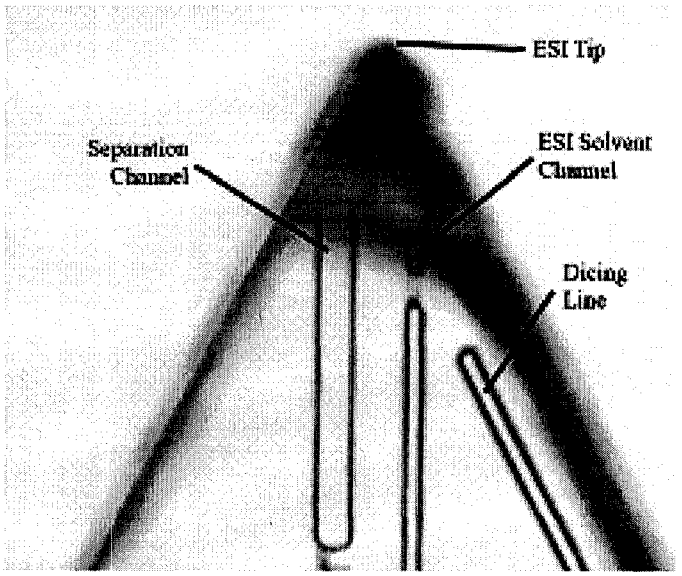

Figure A.9: An image of the tip of a MCE–ESI chip after being diced. The alignment of the separation channel with the ESI tip is poor compared to the chip shown in Figure A.8. The alignment is considered to be poor because the exit of the separation channel from the chip is off to one side of the ESI tip. It is expected that this would adversely affect the formation of a liquid junction with the ESI solvent and the establishment a Taylor cone. This tip was also damaged during the dicing process. A piece of glass chipped away from the tip which is indicated by the refraction of the light passing through the chip. This also made the exact location of the channels difficult to visually assess under the microscope.

ters 3 and 4. Alterations to the protein electrophoresis procedures would require the use of a new sample buffer, running buffer, and standard samples. Native–PAGE has been shown to be feasible in electrophoretic systems similar to those that have been previously discussed in this work [95, 96].

A.2.2 IMS Hardware and Software

Although this section touches on many aspects of the IMS system design that were outside the main scope of my work, this discussion has been included to provide project continuity and address issues discovered during the assembly of the device.

Over the past few years, several generations of IMS hardware based on the designs of Ben Bathgate (Department of Electrical and Computer Engineering, University of Alberta), Eric Cheong (former AML member), Alex Stickel (former AML member), Brent Chizen (former undergraduate AML member), Yujie Han (former postdoctoral AML member), and Loi Hua (former AML member) have been in use. The most recent operational version used by Brent Chizen and Yujie Han, is currently not operational. The system has sat dormant for such a long period of time that documentation regarding changes made to the system during the last few years is severely lacking.

Currently, a redesign of the system mentioned above has been incompletely developed. Largely based on designs by Ben Bathgate, Loi Hua, and Alex Stickel, this new system is intended to replace the one used by Brent Chizen and Yujie Han. It is more compact and features higher levels of design sophistication and integration. The majority of work performed within the scope of this thesis addressed the assembly of this system and some development of the design. Design development was limited to design modifications and fabrication of the shutter gate (see subsequent discussion and Figure A.12) and development of the chip stage to be used with MCE–ESI microchips. Ben Bathgate was responsible for the fabrication of the shutter gate, while work on the chip stage was performed by myself. The subsequent discussion contains an overview of the design and current status of the system.

The IMS ionisation region and drift column are constructed of thirty–one equally spaced printed circuit board (PCB) plates with conductive material on both sides. The center of each PCB plate has a circular cut–out. Because each PCB is conductive on both sides, the column consists of conductive surfaces with alternating spaces of either air or PCB material between them. The conductive surfaces are joined together in series with a $1M\Omega$ resistance between each surface. The $1M\Omega$ resistors are surface mounted to the PCB plates. Connections between conductive surfaces on the same PCB plate are made with PCB vias, whereas connections between conductive surfaces on adjacent PCB plates are made with small wires soldered to conductive pads on each plate. When a voltage is applied across the column, a voltage ladder is formed by the series of conductive surfaces. This ladder produces the electric field required for the IMS column. An image of the IMS

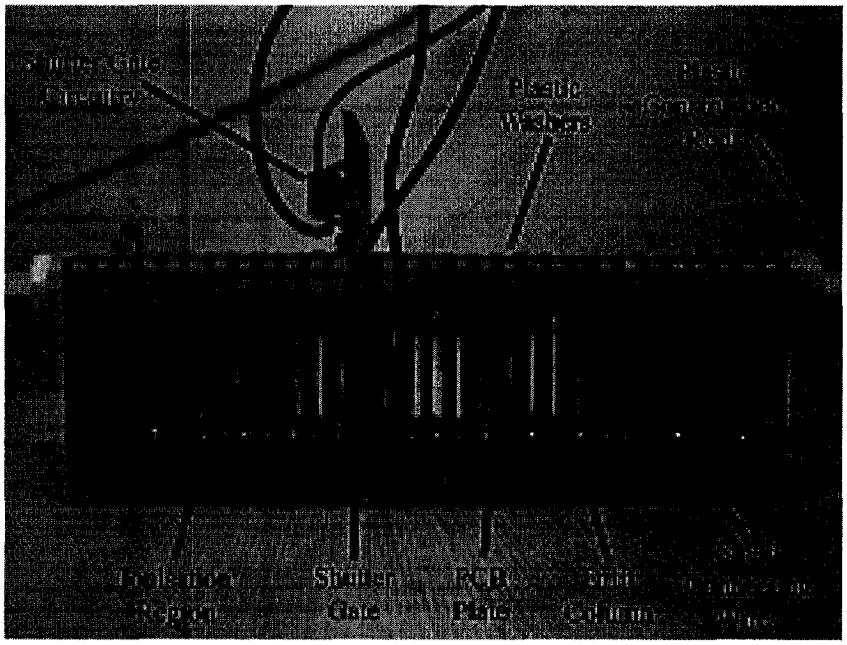

Figure A.10: An image of the partially assembled IMS column showing key features of its construction including the ionisation region, the drift column, the shutter gate and associated circuitry, the construction rods and washers, and the wires connecting adjacent PCB plates.

column is shown in Figure A.10.

The ion shutter gate is also incorporated into the column, and its PCB plate can be seen in Figure A.10. It is the thirteenth plate, and it is placed between the ionisation region and the drift column. This PCB plate contains a series of interdigitated wires that traverse the circular hole in the PCB plate. These interdigitated wires are controlled by signals sent to the switching circuitry located on the shutter gate's PCB plate. When the wires are all held at the same potential, ions are allowed to freely pass through the gate. When adjacent wires are held at different potentials, this creates an orthogonal electric field and prevents the passage of ions into the drift column. Switching of the potentials on these interdigitated wires is achieved by signals sent to optoisolators that are mounted directly on the shutter gate PCB. These optoisolators are denoted as 'Shutter Gate Circuitry' in Figure A.10, but are not shown or mounted to the shutter gate PCB in Figure A.12.

At each end of the IMS column is a focusing grid as shown in Figure A.11. The focusing grid consists of a similar PCB plate to those of the rest of the column, except it has small conductive wires running across the circular cut-out. These wires are held at the potential of the plate they are connected to and are not switchable like the wires of the ion shutter gate.

The column is held together using threaded plastic construction rods, washers, and nuts. A few issues were encountered with the assembly of the column. Firstly, the small wires connecting conductive surfaces on adjacent PCB plates were very

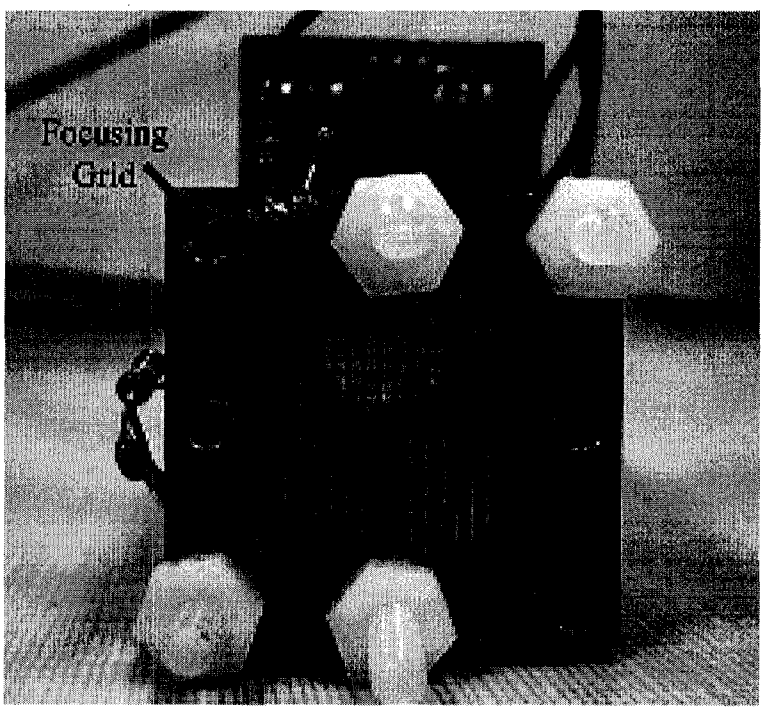

Figure A.11: An image of a focusing grid at the end of the IMS column

difficult to place and properly solder. While the column was tested for short circuits in the IMS column, no high voltages have been applied to the column to date. It is not known if these small wire connections will be sufficient for proper operation of the column. Fabrication of the shutter gate also proved to be problematic. Construction rod holes placed on the sides of the circular cut–out (used for passing the threaded plastic support rods through the PCB plates) were too close to the cut–out and did not allow for proper anchoring of the interdigitated wires (see Figure A.12). Consequently, revisions of the design saw two of the six construction rod holes in the shutter gate removed to allow for a larger supporting area for the wires. This proved effective, although the shutter gates were still extremely difficult to fabricate. Even with the construction rod hole modification, the interdigitated wires were prone to delamination (see Figure A.12). These modifications constitute the only IMS hardware design revisions performed within the scope of the this work.

The ion detector, also known as the Faraday plate, for the IMS has not yet been assembled or fabricated. Ben Bathgate, Eric Cheong, and Loi Hua were responsible for the design of the circuitry used for the detector. The PCB containing the circuitry for the detector (PicoAmpV1a) has been populated (see Figure A.13). To date no testing has been conducted on this circuitry. Care must be taken when handling this PCB, as oil resulting from direct contact with skin can affect the performance of the circuit. Once assembled, care must also be taken in ensuring that the Faraday plate and detection circuitry are properly shielded to mitigate the influence of ambient noise on detection capabilities.

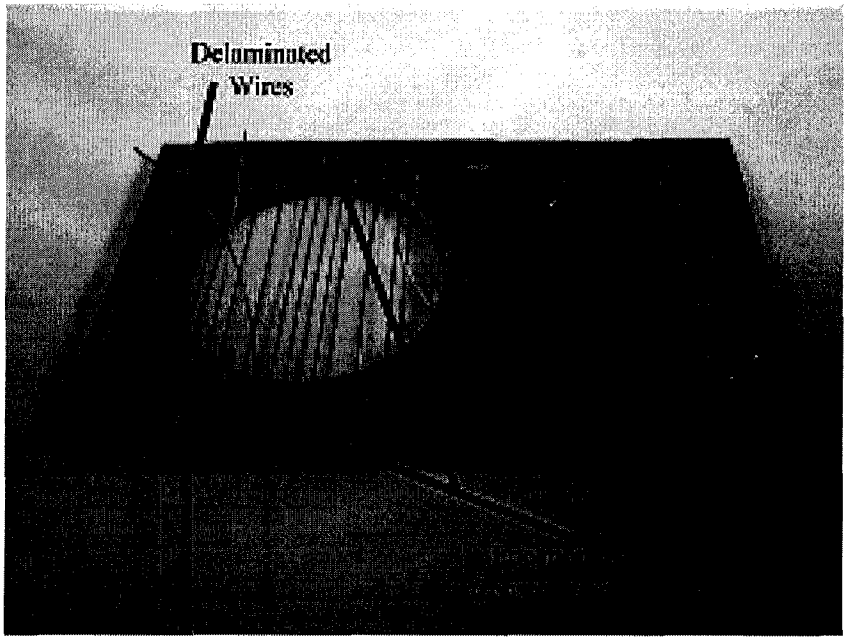

Figure A.12: An image of the redesigned shutter gate PCB plate. As indicated, construction rod holes were removed to increase the surface area on which the interdigitated wires were supported. Despite the redesign, shutter grid construction was tedious and prone to interdigitated wire delamination and breakage.

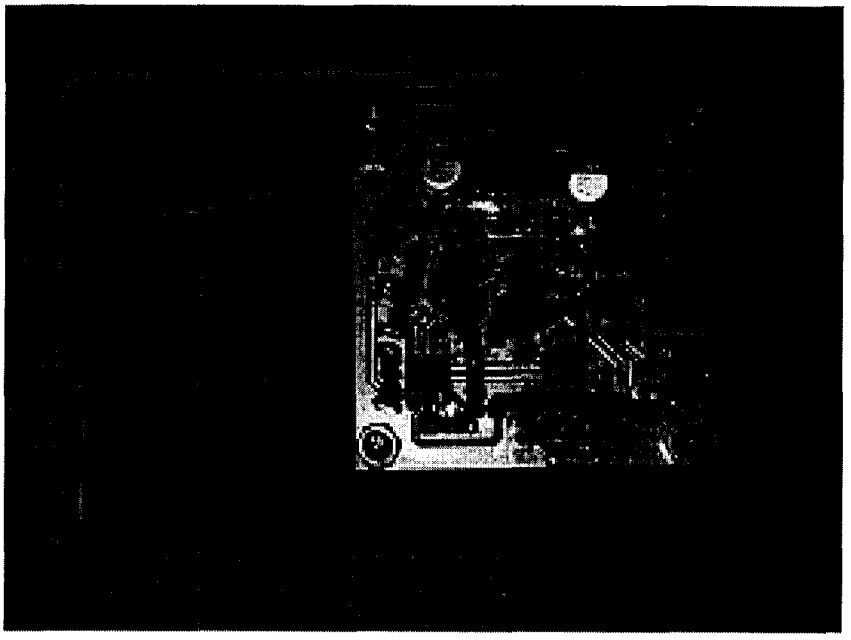

Figure A.13: An image of the populated PCB containing the detection and amplification circuitry required to detect ion current generated at the Faraday plate.

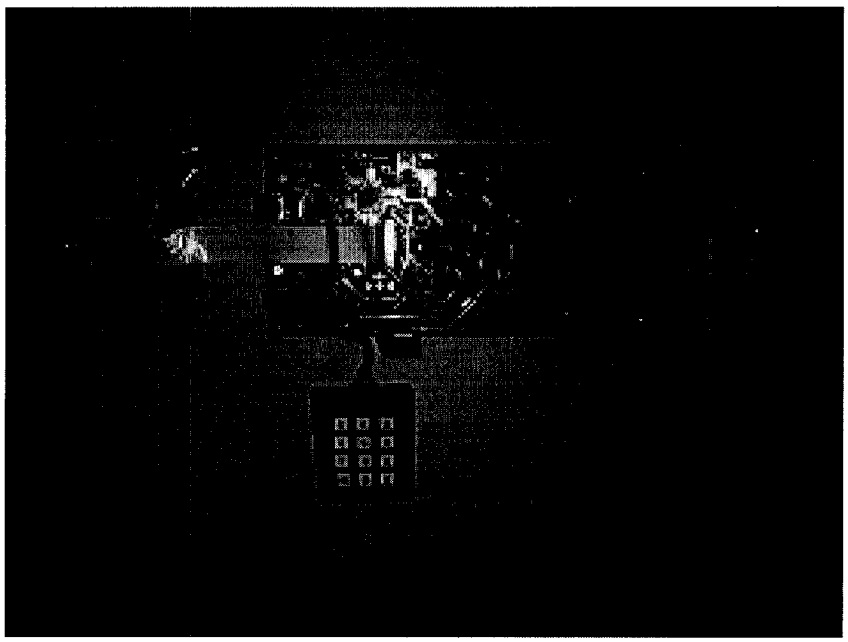

Figure A.14: An image of the populated PCBs containing the control and high voltage circuitry needed to operate the IMS. The larger board has not yet been populated with high voltage power supplies

The electronic hardware required to operate the entire MCE–ESI–IMS system is largely complete. Designed by Alex Stickel and Loi Hua, it consists of a large populated PCB with a design similar to that used by the Capillary Electrophoresis Mobile Oncology Lab (CEMOL) devices developed in the Applied Miniaturisation Laboratory. The intent of such an arrangement is to provide maximum portability of existing CEMOL firmware to the MCE–ESI–IMS system. No work has yet been conducted on adapting CEMOL firmware for use by the MCE–ESI–IMS system. Figure A.14 contains an image of the IMS system's control electronics and Figure A.15 contains a block diagram of the control electronics.

A clear acrylic box intended to house the IMS column, detector, electronic circuitry, and chip stage was constructed prior to my arrival in the AML. Based on the design of the MCE–ESI chip and the constraints of the acrylic box a chip stage was designed. Because the MCE–ESI chip design was within the scope of this work, so too was the chip stage. To date, the design is complete, but fabrication and assembly of the some of the components are still pending. The chip stage is fabricated entirely of polyvinyl chloride and allows for adjustment of the distance between the chip and the focusing grid at the entrance of the ionisation region. The design incorporates a modular chip holder for the chip stage. This holder can be removed and redesigned when new chip designs are tested, thus preventing the need to completely redesign the chip stage. This is similar in concept to the variety of chip stages that are used with the μTk. An acrylic plate attached to the chip stage can be raised or lowered to allow the high voltage electrodes to be placed in or re-

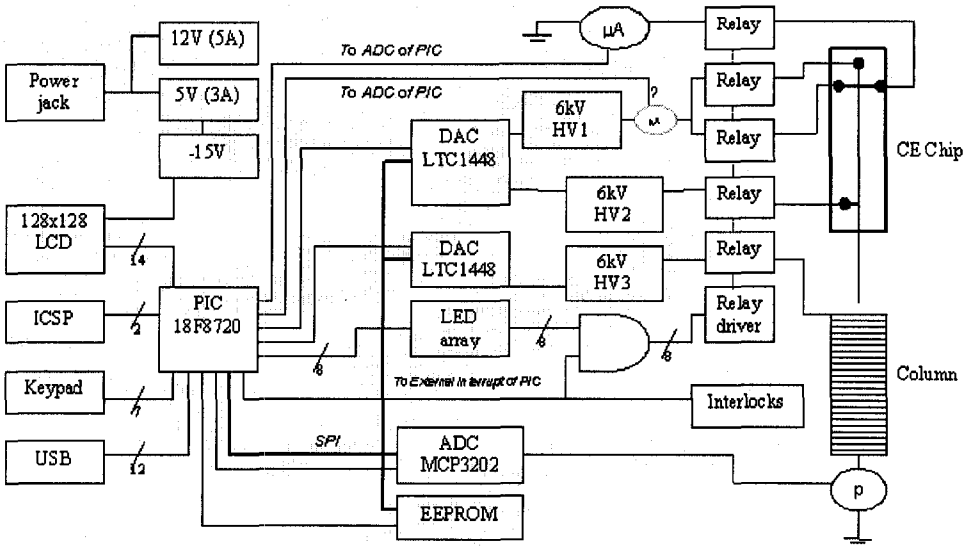

Figure A.15: A block diagram of the key electronic components and interconnections in the IMS control electronics (drawn by Alex Stickel).

moved from the chip wells. This plate can be removed and the hole patterns can be redesigned when necessary.

Complete designs and documentation for all of the chip stage components, IMS hardware, and IMS software are archived in the Applied Miniaturisation Laboratory. This archived documentation has been filed in electronic format on Gaea (the AML's server) and on DVD. Copies of the DVD have been submitted to Dr. Christopher Backhouse and Dr. Dammika Manage (AML member). This documentation includes PCB schematics, MCE–ESI mask design, IMS system operation manuals, electronic hardware datasheets, MCE–ESI–IMS system block diagram, and software and firmware developed by Eric Cheong, Brent Chizen, and Alex Stickel. The work conducted by Yujie Han in the development of the MCE-ESI portion of the system was poorly documented, and as such, was difficult to compile for this documentation in this thesis. Hardware components have been compiled and placed in a box in the AML laboratory labeled 'IMS'. These components include the MCE–ESI microchips, the IMS drift column (along with spare PCB plates), Faraday plate detection circuitry, completed portions of the MCE–ESI chip stage, and other construction materials required for IMS system construction. Incomplete portions of the system include the Faraday plate, detection circuitry shielding, MCE–ESI chip stage, and system firmware and software. All of the design documentation required for the incomplete IMS components has been archived in the 'IMS' box or on DVD. To the best of my knowledge, the data archive noted in this thesis documents all of the work conducted on the IMS system to date. Every effort has been made to ensure all of the required documentation and design work has been included in this data archive. Because of pre–existing documentation gaps that occurred over several years, it is unknown what information has been lost.

A.3 Conclusions

The work contained within this appendix is designed to bridge the gap between the techniques developed in Chapters 2, 3, and 4 and the IMS system developed by AML lab members in previous work. The early developmental phases of the MCE–ESI chip and assembly of the IMS system serve to facilitate future development of the complete MCE–ESI–IMS system.

Bibliography

[1] M. J. Sax. Report for ECE 750: Metabolomic analysis techniques and miniaturization (see supplementary material on DVD, "ECE750TermPaper Metabolomic Analysis.pdf").

[2] M. J. Sax. Report for ECE 559: Fabricating electrospray emitters (see supplementary material on DVD, "ECE559TermPaper Fabricating ESI Emitters.pdf"), 2006.

[3] S. J. Gaskell. Electrospray: Principles and practice. *Journal of Mass Spectrometry*, 32(7):677–688, 1997.

[4] N. B. Cech and C. G. Enke. Practical implications of some recent studies in electrospray ionization fundamentals. *Mass Spectrometry Reviews*, 20(6):362–387, 2001.

[5] B. Bathgate, E. C. S. Cheong, and C. J. Backhouse. A novel electrospray-based ion mobility spectrometer. *American Journal of Physics*, 72(8):1111–1118, 2004.

[6] Stephane Claverol, Odile Burlet-Schiltz, Jean Edouard Gairin, and Bernard Monsarrat. Characterization of protein variants and post-translational modifications: ESI-MSn analyses of intact proteins eluted from polyacrylamide gels. *Mol Cell Proteomics*, 2(8):483–493, 2003.

[7] R. Juraschek, T. Dulcks, and M. Karas. Nanoelectrospray - more than just a minimized-flow electrospray ionization source. *Journal of the American Society for Mass Spectrometry*, 10(4):300–308, 1999.

[8] S. Arscott, S. Le Gac, and C. Rolando. A polysilicon nanoelectrospray-mass spectrometry source based on a microfluidic capillary slot. *Sensors and Actuators B-Chemical*, 106(2):741–749, 2005.

[9] L. W. Beegle, I. Kanik, L. Matz, and H. H. Hill. Effects of drift-gas polarizability on glycine peptides in ion mobility spectrometry. *International Journal of Mass Spectrometry*, 216(3):257–268, 2002.

[10] C. J. Bramwell, M. L. Colgrave, C. S. Creaser, and R. Dennis. Development and evaluation of a nano-electrospray ionisation source for atmospheric pressure ion mobility spectrometry. *Analyst*, 127(11):1467–1470, 2002.

[11] N. B. Cech and C. G. Enke. Relating electrospray ionization response to nonpolar character of small peptides. *Analytical Chemistry*, 72(13):2717–2723, 2000.

[12] Y. H. Chen, H. H. Hill, and D. P. Wittmer. Thermal effects on electrospray ionization ion mobility spectrometry. *International Journal of Mass Spectrometry and Ion Processes*, 154(1-2):1–13, 1996.

[13] A. E. Counterman, A. E. Hilderbrand, C. A. S. Barnes, and D. E. Clemmer. Formation of peptide aggregates during ESI: Size, charge, composition, and contributions to noise. *Journal of the American Society for Mass Spectrometry*, 12(9):1020–1035, 2001.

[14] J. S. Kim and D. R. Knapp. Microfabrication of polydimethylsiloxane electrospray ionization emitters. *Journal of Chromatography A*, 924(1-2):137–145, 2001.

[15] L. M. Matz, W. E. Steiner, B. H. Clowers, and H. H. Hill. Evaluation of micro-electrospray ionization with ion mobility spectrometry/mass spectrometry. *International Journal of Mass Spectrometry*, 213(2-3):191–202, 2002.

[16] T. T. Razunguzwa, J. Lenke, and A. T. Timperman. An electrokinetic/hydrodynamic flow microfluidic CE-ESI-MS interface utilizing a hydrodynamic flow restrictor for delivery of samples under low EOF conditions. *Lab on a Chip*, 5(8):851–855, 2005.

[17] C. A. Srebalus, J. W. Li, W. S. Marshall, and D. E. Clemmer. Gas phase separations of electrosprayed peptide libraries. *Analytical Chemistry*, 71(18):3918–3927, 1999.

[18] S. J. Valentine, A. E. Counterman, C. S. Hoaglund, J. P. Reilly, and D. E. Clemmer. Gas-phase separations of protease digests. *Journal of the American Society for Mass Spectrometry*, 9(11):1213–1216, 1998.

[19] C. Wu, W. F. Siems, J. Klasmeier, and H. H. Hill. Separation of isomeric peptides using electrospray ionization/high-resolution ion mobility spectrometry. *Analytical Chemistry*, 72(2):391–395, 2000.

[20] G. R. Asbury and H. H. Hill. Separation of amino acids by ion mobility spectrometry. *Journal of Chromatography A*, 902(2):433–437, 2000.

[21] L. W. Beegle, I. Kanik, L. Matz, and H. H. Hill. Electrospray ionization high-resolution ion mobility spectrometry for the detection of organic compounds, 1. amino acids. *Analytical Chemistry*, 73(13):3028–3034, 2001.

[22] L. M. Matz, G. R. Asbury, and H. H. Hill. Two-dimensional separations with electrospray ionization ambient pressure high-resolution ion mobility spectrometry/quadrupole mass spectrometry. *Rapid Communications in Mass Spectrometry*, 16(7):670–675, 2002.

[23] P. V. Johnson, H. I. Kim, L. W. Beegle, and I. Kanik. Electrospray ionization ion mobility spectrometry of amino acids: Ion mobilities and a mass-mobility correlation. *Journal of Physical Chemistry A*, 108(27):5785–5792, 2004.

[24] L. Bendahl and B. Gammelgaard. Separation and identification of se-methylselenogalactosamine - a new metabolite in basal human urine - by HPLC-ICP-MS and CE-nano-ESI-(MS)(2). *Journal of Analytical Atomic Spectrometry*, 19(8):950–957, 2004.

[25] T. Soga, Y. Ueno, H. Naraoka, Y. Ohashi, M. Tomita, and T. Nishioka. Simultaneous determination of anionic intermediates for bacillus subtilis metabolic pathways by capillary electrophoresis electrospray ionization mass spectrometry. *Analytical Chemistry*, 74(10):2233–2239, 2002.

[26] M. Sugimoto, S. Kikuchi, M. Arita, T. Soga, T. Nishioka, and M. Tomita. Large-scale prediction of cationic metabolite identity and migration time in capillary electrophoresis mass spectrometry using artificial neural networks. *Analytical Chemistry*, 77(1):78–84, 2005.

[27] M. Dole, L. L. Mack, and R. L. Hines. Molecular beams of macroions. *Journal of Chemical Physics*, 49(5):2240–2249, 1968.

[28] L. A. Agrofolio, X. Cahours, T. T. Tran, H. Dessans, C. Kieda, and P. Morin. Analysis of anti-HIV nucleoside inhibitors by capillary electrophoresis-electrospray ionization mass spectrometry. *Nucleosides Nucleotides & Nucleic Acids*, 20(4-7):375–381, 2001.

[29] Y. R. Chen, M. C. Tseng, and G. R. Her. Design and performance of a low-flow capillary electrophoresis-electrospray-mass spectrometry interface using an emitter with dual beveled edge. *Electrophoresis*, 26(7-8):1376–1382, 2005.

[30] T. Soga, Y. Ueno, H. Naraoka, K. Matsuda, M. Tomita, and T. Nishioka. Pressure-assisted capillary electrophoresis electrospray ionization mass spectrometry for analysis of multivalent anions. *Analytical Chemistry*, 74(24):6224–6229, 2002.

[31] D. S. Lee, C. Wu, and H. H. Hill. Detection of carbohydrates by electrospray ionization ion mobility spectrometry following microbore high-performance liquid chromatography. *Journal of Chromatography A*, 822(1):1–9, 1998.

[32] P. Kebarle and M. Peschke. On the mechanisms by which the charged droplets produced by electrospray lead to gas phase ions. *Analytica Chimica Acta*, 406(1):11–35, 2000.

[33] R. B. Cole. Some tenets pertaining to electrospray ionization mass spectrometry. *Journal of Mass Spectrometry*, 35(7):763–772, 2000.

[34] M. L. Colgrave, C. J. Bramwell, and C. S. Creaser. Nanoelectrospray ion mobility spectrometry and ion trap mass spectrometry studies of the non-covalent complexes of amino acids and peptides with polyethers. *International Journal of Mass Spectrometry*, 229(3):209–216, 2003.

[35] T. Henriksen, R. K. Juhler, B. Svensmark, and N. B. Cech. The relative influences of acidity and polarity on responsiveness of small organic molecules to analysis with negative ion electrospray ionization mass spectrometry (ESI-MS). *Journal of the American Society for Mass Spectrometry*, 16(4):446–455, 2005.

[36] G. J. Van Berkel and F. M. Zhou. Electrospray as a controlled current electrolytic cell - electrochemical ionization of neutral analytes for detection by electrospray mass-spectrometry. *Analytical Chemistry*, 67(21):3958–3964, 1995.

[37] J. V. Iribarne and B. A. Thomson. Evaporation of small ions from charged droplets. *Journal of Chemical Physics*, 64(6):2287–2294, 1976.

[38] B. A. Thomson and J. V. Iribarne. Field-induced ion evaporation from liquid surfaces at atmospheric-pressure. *Journal of Chemical Physics*, 71(11):4451–4463, 1979.

[39] A. D. Zamfir, L. Bindila, N. Lion, M. Allen, H. H. Girault, and J. Peter-Katalinic. Chip electrospray mass spectrometry for carbohydrate analysis. *Electrophoresis*, 26(19):3650–3673, 2005.

[40] A. El-Faramawy, K. W. M. Siu, and B. A. Thomson. Efficiency of nano-electrospray ionization. *Journal of the American Society for Mass Spectrometry*, 16(10):1702–1707, 2005.

[41] M. Karas, U. Bahr, and T. Dulcks. Nano-electrospray ionization mass spectrometry: addressing analytical problems beyond routine. *Fresenius Journal of Analytical Chemistry*, 366(6-7):669–676, 2000.

[42] A. Schmidt, M. Karas, and T. Dulcks. Effect of different solution flow rates on analyte ion signals in nano-ESI MS, or: When does ESI turn into nano-ESI? *Journal of the American Society for Mass Spectrometry*, 14(5):492–500, 2003.

[43] M. Brinkmann, R. Blossey, S. Arscott, C. Druon, P. Tabourier, S. Le Gac, and C. Rolando. Microfluidic design rules for capillary slot-based electrospray sources. *Applied Physics Letters*, 85(11):2140–2142, 2004.

[44] S. Le Gac, S. Arscott, and C. Rolando. A planar microfabricated nanoelectrospray emitter tip based on a capillary slot. *Electrophoresis*, 24(21):3640–3647, 2003.

[45] N. F. Yin, K. Killeen, R. Brennen, D. Sobek, M. Werlich, and T. V. van de Goor. Microfluidic chip for peptide analysis with an integrated HPLC column, sample enrichment column, and nanoelectrospray tip. *Analytical Chemistry*, 77(2):527–533, 2005.

[46] S. Le Gac, C. Rolando, and S. Arscott. An open design microfabricated nib-like nanoelectrospray emitter tip on a conducting silicon substrate for the application of the ionization voltage. *Journal of the American Society for Mass Spectrometry*, 17(1):75–80, 2006.

[47] S. Arscott and D. Troadec. A nanofluidic emitter tip obtained by focused ion beam nanofabrication. *Nanotechnology*, 16(10):2295–2302, 2005.

[48] Q. F. Xue, F. Foret, Y. M. Dunayevskiy, P. M. Zavracky, N. E. McGruer, and B. L. Karger. Multichannel microchip electrospray mass spectrometry. *Analytical Chemistry*, 69(3):426–430, 1997.

[49] K. Huikko, P. Ostman, K. Grigoras, S. Tuomikoski, V. M. Tiainen, A. Soininen, K. Puolanne, A. Manz, S. Franssila, R. Kostiainen, and T. Kotiaho. Poly(dimethylsiloxane) electrospray devices fabricated with diamond-like carbon-poly(dimethylsiloxane) coated SU-8 masters. *Lab on a Chip*, 3(2):67–72, 2003.

[50] M. F. Bedair and R. D. Oleschuk. Fabrication of porous polymer monoliths in polymeric microfluidic chips as an electrospray emitter for direct coupling to mass spectrometry. *Analytical Chemistry*, 78(4):1130–1138, 2006.

[51] W. C. Sung, H. Makamba, and S. H. Chen. Chip-based microfluidic devices coupled with electrospray ionization-mass spectrometry. *Electrophoresis*, 26(9):1783–1791, 2005.

[52] T. Koerner and R. D. Oleschuk. Porous polymer monolith assisted electrospray from a glass microdevice. *Rapid Communications in Mass Spectrometry*, 19(22):3279–3286, 2005.

[53] J. M. Iannacone, J. A. Jakubowski, P. W. Bohn, and J. V. Sweedler. A multilayer poly(dimethylsiloxane) electrospray ionization emitter for sample injection and online mass spectrometric detection. *Electrophoresis*, 26(24):4684–4690, 2005.

[54] J. S. Kim and D. R. Knapp. Miniaturized multichannel electrospray ionization emitters on poly(dimethylsiloxane) microfluidic devices. *Electrophoresis*, 22(18):3993–3999, 2001.

[55] S. Thorslund, P. Lindberg, P. E. Andren, F. Nikolajeff, and J. Bergquist. Electrokinetic-driven microfluidic system in poly(dimethylsiloxane) for mass spectrometry detection integrating sample injection, capillary electrophoresis, and electrospray emitter on-chip. *Electrophoresis*, 26(24):4674–4683, 2005.

[56] V. Gobry, J. van Oostrum, M. Martinelli, T. C. Rohner, F. Reymond, J. S. Rossier, and H. H. Girault. Microfabricated polymer injector for direct mass spectrometry coupling. *Proteomics*, 2(4):405–412, 2002.

[57] Y. Z. Chang, M. W. Yang, and G. J. Wang. A new mass spectrometry electrospray tip obtained via precise mechanical micromachining. *Analytical and Bioanalytical Chemistry*, 383(1):76–82, 2005.

[58] M. H. Fortier, E. Bonneil, P. Goodley, and P. Thibault. Integrated microfluidic device for mass spectrometry-based proteomics and its application to biomarker discovery programs. *Analytical Chemistry*, 77(6):1631–1640, 2005.

[59] J. Kameoka, R. Orth, B. Ilic, D. Czaplewski, T. Wachs, and H. G. Craighead. An electrospray ionization source for integration with microfluidics. *Analytical Chemistry*, 74(22):5897–5901, 2002.

[60] S. Arscott, S. Le Gac, C. Druon, P. Tabourier, and C. Rolando. Micromachined 2d nanoelectrospray emitter. *Electronics Letters*, 39(24):1702–1703, 2003.

[61] S. Arscott, S. Le Gac, C. Druon, P. Tabourier, and C. Rolando. A planar on-chip micro-nib interface for nanoESI-MS microfluidic applications. *Journal of Micromechanics and Microengineering*, 14(2):310–316, 2004.

[62] S. Le Gac, S. Arscott, C. Cren-Olive, and C. Rolando. Two-dimensional microfabricated sources for nanoelectrospray. *Journal of Mass Spectrometry*, 38(12):1259–1264, 2003.

[63] S. Le Gac, J. Carlier, J. C. Camart, C. Cren-Olive, and C. Rolando. Monoliths for microfluidic devices in proteomics. *Journal of Chromatography B-Analytical Technologies in the Biomedical and Life Sciences*, 808(1):3–14, 2004.

[64] J. Carlier, S. Arscott, V. Thomy, J. C. Camart, C. Cren-Olive, and S. Le Gac. Integrated microfabricated systems including a purification module and an on-chip nano electrospray ionization interface for biological analysis. *Journal of Chromatography A*, 1071(1-2):213–222, 2005.

[65] M. Svedberg, A. Pettersson, S. Nilsson, J. Bergquist, L. Nyholm, F. Nikolajeff, and K. Markides. Sheathless electrospray from polymer microchips. *Analytical Chemistry*, 75(15):3934–3940, 2003.

[66] J. Wen, Y. H. Lin, F. Xiang, D. W. Matson, H. R. Udseth, and R. D. Smith. Microfabricated isoelectric focusing device for direct electrospray ionization-mass spectrometry. *Electrophoresis*, 21(1):191–197, 2000.

[67] Y. Z. Deng, J. Henion, J. J. Li, P. Thibault, C. Wang, and D. J. Harrison. Chip-based capillary electrophoresis/mass spectrometry determination of carnitines in human urine. *Analytical Chemistry*, 73(3):639–646, 2001.

[68] Y. N. Yang, C. Li, J. Kameoka, K. H. Lee, and H. G. Craighead. A polymeric microchip with integrated tips and in situ polymerized monolith for electrospray mass spectrometry. *Lab on a Chip*, 5(8):869–876, 2005.

[69] G. E. Yue, M. G. Roper, E. D. Jeffery, C. J. Easley, C. Balchunas, J. P. Landers, and J. P. Ferrance. Glass microfluidic devices with thin membrane voltage junctions for electrospray mass spectrometry. *Lab on a Chip*, 5(6):619–627, 2005.

[70] W. C. Sung, S. Y. Huang, P. C. Liao, G. B. Lee, C. W. Li, and S. H. Chen. Poly(dimethylsiloxane)-based microfluidic device with electrospray ionization-mass spectrometry interface for protein identification. *Electrophoresis*, 24(21):3648–3654, 2003.

[71] S. Ssenyange, J. Taylor, D. J. Harrison, and M. T. McDermott. A glassy carbon microfluidic device for electrospray mass spectrometry. *Analytical Chemistry*, 76(8):2393–2397, 2004.

[72] A. P. Dahlin, M. Wetterhall, G. Liljegren, S. K. Bergstrom, P. Andren, L. Nyholm, K. E. Markides, and J. Bergquist. Capillary electrophoresis coupled to mass spectrometry from a polymer modified poly(dimethylsiloxane) microchip with an integrated graphite electrospray tip. *Analyst*, 130(2):193–199, 2005.

[73] M. Schilling, W. Nigge, A. Rudzinski, A. Neyer, and R. Hergenroder. A new on-chip ESI nozzle for coupling of MS with microfluidic devices. *Lab on a Chip*, 4(3):220–224, 2004.

[74] P. Griss, J. Melin, J. Sjodahl, J. Roeraade, and G. Stemme. Development of micromachined hollow tips for protein analysis based on nanoelectrospray ionization mass spectrometry. *Journal of Micromechanics and Microengineering*, 12(5):682–687, 2002.

[75] G. A. Schultz, T. N. Corso, S. J. Prosser, and S. Zhang. A fully integrated monolithic microchip electrospray device for mass spectrometry. *Analytical Chemistry*, 72(17):4058–4063, 2000.

[76] J. Sjodahl, J. Melin, P. Griss, A. Emmer, G. Stemme, and J. Roeraade. Characterization of micromachined hollow tips for two-dimensional nanoelectrospray mass spectrometry. *Rapid Communications in Mass Spectrometry*, 17(4):337–341, 2003.

[77] A. P. Dahlin, S. K. Bergstrom, P. E. Andren, K. E. Markides, and J. Bergquist. Poly(dimethylsiloxane)-based microchip for two-dimensional solid-phase extraction-capillary electrophoresis with an integrated electrospray emitter tip. *Analytical Chemistry*, 77(16):5356–5363, 2005.

[78] C. S. Creaser, J. R. Griffiths, C. J. Bramwell, S. Noreen, C. A. Hill, and C. L. P. Thomas. Ion mobility spectrometry: a review. part 1. structural analysis by mobility measurement. *Analyst*, 129(11):984–994, 2004.

[79] D. C. Collins and M. L. Lee. Developments in ion mobility spectrometry-mass spectrometry. *Analytical and Bioanalytical Chemistry*, 372(1):66–73, 2002.

[80] J. I. Baumbach and G. A. Eiceman. Ion mobility spectrometry: Arriving on site and moving beyond a low profile. *Applied Spectroscopy*, 53(9):338A–355A, 1999.

[81] V. Ruzsanyi, J. I. Baumbach, S. Sielemann, P. Litterst, M. Westhoff, and L. Freitag. Detection of human metabolites using multi-capillary columns coupled to ion mobility spectrometers. *Journal of Chromatography A*, 1084(1-2):145–151, 2005.

[82] G. A. Eiceman. Ion-mobility spectrometry as a fast monitor of chemical composition. *Trac-Trends in Analytical Chemistry*, 21(4):259–275, 2002.

[83] J. Xu, W. B. Whitten, and J. M. Ramsey. Space charge effects on resolution in a miniature ion mobility spectrometer. *Analytical Chemistry*, 72(23):5787–5791, 2000.

[84] J. Xu, W. B. Whitten, and J. M. Ramsey. Pulsed-ionization miniature ion mobility spectrometer. *Analytical Chemistry*, 75(16):4206–4210, 2003.

[85] P. Dwivedi, L. M. Matz, D. A. Atkinson, and H. H. Hill. Electrospray ionization-ion mobility spectrometry: a rapid analytical method for aqueous nitrate and nitrite analysis. *Analyst*, 129(2):139–144, 2004.

[86] L. M. Matz, H. M. Dion, and H. H. Hill. Evaluation of capillary liquid chromatography-electrospray ionization ion mobility spectrometry with mass spectrometry detection. *Journal of Chromatography A*, 946(1-2):59–68, 2002.

[87] L. M. Matz, H. H. Hill, L. W. Beegle, and I. Kanik. Investigation of drift gas selectivity in high resolution ion mobility spectrometry with mass spectrometry detection. *Journal of the American Society for Mass Spectrometry*, 13(4):300–307, 2002.

[88] G. R. Asbury and H. H. Hill. Using different drift gases to change separation factors (alpha) in ion mobility spectrometry. *Analytical Chemistry*, 72(3):580–584, 2000.

[89] C. Wu, W. F. Siems, G. R. Asbury, and H. H. Hill. Electrospray ionization high-resolution ion mobility spectrometry - mass spectrometry. *Analytical Chemistry*, 70(23):4929–4938, 1998.

[90] C. Wu, J. Klasmeier, and H. H. Hill. Atmospheric pressure ion mobility spectrometry of protonated and sodiated peptides. *Rapid Communications in Mass Spectrometry*, 13(12):1138–1142, 1999.

[91] R. A. Miller, G. A. Eiceman, E. G. Nazarov, and A. T. King. A novel micromachined high-field asymmetric waveform-ion mobility spectrometer. *Sensors and Actuators B-Chemical*, 67(3):300–306, 2000.

[92] H. E. Revercomb and E. A. Mason. Theory of plasma chromatography gaseous electrophoresis - review. *Analytical Chemistry*, 47(7):970–983, 1975.

[93] Z. Karpas and Z. Berant. Effect of drift gas on mobility of ions. *Journal of Physical Chemistry*, 93(8):3021–3025, 1989.

[94] E. C. S. Cheong. *Electrospray Ionization for Applications in Ion Mobility Spectrometry*. PhD thesis, University of Alberta, 2003.

[95] A. E. Herr, D. J. Throckmorton, A. A. Davenport, and A. K. Singh. On-chip native gel electrophoresis-based immunoassays for tetanus antibody and toxin. *Analytical Chemistry*, 77(2):585–590, 2005.

[96] A. E. Herr, A. V. Hatch, D. J. Throckmorton, H. M. Tran, J. S. Brennan, W. V. Giannobile, and A. K. Singh. Microfluidic immunoassays as rapid saliva-based clinical diagnostics. *Proceedings of the National Academy of Sciences of the United States of America*, 104(13):5268–5273, 2007.

Appendix B

Permanent Surface Modification Protocol

B.1 Purpose

This protocol is designed for use with glass chips only. It will apply a permanent linear polyacrylamide coating to the channel walls consisting of a bi–layer that is designed to inhibit DNA and protein adsorption to the channel walls. In addition, this coating can be used in conjunction with a polyacrylamide gel (see Appendix) as the sieving matrix. The bulk of this procedure was adopted from existing papers published by Han and Singh [1], and Hjerten [2].

B.2 Special Precautions

Acrylamide monomer is a potent neurotoxin and should be handled with extreme caution. The proper Personal Protective Equipment for handling acrylamide monomer includes:

- At the very minimum goggles or safety glasses are required.
- Latex gloves to ensure no acrylamide can be absorbed through the skin.
- Lab coat to prevent clothing and exposed skin from absorbing acrylamide.
- Refrain from talking while using polyacrylamide to ensure it is not ingested if it sprays.

Ensure that you review the MSDS for acrylamide monomer prior to working with it.

B.3 Recipes

B.3.1 Silane Functionalisation Layer Solution

This solution is used to create a self–assembled monolayer (SAM) of silane molecules. This SAM makes the channel surface hydrophobic and permits covalent attachment of the linear polyacrylamide molecules used in this permanent coating. This solution should be freshly prepared each time this procedure is conducted, and it should be used immediately after mixing is complete. This recipe is designed to make 1mL of the solution.

Ingredients

1. Milli–Q water
2. Glacial acetic acid (537020, Sigma–Aldrich)
3. 92% 3–(Trimethoxysilyl)propyl acrylate (475149–5ML, Sigma–Aldrich)

Mixing Directions

1. Pipette 990μL of Milli–Q water into an eppendorf tube.
2. Pipette 5.8μL of glacial acetic acid into the eppendorf tube.
3. Pipette 4.2μL of 3–(Trimethoxysilyl)propyl acrylate into the eppendorf tube.
4. Vortex solution to mix thoroughly.

Final Solution Composition

5.75mM acetic acid solution ($pH \approx 3.5$) with 0.4% v/v 3–(Trimethoxysilyl)propyl acrylate.

B.3.2 Linear Polyacrylamide Coating Solution

This solution is designed to polymerise in the channel and form a coating that is covalently bound to the channel wall. This coating is designed to hydrophilic and permanent. The solution used to generate the coating should be mixed immediately prior to use and should not be stored (even for periods as short as 5min) for subsequent use. This recipe is designed to make 1mL of the solution.

Ingredients

1. Milli–Q water
2. 40% w/v acrylamide monomer solution (A4058-100ML, Sigma–Aldrich)

3. N,N,N,N-Tetramethylethylenediamine (TEMED) (T9281-25ML, Sigma–Aldrich)

4. Potassium persulfate (379824-5G, Sigma–Aldrich)

Mixing Directions

1. Pipette 800μL of Milli–Q water into an eppendorf tube.

2. Pipette 100μL of 40% w/v acrylamide monomer solution into the same eppendorf tube.

3. Weigh out 10.0mg of potassium persulfate, and dissolve it in 1mL of Milli-Q water in a new eppendorf tube. Vortex the solution until the potassium persulfate is completely dissolved.

4. Pipette 100μL of the potassium persulfate solution into the eppendorf tube containing the acrylamide monomer solution.

5. Sonicate the acrylamide and potassium persulfate solution in a water bath for 10min. The eppendorf tube can be placed in a small beaker with enough water in it to submerge three–quarters of the eppendorf tube. This beaker can then be placed in the sonication bath. The water level in the surrounding sonication bath should be similar to that in the beaker.

6. Using the fume hood, pipette 1μL of TEMED into the acrylamide and potassium persulfate solution.

7. Swirl solution gently so as to minimise the generation of air bubbles.

Final Solution Composition

4% w/v acrylamide monomer solution with 0.1% w/v potassium persulfate and 0.1% v/v TEMED.

B.4 Procedures

1. When disposing of or rinsing out solutions containing acrylamide, dispose of solutions by aspiration using the vacuum flask in the AML fume hood. Any materials used for soaking up, or delivering acrylamide should be collected and disposed of accordingly. Proper disposal involved placing these materials in a sealed waste bag in the AML fume hood. Also, the chip being coated should be completely clean and should be rejuvenated using the standard AML protocol prior to performing the coating.

2. Using a transfer pipette, dispense 1N NaOH into the chip's wells so as to fill the channels and each of the wells. Allow this solution to remain in the channels for 10min.

3. Evacuate the 1N NaOH solution from the channels using a vacuum.

4. Place Milli–Q water in each of the chips wells and suck water through the channels using a vacuum placed at one of the wells. Repeat two to three times to ensure the channels and wells are adequately rinsed.

5. Dry the channels using the application of the vacuum to each of the channels. Follow up with drying using pressurised N_2. The channels need to be extremely dry.

6. Using a pipette, deposit 3μL of the silane functionalisation layer solution into BW.

7. Allow the separation and injection channels to fill completely. Once they are filled, fill the other wells with the binding layer solution.

8. Place a glass microchip slide over the chip to minimise solution evaporation. Wait for 1h.

9. Remove the covering from the chip.

10. Rinse the channels thoroughly with water to ensure the silane functionalisation layer solution is completely flushed from the channel using the same method used to remove NaOH from the channels. Dry the channels using the aforementioned methods.

11. Mix the linear polyacrylamide coating solution and ensure that it is at room temperature.

12. *Ensure all proper Personal Protective Equipment are in place. Pay full attention to the task at hand, and do not talk during this procedure. Inadvertent exposure to acrylamide monomer is hazardous.* Pipette 3 μL of the linear polyacrylamide coating layer solution into BW. Allow the chip's channels to fill.

13. Examine the channels to ensure there are no air bubbles. If there are air bubbles, aspirate the solution in the channels (using a vacuum) and rinse and dry the channels using previously described methods. If there are not any air bubbles, continue on to the next step.

14. Fill each well with the 3μL of linear polyacrylamide coating layer solution.

15. Place a glass microchip slide over the chip to minimise solution evaporation. Wait 30min.

16. After 30min have elapsed, aspirate the solution in the channels immediately using a vacuum. The solution should be slightly viscous at this point. Once the majority of the solution is aspirated, rinse and dry the channels using the previously described methods.

17. Inspect the channel for contaminants or obstructions. If there are obstructions, repeat rinsing and drying of the channel.

18. Store coated chips submerged in water at 4.

B.5 Troubleshooting

If the linear polyacrylamide coating solution is difficult to remove, it cannot be removed using the application of pressure or standard chip rejuvenation protocols. If this occurs, the only way to remove the coating solution is to take the chip to the University of Alberta Chemistry Department's Glass Blowing Shop and place the chip in the annealing oven overnight. Cleaning often requires two to three nights in the oven. Chips should be picked up each day and examined before they are put back in the oven. The solution is not removable because the solution becomes more viscous during polymerisation. In order to avoid this situation, the following issues should be addressed:

1. Ensure the coating solution reaction is carried out at room temperature (20–25). Higher temperatures may speed up the polymerization reaction.

2. Confirm that the proper amounts of TEMED and potassium persulfate were used. TEMED acts as the reaction catalyst, and potassium persulfate provides the free radicals required for polymerization. Excess amounts of either of these substances will change the reaction rate.

3. This protocol was developed for 4–Port Mini microchips with channels measuring 46μm deep and 102μm wide. Channels with smaller cross–sectional dimensions and/or longer channels make the linear polyacrylamide solution more difficult to evacuate.

4. Reduce the dwell time of the linear polyacrylamide coating solution or reduce the acrylamide monomer concentration in the solution. This should be done as a last resort, as it is unknown what impact this may have on the quality of effectiveness of the coating.

If the coating seems to be ineffective during electrophoretic separations, the linear polyacrylamide coating solution dwell time in the channels can be extended. Otherwise, ensure the following:

1. The proper amounts of TEMED and potassium persulfate were used. Lower amounts than stated will slow the polymerization reaction, thus affecting the quality of the coating.

2. The coating solution was properly degassed by sonicating it for the stated time. Omitting this step may allow dissolved oxygen to remain in the solution. Oxygen inhibits the polymerization reaction by scavenging the free radicals generated by the potassium persulfate that are needed for the reaction to take place. Improper degassing will lead to a slower reaction rate.

3. The acrylamide monomer solution should not be 'old' and should have been stored in a refrigerator. Check with the supplier for storage lifetimes.

For more information on acrylamide polymerization, consult BioRad's Technical Note 1156 [3]. Although it primarily discusses cross–linked polyacrylamide, it is still a good reference that can be used to gain an understanding of the polymerisation chemistry and to troubleshoot the polymerization reaction.

Bibliography

[1] J. Han and A. K. Singh. Rapid protein separations in ultra-short microchannels: microchip sodium dodecyl sulfate-polyacrylamide gel electrophoresis and isoelectric focusing. *Journal of Chromatography A*, 1049(1-2):205–209, 2004.

[2] S. Hjerten. High-performance electrophoresis - elimination of electroendosmosis and solute adsorption. *Journal of Chromatography*, 347(2):191–198, 1985.

[3] P. Menter. Acrylamide polymerization - A practical approach, Bulletin 1156 - Revision E, Bio–Rad Laboratories Ltd., Mississauga, Ontario. Website, 2007. `http://www.bio-rad.com/LifeScience/pdf/Bulletin_1156.pdf`.

Appendix C

In–Situ Polyacrylamide Gel Polymerisation Protocol

C.1 Purpose

This protocol is designed for use with glass chips only. It will form a patterned cross-linked polyacrylamide gel in a portion of a microfluidic channel intended for protein separations. The bulk of this procedure was adopted from an existing paper published by Han and Singh [1].

C.2 Special Precautions

Acrylamide monomer is a potent neurotoxin and should be handled with extreme caution. The proper Personal Protective Equipment for handling acrylamide monomer includes:

- At the very minimum goggles or safety glasses are required.
- Latex gloves to ensure no acrylamide can be absorbed through the skin.
- Lab coat to prevent clothing and exposed skin from absorbing acrylamide.
- Refrain from talking while using polyacrylamide to ensure it is not ingested if it sprays.

Ensure that you review the MSDS for acrylamide monomer prior to working with it.

C.3 Recipes

C.3.1 Polyacrylamide Gel Precursor Solution

This solution is used to generate in–situ polymerised polyacrylamide gels within microfluidic channels coated using the protocol discussed in Appendix B. This

gel acts as a sieving matrix for the separation of SDS–denatured protein molecules via SDS–PAGE. While the gels, could also be used for native protein separations, the solution buffer discussed in this protocol contains SDS, and is thus only useful for SDS–PAGE. These procedures can be adapted to generate a wide range of gel concentrations and also to incorporate alternative solution buffers. This recipe is designed to make 1mL of the solution.

Ingredients

1. Milli–Q water
2. 40% Acrylamide/Bis–acrylamide (37.5:1) solution (A7168-100ML, Sigma–Aldrich)
3. 2,2′–Azobis[2–methyl–N–(2–hydroxyethyl)propionamide] (VA-086 (Sample), Wako Chemicals USA Inc.)
4. 20X NEXT GEL Running Buffer (M259-100ML , Cedarlane Laboratories Ltd.)

Mixing Directions

1. Refer to Table C.1 for reagent quantities. Care should always be taken to minimise the introduction of bubbles into these solutions.
2. Pipette 37.5μL of 20X NEXT GEL Running Buffer into eppendorf tube #1 and 50μL into tube #2. Tube #1 will be used for the final solution, while tube #2 will be used for an intermediate solution of 2,2′–Azobis[2–methyl–N–(2–hydroxyethyl)propionamide] (Azo–Initiator).
3. Add the required amount of Milli–Q water to each tube. In the case of tube #2, this will always be 950μL.
4. Add the required amount of 40% Acrylamide/Bis–acrylamide solution to tube #1.
5. Weigh out 20mg of Azo–Initiator powder and dissolve it in the solution contained in tube #2. Vortex the solution until the powder is completely dissolved.
6. Pipette 250μL of the intermediate Azo–Initiator solution in tube#2 into the solution in tube #1. Pipette the solution up and down to ensure proper mixing. Do not vortex this solution.
7. Wrap tube #1 in aluminum foil to ensure minimal exposure to light. This is now a photoactive solution and exposure to UV light may initiate the polymerisation reaction.

8. Sonicate the solution in tube #1 in a water bath for 30min. The eppendorf tube can be placed in a small beaker with enough water in it to submerge three–quarters of the eppendorf tube. This beaker can then be placed in the sonication bath. The water level in the surrounding sonication bath should be similar to that in the beaker.

Gel Concentration	4%	5%	6%	8%	10%	12%	15%
Milli-Q water added to Tube #1 (μL)	613	588	563	513	463	413	338
40% Acrylamide/Bis-acrylamide added to Tube #1 (μL)	100	125	150	200	250	300	375

Table C.1: Polyacrylamide gel recipes

Final Solution Composition

Acrylamide/bis–acrylamide solution of given concentrations %T and %C with a monomer to cross–linker ratio of 37.5:1. 0.5% w/v Azo–Initiator and 1X running buffer.

C.4 Procedures

1. When disposing of or rinsing out solutions containing acrylamide, dispose of solutions by aspiration using the vacuum flask in the AML fume hood. Any materials used for soaking up, or delivering acrylamide should be collected and disposed of accordingly. Proper disposal involved placing these materials in a sealed waste bag in the AML fume hood. Also, the chip being coated should be completely clean and should be rejuvenated using the standard AML protocol prior to performing the coating.

2. Mix the polyacrylamide gel precursor solution with the desired %T as per the instructions in Section C.3.1.

3. Cover the polyacrylamide gel precursor solution's eppendorf tube with aluminum foil to prevent exposure to light.

4. Sonicate the polyacrylamide gel precursor solution in a water bath for 30min. The eppendorf tube can be placed in a small beaker with enough water in it to submerge three–quarters of the eppendorf tube. This beaker can then be placed in the sonication bath. The water level in the surrounding sonication bath should be similar to that in the beaker.

5. Adjust the stage in the UV box (Applied Miniaturisation Laboratory) such that it is approximately 3cm from the UV lamp. With the UV box exhausted to the fume hood and the fume hood turned on, turn on the UV lamp (Part No. 88–9213–02, BHK Inc., Claremont, CA, USA) and allow it to warm up until the first chip exposure is conducted. This should be approximately 40min. Ensure the door on the UV box is closed. Intensity measurements, performed after a thirty minute lamp warm–up time, at 254nm, 365nm, and 400nm, yielded values of $1.64 mW/cm^2$, $15.7 mW/cm^2$, and $4.5 mW/cm^2$ respectively.

6. Approximately 10min prior to the completion of polyacrylamide gel precursor solution sonication, remove the chips in which the gel will be polymerised from their storage water. Dry the channels thoroughly using pressurized N_2.

7. Remove the polyacrylamide gel precursor solution from the sonicator.

8. *Ensure all proper Personal Protective Equipment are in place. Pay full attention to the task at hand, and do not talk during this procedure. Inadvertent exposure to acrylamide monomer is hazardous.* Pipette 3 μL of the polyacrylamide gel precursor solution into CB3. Allow the chip's channels to fill.

9. Examine the channels to ensure there are no air bubbles. If there are air bubbles, aspirate the solution in the channels (using a vacuum) and rinse and dry the channels using previously described methods. If there are not any air bubbles, continue on to the next step.

10. Fill each remaining well with 3 μL of polyacrylamide gel precursor solution.

11. Turn off the UV lamp.

12. Place the chip on a glass microscope slide and place the chip and slide on the stage inside the UV box. Close the door on the UV box.

13. Set the countdown timer on the UV lamp to 8min and start the countdown. The lamp should automatically turn on when the countdown is started and shut off when the countdown is complete.

14. Once the exposure is complete remove the slide and chip from the UV box. Examine the channels to see if any bubbles/voids formed in the gel. If bubbles/voids did form, set aside the chip for cleaning. If bubbles/voids did not form, the chip can undergo a second exposure. Also examine the consistency of the gel in the wells by probing it with a 10μL pipette tip. If the polymerisation is progressing at the desired reaction rate polymerisation should have taken place and the gel in the wells should have a consistency similar to JELL–O.

15. Top up each well with 3μL of polyacrylamide gel precursor solution.

16. Place the chip and slide in the UV box and conduct a second 8min exposure. When the exposure is complete inspect the channels again and top up the well with polyacrylamide gel precursor solution as before.

17. Place the chip and slide in the UV box and conduct a 5min exposure. When the exposure is complete inspect the channels again. If the gel in the channels is free of bubbles/voids. Store the chip completely submerged in 1X NEXT GEL Running buffer at approximately 4°C.

18. Store the chip overnight before attempting separations. This allows any polymerisation reagents to diffuse out of the channels and ensures fresh running buffer is present in all regions of the chip.

19. Dispose of all solutions by aspirating them into the waste solution flask in the Applied Miniaturisation Laboratory fume hood.

20. Allow the UV box to exhaust for approximately 10min after the final exposure by leaving the exhaust connected to the fume hood.

21. Unplug the power cord leading to the UV box to ensure the UV lamp is not inadvertently turned on while it is unattended.

Bibliography

[1] J. Han and A. K. Singh. Rapid protein separations in ultra-short microchannels: microchip sodium dodecyl sulfate-polyacrylamide gel electrophoresis and isoelectric focusing. *Journal of Chromatography A*, 1049(1-2):205–209, 2004.

Appendix D

SDS–PAGE Protocols

D.1 Purpose

These protocols are designed for use with microfluidic chips permanently coated with linear polyacrylamide and with a cross–linked polyacrylamide gel sieving matrix in the channels. The procedures discussed herein cover the electrophoretic separation of a pre–labeled protein ladder, an unlabeled protein ladder, and the collection and analysis of a unstimulated whole saliva sample, also known as sialometry.

D.2 Special Precautions

Special care should be taken when handling 2–mercaptoethanol and solutions containing 2–mercaptoethanol. This substance has a pungent odour that is irritating and potentially harmful. Ensure the MSDS for 2–mercaptoethanol is reviewed prior to use. Any solutions for which 2–mercaptoethanol is required should be prepared in a fume hood and once prepared, the eppendorf tubes in which these solutions are contained should be stored in a capped vial to minimise odours.

Special care should also be taken when handling potassium cyanide (KCN). The major hazard associated with KCN is the formation of toxic cyanide gas when it is combined with acids. Always handle KCN with care and review its MSDS prior to use.

D.3 Recipes

D.3.1 Sodium Borate Buffer

A dilution of this buffer solution is used as the sample buffer in all protein separations. This recipe specifies the ingredients required for making a 100mL aliquot of 20mM of sodium borate buffer.

Ingredients

1. Milli-Q water
2. Sodium tetraborate decahydrate ($Na_2B_4O_7 \cdot 10H_2O$) (AC205950010, Fisher Scientific)
3. Boric acid (B115, Biochemistry Stores, University of Alberta)

Mixing Directions

1. Add 100mL of Milli–Q water to a container suitable for storing solution aliquots.
2. Weigh out 124mg of boric acid and add it to the Milli–Q water.
3. Weigh out 763mg of $Na_2B_4O_7 \cdot 10H_2O$ and add it to the Milli–Q water.
4. Stir the solution until all ingredients are completely dissolved.
5. Measure the pH.
6. Adjust the pH using a suitable acid (e.g. HCl) to a value of approximately 8.5.
7. Store the solution at room temperature. Replace after one month.

Final Solution Composition

20mM sodium borate buffer with pH of 8.5.

D.3.2 Pre–Labeled Protein Ladder Sample Solution

This solution is intended to be mixed in the sample well (SW) of the microfluidic chip in which the electrophoretic separation will take place.

Ingredients

1. Milli–Q water
2. Benchmark™ Fluorescent Protein Ladder (BFPS) (LC5928, Invitrogen Inc.)
3. 20mM Sodium borate buffer
4. 10% Sodium dodecyl sulfate (SDS) solution (71736-100ML, Sigma–Aldrich)

Mixing Directions

1. Pipette 12μL of 20mM (see Section D.3.1) into a small eppendorf tube.
2. Add 20μL of 10% SDS solution to the buffer in the small eppendorf tube.
3. Add 68μL of Milli–Q water to the small eppendorf tube. Vortex this solution and store it at approximately 4°C when not in use. This is a 100μL sample buffer solution containing 2.4mM sodium borate buffer with 2.0% SDS.
4. Vortex the BFPS solution. Pipette 0.5μL of the solution into the sample well.
5. Pipette 2.5μL of the 2.4mM sodium borate sample buffer into the well. Mix the well by pipetting the solution up and down.

Final Solution Composition

0.16X BFPS sample solution with 2.0mM sodium borate buffer and 1.7% SDS.

D.3.3 Unlabeled Protein Ladder Sample Solution

The final solution is intended to be mixed in the sample well (SW) of the microfluidic chip in which the electrophoretic separation will take place. This sample solution is designed to label an unlabeled protein ladder in the SW of the microfluidic chip.

Ingredients

1. Milli–Q water
2. Benchmark™ Protein Ladder (BPL) (10747012, Invitrogen Inc.)
3. 20mM Sodium borate buffer
4. 10% Sodium dodecyl sulfate (SDS) solution (71736-100ML, Sigma–Aldrich)
5. Potassium cyanide KCN (207810-25G, Sigma–Aldrich)
6. ATTO–TAG FQ (A-10192, Invitrogen Inc.)
7. Methanol (M112, Biochemistry Stores, University of Alberta)

Mixing Directions

1. In an eppendorf tube, dissolve 13mg of KCN into 1mL of Milli–Q water (0.2M KCN). Vortex this solution to ensure it is mixed well. Dilute and aliquot this solution by pipetting 1μL into 99μL of Milli–Q water in small eppendorf tubes (2mM KCN). Store these solutions at approximately -20°C when not in use.
2. Dissolve 2.5mg of ATTO–TAG FQ in 1mL of methanol (10mM ATTO–TAG FQ). Dilute an aliquot this solution by pipetting 2μL into 8μL of methanol in small eppendorf tubes (2mM ATTO–TAG FQ). Store these solutions at approximately -20°C when not in use and ensure the eppendorf tubes are covered in aluminum foil to prevent exposure to light.
3. Pipette 14μL of 20mM (see Section D.3.1) into a small eppendorf tube.
4. Add 20μL of 10% SDS solution to the buffer in the small eppendorf tube.
5. Add 66μL of Milli–Q water to the small eppendorf tube. Vortex this solution and store it at approximately 4°C when not in use. This is a 100μL sample buffer solution containing 2.8mM sodium borate buffer with 2.0% SDS.
6. Vortex the BPL solution. Pipette 0.5μL of the solution into the sample well.
7. Pipette 0.2μL of the 2mM KCN solution (ensure the solution is completely thawed and well mixed) into the well.
8. Pipette 0.2μL of the 2mM ATTO–TAG FQ (ensure the solution is completely thawed and well mixed) solution into the well.
9. Pipette 2.1μL of the 2.8mM sodium borate sample buffer into the well. Mix the well by pipetting the solution up and down.
10. Allow the solution to react for approximately 10min in a dark location (i.e. inside the μTk) prior to conducting electrophoretic separations.

Final Solution Composition

0.16X BPL sample solution with 2.0mM sodium borate buffer, 0.33mM ATTO–TAG FQ, 0.33mM KCN, and 1.7% SDS.

D.3.4 Saliva Sample Solution

The final solution is intended to be placed directly in the SW of the microfluidic chip immediately prior to electrophoretic separation. This sample solution is designed to fluorescently label and denature proteins in an unstimulated saliva sample.

Ingredients

1. Milli–Q water
2. Unstimulated saliva sample
3. 20mM Sodium borate buffer
4. 10% Sodium dodecyl sulfate (SDS) solution (71736-100ML, Sigma–Aldrich)
5. 0.2M Potassium cyanide KCN (see Section D.3.3)
6. 10mM ATTO–TAG FQ (see Section D.3.3)
7. 2–mercaptoethanol (M108, Biochemistry Stores, University of Alberta)

Mixing Directions

1. Conduct the following step in a fume hood. In a small eppendorf tube combine 45μL of Milli–Q water, 20μL of 20mM sodium borate buffer, 20μL of 10% SDS solution, 20μL of 10mM ATTO–TAG FQ solution, and 5μL of 2–mercaptoethanol. Cover the eppendorf tube in aluminum foil, seal it in a vial with a screw–on cap, and store at approximately 4°C. This will be called the sample buffer.
2. Obtain informed consent before getting saliva sample. Ethics coverage may also be required when obtaining samples, so ensure that proper documentation has been filed and that the required approval for gathering of such samples has been granted. Do not proceed with any sample collection in the absence of ethics approval.
3. Have the subject rinse out their mouth extensively with water over 2 to 3min repeatedly expectorating water and replacing it with fresh water. The sample should then allow saliva to gradually accumulate in their mouth for a period of 5min. At the end of the 5min period, have the subject expectorate the saliva into an eppendorf tube.
4. Pipette 99μL of the saliva sample into a small eppendorf tube. Store the remaining sample at -20°C.
5. Add 1μL of 0.2M KCN solution to the saliva. Vortex this solution (sample solution).
6. Add 25μL of sample solution to the sample buffer. Vortex this solution (labeled sample solution). At this point the solution should be clear.
7. Heat the solution to 90°C for 5min using a thermocycler. This will denature the proteins and allow for labeling of the proteins with ATTO-TAG FQ.

8. Allow the sample to return to room temperature. Remove it from the thermocycler. The solution should now have a slightly pinkish hue.

9. Pipette this solution into the sample well immediately prior to conducting an electrophoretic solution.

10. Any unused sample should be stored at -20°Cand should be covered in aluminum foil to prevent exposure to light.

Final Solution Composition

0.5X saliva sample solution with 2.0mM sodium borate buffer, 1mM ATTO–TAG FQ, 1mM KCN, and 1% SDS.

D.4 Procedures

1. All operating conditions (i.e. electric field strengths) are quoted for 4–Port Mini chips with 46μm deep and 102μm wide channels.

2. Remove the microfluidic chip from its storage buffer. If the chip has not been used before, scrape the gel out of each well using a 10μL pipette tip.

3. Fill each well of the microfluidic chip with 3μL of 1X NEXT GEL Running buffer (1XNGB).

4. Place the chip in the μTk, focus the laser at the intersection, and conduct electrokinetic flushing. Apply a 300V potential across the injection channel (approximately 160V/cm, SR = GND, SW = 300V) for ten minutes, then apply a 300Vpotential across the separation channel (approximately 140V/cm, BR = GND, BW = 300V) for an equal duration. This procedure is repeated until the sample fluorescence generates a photomultiplier tube (PMT) voltage of less than 0.5V (PMT gain = 0.8). Currents should also be monitored to ensure they are stable. Periodic replacement of 1XNGB in each well may be required to help lower

5. Pipette the 1XNGB out of each well.

6. Pipette 3μL of 1XNGB in the SW, BR, and BW wells.

7. Pipette the one of the desired sample solutions from Sections D.3.2, D.3.3, or D.3.4.

8. Place the microfluidic chip into the μTk.

9. Focus the laser at a detection point between 3mm and 10mm. Commonly used detection points are 3mm, 4mm, 9mm, and 10mm because they are easy to landmark on 4–Port Mini chips.

10. Conduct sample injection and separation. The electric field strength used for the injection is approximately 215V/cm (SR = GND, SW = 400V). Injection times vary, but are generally between 90s and 120s for the initial injection, and between 10s and 20s for subsequent injections in 4–Port Mini chips using 6% and 8% gels. The separation field strength can vary between 230V/cm and 460V/cm(BR = GND, BW = 500V-1000V). Separation times are based on detection distance, electric field strength, and sample content. Generally, separations last less than 150s at 230V/cm with detection conducted at 10mm for sample proteins as large as 220kDa.

11. After the final separation is complete, pipette the solutions out of the wells.

12. Repeat the aforementioned electrokinetic flushing procedure to ensure a minimal amount of sample is left in the channels, and to flush out any remaining sample buffer (sodium borate buffer).